NASA
Contractor Report 191057

Army Research Laboratory
Contractor Report ARL-CR-14

Advanced Rotorcraft Transmission (ART) Program – Final Report

Gregory F. Heath
McDonnell Douglas Helicopter Company
Mesa, Arizona

and

Robert B. Bossler, Jr.
Lucas Western, Incorporated
Applied Technology Division
City of Industry, California

January 1993

Prepared for
Lewis Research Center
Under Contract NAS3-25454

National Aeronautics and Space Administration

U.S. ARMY RESEARCH LABORATORY

PHASE I
FINAL REPORT

ADVANCED ROTORCRAFT TRANSMISSION PROGRAM
(ART)

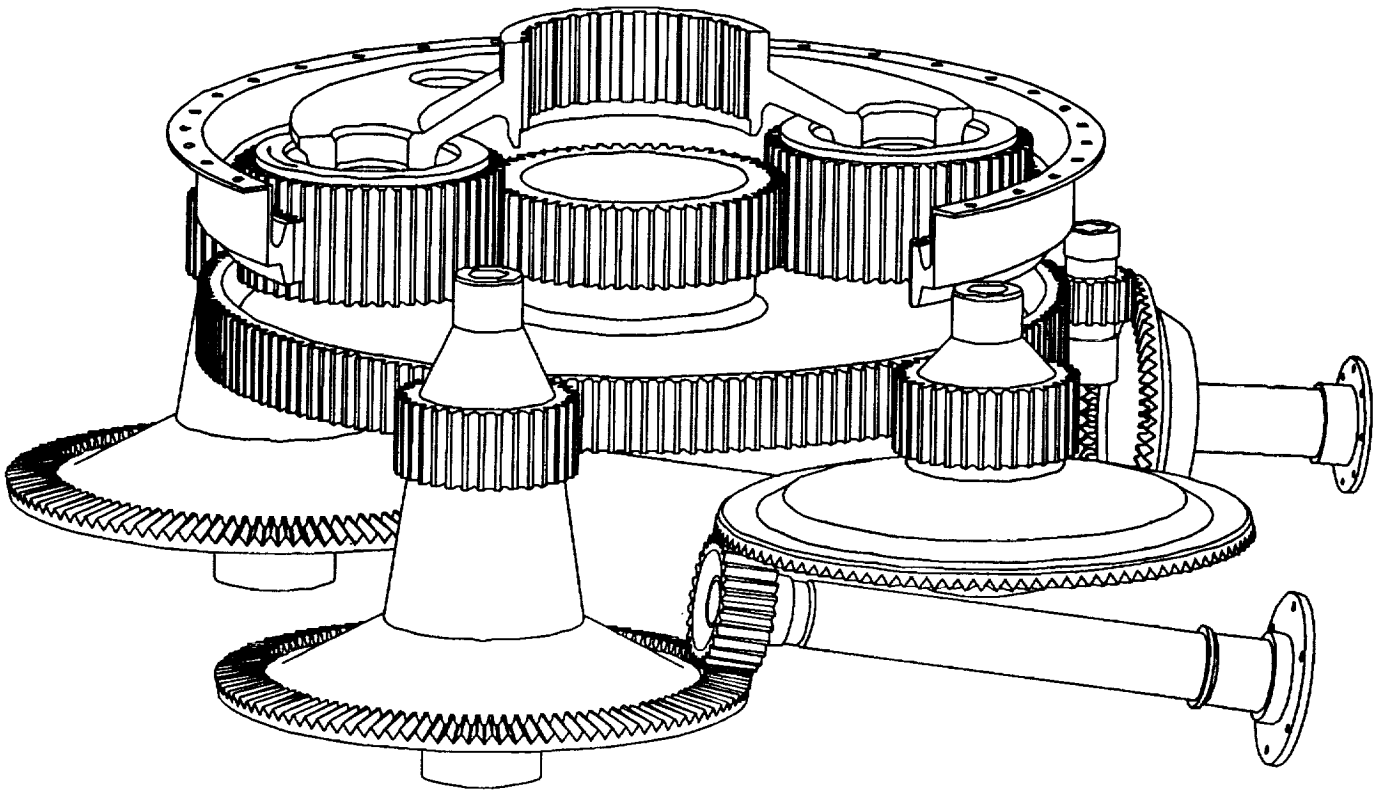

Prepared For:

U.S. Army Propulsion Directorate
National Aeronautics and Space Administration
Lewis Research Center
Cleveland, Ohio 44135

CONTENTS

CONTENTS (Continued)

CONTENTS (Continued)

CONTENTS (Continued)

FIGURES

FIGURES (Continued)

FIGURES (Continued)

FIGURES (Continued)

LIST OF TABLES

LIST OF TABLES

LIST OF TABLES

LIST OF TABLES

This page is intentionally left blank.

I. SUMMARY

The Team of McDonnell Douglas Helicopter Company (MDHC) and teammate/subcontractor Lucas Western, Inc. (LWI) have developed a concept which meets or exceeds all of the goals of the Advanced Rotorcraft Transmission (ART) Program. The total calculated weight of the transmission assembly is 40 percent below the SOA transmission weight compared to the goal of 25 percent. The noise reduction goal of 10 dB is essentially met with a predicted reduction of 9.6 dB. Reliability of the ART exceeds the 5000-hour MTBR goal by 1270 hours.

This report summarizes design work performed by MDHC and LWI, within the Army/NASA ART Program. It describes the ART Program Task IV detail design of a 5000-horsepower transmission for an early 21st century Future Attack Air Vehicle (FAAV) weighing about 16,000 pounds. Government goals set for the program were to define technology and detail design the ART to meet, as a minimum, a weight reduction of 25 percent, an internal noise reduction of 10 dB plus a Mean Time Between Removal (MTBR) of 5000 hours compared to a state-of-the-art (SOA) baseline transmission.

A novel three-stage ART transmission concept was developed to meet the requirements. It features a torque splitting configuration using face gears. On each side of the transmission, a single input spur gear drives two face gears simultaneously. This splits the torque into two nearly equal load paths, each face gear shaft transmitting reduced torque until a recombination occurs at a second stage collector gear. The separate load paths allow significant downsizing of first and second stage components beyond the high-volume geometries that would have been required to carry full load. A high contact ratio third stage planetary with a flexured ring gear also yields reduced weight and noise levels for the transmission. Optimized gear web design and selection of advanced housing materials represent other technology improvements. Overrunning positive engagement clutches on the input shafts and an advanced lubrication system further advance the weight and reliability advantages of the configuration. System design methods such as an optimized combination of gear ratios, computerized reliability methodology interactive with gear and bearing design allowables, and partially overlapping second and third stages were also used to reduce weight. The total calculated weight of the transmission assembly is 815 lb, 40 percent below the SOA transmission weight. The predicted source noise level for the ART is 98.3 dB, which is 9.6 dB below the 107.9 dB SOA noise level for the upscaled baseline 5000-horsepower Apache transmission. The Army/NASA goal for noise reduction was 97.9 dB, 10 dB below the 107.9 dB SOA noise level. Reliability of the ART is 6270 hours MTBR, 1270 hours above the 5000 hour goal. MDHC mission analysis shows that the above FAAV with ART produces a 17 to 22 percent improvement in the loss exchange ratio compared to the baseline FAAV. In addition, the improvement in mission reliability translates to a 22 percent increase in MTBF, while system reliability increased 25.5 percent in MTBF. Also, transmission direct operating cost decreased above 33 percent. The three stage, single planetary split torque design offers substantial improvement over conventional 5000 horsepower design practice.

The mission performance improvements and cost savings resulting from the ART transmission design achievements described above are substantial. Installing the 5000 HP ART transmission in a 16,000-lb FAAV, rather than a 5000 HP state-of-the-art baseline transmission, would result in a 17 to 22 percent improvement in loss-exchange ratio during combat, a 12 percent improvement in the ability to sustain a given level of combat operations and a 22 percent improvement in MTBF. Use of the ART would also result in a transmission acquisition cost savings of 23 percent or $165K, per unit. An average transmission direct operating cost savings of 33 percent, or $24 per flight hour, would also be realized.

Tooth scoring tests, single tooth bending tests, Charpy impact energy tests and compact tension fracture toughness tests were performed with five high temperature gear materials. Also, compact tension fracture toughness tests and tensile strength tests were performed with three advanced housing materials. Recommendations for additional detail design, analysis, fabrication, and testing are made for follow-on work to the ART Program Phase I work described in this report.

II. INTRODUCTION

The U.S. Army, in cooperation with the National Aeronautics and Space Administration, initiated the Advanced Rotorcraft Transmission (ART) Program to develop and demonstrate improvements in state-of-the-art (SOA) rotorcraft transmissions. The main focus of the ART Program is to develop key emerging material, component, subsystem and manufacturing technologies along the same pathways traditionally followed in new engine development. Engines typically are tested and perfected over a period of years, long before transmission design and development begins for aircraft application.

The McDonnell Douglas Helicopter Company (MDHC) and teammate, Lucas Western, Inc. (LWI), ART is sized for the Future Attack Air Vehicle (FAAV) of the early 21st century. The FAAV is visualized as a rotorcraft having extremely enhanced maneuverability at nap-of-the-earth altitudes along with improved performance in all flight regimes. FAAV requirements and vehicle concepts were evaluated early in the program to define a rotorcraft in the 10,000 to 20,000 pound gross weight range using an ART rated in the 5000 horsepower class. A 5000 horsepower version of the AH-64A Apache helicopter was used as the FAAV baseline aircraft, and an Apache main transmission parametrically upscaled to 5000 HP served as the baseline SOA transmission for comparison with the ART.

II.A ART PHASE I TRANSMISSION PRELIMINARY DESIGN AND COMPONENT DEVELOPMENT TASK DESCRIPTIONS

Task 1 - Selection of Evaluation Procedures and Assumptions

Select the procedures and ground rule assumptions for conducting tradeoff studies for the design of an advanced technology transmission for an FAAV. These procedures and ground rules shall be used in conducting Task 2 and Task 3.

Task 2 - Transmission Configuration and Operation Evaluation

Prepare the preliminary designs for and evaluate advanced technology transmissions applicable to the FAAV. The goals are to reduce transmission weight by 25 percent, reduce source noise in the transmission by 10dB, and increase the MTBR to 5,000 hours.

Recommend a transmission configuration and present the study results to the U.S. Army Propulsion Directorate Project Manager for approval.

Task 3 - System Performance Evaluation

Conduct a mission analysis to determine the effects on performance of the selected FAAV.

Task 4 - Detail Design and Analysis of ART Components for Test

Based on the transmission configuration approved in Task 2, proceed with the detailed design and analysis of all components and subsystems. The design layout and analysis shall be used to determine estimated system weight (including lubrication and cooling requirements), probable noise levels, theoretical component life, and assembly integrity under loading and operating conditions expected in the transmission.

Identify the crucial components and subsystems for test.

Task 5 - Development of Component and Subsystem Test Plan

Develop a detailed component test plan based on the results of Task 4. The test plan shall provide rationale for the types of tests to be conducted and data to be acquired from the tests. Submit the test plan to the U.S. Army PM for approval.

Task 6 - Preparation of Component Test Rig

Provide or make arrangements for component test rigs.

Task 7 - Fabrication of Component Test Articles

Fabricate the number of test articles of components or subsystems identified in Task 4 for verification testing to complete the plan developed in Task 5.

Task 8 - Performance of Component Verification Test and Individual Assessment

Perform the component tests called for in the approved test plan submitted under Task 5.

Task 9 - Report Requirements

Submit a written Final Report covering all the effort conducted.

Art Program Phase I was started in 1988 and is now complete. It was structured for performance of transmission preliminary design and component development. ART Program Phase II is scheduled as a demonstrator phase, during which an ART transmission or individual subsystems will be detail designed, fabricated and tested. The main purpose of the Phase I design and analysis efforts has been to attain the U.S. Army/NASA goals for the transmission weight, noise and reliability. Specifically, the Army/NASA goals were to design an ART that, relative to the SOA baseline transmission, achieved at least a 25% weight reduction, a 10 dB reduction in source noise and a mean-time-between-removal (MTBR) life of 5000 hours. Testing performed to substantiate the transmission component and subsystem concepts developed and materials utilized indicated the progress attained in meeting the goals and validating new design concepts.

This report covers the work performed by MDHC and teammate/subcontractor LWI under Phase 1 of the Advanced Rotorcraft Transmission (ART) Program. The efforts concentrated on high gain and comparatively high risk developments that were evaluated systematically to solve problems prior to full scale development. Advanced and innovative technology has been identified in the MDHC/LWI candidate for further development and testing as part of the ART program.

Section III, Preliminary Design, covers Tasks 1 and 2. To satisfy Task 1, Selection of Evaluation Procedures and Assumptions, a letter was written to specify the procedures and ground rules to be used in carrying out the design processes. We identified the FAAV as an upscaled AH-64A Apache, having two engines driving a main rotor, anti-torque fan and accessories through a main transmission. The input shaft speed from each engine is 20,952 rpm, and the main rotor speed is 289 rpm. The dual engine rated power for the transmission baseline is 5000 horsepower, and the maximum continuous single-engine power is 2500 horsepower. The one-engine-inoperative (OEI) power requirement for emergency single engine flight is 3000 horsepower. All gears of the preliminary design candidates were to be designed to carry the OEI horsepower for thirty minutes or more. In addition, all gears and bearings were to be designed without exceeding American Gear Manufacturers Association (AGMA) and Anti-Friction Bearing Manufacturers Association (AFBMA) stress allowables while achieving at least the minimum component lives required to attain a 5000 hour system MTBR.

In performing Task 2, Transmission Configuration and Operation Evaluation, candidate transmission configurations were defined to meet the design requirements of the FAAV and the allowables selected in Task I. Load and speed carrying capabilities, preliminary bearing and gear lives, and preliminary weight and noise design considerations were analyzed and sketches of the transmission concepts under consideration were produced. Weight, reliability and noise analysis methods were then applied to the designs to evaluate these key operational parameters. Results of the analysis work are presented in this report. A final downselection was made between the two most promising configurations using a matrix evaluation process. This evaluation procedure rated the candidate configurations in terms of apparent progress made in meeting Army/NASA goals in addition to secondary factors such as direct operating cost and risk assessment. The goal factors were given a weighted priority of importance of 0.5, 0.3 and 0.2 respectively for the evaluation. Direct operating cost and risk assessment factors were evaluated for use in the event of a near-tie between the configurations scored.

The ART transmission chosen through the above downselection process was a novel three stage, single planetary, split torque concept using face gears. A spur gear pinion located on each input drive shaft drives two face gears simultaneously, providing a split of the torque at the first stage. The face gears rotate in the same direction, and the torque is recombined on a large bull gear above through two second stage spur pinions. The bull gear drives a high contact ratio planetary, which in turn drives the main rotor. Key subsystems of the transmission include two positive engagement input clutches and an advanced lubrication system.

Section IV, ART Transmission Design, covers Task 4, Detail Design and Analysis of ART Components for Test. The three stage split torque configuration selected in Task 2 was further developed and refined during Task 4. The design effort focused on attaining the U.S. Army/NASA weight, noise and reliability goals described previously.

The three stage split torque configuration, first sized in Task 2, provided a low weight starting point for Task 4. During Task 4, weight reduction was enhanced when the combination of gear reduction ratios used for the three stages of the split torque transmission was optimized to achieve a minimum weight for the configuration. This minimum weight assessment was based on iterative computer runs performed with a parametric weights

analysis program which considered the gear and bearing arrangements as well as component materials and geometries. As in the design processes for earlier downselection, AGMA and AFBMA stress analyses and life calculations were performed in assuring an ART with a system life of 5000 hours MTBR and OEI operational capability. Additional weight reduction was achieved during the detail design of individual transmission components.

Stress analyses performed on the transmission included modeling the gear webs, rims, and shafts of the three individual stages to analyze deflections. Deflections of the two first stage face gears were equalized and minimized through a design-interactive process. Equalized stiffness, in addition to first and second stage tooth phasing and a flexible input pinion support, assured near-equal torque splitting to the gears. Planetary carrier deflections were analyzed during the design process to achieve good strength-to-weight design. Deflections of the cantilevered planetary ring gear were also determined to assure controlled radial motion of the six pinions and to provide suitable fatigue life.

As the ART design neared completion, a NASTRAN finite element model of the transmission was produced to obtain output vibration levels of the transmission during operation. This information was then used for the acoustic calculations, which were accomplished by two distinctly different procedures. A deterministic approach, based on the boundary element method, was used for determining the case-radiated noise at the lowest gear mesh frequencies. Given the demand for large amounts of computer memory for the boundary element method, it was found practical to supplement this method with a stochastic approach, based on statistical energy analysis (SEA), for evaluation of the higher frequencies. SEA could not be used exclusively because of its limited precision at the lower frequencies where the boundary element method performed best. The overall noise prediction methodology, which incorporates a combination of both approaches, was implemented to evaluate the noise emissions of a transmission currently used in the AH-64 Apache helicopter. Vibration and noise levels from the Apache transmission models were correlated with actual test data. This test-correlated methodology was then used in developing and analyzing ART. The methodology is intended to allow for "design-to-noise" capability.

Noise reduction methods employed during the design process included minimizing gear web, rim and shaft deflections. Also, a high contact ratio (HCR) third stage planetary having properly phased gear tooth numbers, profile modification and a cantilevered ring gear was implemented. The ART split torque configuration, with divided power paths, provides additional noise reduction. The transmission housing structural shape, webs and stiffeners were also designed to minimize vibratory deflections.

The MDHC ART split torque configuration, design features and analysis methodologies are described in this report. The completed transmission design was found to offer substantial progress towards the Army/NASA weight, noise and reliability goals, and can provide increased capabilities in a fielded aircraft.

Section V, Mission Effectiveness, covers Task 3, System Performance Evaluation. This section is segmented into three subsections:

- Mission Analysis
- Reliability
- Life-Cycle Costs

Mission Analysis is an assessment of lethality and survivability of the aircraft. As part of the ART program, an evaluation of how the improved transmission impacted mission effectiveness was studied. Although the changes being considered affected all areas of mission performance, past experience indicated that the most

demanding area would be a close-in, air-to-air engagement. Accordingly, the air-to-air engagement was the focus of this analysis. The FAAV with ART produced a 17 to 22 percent increase in the loss-exchange ratio compared to the baseline FAAV.

FAAV Reliability will be much improved over current generation aircraft. The amount of improvement is estimated by trending previous and current design reliabilities. Assuming the FAAV is a next-generation design, the trend is to double reliability requirements every generation. This results in an FAAV system reliability of 18 hours with mission reliability increasing from 22 to 75 hours.

Life Cycle Costs (LCC) estimates were made for three configurations: baseline FAAV, ART improved FAAV, and optimized FAAV with ART. This report contains the estimates and a discussion of the techniques and assumptions used to make those estimates. The LCC estimate is reflective of the technological advances (composites and integrated mission equipment) and operating conditions inherent in designing and fielding an aircraft in the next century. The estimated life cycle costs show significant savings for the FAAV with ART, compared to the baseline FAAV.

Several key performance parameters of the FAAV were evaluated to determine the benefits that would be derived from the performance characteristics of the selected ART configuration. These analyses focus on the system, not just the transmission, and consider the synergism of the transmission performance on the FAAV as a total system.

Section VI, Material Characterization Tests, covers Task 5, Development of Component and Subsystem Test Plan, Task 6, Preparation of Component Test Rig, Task 7, Fabrication of Component Test Articles, and Task 8, Performance of Component Verification Test and Individual Assessment. Material testing was performed as tabulated below, with the stated results.

II.B TOOTH SCORING TESTS, SINGLE TOOTH BENDING FATIGUE TESTS, AND CHARPY IMPACT ENERGY TESTS - GEAR MATERIALS

These tests were performed on specimens fabricated from five different steels as tabulated.

		Number of Tests		
Material	Spec.	Tooth Scoring	Tooth Bending	Charpy
M50 MIL	6278	70	20	12
X53 Pyro.	6308	72	20	12
CBS 600	6255	6	12	12
AISI 9310	6265	96	24	12
300M	6514	6	12	12

II.C FRACTURE TOUGHNESS TESTS - GEAR AND HOUSING MATERIALS

These tests were performed on specimens fabricated from two magnesium alloys, one aluminum alloy, and two steel alloys, as tabulated.

Material	Spec.	Heat Treatment	No. of Tests
WE43	4427	Solution Heat Treat	7
ZE41A	4439A	Solution Heat Treat	7
C355T7	4215	Solution Heat Treat	6
M50 MIL	6278	Pseudocarburized/Hardened	6
X53 Pyro.	6308	Pseudocarburized/Hardened	7

II.D TENSILE TESTS - HOUSING MATERIALS

These tests were performed on specimens fabricated from two magnesium alloys and one aluminum alloy, as tabulated.

Material	Spec.	Heat Treatment	No. of Tests
WE43	4427	Solution Heat Treat	24
ZE41A	4439A	Solution Heat Treat	24
C355T7	4215	Solution Heat Treat	24

The relative rankings of the tested gear materials and housing materials, based on the test results, are shown in Tables 1 and 2.

TABLE 1. GEAR MATERIALS - RELATIVE RANKINGS

Material	Single Tooth Bending	Scoring	Fracture Toughness	Charpy Impact
X53	1	3	1	2
M50Nil	3	1	2	5
CBS600	2	2		3
M300	4	4		4
AISI 9310	5	5		1

TABLE 2. HOUSING MATERIALS - RELATIVE RANKINGS

Material	Tensile Strength	Fracture Toughness
C355T7	1	1
WE43	2	2
ZE41A	3	3

Section VII, Recommended Redesign and Retest, covers future activities recommended for the ART Program in Phase II. During performance of ART Phase I, areas of the design and analysis investigations with great potential presented themselves. In addition to the ART prototype design and tests, other areas might be profitably investigated, such as two stage ART design and tests, positive engagement clutch tests, an expanded face gear capacity test program with variations in material and manufacturing methods (including ground face gears), acoustic modeling, and advanced materials investigation and implementation. Tested materials which showed the highest performance during Phase I tests are recommended for high temperature tests and subsystem integration tests.

III. PRELIMINARY DESIGN

III.A INTRODUCTION

The ART transmission selection and related methodology is presented herein. Design baselines and allowables were established in Task 1 for use in the preliminary design of candidate transmission configurations. Load and speed carrying capabilities, preliminary bearing and gear lives, and preliminary weight and noise design considerations were analyzed for the two most promising configurations selected for Task 2. Two sketches were produced, and weight, reliability and noise analysis methods were then applied to the designs to evaluate these key operational parameters set forth within the original MDHC ART proposal. Results of the analysis work are presented in this report. Weighting factors and comparative analyses were applied to the results to yield a unique ART design that promises to substantially advance the state of the rotorcraft transmission art.

III.B ART TEAM DRIVE SYSTEMS ENGINEERING METHODOLOGY

The transmission preliminary design analysis methodology used to develop the two candidate ART transmission configurations began with establishing basic transmission requirements. Materials assumed for both the gears and bearings used in this preliminary design phase were basic 9310 gear steel and 52100 bearing steel. The necessary power capacity, input and output speeds, loading and life allowables, and design envelope criteria were determined. Table 3 lists the baselines and allowables used in preliminary design of the candidate configurations. The next step in the design process was to select types of gearing, determine gear ratios, and size the gears as a system to optimize weight and meet life requirements. The gear train designs conformed to the established bending stress, hertz stress, pitch line velocity and flash temperature allowables of 9310 gear steel.

Once gearing types and sizes were established, bearings were selected as per required type and basic C/P load carrying capacity, based on allowables of 52100 bearing steel.

Computer programs were used to facilitate stress calculations for each gear type, geometry, and ratio combination analyzed in preliminary design iterations. Existing programs used were the Gleason dimension sheet program, the modified NASA CHOPR program, and AGMA-based spur and helical gear analysis programs. The modified CHOPR program was used to calculate hertz stresses needed on each gear mesh to achieve a minimum overall 5000 hour MTBR for the gear trains of each candidate ART configuration.

Concurrent with the analyses described above, preliminary design sketches of the two candidate ART transmission configurations were developed. Descriptions of the two configurations follow.

The first candidate transmission presented was the initial design version of a split-torque, 3-stage configuration. As shown in Figure 1, input shafting, from two engines which are parallel drives through clutches on both sides of the transmission. Each of the two first stage gear meshes involves a spur gear type pinion simultaneously driving two face gears, one above and one below the pinion. This results in an even split of the input torque between the two face gears. Spur gears are located above and on the same shaft as the face gears. These four spur gears, two on either side, simultaneously drive a large combining (bull) gear. Splined at the hub of the bull gear is a planetary sun gear. The sun gear drives eight planet gears which rotate within a large internal ring gear. All planetary gearing is of the spur gear type. The planets are positioned by, and drive a carrier, which is splined to the main rotor drive shaft.

TABLE 3. PRELIMINARY DESIGN BASELINES AND ALLOWABLES

DESIGN BASELINES	
Engine Input Speed	20,950 RPM at engine output shaft
Main Rotor RPM	289 RPM
Horsepower to Main Rotor	5000 HP
Overrunning clutches at transmission inputs from engine. Engines parallel or at 40-degree maximum included angle.	

DESIGN ALLOWABLES		
Gears	**Hertz Stress Allowables**	**Bending Stress Allowables**
Spiral Bevel Gears	220 ksi [1]	40 ksi [2]
Spur and Helical Gears	190 ksi [3]	60 ksi [3]
Pitch line velocity allowable = 22,500 ft/minute (for Rc 62 9310 steel, all gearing). Flash temperature less than 400°F [4].		
Bearings: B10 lives all exceeded 10,000 hours for ART Preliminary Design. C/P ratings per allowables for 52100 steel bearings [5,6].		

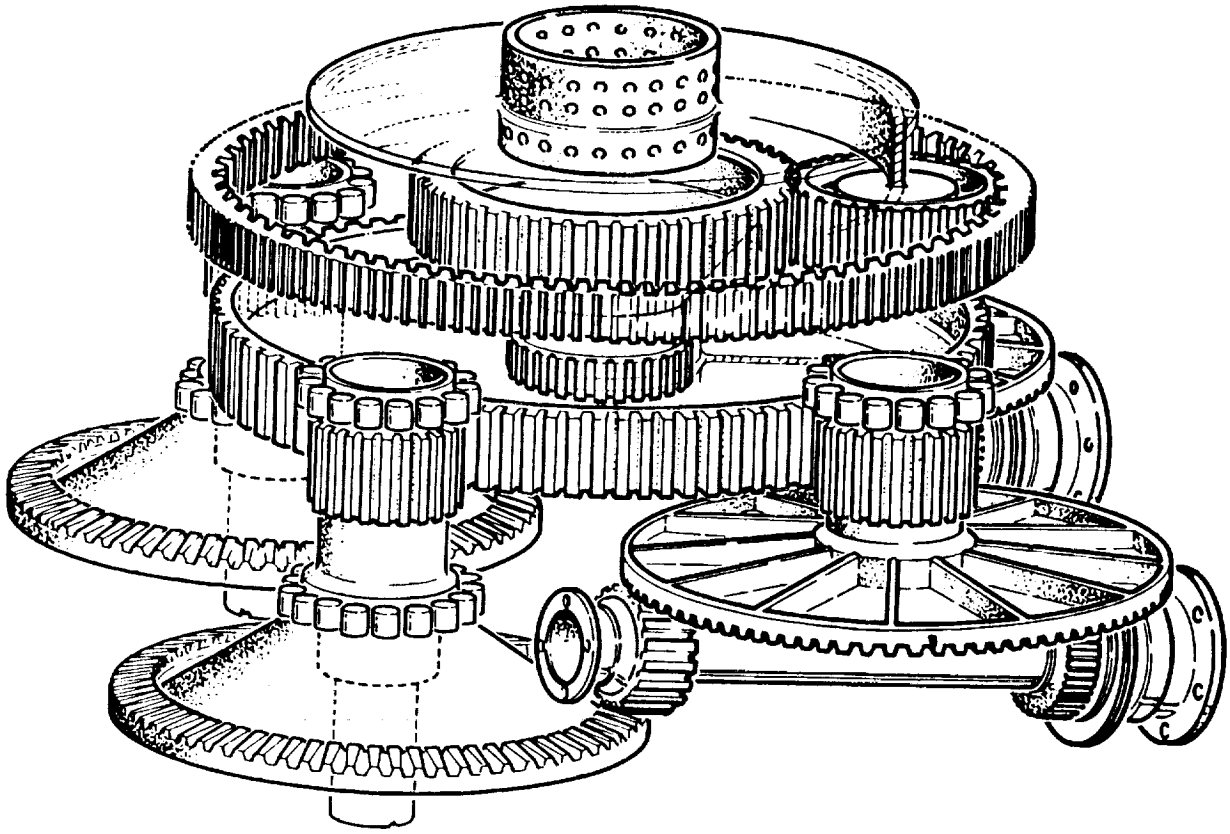

Figure 1. Three-Stage Split Torque Transmission Preliminary Design

The second preliminary design candidate ART transmission was a 4-stage, single planetary configuration. This transmission, shown in Figure 2, runs the two engine inputs through two spiral bevel nose gearboxes. This first speed reduction ratio is about 2.22 to 1. The output shafting of each nose gearbox feeds into the main transmission through a clutch and inputs to a second spiral bevel gearset. Here a reduction of 2.45 to 1 occurs. Driven on the output shaft of this spiral bevel gear set is a herringbone gear. These double helical gears, one on either side, simultaneously drive a large herringbone combining (bull) gear, and this gear ratio is 3.46 to 1. Located above the bull gear and splined to the same shaft is a planetary sun gear. This gear drives six planet gears which rotate within a large internal ring gear. This final planetary ratio is 3.86 to 1. The planet gears are retained on a carrier which is splined to the main rotor driveshaft. The carrier is driven by rotation of the planets about the sun gear.

III.C WEIGHT DESIGN INFORMATION

The baseline helicopter is the Army AH-64 Apache upgraded to FAAV requirements. The industry weight trend for a 5000 HP helicopter main transmission with an Apache main rotor speed of 289 RPM is 1792 lb (installation weight, includes main rotor driveshaft, static mast, and lubrication system) while the weight goal of the ART, with a 25 percent weight reduction is 1344 lb. The corresponding weights for the transmission assembly only are 1347 lb for the industry weight trend and 1010 lb for the ART goal with a 25-percent weight reduction.

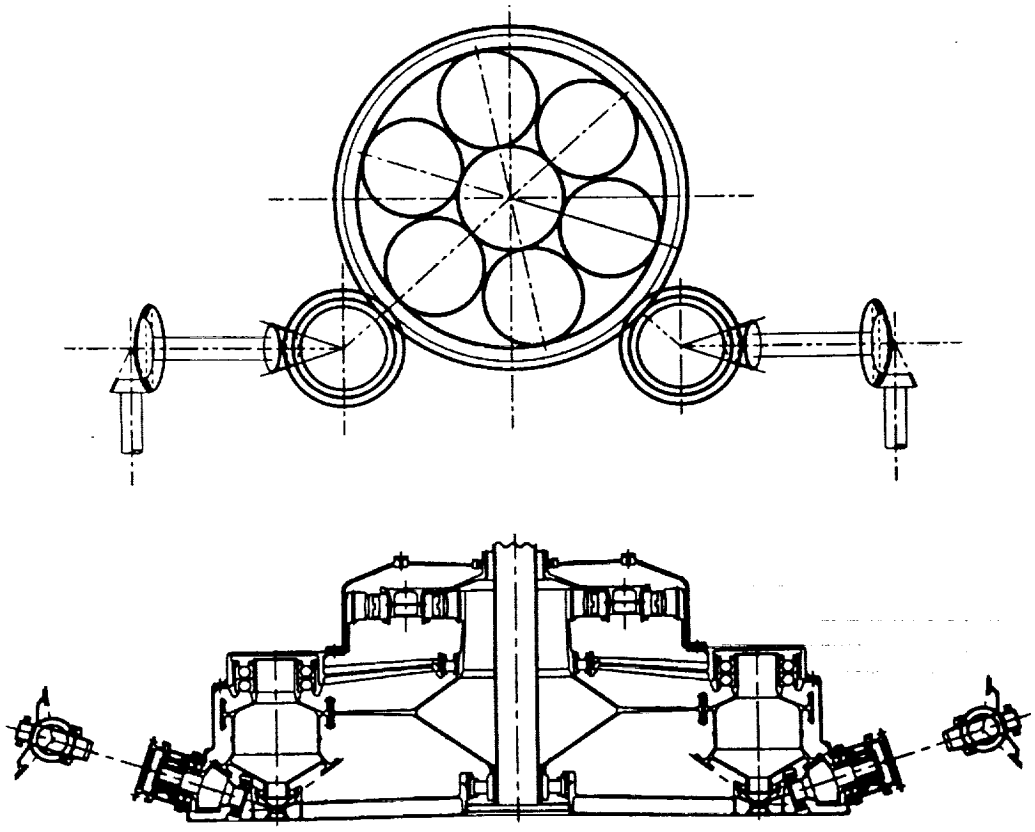

Figure 2. Four-Stage Single-Planetary ART Candidate Configuration

III.C.1 Weight Prediction Methodology

Weights of the Task 2 split torque transmission and the four stage single planetary transmission were estimated by a parametric methodology described in Reference [7]. Using this method, the weight estimates for 39 gearboxes versus actual gearbox weights had a standard deviation of 9.3% with a correlation coefficient of .998. The methodology was calibrated to the current Apache main transmission weight, and the estimated weight was above, but within 6% of the actual weight.

The weight prediction methodology is based on the three main components of transmissions (gears, bearings, and housing), input and output drive train speeds and power capacities, and a sketch of the gear train. Predicted weights were calculated based upon the above gearbox data.

III.C.2 Transmission Weight Results

The weight predictions used in down selecting the ART design were considered to be sufficiently accurate for weight comparisons made during preliminary design. For the two candidate transmissions, the split torque transmission and the four stage, single planetary transmission, weights are directly comparable to each other. They do not include weights of the drive shaft(s), the static mast, and lubrication system. They use no weight saving material or technologies other than the split torque transmission with face gears. The predicted transmission assembly weights are as follows:

Split Torque Design	Four-Stage Single Planetary Design	Industry Trend	ART Goal
1048 lb	1757 lb	1347 lb	1010 lb

The four-stage single planetary transmission design weight is 30% higher than the industry trend line. This indicates there may be other transmission designs (i.e., three stage with component planetary, three stage with self-aligning bearingless planetary, four stage counter rotating, etc.) that are more weight effective than the four-stage, single planetary design. Task 2, however, evaluated only two designs. The weight advantage of the split torque design is evident and there is great potential for further weight savings from improved materials, technologies, and optimization techniques. Weights resulting from application of recent technologies and optimization techniques are shown in section IV of this report.

III.C.3 Weight Comparison Summary

The split torque transmission design is significantly lighter than the four-stage, single planetary transmission design because of two factors:

1. Elimination of two spiral bevel gear reduction stages.

2. Innovative split torque/face gear design.

The main risk area in the split torque transmission design is the development and application of face gear technology for gear box designs. The four-stage, single planetary transmission design is conservative and offers little or no risk. However, future weight savings in this design can only arise from optimized packaging, and material technology, and thus offers no advantage in these two areas over the split torque transmission.

III.D RELIABILITY EVALUATION

This section explains how the component reliability requirements were developed from the Advanced Rotorcraft Transmission's design goal of 5000 hour MTBR. The estimated preliminary design MTBR for the three stage split torque transmission was 5388 hours and for the four-stage single planetary transmission was 5323 hours.

Given an MTBR of 5000 hours as a design goal, the following was assumed:

- Applies to main rotor drive components only.
- An allowance of 0.00004 failures/hour for random and unknown failures.
- The MTBR is approximately the Mean Time To First Failure.
- The optimum transmission will have equal component L10 lives.
- Only failures due to contact stress need to be considered.
- All component failures are modeled as Weibull distributions.

Component	Weibull Shape Parameter
Gears	4.0
Bearings	2.5
Clutches	3.5

- Effective operating power is 2/3 of MCP.

A series model was used. An equation relating system life to component reliability in which the component failures are modeled as Weibull distributions was developed expanding principles developed in Reference [8] (Appendix B1). Component L_{10} lives were generated by setting the system median life equal to 5000. The resulting component lives then were used to numerically calculate the mean. The median was then adjusted to produce a MTTFF of 5000.

Component L_{10} lives were given as inputs to the designs. For gears, L_{10} lives were converted to contact stress allowables using AGMA standards. The actual contact stresses were used to calculate the estimated reliability of each design. Because the new configurations were designed to the allowable, the estimate is very close to the requirement.

The initial estimates are based on preliminary information. As more design detail becomes available, more accurate MTBR's will be calculated. Implementing the principles of concurrent engineering by monitoring MTBR throughout design will assure the transmission design meets all reliability objectives.

III.D.1 Reliability Introduction

To model the complex, real-world process that a helicopter transmission represents, several assumptions and simplifications were made to allow current theories and computer technologies to be applied. Currently only mean time to first failure (MTTFF) for components requiring removal is calculated. It is approximately equal to MTBR, and approaches MTBR as inspection accuracy increases.

During preliminary design, an allowance of 25,000 hours MTBR was made for random and unknown failures. This is a valid number that is based on extensive experience with transmissions [9,10,11].

Many assumptions were necessarily made because the transmission designs were preliminary, and incomplete. As the designs are developed, more information and complexity is added to the model to improve accuracy. During the ART program preliminary design, only the main rotor power path was compared, and it was limited to the gear, bearing and clutch components. To avoid possible arbitrary penalties from the rest of the system, other components were excluded from the MTBR calculation.

Balancing lives of components tends to optimize components with equal weight and noise factors. As design refinement progresses, trade-offs may be indicated, and,if so, they will be investigated.

Component failures are modeled as Weibull distributions, with the mode of failure modeled is surface fatigue resulting from contact stress. The design of the ART will eliminate the likelihood of other failure modes. The shape parameter for gears used is 4. This number is higher than 2, and represents improvements in gear manufacturing processes and materials. The shape parameter for clutches has not been determined, the number used is based on similar bearing and gear failure modes.

The ART candidate configuration design and analysis is based on a power usage spectrum value of 66.67%, based on Apache design and usage. This number is conservative because the FAAV will have a higher power/weight ratio than any existing rotorcraft.

III.D.2 Reliability Evaluation Procedure and Results

The equation used to calculate required component L10 lives is developed in Appendix B1. The initial inputs are counts of components.

Component	Four-Stage Single Planetary Design	Split Torque Design
Gears	19	21
Bearings	28	30
Clutches	2	2

The three stage split torque design required a component L_{10} life of 10,100 hours for each of its 53 components. The four stage single planetary design with 49 components required L_{10} lives of 9900 hours. Gear contact stress allowables were then calculated from AGMA standards (Reference [12]). The designs were limited to contact stresses below the allowable at operating power (3333 HP). The designer calculated contact stress. Bearing and clutch lives were not available at this time and were set to required life for 5000 hours. These numbers were then fed back into the system model to calculate system MTBR.

Transmission	Required	Four-Stage Single Planetary Design	Split Torque Design
MTBF	5000	5323	5388

These results are sensitive to slight changes in the design.

III.D.3 Reliability Evaluation Discussions and Conclusions

Because components with high speed and/or multiple contacts per revolution accumulate cycles fastest, they were most often affected by the adjusted allowables. The allowable contact stresses are based on commonly used materials. The ART will most likely incorporate advanced materials with higher allowables. Processes and tolerance improvements will also increase the MTBR. This increase will be offset to some degree when other components are included in the MTBR calculation. Designs will minimize other components' negative effect on MTBR by not requiring transmission removal for repair.

The calculated MTBR's should not be considered an accurate prediction of the design's reliability, because of the designer's ability to adjust weak spots and dramatically improve system life. The process serves to focus design on even component lives and potential areas for weight reduction. Reliability analysis concurrent with the design process will enhance the transmission's reliability and lengthen it's life.

III.E NOISE PREDICTION

Transmission noise varies from being a mild annoyance to causing physical discomfort. In the case of large, high power, high speed helicopter transmissions, noise considerations may be compromised by the need for high reliability, light weight and compact packaging. Transmission noise presents an especially difficult problem because of three factors - high sound pressure levels, frequencies in the range most sensitive to the ear, and pure tonal content. The significance of these factors varies somewhat with the size and speed of the gearbox in question, but the general treatment of each is the same.

III.E.1 Estimation of Transmission Noise Levels

Current transmission noise level estimation procedures may be either very complex or very simple. The complex procedures require details of the dynamic system, the casings and mounting systems which are not defined as part of the preliminary design, and will not be available until a detail design of the main transmission is complete. Therefore, a very simple method utilizing empirical information was used for the estimation of each gearbox noise level in the preliminary design downselect.

The empirical procedure used here to predict installed transmission noise level is derived from a data base which includes single main rotor helicopters (both reciprocating and turbine powered) in the 6000 to 50,000 pound gross weight and 400 to 10,000 HP range. In every case, noise levels were measured at multiple locations inside cabins that were aluminum monocoque structure. The spectrum of each measurement was analyzed and each of the gear mesh noise peaks identified by frequency. The average sound power level was determined for each of the mesh frequencies using standard room acoustics techniques, and included a wide variety of gear types, such as planetary (either phased or unphased), spur and bevel. These data for many helicopter types were consolidated to establish trends for each gear mesh type defined by curve fitting. This forms the basis of the prediction method used here.

Contact ratio and pitchline velocity (in addition to gear type and power transmitted) are important factors which influence the amount of sound power radiated from a mesh point. Noise generation analytical techniques, as a function of these parameters, can also be used to estimate average sound power level in the helicopter cabin. They can be applied in addition to the basic empirical method, to arrive at the final estimate of average sound power level at each mesh frequency generated by the transmission.

Once the sound power level has been determined for each gear mesh frequency, the levels of the various bands making up the speech interference level (SIL) can be determined and the SIL computed. However, some judgement must be used to define levels for bands which do not contain a gear mesh. Here the SIL is defined as the arithmetic average of the noise levels in the octave bands at 500, 1000, 2000, and 4000 hertz.

III.E.2 Noise Prediction Results

The empirical method was applied to both the four-stage, single planetary and three-stage split torque configurations, and it was estimated that the conventional planetary design is 5.7 dB quieter for gear mesh frequencies that fall in the audible range.

III.F SUMMARY OF RESULTS

A tabulation of the results determined through the weight, noise and reliability methodologies above is given in Table 4. The numerical column to the left of the table lists the ART goal weight of 1010 lb and the goal MTBR of 5000 hours. As established in the original MDHC ART proposal, the weighting factors for weight, noise and MTBR are 0.5, 0.3, and 0.2, respectively. These factors were multiplied by relative scores for the two configurations for each weight, noise, and MTBR. The relative scores were evaluated against a 5 value which represented the ART goals. Therefore, values of 6 to 10 represent relative improvements over the goal score,while values of 1 to 4 are below the goal. The product of weighting factor times relative score represents the weighted value for each of weight, noise and MTBR. The weighted values are totaled for each configuration. Since these totals of 2.1 for the four stage configuration and 3.8 for the split torque configuration had a 1.7 point spread, neither risk factors nor direct operating cost determinants were applied. The three stage split torque configuration was selected for further design and analysis.

TABLE 4. CANDIDATE ART CONFIGURATION RATING TABLE

		Configuration	
	ART Goal	**Four Stage**	**Split Torque**
Actual Weight (lb)	1010	1757	1048
Weight Score	(5)	0	4
Weighting Factors	0.5	-	-
Weighted Weight	-	0	2.0
Actual Noise (dB)	TBD	100.15	105.85
Noise Score*	(5)	3	2
Weighting Factor	0.3	-	-
Weighted Noise	-	0.9	0.6
Actual MTBR (hours)	5000	5323	5388
MTBR Score	(5)	6	6
Weighting Factor	0.2	-	-
Weighted MTBR	-	1.2	1.2
Summation	-	2.1	3.8
Risk Factor**	-	-	-
Score	-	2.1	3.8
Intermediate Ranking	-	2	1
DOC $/HR**	-	-	-
Final Ranking	-	-	Choice

*Noise score was based on the noise difference (dB) between the configurations.
**Not used due to large score difference between configurations.

III.G CONCLUSIONS

The three-stage split torque configuration featuring face gearing was the most promising ART transmission investigated in the preliminary design effort. As shown by the weight savings over the four stage configuration and early progress towards the ART goal, this is a viable concept in the 5000 horsepower and above range. Though noise was not a major driver in the down-selection ratings, the detail design phase will implement applicable current noise reduction technologies to yield the quietest gearbox. One major area of investigation for noise reduction will be to implement high contact ratio gearing in the transmission. This, combined with gear phasing in the planetary section of the transmission, offers particular promise for noise reduction. The face gearing in the first reduction stage is recognized as unconventional, but it has great potential and will be analyzed in further detail. The small space requirements and high load and speed capabilities of this type of gearing supports its further study. In addition, MTBR will be monitored throughout the detail transmission design. The modified CHOPR program will be further expanded to allow analysis of more complex design of this and future transmissions. The prospects are bright for further development of the selected three stage split torque ART transmission.

Section IV summarizes additional design and analysis work performed for this concept.

IV. ART TRANSMISSION DESIGN AND ANALYSIS

IV.A TRANSMISSION CONFIGURATION

This section summarizes the design of the MDHC/LWI 5,000 HP ART transmission. Included are descriptions of the transmission engine and main rotor drive interfaces, input clutches, transmission configuration, individual stages, housing design, and lubrication system. Stress and deflection analyses for the transmission are also provided in the latter part of this section.

The ART transmission, shown in Figure 3, is a split torque configuration having three reduction stages. The gearbox is designed to provide an overall reduction ratio of 71.844:1 from the engine inputs to the main rotor drive shaft, and a reduction ratio of 5.170:1 from the input to the NOTAR/accessory output. The input quills from the two engines are laterally separated approximately 12.5 inches to either side of the main rotor drive shaft centerline and tilted down five degrees with respect to the aircraft waterline. The main rotor drive shaft and ART transmission are also tilted five degrees forward relative to vertical.

On each side of the transmission, engine power enters an input quill shaft through a 15-5 PH bolted flanged stainless steel adapter, which is integral with an overrunning positive engagement clutch. The positive engagement clutch is shown in the exploded view in Figure 4 in the engaged or driving position. The clutch has the advantage of driving by engaged spline teeth, not by friction as found with sprag, ramp roller or wrap spring clutches. This type of clutch is more reliable and is always lighter than the friction types. The weight advantages increase with torque, so in the ART application there is not a significant weight advantage in the clutch hardware but there is a weight savings of about 12 lb in the lubrication system. This is because the high speed friction clutches require about three gallons of oil per minute to cool the sprags and inner race when they are overrunning. This heat generation is not present in the ART clutch since it is not a friction type clutch.

The essential elements of the clutch are those of the famous Synchro Self Shifting clutch in which a ratchet and pawl system guides spline engagement until a torque reversal causes disengagement. The "triple S clutch" is in worldwide use and transmits millions of horsepower daily.

The input adapter has an internal helical spline that mates with an external helical spline on the synchronizer. The synchronizer carries two pawls that engage a ratchet mounted on the output member. If the output member is stationary, the synchronizer must translate (move toward the output member) when the input rotates. This translation moves the curvic coupling half on the synchronizer into engagement with the curvic coupling half on the output member. The pawl and ratchet orientation is synchronized with the curvic coupling engaged position so there is not possibility of curvic disengagement.

The sloping sides of the curvic coupling are also used to advantage. The engaging motion is designed to rotate the ratchet with respect to the pawl, so that the toe of the pawl is withdrawn slightly from contact with the ratchet. Thus, the pawls cannot transmit more torque than is required to move the synchronizer.

If the engine stops, the torque flow is from the output member to the synchronizer. Because the input member is stationary, the sloping sides of the curvic coupling and the helical spline reaction cause the synchronizer to move out of engagement with the output member. At this point, the only contacts with the output member are the pawls mounted on the synchronizer, which are hydroplaning on the cylindrical surface of the ratchet portion of the output member. This hydrodynamic bearing behavior has infinite life and very high efficiency.

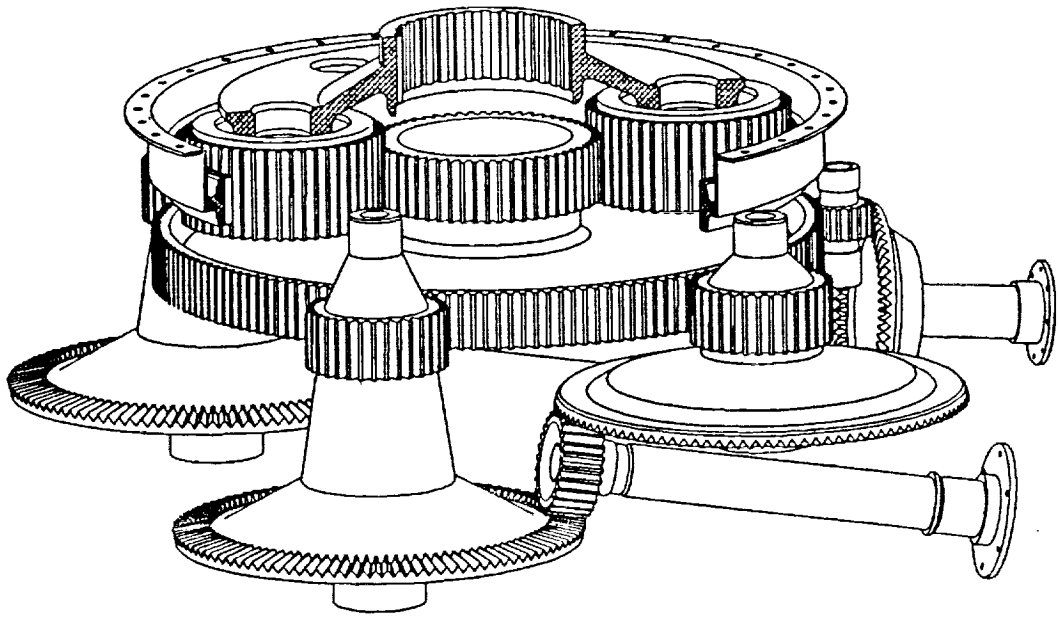

Figure 3. ART Transmission Configuration

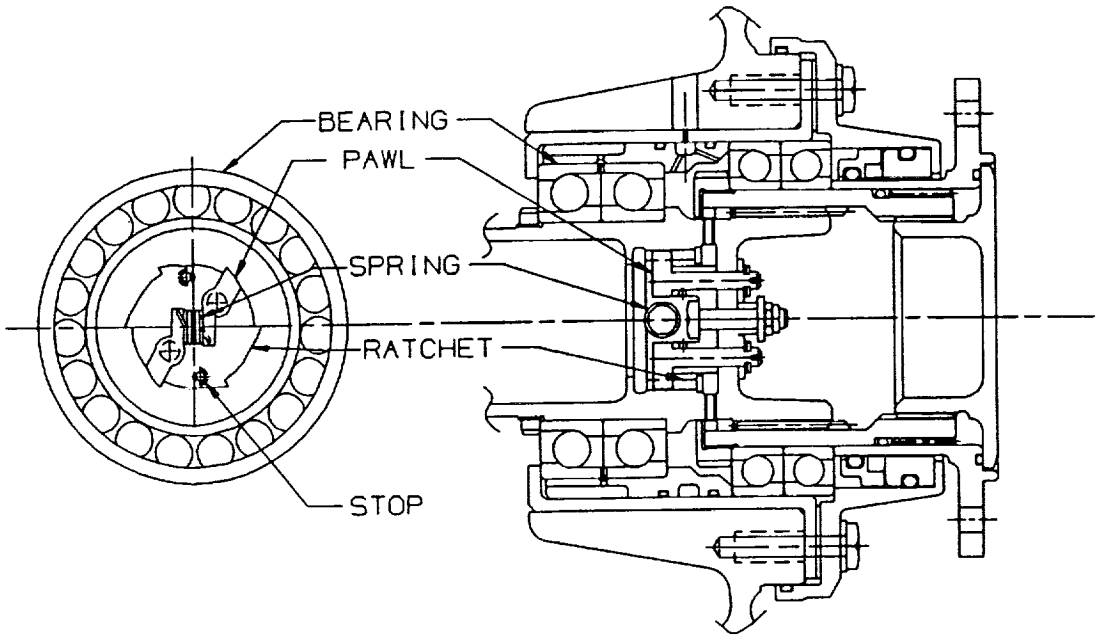

Figure 4. ART Positive Engagement Clutch

When an engine is started and brought up to synchronous speed with a rotating output shaft, the pawl-ratchet combination is a true spring mass system which is excited by the passage frequency of the ratchet gaps. A relatively weak spring is required to keep the hydroplaning load small. As the engine is brought up to speed, the speed differential decreases between the ratchet and the spring-loaded pawl. The pawls initially hydroplane, go through resonance, then dip toward each passing gap, synchronize and drive the curvic coupling halves together.

Appendix A provides calculations for curvic coupling stress, helical spline stress, resonant frequencies, pawl balance, hydroplaning, spring stress, and engagement system analysis.

Power from each engine is then transmitted at 20,952 RPM from the clutch to the input spur gear pinion. The pinion splits the torque to two face gears and provides the first stage reduction of 3.821:1. The speed of the face gears is reduced to 5,483 RPM. The spur gear pinion is supported by a roller bearing housed in a flexible support which is as compliant as possible for gear load sharing yet stiff enough to ensure that the frequency of the first vibrational mode is higher than the rotating speed of the pinion shaft to avoid resonance. The load sharing split has been calculated to be within two percent. The torque sharing analysis considers the deflections of the gears, bearings, and housing as well as the backlash difference between both face gears due to manufacturing tolerance and indexing.

Gear tooth stress calculations for the preliminary design were based on established techniques for spur gears. The gears are analyzed using an MDHC computer program which uses standard AGMA analysis techniques for determining bending and pitting stresses. The gear and bearing stress analyses are presented in the last part of this section. The parts list and drawing views shown previously provide design reference to the gears and bearings analyzed. Figure 5 is a schematic with alphanumeric identification of the ART gears and shafts. Tables 5 and 6 show the ART gear and shaft operating parameters for these upon which load and life calculations for all dynamic components were based.

Figure 6 gives a plan view of the ART transmission with several major cross sections shown. Figure 7 shows Section B-B taken through the input shaft of the transmission. Table 7 gives the parts list for the transmission assembly, with part find numbers cross-referenced in the section views. Shown in Figure 7, the face gears for the first reduction have significant advantages over spiral bevel gears. The largest advantage is the ability to split the power using one pinion with an 80-degree shaft angle to two parallel shafts rotating in the same direction. This reduces the total number of gears and bearings in the transmission. The input pinion is a conventional involute spur gear. It can be developed, manufactured, inspected and installed for much less cost and weight than a spiral bevel pinion. It can move axially within the limits of its face width with no effect on the mesh. It can move toward or away from the face gear with the same tolerance as a center distance change with spur gears. There is no axial force on the pinion and the mesh has true conjugate action. The face gear tooth contact patterns are analyzed and the teeth are crowned by the manufacturing process so slight misalignments are tolerated. Further, analysis indicates face gear tooth misalignment does not cause as much transmission error (nonconjugate action) as it does with spiral bevel gears and therefore operation is quieter. Face gear measured efficiency appears as good as spiral bevel efficiency. Face gears in general exhibit high contact ratios at high reduction ratios. A contact ratio over two is predicted for this reduction mesh.

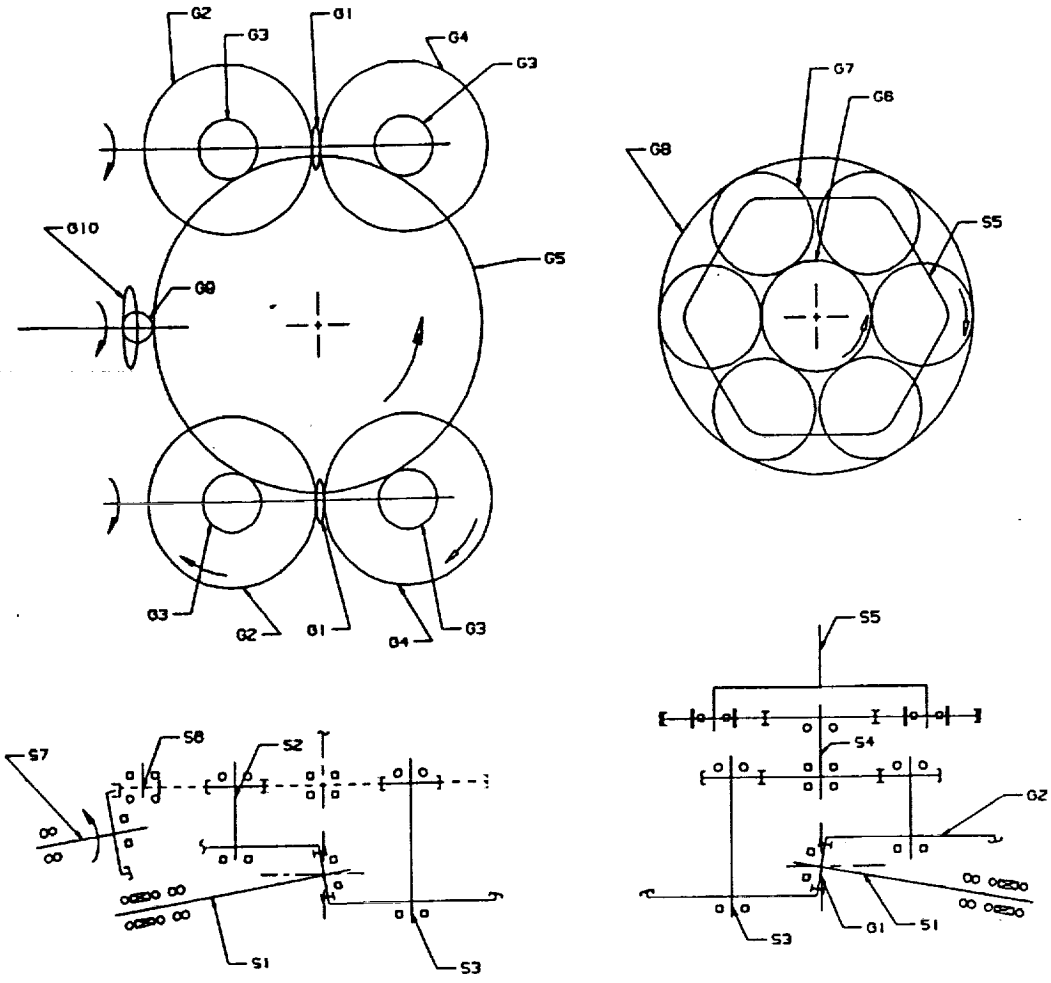

Figure 5. ART Gear and Shaft Schematic

TABLE 5. SHAFT SPEED/LOAD TABLE

Shaft	RPM	HP	Torque (in.-lb)
S1	20,952.0	3000	9,024.2
S2	5,482.8	1500	17,242.7
S3	5,482.8	1500	17,242.7
S4	1,116.3	5000	282,306.4
S5	291.6	5000	1,080,552.0
S6	12,428.1	563	3,616.6
S7	4,052.51	563	8,755.9

TABLE 6. GEAR SPEED/LOAD TABLE

Gear	No. of Teeth	RPM	HP	Torque (in.-lb)
G1	28	20,952.0	3000	9,024.2
G2	107	5,482.8	1500	17,242.7
G3	34	5,482.8	1500	17,242.7
G4	107	5,482.8	1500	17,242.7
G5	167	1,116.3	5000	282,306.4
G5	167	1,116.3	563	31,787.7
G6	58	1,116.3	5000	282,306.4
G7	51	937.8	833.3	0.0 (Idler)
G8	164	0.0	5000	798,246.3
G9	15	12,428.1	563	0.0 (Idler)
G10	46	4,052.51	563	8,755.9

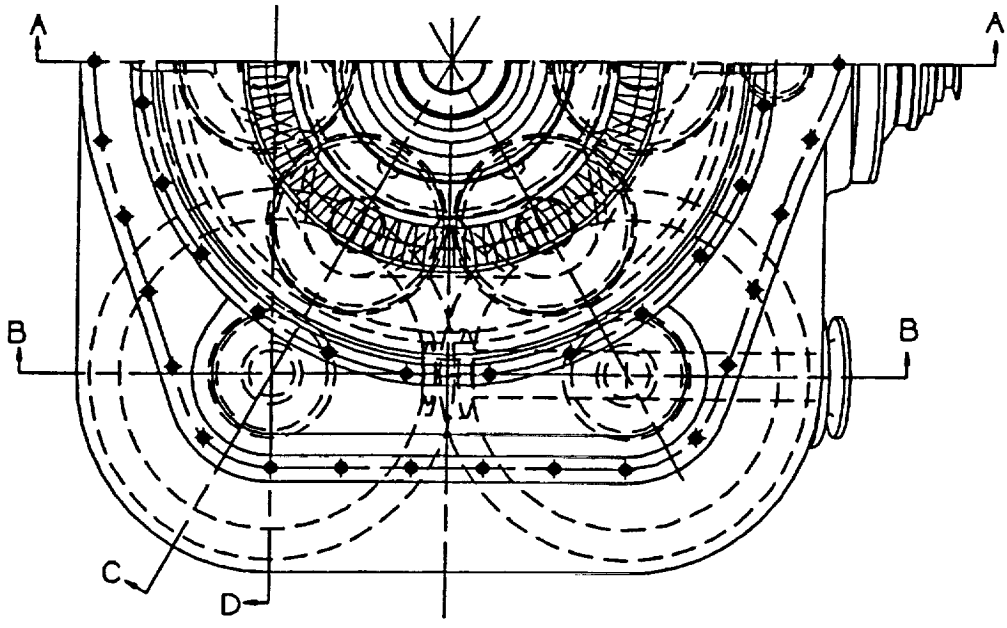

Figure 6. ART Plan View

TABLE 7. ART DESIGN PARTS LIST

Find No.	Dwg Zone	Qty	Description	Components	Notes	Goes Into
1	5A	1	Assembly, Transmission	(2-15,35,59,73,75)		
2	6A	1	Assembly, Lower Housing	(18,28,33,39,48,67,69, 79,85,86)		1
3	7A	2	Assembly, Input Quill	(80,81,82,83,84,87,88,8 9,92,93,94,98,99,100, 101,102,103,104,113, 114,119)		1
4	4B	1	Assembly, NOTAR Drive	(19,20,21,22,24,25,27, 34,40,43,68)		1
5	4C	1	Assembly, Spur Gear Shaft	(29,30,32,44)		1
6	4D	1	Assembly, Middle Housing	(17,31,66)		1
7	5E	1	Assembly, Upper Housing	(16,72,78,120,121,122)		1
8	5E	1	Assembly, Carrier	(70,71,74,76,77)		1
9	6E	1	Assembly, Sleeve	(36,54,55)		1
10	6C	1	Assembly, Sun/Combining Gear	(37,38,41)		1
11	6B	1	Assembly, Clutch	(91,95,96,97,105,106, 107,108,109,110,111, 112,115,116,117,118)		1
12	7D	2	Assembly, Face-Down Face Gear	(49,50,63,64)		1
13	8D	2	Assembly, Face-Up Face Gear	(45,46,49,50)		1
14	3D	1	Assembly, Main Oil Pump	(51,52,53,57)		1
15	1C	1	Assembly, Secondary Oil Pump	(58,60,61,62)		1
				Material		
16	6D	1	Housing, Upper	Aluminum Alloy		7
17	6C	1	Housing, Middle	WE 43 Magnesium		6
18	6B	1	Housing, Lower	WE 43 Magnesium		2
19	4B	1	Shaft, NOTAR Drive	4340 Steel		4
20	3A	1	Housing Cover	WE 43 Magnesium		4
21	4B	1	Gear, Face - NOTAR	EX-53 Steel		4
22	3C	2	Bearing, Ball, NOTAR	M-50 Nil Steel	#210	4
23						
24	3C	1	Sleeve	4140 Steel		4
25	4C	1	Screw, Self-Lok	4140 Steel		4
26						

TABLE 7. ART DESIGN PARTS LIST (Continued)

Find No.	Dwg Zone	Qty	Description	Material	Notes	Goes Into
27	4B	1	Nut, Self-Lok	4140 Steel		4
28	5A	1	Bearing, Roller, NOTAR	M-50 Steel	#305	2
29	5C	1	Bearing, Ball, NOTAR Idler	M-50 Steel	#308	5
30	5B	1	Nut, Self-Lock	4140 Steel		5
31	5C	1	Bearing, Roller, NOTAR Idler	M-50 Steel	#306	6
32	4B	1	Screw, Self-Lok	4140 Steel		5
33	5C	1	Liner, Bearing	M-50 Steel		2
34	3C	1	NOTAR Drive Flange	4340 Steel		4
35	6E	1	Retainer	4140 Steel		1
36	6E	1	Bearing, Ball, Mast Support	SAE 52000 Steel	Special	1
37	6A	1	Bearing, Roller Set, Combining Gear	M-50 Steel	Special	10
38	5A	1	Gear, Combining/Sun	M-50 Steel		10
39	5A	1	Race, Inner	M-50 Steel		2
40	3A	1	Seal, Double Lip	Special		4
41	5A	1	Retaining Ring	301 Stainless		10
42						
43	3A	1	Cap Screw Retainer	Steel		4
44	4C	1	Gear, Spur - Idler	EX-53 Steel		5
45	8D	1	Gear, Face-Up Face	EX-53 Steel		13
46	8B	1	Plate	4340 Steel		13
47						
48	3D	2	Bearing, Ball, Face Gear	M-50 Steel	#217	2
49	3D	1	Roll Pin	Steel		12,13
50	8A	1	Coupler, Splined	4340 Steel		12,13
51	3C	1	Housing, Pump	WE 43 Magnesium		14
52	2C	1	Pump, Main Lube	Gerotor 10 GPM		14
53	2C	1	Shaft, Splined	4340 Steel		14
54	4F	1	Sleeve	4340 Steel		9
55	5E	1	O'Ring			9
56						
57	2C	1	O'Ring			14
58	1C	1	O'Ring			15
59	7C	4	Nut, Self-Lock	4140 Steel		1

TABLE 7. ART DESIGN PARTS LIST (Continued)

Find No.	Dwg Zone	Qty	Description	Material	Notes	Goes Into
60	1C	1	Pump, Secondary Lube	Gerotor 1.5 GPH		15
61	1C	1	Housing, Pump	WE 43 Magnesium		15
62	1D	1	Shaft, Splined	4340 Steel		15
63	7C	1	Plate	4340 Steel		12
64	7D	1	Gear, Face-Down Face	EX-53 Steel		12
65						
66	2F	4	Bearing, Roller, Face Gear	M-50 Steel	#308 Sp	6
67	7d	2	Bearing, Ball - Face Down Gear	M-50 Steel	#118	2
68	4A	2	O'Ring			4
69	3E	2	O'Ring			2
70	4G	6	Gear, Planet Pinion	EX-53 Steel		8
71	4G	1	Planetary Carrier	EX-53 Steel		8
72	4F	1	Seal, Split Lip			7
73	4E	1	Spring	Steel		1
74	4E	6	Bearing, Spherical, Planetary	M-50 Steel	Special	8
75	4E	1	Gear, Ring	EX-53 Steel		1
76	3D	6	Cover	2024-T4 Aluminum		8
77	3D	6	Screw Cap	6061-T6 Aluminum		8
78	4F	1	Adapter/Seal Ring	6061-T6 Aluminum		7
79	7D	2	Sleeve, Bearing	M-50 Steel		2
80	8A	2	Nut, Self-Lock	4140 Steel		3
81	8A	2	Gear, Input - Spur	EX-53 Steel		3
82	7A	1	Bearing, Roller, Input Quill	M-50 Steel	#108	3
83	7A	1	Resilient Mount	4340 Steel		3
84	7A	1	Anti-Flail Ring	4140 Steel		3
85	7A	2	Cover, Access	6061-T6 Aluminum		2
86	7A	2	Retainer	4140 Steel		2
87	7A	2	Tube, Spacer	4140 Steel		3
88	7D	1	Screw, Set	Steel		3
89	7A	1	Shaft, Input	4340 Steel		3
90						
91	7H	1	Spacer	Steel		11

TABLE 7. ART DESIGN PARTS LIST (Continued)

Find No.	Dwg Zone	Qty	Description	Material	Notes	Goes Into
92	7F	6	Bolt, Hex	Cres		3
93	7F	6	Washer	Steel		6
94	7F	6	Thread Insert	Steel		6
95	7F	1	Ratchet	M-50 Steel		11
96	7F	1	Nut, Lock	Steel		11
97	7G	1	Spring	Steel		11
98	7F	1	O'Ring			3
99	6F	1	O'Ring			3
100	6G	1	Drive Flange	4340 Steel		3
101	6G	1	Cover, Retainer	4340 Steel		3
102	7H	1	Seal, Magnetic			3
103	6H	1	Housing, Retainer Cap	6061-T6 Aluminum		3
104	7H	1	O'Ring			3
105	7H	2	Bearing, Ball, Input	M-50 Steel	#013	11
106	7H	1	Coupler, Splined	4340 Steel		11
107	7H	1	Synchronizer	M-50 Steel		11
108	7G	1	O'Ring			11
109	7G	2	Pawl	M-50 Steel		11
110	7G	1	Bolt, Hex	Steel		11
111	7G	2	Washer	Steel		11
112	7F	1	Nut, Hex	Steel		11
113	7F	2	Nut, Lock	Steel		3
114	7F	2	Bearing, Ball, Clutch	M-50 Steel	#110	3
115	7F	1	Spacer	4140 Steel		11
116	7F	1	Sleeve	4140 Steel		11
117	7G	2	Retaining Ring			11
118	7G	A/R	Washer			11
119	7A	1	Tube, Lube	4140 Steel		3
120	6D	2	Tube, Lube	4140 Steel		7
121	6D	8	O'Ring			7
122	6C	2	Tube, Transfer	4140 Steel		7

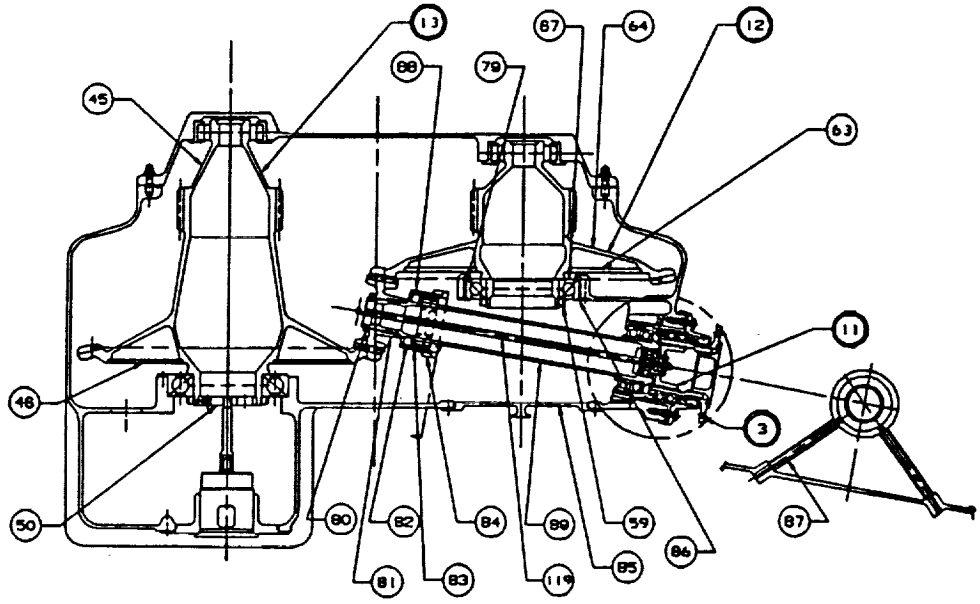

Figure 7. ART Input Stage

Figure 8 shows Section C-C taken through two of the second stage pinions. The second stage reduction spur gear is integral with the face gear. This spur gear is identical on both the upper and lower face gear shafts.

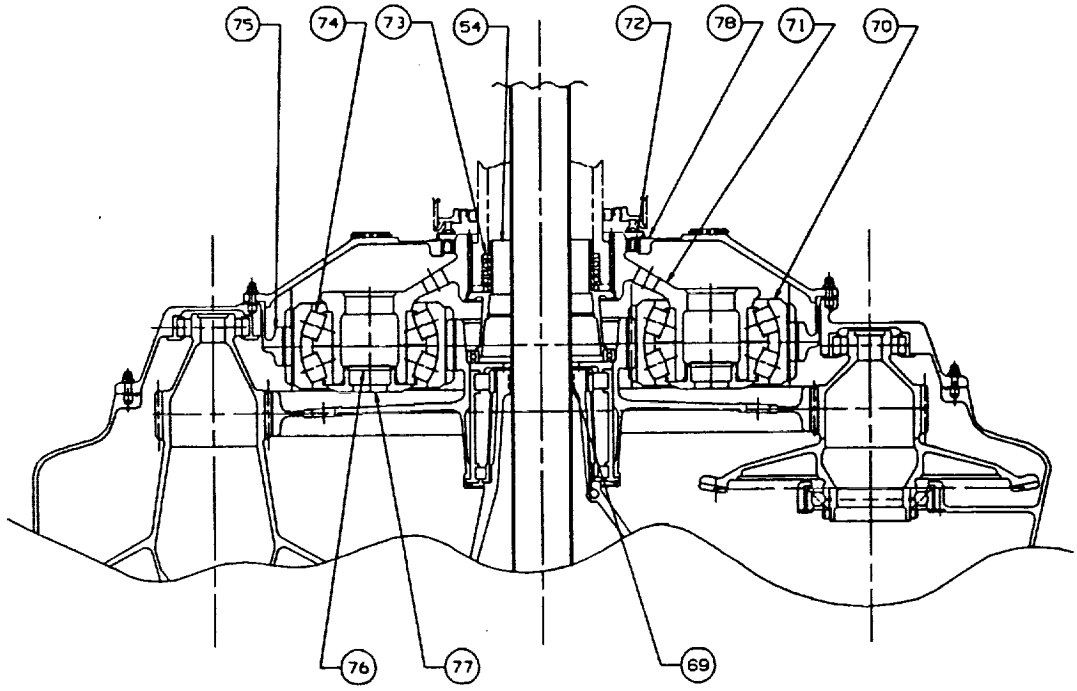

Figure 8. ART Second Stage and Planetary Third Stage

Thus four pinions total, two on either side, combine to drive the collector gear which rotates at 1116 RPM. This provides a 4.912:1 reduction ratio at the second stage. The upper face gear shaft requires an E.B. weld because there is not enough clearance between the spur gear and the face gear web to grind the teeth. A secondary web is also welded on the upper and lower face gear shafts to provide a lightweight box structure for face gear stiffness.

The face gear webs and rims were designed to achieve nearly equal radial, axial, and tangential stiffness between the two. Matched web stiffness resulted in a near equal torque split to the two face gears, as obtained in a finite element static systems analysis. In addition, the magnitude of axial deflection, which occurs along the face gear tooth height, was limited in the designs to approximately 0.005 inch. This represents less than 2 percent of the tooth whole depth. Analysis showed the designs of both gear shafts effectively limit gear deflection while reducing weight and shaft length.

As shown in Figure 9, Section D-D, the transmission main lubrication pump is driven by the left hand lower face gear shaft and the emergency lubrication pump is driven by the right hand lower face gear shaft.

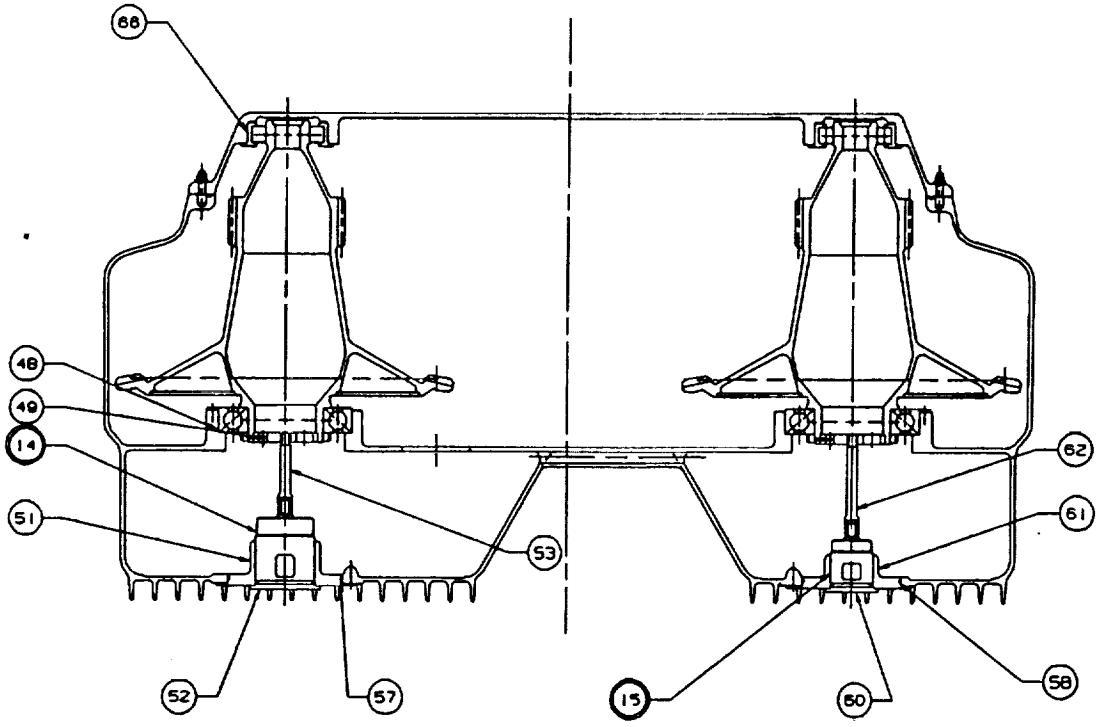

Figure 9. ART Face-Up Face Gears/Lubrication Pump Drives

The collector gear recombines the power from the upper and lower face gears and also combines the power from the left- and right-hand engines. The collector in turn drives the NOTAR/accessory output and the integral sun gear for the high contact ratio (HCR) planetary. Figure 10, Section A-A, shows this section of the transmission. The collector gear is supported by a dual roller bearing set which is designed to handle the small thrust load produced by gear tooth errors, torsional windup, and the gear weight. The roller bearing set was sized for OEI power which produces the larger bearing loading. In the twin engine operation, much of the bearing load is cancelled leaving only the NOTAR/accessory loads to be reacted by the roller bearing set.

The final transmission reduction is a simple HCR planetary design with the sun gear integral with the collector gear. Shown in Figure 10, six equally spaced planet idler gears orbit around the sun and drive the planetary carrier. The carrier in turn drives the main rotor drive shaft through a grease-packed crown tooth spline coupling. The planet pinions contain double row spherical bearings which run on common spherical raceways integral with the planet pinions. The bearings are self-aligning and thus insensitive to misalignment of the cantilevered carrier posts. The flexured planetary ring gear provides controlled radial motion of the planets and is attached to the transmission housing at a bolted flange. The ring gear has no working spline to generate wear debris and isolates the meshing tooth noise from the housing at the bolt flange. The planetary is a high contact ratio, dropped tooth design in which the sun, pinion, and ring meshes have contact ratios of about 2.22, and the ring gear action is almost fully recessed. The planetary is designed to employ the highest profile contact ratio that can be gainfully used in a spur gear planetary drive. Table 8 compares a standard spur gear planetary with a high contact ratio planetary similar to the ART design described and notes a noise reduction of about 9.5 dB [13]. Both planetaries given in Table 8 are sized to transmit the same torque with the same gear tooth bending stresses. The dropped tooth gearing technique used permits the use of six planets at a ratio where normally only five could be used. The planet idler gears have two teeth less than what would normally be employed at this ratio. This allows the ring gear to become smaller for the same reduction ratio, consequently reducing weight. The planet gears are equally spaced, but their tooth numbers provide a hunting ratio with respect to their mesh with the sun and ring gears and allow the planetary system to be phased. Emphasis was placed on system-phasing the individual planet-gear mesh points and preventing all the pinions from meshing at the same time. The system was phased so the sequences of engagement and sliding impulses between the six pinions cancelled. This eliminated external force or moment reactions. This method has demonstrated noise reductions of up to 11 dB [14].

The final planetary design evolved from a trade-off study comparing two different planetary concepts primarily to consider weight, noise and reliability. The baseline configuration, shown in Figure 11 centered around a rigid cantilevered planetary containing six planetary pinions with integral single row cylindrical roller bearings. The bearings contained fourteen 30x42 mm rollers closely housed in a steel cage. The cantilevered carrier for the baseline planetary was designed using finite element modeling with a goal limiting deflection of the cantilevered planet pins to 0.001 inch per inch of length at maximum load. This value was chosen to maintain line contact on the cylindrical rollers. A conical web directly connects the carrier plate to the hub. The cylindrical I-beam above the plate is required to resist planet pin deflection. The carrier material is carburized AMS 9310, chosen for the integral splined crown tooth coupling required to drive the main rotor mast. Because the design criteria was stiffness rather than strength, the stresses are extremely low and the weight is almost double that of the alternate carrier design. The baseline planetary gearing consists of a 58-tooth sun gear integral with the 167-tooth collector gear driving six 53-tooth planet idler pinions. The ring gear has 164 teeth which yields a planetary reduction ratio of approximately 3.83:1 at a 7.500-inch center distance. The gearing has a 25-degree pressure angle and operates at 7.400 diametral pitch. The gears have standard tooth proportions with the face widths sized for infinite tooth bending strength at 100 percent power. This yielded L_{10} pitting lives which greatly exceeded the 15,000 hour component life requirement for life equivalent power.

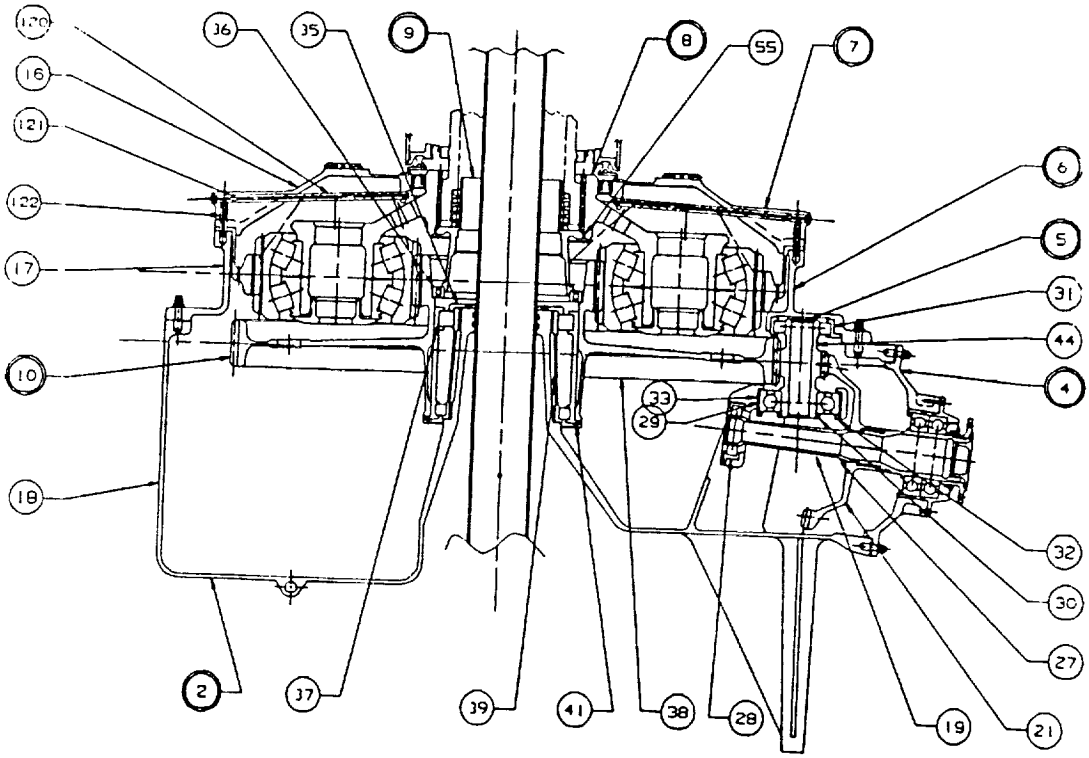

Figure 10. ART Combining Gear/NOTAR Drive and Planetary Stage

TABLE 8. PLANETARY COMPARISON TABLE

	Weight (lb)	Efficiency (%)	Noise (dB)	Life
Standard (XV-15 Final Stage) Spur Gear Planetary Design	40	99.7	X	X
High Contact Ratio (Model 222) Spur Gear Planetary Design	38	99.4	X - 9.5	2X

The alternate planetary design analyzed in the trade-off study is described at the beginning of this section. This configuration was selected as the final design because of the weight savings advantage and the potential to reduce the noise level with no decrease in gear or bearing life. The alternate planetary gearing consists of a 58-tooth sun gear integral with the 167-tooth collector gear driving six 51-tooth planet idler pinions. The ring gear has 164 teeth which yields a planetary reduction ratio of about 3.83:1 at a 7.500-inch center distance. The sun-pinion mesh has a 16.01-degree pressure angle and operates at 7.533 diametral pitch. The gear tooth proportions are 37.8 percent greater than standard tooth proportions with the face widths sized for infinite tooth bending strength at 100 percent power and well over 15,000 hours L_{10} pitting life at the life equivalent power. Table 9 gives a comparison between the baseline planetary design and the high contact ratio planetary design selected. A detail weight analysis indicated a difference of 68.5 lb between the two planetary stage designs with both falling under the parametric ART weight allocation.

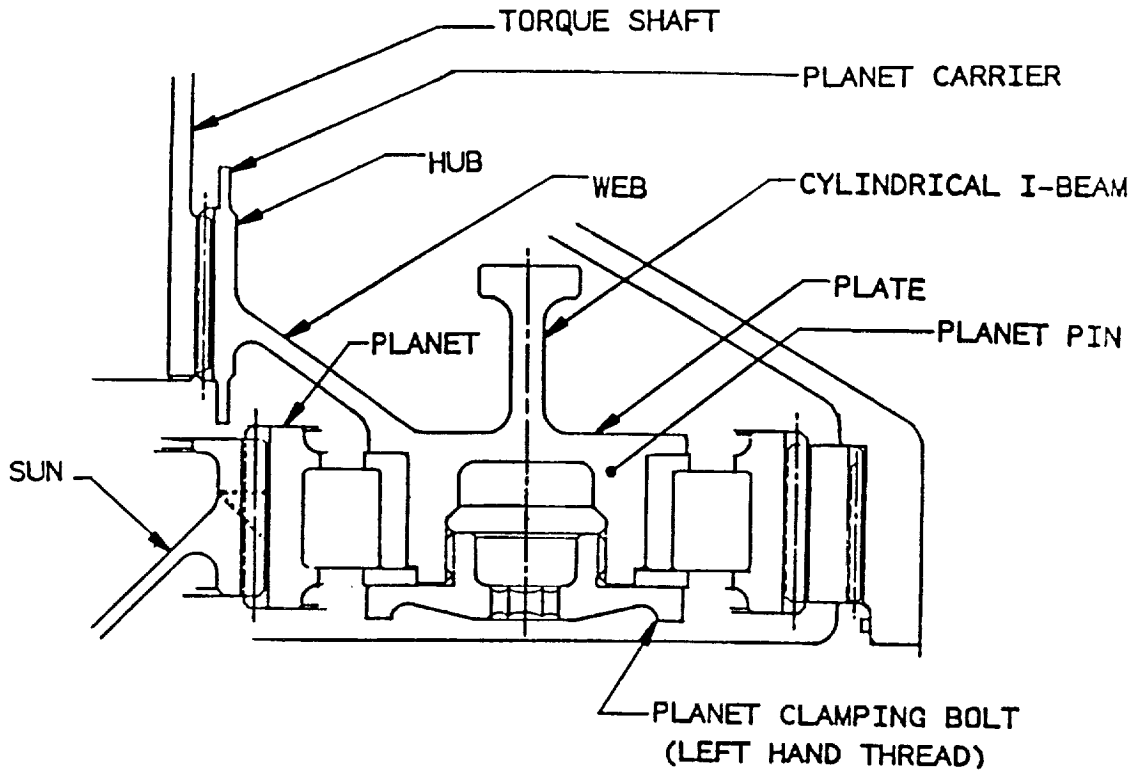

Figure 11. ART Baseline Planetary Design

TABLE 9. BASELINE PLANETARY VERSUS HIGH CONTACT RATIO PLANETARY DESIGN

	Contact Ratio	Fitting L1 Life	Face Width	Efficiency	Contact Temperature
Standard Planetary	1.59	>10,000 hrs	3.93 in.	99.93%	267.1°F
High Contact Ratio Planetary	2.22	>10,000 hrs	3.25 in.	99.85%	337.5°F

The NOTAR spur gear idler is driven from the collector gear at a speed of 12,428 RPM and provides the speed up ratio required for the NOTAR face gear. The NOTAR face gear drives the NOTAR and the accessory gearbox and is attached to the bolted flange output shaft with a double piloted splined connection. The face gear has a speed reduction ratio of 3.067:1 which is about the smallest reduction ratio possible to retain an adequate tooth profile on the face gear. The face gear angles the output shaft along the 0.00 aircraft waterline and provides a NOTAR shaft speed of 4,052 RPM. The NOTAR shaft is on the centerline of the transmission.

The transmission attachment and main rotor drive configuration is identical to the AH-64 Apache helicopter design, whereby the transmission housings are designed to handle drive loads only and the rotor loads are taken out through the mast support structure. This feature not only minimizes weight and increases reliability, but allows the transmission to be removed from the aircraft in a simple manner without disturbing the rotor or the controls. The transmission is simply supported from the top by tension bolts with the torque being reacted by a curvic type coupling. The drive shaft from the main transmission to the rotor is a full-floating-type unit having grease lubricated spherical gear couplings at each end. It is supported from the top and provides torque transmission only and accommodates the small angular misalignment of the transmission to static support and the static support to rotor.

The transmission housing is a three-piece housing bolted together as an assembly. Figures 12, 13, 14, 15, and 16 show outside views of the ART housing. The housings are proposed to be manufactured from Elektron WE43 high-strength, corrosion-resistant sand castings. The housings contain internal cored passages for lubricant transfer. The choice of housing material was made after a preliminary trade-off was conducted looking at weight, corrosion resistance, strength, method of fabrication, and fatigue characteristics.

The lubrication system for the ART is schematically shown on Lucas Western Drawing 42499-1037, shown here as Figure 17. The system is self contained, except the external heat exchanger. The lubrication system is an extension of current practice. The extension is directed toward taking advantage of advanced technology materials and components. These materials and components allow an oil-out temperature from the gearbox of 400°F and an oil-in temperature from the oil cooler of 230°F. This allows a 10 gallon per minute (GPM) pump where conventional practice for a 5000 HP transmission would require 27 GPM. Conventional practice uses a 16 second cycle time, which would require 7.2 gallons of oil for the 27 GPM case versus 2.2 gallons for our 10 GPM case which uses a 13 second cycle time. At 7.6 pounds per gallon, a direct savings of 38 pounds results plus added savings from a smaller system. Cycle times as short as 8 seconds are being used successfully so the 13 second cycle time is somewhat conservative.

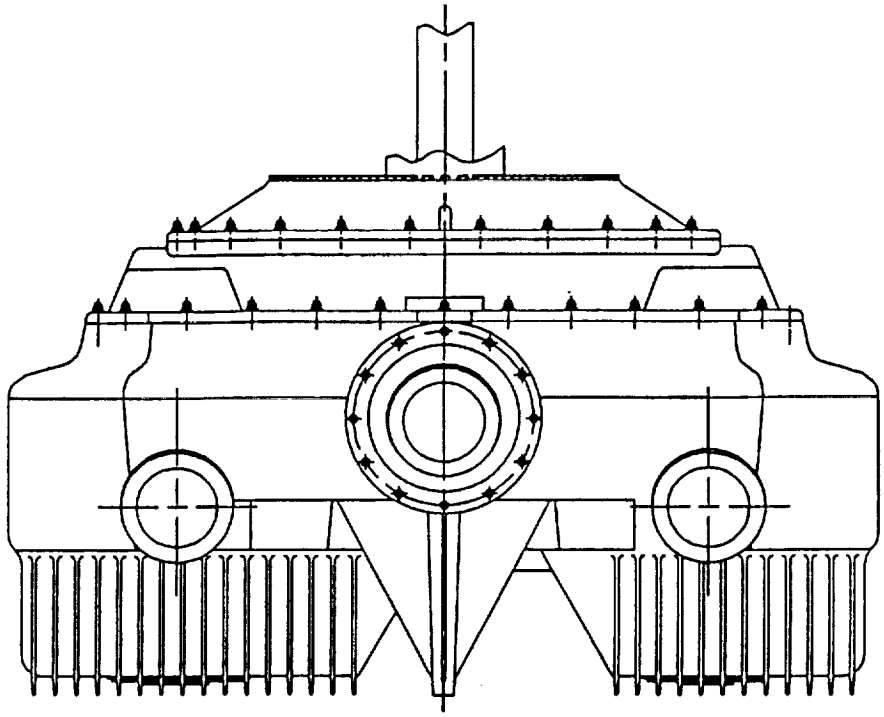

Figure 12. ART Aft View of Housing

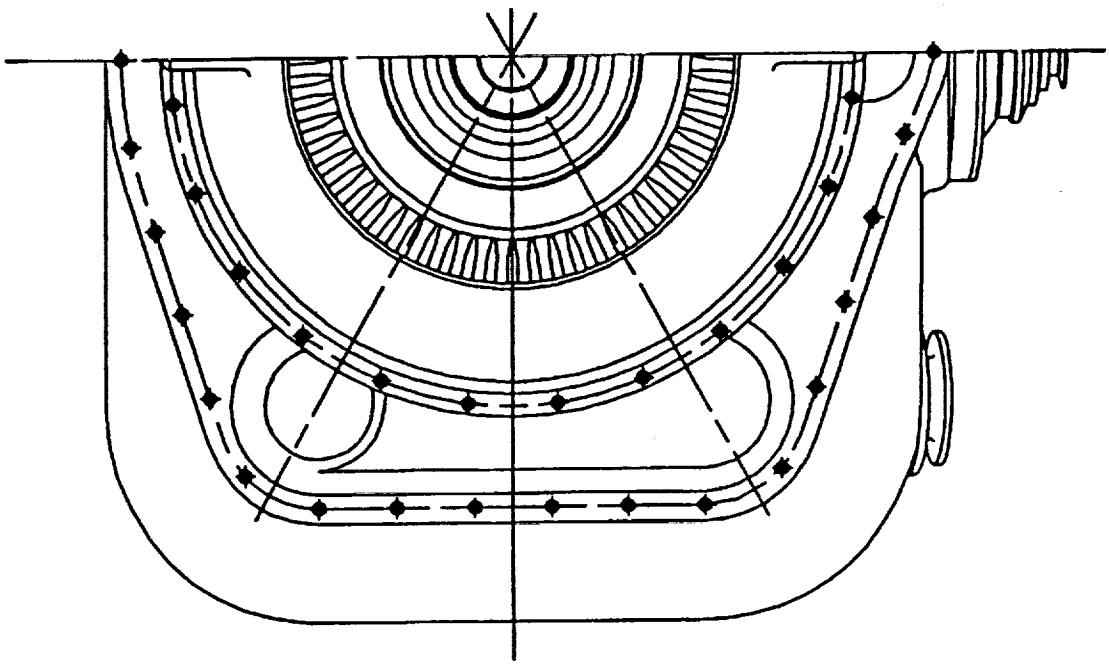

Figure 13. ART Plan View of Housing

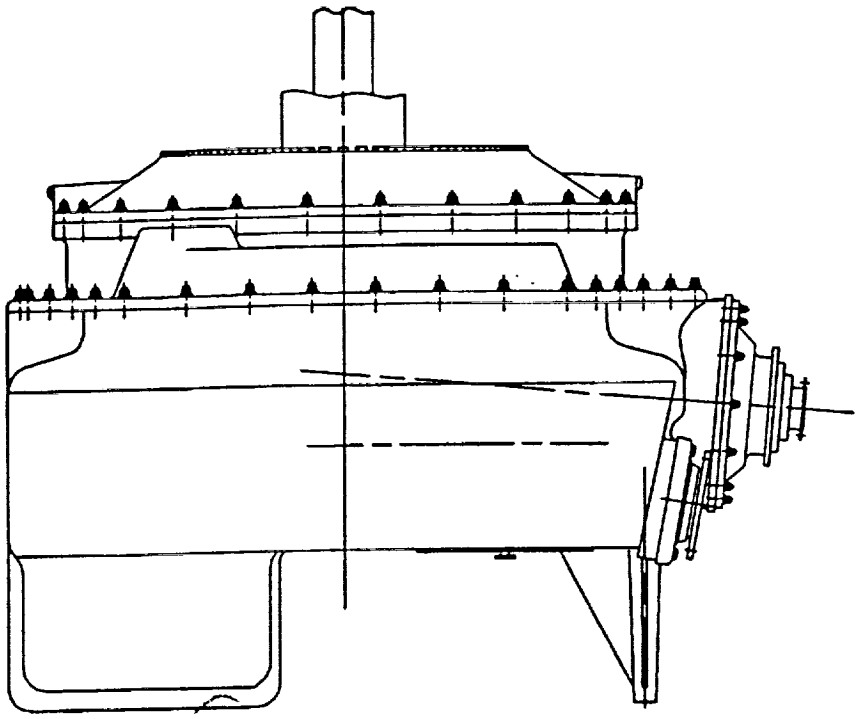

Figure 14. ART Profile View of Housing

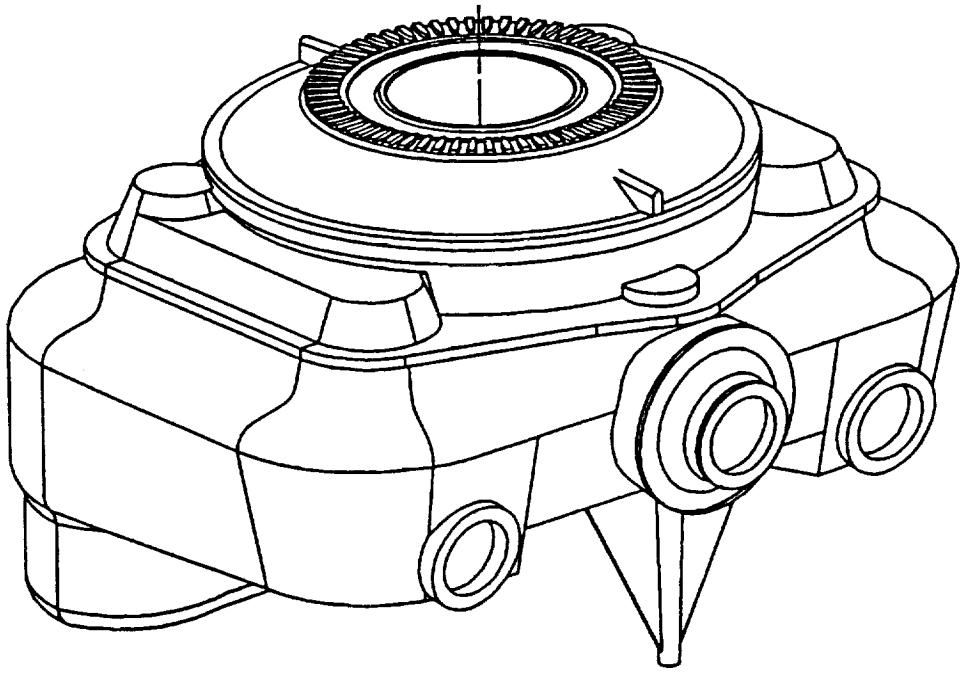

Figure 15. ART Transmission Case, Tri-Metric View Looking Down

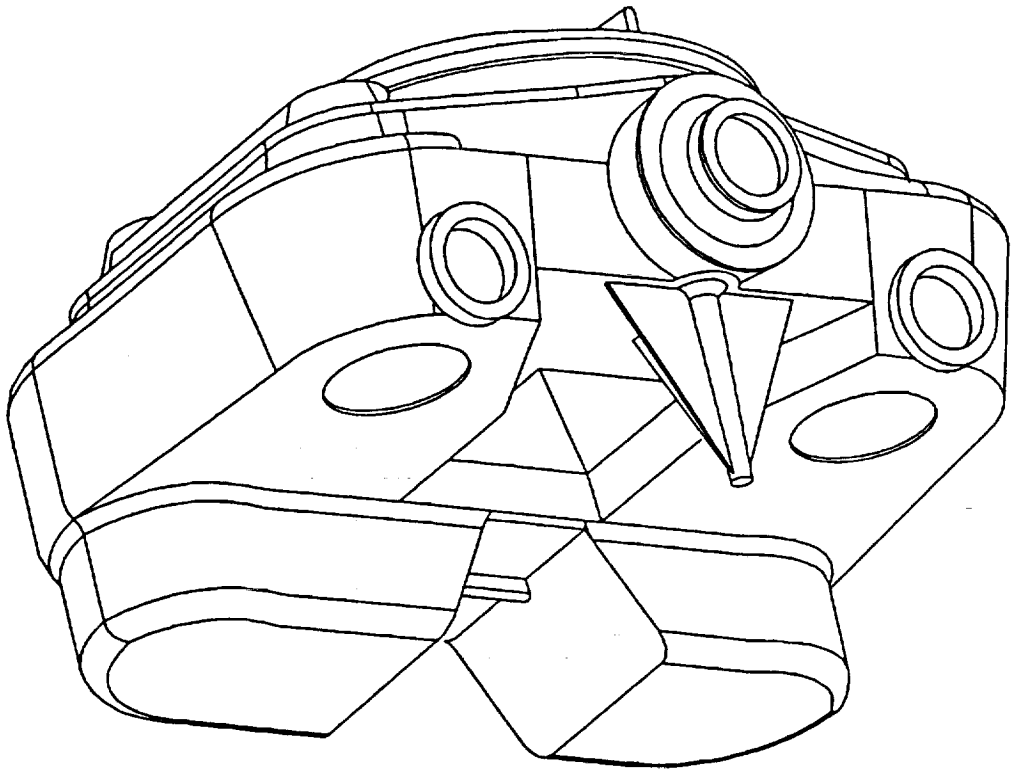

Figure 16. ART Transmission Case, Tri-Metric View Looking Up

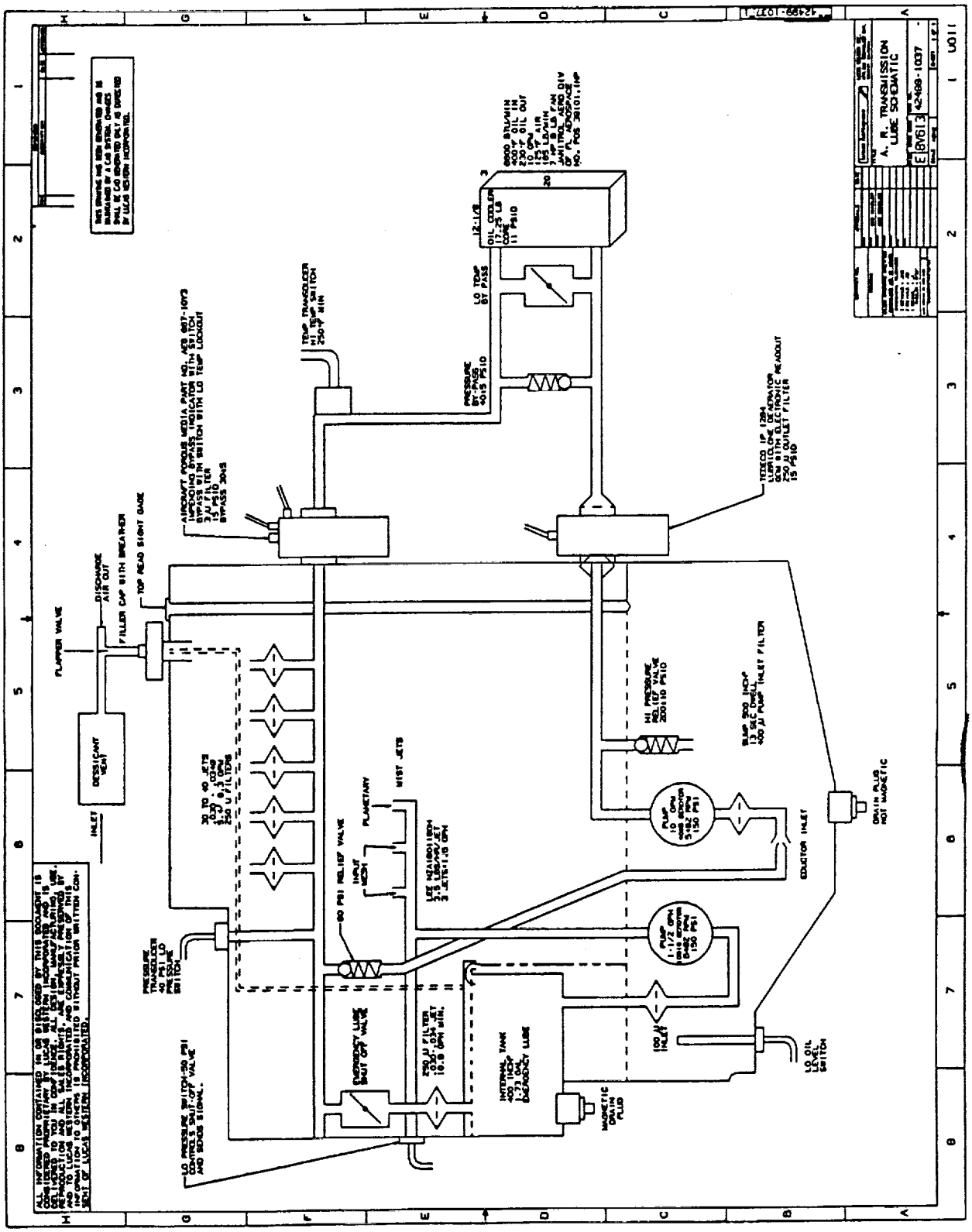

Figure 17. Lubrication System Schematic

The benefits of using high oil temperature carry over into the oil cooling system. The greater the difference in oil and air temperatures, the more heat is rejected directly by the gearbox. The higher the allowable oil temperature out of the cooler, the smaller the air/oil heat exchanger. Taking both these factors into account results in an oil cooler having a core weight of 17 pounds when optimized with respect to pressure drop through the cooler, air flow, air pressure, blower power, and blower weight.

A conventional design using 27 GPM, 275°F oil out of the gearbox, 205°F oil out of the cooler and the same air temperature of 125°F results in a core weight of 61 pounds. Oil weight savings and core weight savings is 82 pounds directly. The total weight savings from secondary effects would be considerably higher.

A third approach of interest is the provision of emergency lubrication after oil is lost from the gearbox. It is planned to provide a constantly filled separate oil tank within the gearbox which feeds a 1.5 gallon per hour pump. The oil is delivered under pressure to three mist jets, one on each input pinion, and one directed into the zone between the combining gear and the output planetary. The system is designed for over one hour endurance and is entirely independent of the primary oiling system. It operates all the time, and provides a signal if it becomes inoperative. The basic concept is that either oil system will function independent of loss of oil in the other.

The lower part of the transmission acts as the lubricant sump and has an approximate capacity of 500 cubic inches. The oil circuit is described later in this section.

Starting at the sump, oil passes through a 400 micron screen into a 4065 gerotor lube pump which has a capacity of 10.0 GPM. At this point, the system contains a high pressure relief valve set at 200±10 PSID. The high pressure relief valve protects the system by limiting excessive pressure due to very cold oil or other reasons. The oil then enters a Tedeco Lubriclone Deaerator with a quantitative debris monitor (QDM), Part No. 1P 1284. Entrained air is removed by the lubriclone which delivers solid oil to the QDM.

QDM is a technology for determining the operating condition of oil-wetted mechanical parts such as bearings and gears. Abnormal wear and mechanical damage can be detected well in advance of complete mechanical failure. Measurement of debris particle generation rate within certain particle size categories provides the information necessary to detect the onset of failure in time to take corrective safety action and trend information required to implement a cost-effective maintenance and repair program.

The QDM sensor is located in the lubrication system where it is exposed to the entire lubricant flow to assure most effective capture of damage debris and early notification of impending failure. The QDM sensor incorporates a magnet to attract and capture ferrous debris and a coil which generates a voltage pulse proportional to the magnetic flux disturbance caused by the capture of the debris. This design approach has the advantage of not only signaling the existence of debris, but also retaining the debris for subsequent analysis. Since the magnetic flux disturbance is a function of the mass of the debris particle, the resultant signal amplitude indicates the size of debris captured by the sensor. The signal conditioner contains built-in test circuitry. The circuit is activated by a pushbutton on the unit and generates a pulse simulating a large chip.

Oil exits the QDM through a 250 micron barrier screen. The barrier screen prevents foreign objects from entering the QDM when the external line is not present. The barrier screen also prevents non-ferrous debris, which can escape the QDM, from entering the oil cooler. The screen is removable to allow inspection for accumulation of non-ferrous debris. The pressure drop through the Lubriclone/QDM is 15 psi.

The oil cooling system has been optimized by the Janitrol Aero Division of FL Aerospace, Part No. POS 39101, INP. The design features a 17.25 pound core measuring 12-1/8 x 3 x 20 inches. The heat load is 6600 Btu/minute, 400°F oil in, 230°F oil out. The cooler passes 10 gallons of oil/minute with an 11 PSI drop. Cooling requires 165 pound/minute of 125°F ambient air furnished by a 7 HP 8 pound fan. The cooler has a low temperature by-pass and a high pressure by-pass which induces a 40±5 psi drop.

After the oil exits the cooler it passes the high temperature warning switch, set at 250°F minimum, which will indicate an oil over-temperature condition.

The oil then enters the filtration system, Aircraft Porous Media Part No. AEB 667-10Y3. Three micron filtration, which has demonstrated significant advantages and has been widely adopted in helicopter engines and transmissions, is provided. The basic concept is that particles smaller than 3 microns are smaller than the thickness of the oil film which separates gear teeth and rolling elements in bearings from the bearing races. To over simplify, since wear is generated by debris, if the debris is removed, there will be no wear. This has proven to be generally true. By actual test, oil service life increased from 100 to 1000 hours, filter life after initial clean-up increased from 400 hours to 1000 hours, bearing life increased 100% with a potential for no fatigue limit. Three micron filtration also eliminates SOAP analysis. The filter includes an impending bypass indicator with switch, bypass with switch and a low temperature lockout. The filter has a 15 PSI drop while the bypass has a 30±5 psi drop. Oil then passes to multiple jets which direct and meter oil flow, as needed, to lubricate and cool the transmission gears, bearings and splines. Jets orifice size will be 0.030-0.034 inches. It is estimated that 30 to 40 jets will be used for a total flow of 5.4 to 9.3 GPM. Each jet is protected by a 250 micron contaminant barrier screen. A low pressure relief valve, set at 80±5 PSID, is included in this part of the oil circuit and establishes pressure at the lube jets and bypasses excess oil to the sump. The last monitor before the return to the sump is the low pressure warning switch, set at 40±5 psi.

The sump return line terminates in a nozzle directed into an eductor, or jet pump, inlet. The eductor inlet is in fact the oil pump inlet. This technique accelerates sump oil into the pump inlet, reduces entrained air into the pump and will compensate for a low oil condition by reducing sump dwell time. In fact, this technique is used in one application with a dwell time of 8 seconds.

The oil is added to the transmission via a filter cap with breather. The breather has a flapper valve to let air in through a desiccant filter or air out as required by pressure changes. The desiccant filter is intended to reduce water entering the gearbox through the air inlet. Even minute amounts of water can cause damaging rust and accelerate crack growth.

The filter cap leads to the emergency lube tank which overflows into the main sump. The sight gage monitors the oil level in the main sump. Thus both tanks are full when the sight gage indicates full. The main sump contains a low oil level switch in addition to the sight glass. The main sump is drained by a non-magnetic drain plug because all ferrous debris must be routed to the QDM.

The emergency lube system is a separate entity. The gearbox contains a closed internal tank fed by one of the standard oil jets at 10.8 gallons per hour. The internal tank contains 400 cubic inches. Overflow oil is returned to the main sump. From the emergency tank, the oil goes through a 100 micron screen into a 10010 gerotor pump delivering 1.5 gallons per hour to three mist jets, LEE Part No. NZA 180118H. Each jet uses 0.5 gallon per hour. One jet is directed at each input pinion and one jet is directed into the zone between the combining gear and the planetary. The emergency lube system operates continuously and has over one hour endurance. The emergency lube circuit contains a low pressure switch set at 40 psi which operates a shut-off valve controlling the jet feeding the emergency lube tank. This switch also sends a signal that the emergency lube system is

inoperative. Ferrous particles entering the emergency lube tank cannot be allowed to escape. Therefore this tank has a magnetic drain plug to capture debris that might damage the pump.

Both the primary and emergency pumps are driven by shafts connected to first stage gears. Therefore no gears or bearings are added to the transmission to drive the oil pumps.

In summary, there are seven lubrication system sensor components that provide transmission condition monitoring signals. These are:

Sensor	Indication
Quantitative Debris Monitor	Abnormal wear
High Temperature Switch	Oil cooler malfunction, low oil supply, oil leak
Filter Element Switch	No filter element present
Impending Bypass Switch	Filter collecting debris
Bypass Switch	Filter plugged, oil contaminated
Low Pressure Switch	Low oil, oil leak
Emergency Lube Low Pressure Switch	Emergency oil low or leaking

The seven switch signals can be provided as cockpit warnings of each condition sensed; or, ganged to provide one transmission problem signal. The concept behind one transmission problem signal is that a combat aircraft should be designed to refuel and rearm with as little maintenance as possible. Either all systems are ready or not ready with no panel openings and ground inspection required. Certain signals may also be used for maintenance status panels, if provided on the aircraft. It is the responsibility of the aircraft systems integrators to decide what, and how, to display transmission condition monitoring signals for the cockpit crew and maintenance personnel.

IV.B GEAR ANALYSIS

Structural analyses for the gear components were performed in support of the Advanced Rotorcraft Transmission (ART) Design. Analyses of the gear tooth bending stresses, the compressive (Hertzian) stresses and the scoring risk evaluations were conducted. All the gear components in the main transmission as well as the NOTAR and accessory power drive were analyzed.

The gear tooth stress analyses for the spur gear components were carried out per AGMA standards. Due to the unusual geometry of the face gear [15], the formulas are not available in any of the standards for stress analysis. An approximate method for analyzing the face gears is used in the first stage and the NOTAR/accessory power drive gear analyses. This method tends to give conservative values of both tooth bending and compressive stresses. The results of the gear tooth stress analyses are tabulated in Tables 10 and 11.

TABLE 10. SUMMARY OF GEAR STRESS ANALYSIS

Stage	Part	No. of Teeth	Bending S_t (psi)	Compressive S_c (psi)	Load (HP)
1	Pinion	28	36,112	143,590 (@)	1500 (OEI)
1	Face Gear	107	< 36,112	143,590 (@)	1500 (OEI)
2	Pinion	34	43,292	158,531	1500 (OEI)
2	Gear	167	40,787	158,531	1500 (OEI)
3	Sun	58	52,142	158,900	5000/6, MCP
3	Planet (#)	51	41,760	158,900	5000/6, MCP
3	Planet (#)	51	45,941	122,603	5000/6, MCP
3	Ring	164	48,307	122,603	5000/6, MCP
NOTAR	Gear	167	12,637	152,512	563 * (71%)
NOTAR	Idler	15	19,017	152,512	563 * (71%)
NOTAR	Idler	15	23,317	177,857 (@)	563 * (71%)
NOTAR	Face Gear	46	< 50,896	177,857 (@)	563 * (71%)

\# Bending stress should be divided by a factor of 0.7 to account for the effect of reverse bending on the planet.

@ The compressive stress for the face gear drive is the value calculated at the pitch point, which is closer to the test results.

TABLE 11. SUMMARY OF ART GEAR DESIGN LIFE VALUES

Gears Item No.	Description	Qty	RPM	No. of Meshes	Hertz Stress	Load (HP/mesh)	L10 Life (hrs)
-081	Input Spur Pinion	2	20,952.0	2	99,478	1,000	1.5E+08
-012	Upper Face Gear	2	5,482.8	1	99,478	1,000	1.2E+09
-012	Collector Pinion (2)	2	5,482.8	1	131,002	1,000	8666102
-013	Lower Face Gear	2	5,482.8	1	99,478	1,000	1.2E+09
-013	Collector Pinion (2)	2	5,482.8	1	131,002	1,000	8666102
-010	Collector Gear	1	1,116.3	4	131,002	1,000	10641070
-010	Collector Gear - NOTAR Mesh	1	1,116.3	1	152,512	.71*563	2818434
-010	Planetary - Sun Gear	1	1,116.3	4.432	142,124	666.7	2241069
-070	Planet Gear - Sun Gear Mesh	6	902.41	1	142,124	666.7	12287599
-070	Planet Gear - Ring Gear Mesh	6	902.41	1	101,854	666.7	4.7E+09
-075	Ring Gear	1	291.63	6	101,854	666.7	2.4E+09
-005	NOTAR Idler Gear - Collector Mesh	1	12,428.14	1	152,512	.71*563	253152.8
-005	NOTAR Idler Gear - Face Gear Mesh	1	12,428.14	1	150,909	.71*563	305722.1
-021	NOTAR Face Gear	1	4,052.65	1	150,909	.71*563	937549.0

NOTES:

(1) A factor of 1.389 is used to account for the high contact ratio of the face gear drive.

(2) Calculated gear L10(L1) life and cycles are based on AGMA compressive stress.

(3) Life equivalent power per engine = 80%* (single engine MCP) = 0.8 * 2500 HP = 2000 HP
Life equivalent power for NOTAR and accessory drive = 0.71 * 563 = 400 HP

(4) AGMA compressive stress allowable of 225,000 psi for 10^7 cycles and .99 reliability is used in life calculation.

IV.C BEARING ANALYSIS

This section summarizes the bearing life analyses for the bearing components in ART design. The design lives (B10) for the bearing components are aimed at 15,000 hours. A Life Equivalent Power (LEP), which is equal to 67 percent of the Maximum Continuous Power (MCP), is used for the bearing life analyses.

The ball and cylindrical roller bearing lives are calculated using the "Rolling-Element Bearing Analysis Program" developed by A.B. Jones, Newington, Connecticut. Table 12 gives the bearing lives calculated. The lives reported are the adjusted lives using the EHD film thickness life adjustment factor. The total life adjustment factor for the bearings associated with main transmission gear shafts (S1 through S4) is 12.0. The factor is a combination of a material factor of 2.0, a process factor of 3.0, and a life improvement factor of 2.0 for the use of the three micro filter. All other factors are considered to be 1.0. In analyzing the collector-to-sun-gear shaft (S4), the loadings are balanced under an even twin engine input condition. Therefore, the size of the bearings are designed for a more critical OEI condition.

TABLE 12. ART BEARING DESIGN AND CALCULATED LIFE VALUES

Find No.	Qty	Descriptions	RPM	B10 Hours
114	4	Input Shaft Bearing: Duplex Ball, Clutch	20952	>50000
105	4	Input Shaft Bearing: Duplex Ball, Adapter	20952	>50000
82	2	Input Shaft Bearing: Roller, Input Quill	20952	>50000
48	2	Face-Up Gear Shaft Bearing: Ball, 217B	5483	28315
66	2	Face-Up Gear Shaft Bearing: Roller, 308R	5483	22484
67	2	Face-Down Gear Shaft Bearing: Ball, 118B	5483	44256
66	2	Face-Down Gear Shaft Bearing: Roller, 308R	5483	21926
36	1	Collector Gear S4 Bearing: Ball	1116	>50000
37	1	Collector Gear S4 Bearing: Roller, 121R	1116	>50000
37A	1	Collector Gear S4 Bearing: Roller, 021R	1116	>50000
74	6	Planet Spherical Roller Bearing	902	16629
31	1	NOTAR Idler S6 Bearing: Roller, 306R	12428	20014
29	1	NOTAR Idler S6 Bearing: Ball, 308B	12428	14735
28	1	NOTAR Output S7 Bearing: Roller, 305R	4053	31379
22	1	NOTAR Output S7 Bearing: Duplex Ball, 210B	4053	39409

The supporting bearing for the idler and output shafts (S6 and S7) is also analyzed using A.B. Jones' Computer program. A combined material, process and life improvement factor of 22.0 [16] is used for VIM-VAR M-50 bearing material in the bearing life analyses of NOTAR and accessory power drive.

The bearings of the engine input shaft (S1) theoretically are not loaded by any bending moment or radial force due to the split torque configuration of the ART design. This assumption is based on the ideal condition that the torque is evenly divided into the two output shafts. The flexural mounting design for the engine input shaft support at the front end allows for nearly even torque splitting. Another ART design advantage results from the application of face gear drives using a spur pinion to drive the generated face gears. No thrust load is generated in this type of gear meshing. Therefore, the bearing lives (B10) of bearing components associated with the engine input shaft are conceptually determined to be higher than 50,000 hours.

The planet spherical roller bearing lives are calculated using the PLANETSYS computer program and the NASA model. The lives reported are the adjusted lives. The computer program's film thickness lubrication life adjustment factor was modified from 0.21 to 3.0. This is based on the paper "Life Adjustment Factors for Ball and Roller Bearings," sponsored by the Rolling-Elements Committee and verified by helicopter transmission experience. The total life adjustment for the spherical roller bearing is 3.6. The factor of 3.6 is set using a material factor of 2.0, a process factor of 3.0, a lubrication factor of 0.3, and a life improvement factor of 2.0. All other factors are considered to be 1.0.

IV.D GEAR SHAFT STRUCTURAL ANALYSIS

Structural analyses of the gear shafts were conducted in support of the ART design. Static analyses were performed at critical cross-sections of all gearshafts. shear force and bending moment diagrams were constructed using the gear meshing loads and the reactions at the bearings as input. The reactions at the bearings were derived from high speed roller bearing analyses using the A. B. Jones program. The analyses, in general, showed high margins of safety for each gear shaft in the current design.

Because of the complexity of the conical-box shaped gear blank design and the concentrated applied loads at the edge, the deflections and the maximum stresses for the face-down gear shaft and the face-up gear shaft can not be easily solved by equations. Analytical methods for evaluating the strength and the stiffness of the conical plate or the conical box configurations are commonly required in bevel type gear design, face gear drive (loaded by the separating force), and the helical gear design (loaded by the thrust force). Therefore, a parametric study of the gear blank structures using the finite element method was conducted. Fatigue analyses were carried out for the ring gear structure, which is subjected to cyclic load in normal operation. The analyses were conducted at the planet spindle and at the critical section near the lubrication holes of the carrier plate. Design criteria used in performing all analyses are listed below.

IV.D.1 Design Criteria and Loads for Gear Shaft Analysis

Ultimate Horsepower:

a. Ultimate HP for the first stage is based on (OEI Power) * 1.5

OEI Power: One Engine Inoperative Horsepower
MCP: Maximum Continuous Horsepower
OEI Power = 1.2 * MCP = 1.2 * 2500 HP = 3000 HP
Ultimate Power = 3000 HP * 1.5 = 4500 HP

b. Ultimate HP for the combining stage and the planetary stage is (twin engine MCP) * 1.5

5,000 HP * 1.5 = 7,500 HP

c. Ultimate HP for the NOTAR and accessory drive

563 HP * 1.5 = 844.5 HP

Fatigue Analysis:

For adequate fatigue strength, gearshafts are to be designed for infinite life at the following loads:

a. For Gear Shafts S1, S2, and S3

(50% $\pm$ 50%) * (OEI Power)
(50% $\pm$ 50%) * 3000 HP = 1500 HP $\pm$ 1500 HP

b. For Gear Shafts S4, S5 and Other Planetary Stage Components

(50% $\pm$ 50%) * (twin engine MCP)
(50% $\pm$ 50%) * 5000 HP = 2500 HP $\pm$ 2500 HP

c. NOTAR and Accessory Power Drive (Shafts S6 and S7):

(50% + 50%) * (NOTAR/Accessory Drive MCP)
(50% + 50%) * 563 HP = 281.5 HP + 281.5 HP

Such a loading also represents the GAG (ground-air-ground) condition as the spectrum for fatigue life calculation.

Material Properties:

The material properties for 9310 Steel, CEVM per AMS 6265, Rc 33-41 Core used in AH-64 Drive System Fatigue Analysis are

F_{tu} = 150 ksi
F_{su} = 90 ksi
F_e = 30 ksi (design endurance limit)

A summary of gear shaft stress analysis is shown in Table 13.

Table 13. SUMMARY OF GEAR SHAFT STRESS ANALYSIS

Components	Type of Stress	Margin of Safety
Input Pinion Shaft		
Most critical shaft section	Torsion	+2.75
Spline section	Torsion	+2.35
Face-down Gear Shaft (FEA)		
Web	Combined stress	+7.24
Most critical shaft section	Combined stress	+11.5
Face-up Gear Shaft (FEA)		
Web	Combined stress	+16.22
Most critical shaft section	Combined stress	+11.5
Collector Gear to Sun Gear Shaft		
Most critical web section	Torsion	+4.65
Most critical shaft section	Torsion	+2.45
Planetary Stage, Ring Gear	Hoop stress (fatigue)	$S_{alt} < F_e$(*)
Planet Carrier		
Most critical shaft section	Torsion	+1.186
Most critical web section	Torsion	+1.62
Weight-reduction hole	Stress concentration	+1.06
Planet spindle	Bending	+4.47
For all of the above	Fatigue	$S_{alt} < F_e$
NOTAR/Accessory Power Drive, Idle Shaft		
Most critical shaft section	Combined stress	+6.747
NOTAR/Accessory Power Drive, Output Shaft		
Most critical shaft section	Combined stress	+1.07
Spline section	Torsion	+0.783

Note: (*) S_{alt} - Calculated alternate stress
F_e - Adjusted endurance limit (considering the effect of mean stress)

IV.E MASS PROPERTIES ANALYSIS

IV.E.1 Introduction

This report details the history and results of generating the weight estimates for the Advanced Rotorcraft Transmission (ART) design concept formulation. Parametric weight estimation methodology was used to size the design concept followed by a UGII volumetric mass properties analysis using the R800-0001 drawing file. This then was added to the main rotor driveshaft, static mast, lube system, and miscellaneous component weights resulting in a total installation weight. The total installation weight for ART can then be assessed against the current status of the design. The latest weight status shows that there is still enough buffer to meet the weight goals.

IV.E.2 Summary Profile and Outline of ART Weight Goals

The following summary table profiles the original drive system weight estimate prior to incorporating advanced technology, the ART weight goal incorporating the 25 percent weight reduction, and the current volumetric weight estimate.

The baseline helicopter is the Army AH-64 Apache upgraded to FAR requirements as described in the Baselines and Allowables section. The industry weight trend for a 5000 HP helicopter main transmission with an Apache main rotor speed of 289 rpm is 1792 lb. This in turn results in a weight goal for the Advanced Rotorcraft Transmission, with a 25 percent weight reduction, of 1344 lb. Additional component breakout as shown in Table 14 is the result of approximating to the AH-64A Drive System component relative weights.

TABLE 14. ART WEIGHT PROFILE

Component	Original Parametric Weight (lb)	ART Goal Weight (lb)	Current Volumetric Weight (lb)
ART Transmission Assembly	1347	1010	815
Main Rotor Driveshaft	143	105	115
Static Mast	112	95	102
Lube System (not including oil)	120	80	83
Miscellaneous Components	70	54	55
Total Install Weight	1792	1344	1170

The parametric weight estimation methodology which was used to estimate the weight of the drive system major components was derived and documented in Reference [7]. This methodology is based on a stage-by-stage dimensional analysis. The methodology used 39 gearboxes in the derivation process resulting in a standard deviation of 9.3 percent. The method estimates the weight of the gears, pinions, bearings, supports, and case (in effect, a 'dry gearbox'). The weight estimation methodology was correlated to the AH-64A main transmission. The uncorrected weight estimate was 6 percent greater than actual.

A parametric weight check was performed using the Advanced Rotorcraft Transmission design and dimensional inputs to generate a weight profile of the gearbox arrangement. A total composite of this analysis is shown on Table 15. This total weight (1036 lb) is equivalent to the ART transmission assembly weight goal of 1010 lb (refer to Table 14). The purpose of this exercise is to show parametrically that with the dimensional inputs of the ART transmission assembly, the weight goal is achievable.

TABLE 15. ART TRANSMISSION ASSEMBLY PARAMETRIC WEIGHT CHECK

PARAMETRIC WEIGHT CHECK SUMMARY SHEET	
Component	**Weight (lb)**
Input Stages (2) Input Gears** (2) Combining Gear (1) Combining Gear Pinions (3) Planetary (1)	147.0 111.4 243.5 117.8 416.7
Total Parametric Weight	1036.4
**Input Gears weight determined by the following operation:	
Input Stages (2) Remove Input Pinions (2)	147.0 -35.6
Input Gears (2)	111.4

IV.E.3 Volumetric Weight Analysis

A volumetric weight analysis was completed using the existing ART Unigraphics model (R800-0001). The approach taken was to analyze only those components which were comparable to the parametric equation. Components calculated include all main transmission gears, pinions, associated bearing assemblies with supports, and the case surrounding these components. The components calculated (ART transmission assembly) represents approximately 70 percent of the total installation weight.

The general procedure followed to obtain the component volume for weight calculations is as follows. A majority of the transmission components are currently modelled in 2D only. To obtain volumes, those parts which were symmetric were revolved about their axis. These parts included all gears, pinions, shafts, bearings, bearing races, etc. For those parts which were not symmetric, in particular the housing, a cross-sectional area was obtained and then extended the appropriate length to obtain the volume.

To save time, some compromises were made in the volumetric analysis. For example, those component areas which contained numerous fillets and bends were simplified with straight line segments. For those components which were non-symmetrical, average cross-sectional areas were sometimes taken. An attempt was made to never remove material with these approximations. Depending on the complexity of the component and number of approximations used, a percentage of the calculated volume was added to account for undefined areas before the weight calculation was performed.

IV.E.4 Conclusions

The current status of the ART mass properties is shown in Table 16.

TABLE 16. ART VOLUMETRIC WEIGHT SUMMARY

Component	Current Weight (lb)
ART Transmission Assembly	815
Main Rotor Driveshaft	115
Static Mast	102
Lube System (not including oil)	83
Miscellaneous Components	55
Total Installation Weight	1170
Installation Goal Weight	1344
Weight buffer to Date = 15%	

Table 17 provides a detailed weight breakout for the transmission assembly weight shown in Table 16. All the weights shown were generated through calculations on the UGII from drawing R800-0001. Additional installation weight increases of 10 percent were included and noted on Table 17 as appropriate.

TABLE 17. ART GEARBOX DETAIL WEIGHT

Find No.	Dwg Zone	Description	Material	Volume/Part (cu in)	Density (lb/cu in)	Wt/Part (lb)	Qty	Total Wt (lb)	Miscellaneous Comments
1	5A	Assembly, Transmission (2→15, 35,59,73,75)					1	815.21	
2	6A	Assembly, Lower Housing (18,28,33,39,48,67,69,79,85,86)				121.96	1	134.16	+10% for nuts, bolts, etc.
3	7A	Assembly, Input Quill (80→84, 87→89, 92→94, 98→104, 113,114,119)				11.56	2	25.44	+10% for nuts, bolts, etc.
4	4B	Assembly, NOTAR Drive (19,20→22, 24,25,27,34,40,43,68)				18.04	1	19.85	+10% for nuts, bolts, etc.
5	4C	Assembly, Spur Gear Shaft (29,30,32,44)				3.09	1	3.09	
6	4D	Assembly, Middle Housing (17,31,66)				31.67	1	34.84	+10% for nuts, bolts, etc.
7	5E	Assembly, Upper Housing (16,72,78, 120→122)				18.82	1	20.71	+10% for nuts, bolts, etc.
8	5E	Assembly, Carrier (70,71,74,76,77)				268.21	1	268.21	
9	6E	Assembly, Sleeve (36,54,55)				5.60	1	5.60	
10	6C	Assembly, Sun/Combining Gear (37,38,41)				78.41	1	78.41	
11	6B	Assembly, Clutch (91, 95→97, 105→112, 115→118)				6.01	2	13.22	+10% for nuts, bolts, etc.
12	7D	Assembly, Face-Down Face Gear (49,50,63,64)				38.21	2	76.41	
13	8D	Assembly, Face-Up Face Gear (45,46,49,50)				42.09	2	84.19	
14	3D	Assembly, Main Oil Pump (51→53, 57)				3.15	1	3.15	

TABLE 17. ART GEARBOX DETAIL WEIGHT (Continued)

Find No.	Dwg Zone	Description	Material	Volume/Part (cu in)	Density (lb/cu in)	Wt/Part (lb)	Qty	Total Wt (lb)	Miscellaneous Comments
15	1C	Assembly, Secondary Oil Pump (58, 60→62)				1.52	1	1.52	
16	6D	Upper Housing	Aluminum	154.50	0.100	15.45	1	15.45	
17	6C	Middle Housing	WE 43 Magnesium	350.26	0.066	23.12	1	23.12	
18	6B	Lower Housing	WE 43 Magnesium	1552.78	0.066	102.48	1	102.48	
19	4B	Shaft, NOTAR Drive	4340 Steel	12.86	0.283	3.64	1	3.64	
20	3A	Housing Cover	WE 43 Magnesium	24.15	0.066	1.59	1	1.59	
21	4B	Gear, Face - NOTAR	EX-53 Steel	23.29	0.286	6.66	1	6.66	
22	3C	Bearing, Ball, NOTAR	M-50 Nil Steel	4.94	0.286	1.41	2	2.83	
23									
24	3C	Sleeve	4140 Steel	5.43	0.283	1.54	1	1.54	
25	4C	Screw, Self-Lock	4140 Steel	0.17	0.283	0.05	1	0.05	
26									
27	4B	Nut, Self-Lock	4140 Steel	0.07	0.283	0.02	1	0.02	
28	5A	Bearing, Roller, NOTAR	M-50 Steel	2.11	0.286	0.60	1	0.60	
29	5C	Bearing, Ball, NOTAR Idler	M-50 Steel	5.67	0.286	1.62	1	1.62	
30	5B	Nut, Self-Lock	4140 Steel	0.39	0.283	0.11	1	0.11	
31	5C	Bearing, Roller, NOTAR Idler	M-50 Steel	3.19	0.286	0.91	1	0.91	
32	4B	Screw, Self-Lock	4140 Steel	0.69	0.283	0.20	1	0.20	
33	5C	Liner, Bearing	M-50 Steel	1.84	0.286	0.53	1	0.53	

TABLE 17. ART GEARBOX DETAIL WEIGHT (Continued)

Find No.	Dwg Zone	Description	Material	Volume/Part (cu in)	Density (lb/cu in)	Wt/Part (lb)	Qty	Total Wt (lb)	Miscellaneous Comments
34	3C	NOTAR Drive Flange	4340 Steel	4.00	0.283	1.13	1	1.13	
35	6E	Retainer	4140 Steel	1.84	0.283	0.52	1	0.52	
36	6E	Bearing, Ball, Mast Support	SAE 52000 Steel	2.45	0.286	0.70	1	0.70	
37	6A	Bearing Set, Combining Gear	M-50 Steel	6.39	0.286	1.83	1	1.83	
38	5A	Gear, Combining/Sun	M-50 Steel	266.82	0.286	76.31	1	76.31	
39	5A	Race, Inner	M-50 Steel	8.95	0.286	2.56	1	2.56	
40	3A	Seal, Double Lip	Special	1.08	0.286	0.31	1	0.31	
41	5A	Retaining Ring	301 Stainless	0.96	0.285	0.27	1	0.27	
42									
43	3A	Cap, Screw Retainer	Steel	0.92	0.286	0.26	1	0.26	
44	4C	Gear, Spur-Idler	EX-53 Steel	4.08	0.286	1.17	1	1.17	
45	8D	Gear, Face-Up Face	EX-53 Steel	120.00	0.286	34.32	1	34.32	
46	8B	Plate	4340 Steel	24.30	0.283	6.88	1	6.88	
47									
48	3D	Bearing, Ball, Face Gear	M-50 Steel	13.33	0.286	3.81	2	7.62	
49	3D	Roll Pin	Steel	0.01	0.286	0.00	1	0.00	
50	8A	Coupler, Splined	4340 Steel	3.16	0.283	0.89	1	0.89	
51	3C	HSG, Pump	WE 43 Magnesium	13.16	0.066	0.87	1	0.87	
52	2C	Pump, Main Lube	Steel	7.35	0.286	2.10	1	2.10	Estimated weight

TABLE 17. ART GEARBOX DETAIL WEIGHT (Continued)

Find No.	Dwg Zone	Description	Material	Volume/Part (cu in)	Density (lb/cu in)	Wt/Part (lb)	Qty	Total Wt (lb)	Miscellaneous Comments
53	2C	Shaft, Splined	4340 Steel	0.59	0.283	0.17	1	0.17	
54	4F	Sleeve	4340 Steel	17.12	0.283	4.84	1	4.84	
55	5E	O'Ring	Rubber	1.25	0.040	0.05	1	0.05	
56									
57	2C	O'Ring	Rubber	0.25	0.040	0.01	1	0.01	
58	1C	O'Ring	Rubber	0.15	0.040	0.01	1	0.01	
59	7C	Nut, Self-Lock	4140 Steel	1.18	0.283	0.33	4	1.34	
60	1C	Pump, Secondary Lube	Steel	2.40	0.286	0.69	1	0.69	Estimated weight
61	1C	HSG, Pump	WE 43 Magnesium	9.13	0.066	0.60	1	0.60	
62	1D	Shaft, Splined	4340 Steel	0.79	0.283	0.22	1	0.22	
63	7C	Plate	4340 Steel	22.00	0.283	6.23	1	6.23	
64	7D	Gear, Face-Down Face	EX-53 Steel	108.68	0.286	31.08	1	31.08	
65									
66	2F	Bearing, Roller, Face Gear	M-50 Steel	6.68	0.286	1.91	4	7.64	
67	7D	Bearing, Ball - Face Down Gear	M-50 Steel	7.69	0.286	2.20	2	4.40	
68	4A	O'Ring	Rubber	0.18	0.040	0.01	2	0.02	
69	3E	O'Ring	Rubber	0.14	0.040	0.01	2	0.02	
70	4G	Gear, Planet Pinion	EX-53 Steel	80.07	0.286	22.90	6	137.40	
71	4G	Planetary Carrier	EX-53 Steel	232.00	0.286	66.35	1	66.35	

TABLE 17. ART GEARBOX DETAIL WEIGHT (Continued)

Find No.	Dwg Zone	Description	Material	Volume/Part (cu in)	Density (lb/cu in)	Wt/Part (lb)	Qty	Total Wt (lb)	Miscellaneous Comments
72	4F	Seal, Split Lip	Steel	7.93	0.286	2.27	1	2.27	
73	4E	Spring	Steel	3.70	0.286	1.06	1	1.06	
74	4E	Bearing, Spherical, Planetary	M-50 Steel	36.30	0.286	10.38	6	62.29	
75	4E	Gear, Ring	EX-53 Steel	152.10	0.286	43.50	1	43.50	
76	3D	Cover	2024-T4 Aluminum	0.39	0.100	0.04	6	0.23	
77	3D	Screw Cap	6061-T6 Aluminum	3.29	0.098	0.32	6	1.93	
78	4F	Adapter/Seal Ring	6061-T6 Aluminum	5.60	0.098	0.55	1	0.55	
79	7D	Sleeve, Bearing	M-50 Steel	2.16	0.286	0.62	2	1.24	
80	8A	Nut, Self-Lock	4140 Steel	0.15	0.283	0.04	1	0.04	
81	8A	Gear, Input - Spur	EX-53 Steel	4.72	0.286	1.35	1	1.35	
82	7A	Bearing, Roller, Input Quill	M-50 Steel	2.31	0.286	0.66	1	0.66	
83	7A	Resilient Mount	4340 Steel	0.67	0.283	0.19	1	0.19	
84	7A	Anti-Flail Ring	4140 Steel	1.18	0.283	0.33	1	0.33	
85	7A	Cover, Access	6061-T6 Aluminum	7.66	0.098	0.75	2	1.50	
86	7A	Retainer	4140 Steel	1.80	0.283	0.51	2	1.02	
87	7A	Tube, Spacer	4140 Steel	0.37	0.283	0.10	2	0.21	
88	7D	Screw, Set	Steel				1		Part of installation weight
89	7A	Shaft, Input	4340 Steel	13.40	0.283	3.79	1	3.79	
90									

TABLE 17. ART GEARBOX DETAIL WEIGHT (Continued)

Find No.	Dwg Zone	Description	Material	Volume/Part (cu in)	Density (lb/cu in)	Wt/Part (lb)	Qty	Total Wt (lb)	Miscellaneous Comments
91	7H	Spacer	Steel				1		Part of installation weight
92	7F	Bolt, Hex	Cres				6		Part of installation weight
93	7F	Washer	Steel				6		Part of installation weight
94	7F	Thread Insert	Steel				6		Part of installation weight
95	7F	Ratchet	M-50 Steel	0.17	0.286	0.05	1	0.05	
96	7F	Nut, Lock	Steel	1.44	0.286	0.41	1	0.41	
97	7G	Spring	Steel	0.02	0.286	0.01	1	0.01	
98	7F	O'Ring	Rubber	0.02	0.040	0.00	1	0.00	
99	6F	O'Ring	Rubber	0.02	0.040	0.00	1	0.00	
100	6G	Drive Flange	4340 Steel	4.43	0.283	1.25	1	1.25	
101	6G	Cover, Retainer	4340 Steel	2.45	0.283	0.69	1	0.69	
102	7H	Seal, Magnetic	Steel	1.90	0.286	0.54	1	0.54	
103	6H	Housing Retainer Cap	6061-T6 Aluminum	6.75	0.098	0.66	1	0.66	
104	7H	O'Ring	Rubber	0.14	0.040	0.01	1	0.01	
105	7H	Bearing, Ball, Input	M-50 Steel	1.50	0.286	0.43	2	0.86	
106	7H	Coupler, Splined	4340 Steel	4.90	0.283	1.39	1	1.39	
107	7H	Synchronizer	M-50 Steel	2.21	0.286	0.63	1	0.63	
108	7G	O'Ring	Rubber	0.09	0.040	0.00	2	0.01	
109	7G	Pawl	M-50 Steel	0.10	0.286	0.03	2	0.06	

TABLE 17. ART GEARBOX DETAIL WEIGHT (Continued)

Find No.	Dwg Zone	Description	Material	Volume/Part (cu in)	Density (lb/cu in)	Wt/Part (lb)	Qty	Total Wt (lb)	Miscellaneous Comments
110	7G	Bolt, Hex	Steel	0.05	0.286	0.01	1	0.01	
111	7G	Washer	Steel	0.01	0.286	0.00	1	0.00	
112	7F	Nut, Hex	Steel	0.04	0.286	0.01	1	0.01	
113	7F	Nut, Lock	Steel	0.20	0.286	0.06	1	0.06	
114	7F	Bearing, Ball, Clutch	M-50 Steel	2.40	0.286	0.69	2	1.37	
115	7F	Spacer	4140 Steel	3.40	0.283	0.96	1	0.96	
116	7F	Sleeve	4140 Steel	5.70	0.283	1.61	1	1.61	
117	7G	Retaining Ring					2		Part of installation weight
118	7G	Washer					A/R		Part of installation weight
119	7A	Tube, Lube	4140 Steel	1.40	0.283	0.40	1	0.40	
120	6D	Tube, Lube	4140 Steel	0.86	0.283	0.24	2	0.49	
121	6D	O'Ring	Rubber	0.01	0.040	0.00	8	0.00	
122	6C	Tube, Transfer	4140 Steel	0.12	0.283	0.03	2	0.07	

IV.F SUPPORTABILITY

IV.F.1 Abstract

This section presents the supportability analysis of the Advanced Rotorcraft Transmission (ART) design. Supportability includes Reliability, Maintainability, Survivability/Vulnerability (S/V), and Integrated Diagnostics. The ART program has a reliability goal of 5000 hours Mean Time Between Removal (MTBR). The plan to attain that reliability is outlined as well as an assessment of the ART MTBR. Strategies for increasing reliability during production design are presented. Maintainability, Integrated Diagnostics and Survivability/Vulnerability assessments were completed.

IV.F.2 Introduction

There is a high degree of interrelationship between all design criteria, so a formalized systems approach is taken. This approach is based on the evaluator function, a mathematical model for doing trade studies [17]. The evaluator function provides perspective for choosing design trades. An example of this is the relative merit of a high maintainability/low reliability vs. high reliability low maintainability applied to seal selection.

Supportability includes features of the design that have the highest effect on the operational phase. This phase contains the bulk of the life cycle costs of the unit as shown in Figure 18. To reduce costs, military and commercial customers are paying increasing attention to the supportability features of the design.

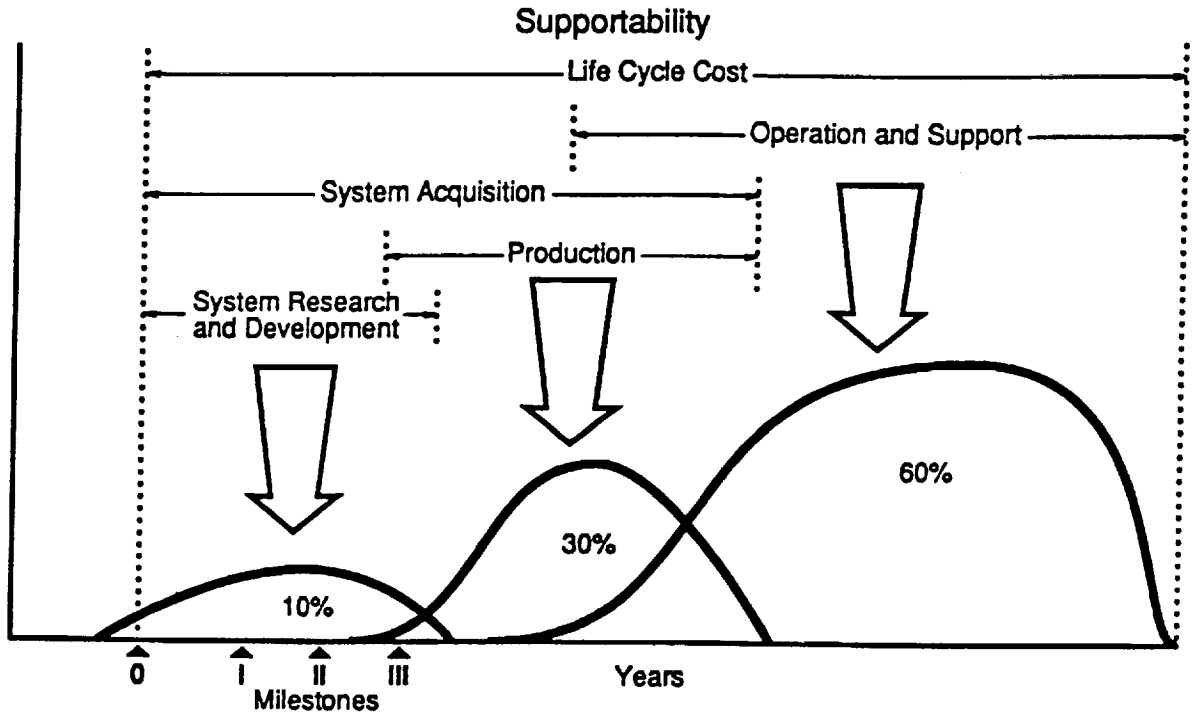

Figure 18. Nominal Cost Distribution of a Typical DoD Program

The following sections focus on the individual disciplines within supportability. They are followed with a discussion of how the individual conclusions relate to one another. The early analysis has been preserved to document the basis of the design decisions. This will be useful during the pre-production design and manufacturing stages in that changes will be made with awareness of the design intent. Loss of design intent is a major issue in concurrent engineering [17].

IV.F.3 Reliability

In the effort to meet weight and performance goals with any given technology, there is a trade-off with reliability. Every excess pound of unnecessary material reduces available payload. Where can design reduce weight and not affect reliability? Which configuration has the best prospects from a reliability standpoint? Transmission design is such that any degree of reliability can be achieved by sacrificing weight, performance and cost. MDHC's method for achieving the reliability goals for the ART was to engineer them in through:

1. Using the established Failure Modes, Effects, and Criticality Analysis (FMECA) procedures (see Appendix B2). Although this is not a production effort, the groundwork is laid for detail reliability evaluation. By staying consistent with the FMECA process, we are ensuring continuity in reliability support should the design go into production.

2. Using concurrent engineering [feed-forward (reliability apportionment) and feed-back (reliability evaluation) cycles].

3. A high degree of communication between designer and engineer during the conceptual design. This is facilitated electronically where efficient, i.e., E-mail.

4. Use of Computer-Aided Engineering codes to automate analysis as much as possible.

The strategy is to base ART reliability on AH-64A reliability. AH-64A reliability is analyzed by failure mode. Prospective improvements designed to reduce selected failure modes are sought and analyzed for their overall impact on the design.

IV.F.3.i Measures of Reliability

Reliability is a critical attribute of helicopter transmissions. There are many measures and criteria of reliability that a transmission must meet. The main criteria used by the military are mission reliability and system reliability. These two criteria are very useful in understanding how an aircraft is performing.

1. Mission reliability is the measure of mission time units (typically hours) divided by the number of critical failures during a stated series of missions. This would include chip lights, high-temperature lights, and failure of basic drive components.

2. System reliability is a basic measure of reliability for repairable items: the mean number of life units during which all parts of the item perform within their specified limits, during a particular measurement interval under stated conditions. Note that this includes all mission-critical failures and non-critical failures such as loss of redundant units and non-critical indications.

ART TASK III, mission analysis reports significant impact of the ART transmission to the helicopter's reliability. At this design stage we are interested primarily in transmission mission reliability, using system reliability and Maintenance-Man-Hours-per-Flight-Hour as a trade-off measure. An example of this was the recommendation to use split seals. The ease and level of maintenance outweighs their inherently lower life.

IV.F.3.ii Reliability Apportionment

Insuring that the ART meets its 5000 hour MTBR requirement is the main goal of reliability's support to design. This is accomplished by apportioning reliability requirements down to the component level. This gives the designer a clear goal. The first level of apportionment is a split between dynamic components which wear out, and more randomly occurring Miscellaneous modes. Existing (AH-64A) Miscellaneous modes are analyzed for frequency, effects and criticality. This leads to design changes which reduce or eliminate them. On acceptance of these changes, the Miscellaneous failure rate is modified. The dynamic components are then apportioned equal L_{10} lives based on the overall reliability goal. This is converted to stress levels for gears. Design then calculates gear stress and converts to L1 or L_{10} life for feedback into the model.

This task must occur early and often in the design cycle. Additionally, the designer and reliability engineer work closely together to:

1. Meet on a regular basis to discuss potential configurations with respect to reliability
2. Identify mission critical components
3. Identify components which would cause a removal on failure
4. Transfer reliability apportionments and implications.
5. Implement Computer-Aided Engineering software specific to the design goals

As the preliminary design solidifies and moves into detail design, the focus of reliability stays with the focus of the current design work. The goal of reliability in detail design includes minimizing the impact of failures of these components on mission-critical systems. The strategy is that component failures will mostly affect system reliability, not require a transmission removal to service, or be extremely unlikely. This is known as the FMECA. There are many good sources for guidances to this strategy, References [12,18,19]. In addition, the reliability engineer should provide alternatives to design that will improve the system's characteristics.

IV.F.3.iii Miscellaneous Failure Modes

The design then progresses to non-dynamic or non-removal-inducing components including seals, clutches, and the lubrication. There is sufficient design and historical data to make a reasonable estimate of the failure rate due to failure modes which have not been designed out [20]. This provides input to the reliability model, and a basis for design to reduce these failure modes. The data was collected and analyzed in the following maintainability section. Please refer to Figure 19 for the failure modes used in the following analysis. Other failures are unknown and missing data records. Phase inspection removals are due to a discrepancy during a detailed inspection (the exact reason is not listed). The causes of these Other removals are assumed to be distributed like the rest of the population. Therefore the other failure rates are increased by the percentage:

$$\frac{\text{Total}}{(\text{Total-Other})}$$

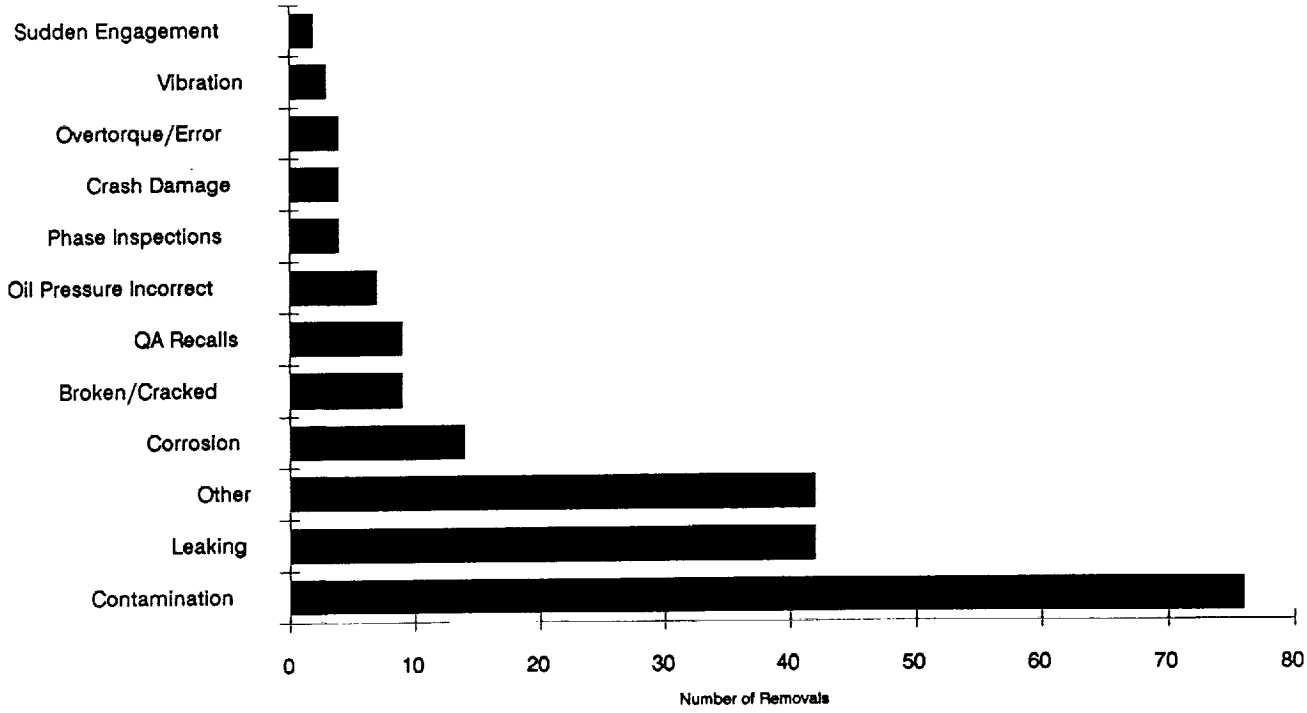

Figure 19. Reasons for Transmission Removals

Excessive Vibration is a sign of dynamic component wear. This modes are covered in the following section on dynamic components.

Oil Contamination is due to water, dust and Foreign Object Damage (FOD). This is eliminated by the desiccant breather, and complete sealing. The new clutch design eliminates wearout of the sprags, another contributor to oil contamination.

Leaking is due to seals and housing split failures. Only one seal in the ART design is not field-replaceable. Reliability criteria for seals will primarily affect the transmission's maintainability and operating cost (since seals are field-replaceable). Housing spilt leaks are avoided by using tighter bolt spacings. The estimated reduction of these failures is 90%.

Broken/Cracked housings, flanges and other structure failure rate may be improved by increased testing. These failures are most likely due to unexpected loads or overloads. A thorough test program should include housing load testing, i.e., flanges, supports, etc. In addition, the ART has fewer interfaces where these failures can occur. These modes are reduced 90% for ART reliability estimation.

Q/A recalls, Crash, Overtorques, Sudden engagement and Maintenance errors are induced modes that are not inherent to the design. They are deleted from the calculation.

Oil Pressure Incorrect modes are failures of the lubrication system. The AH-64A transmission's lubrication system is considered highly reliable. This failure mode and frequency of occurrence will conservatively be left in at 100 percent. Corrosion failures will be reduced at least 50% by following recommendations in the maintainability section. The results of this analysis are presented in Table 18 and Figure 20.

Failure rates for the ART transmission are predicted at .0000789 which is equal to 12674 hours MTBR. This is not as good as we had hoped for (25,000 hours MTBR), but better than our expectations(10,000 hours MTBR). The most difficult part about reducing non-dynamic component failure rates is knowing what they are. Once they are identified, it is easy to fix them unless you are already in production, in which case it is nearly impossible.

IV.F.3.iv MTBR evaluation

The ART has a requirement of 5000 hours MTBR. To provide design guidance and a criteria to evaluate the design, the following assumptions and conditions were made:

Assumptions

1. The criteria applies to main rotor drive system only. Includes main transmission and accessory take-off, but not accessory gearbox and tail-rotor drive.

2. Only failures due to contact stress need to be considered. All other types of failures (corrosion, tooth bending, etc.) will be essentially designed out or are covered by the Miscellaneous failure rate.

3. An allowance of .0000789 failures/hour is made for Miscellaneous failures.

4. The MTBR is approximately the Mean Time To First Failure. When a transmission fails, is removed for overhaul, and returned to service, that transmission will be equivalent to a newly built transmission.

5. The optimum transmission will have equal component L_{10} lives. The transmission's reliability will be affected most by the component with the lowest life. There is little value in having a transmission with all very reliable components except one. L_{10} lives are chosen since they are close to the expected life of the transmission, and failure distribution shapes will have little effect on accuracy.

6. All component failures are modeled as Weibull distributions. The Weibull distribution is a good fit for a wear-out failure distribution. The shape parameters used are:

Gears	2.5
Bearings	2.5

7. Any component failure causes a system failure. System reliability is the product of component reliabilities.

TABLE 18. MISCELLANEOUS FAILURES AND FAILURE RATES

Type of Failure	Count	Percent Occurrence	Apache Failure Rate * 1000	Reduction factor	ART Analysis Failure Rate * 1000
Contamination	76	44.7	.3144	0	0
Leaking	42	24.7	.1737	.1	.0174
QA recall	9	5.3	.0372	0	0
Crash damage	4	2.4	.0165	0	0
Oil Pressure Incorrect	7	4.1	.0290	1	.0289
Overtorque/ maintenance error	4	2.3	.0166	0	0
Corrosion	14	8.2	.0579	.5	.0289
Excessive vibration	3	1.8	.0124	0	0
Broken/Cracked	9	5.3	.0372	.1	.0037
Sudden engagement	2	1.2	.0083	0	0

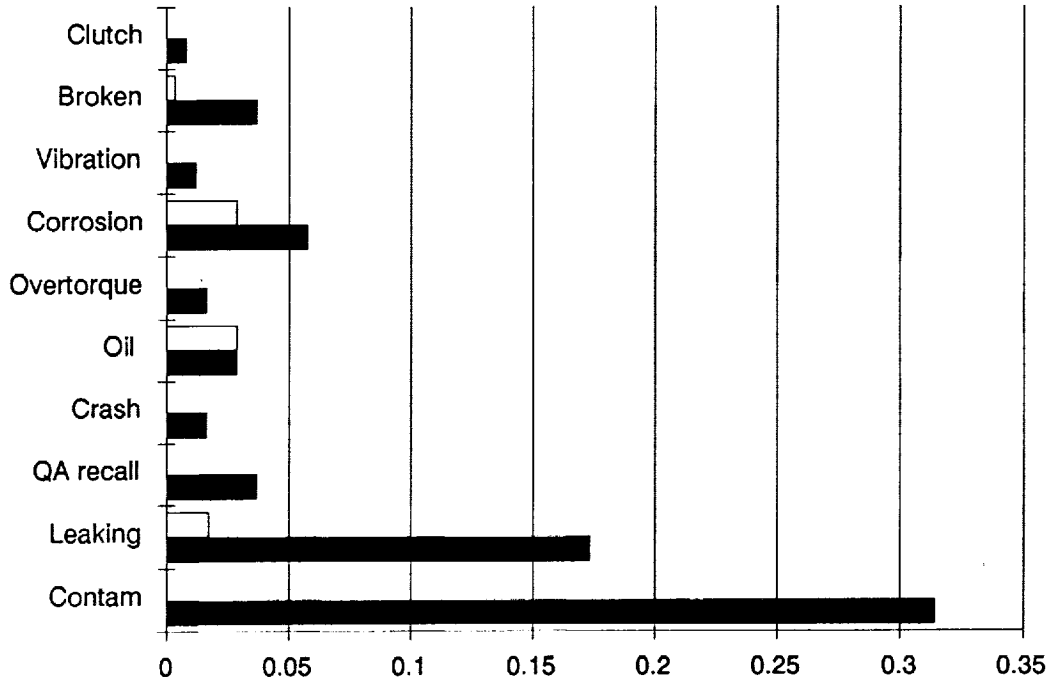

Figure 20. ART (top) vs. Apache Miscellaneous Failure Rates

Conditions

Constraints on design imposed by reliability so that the design can meet it's goals:

1. Seal failures are field-replaceable. The use of seal housings and field replaceable interface shafts to facilitate replacement appears feasible except at the main rotor output. This has been taken into account in the Miscellaneous failure rate.
2. The lubrication system will have extremely high reliability. Lube systems are not currently prone to failure. Using redundancy, Integrated Diagnostics and proven components will further improve reliability.
3. The clutches will have very high reliability or will not induce a removal when they fail. This is considered not necessary at this time as this clutch has been proven in many hours of non-helicopter operation.

Component L_{10} life required

Component L_{10} life is the number of hours of operation of a component at which the probability of having failed is 10%. Component L_{10} life is the basic measure of reliability used in the ART reliability analysis. Component L_{10} life is a function of the number of each of the types of components. (See Appendix B1 for a discussion of the mathematics.)

Using the values provided by design, a component L_{10} required life of 14,100 hours was found. Design was asked to work to a 15,000 hour L_{10} life for all components.

Calculating Component Lives

Component lives are functions of geometry, materials, speed and force. These parameters are generally fixed by design except force (torque). Torque is a characteristic of transmission operation that greatly affects life and reliability. MDHC Reliability, therefore, has studied helicopter mission spectrums to improve the accuracy of reliability predictions. The results are that a factor of Maximum Continuous Power (MCP) for each type of component has been developed. This factor is known at MDHC as the Life Equivalent Power (LEP) factor. This factor applies to the torque or horsepower used in determining the life of a component. The LEP factor accounts for the reaction of the component to the spectrum of loads that the component sees over its life.

Life Equivalent Power (LEP)

The ART mission spectrum is based on the AH-64A transmission. The primary difference is that the ART will be subject to a greater dynamic range. That is, the ART will have a greater amount of reserve power available for combat and emergency maneuvers. The ART will have a lower LEP percentage than the AH-64A. It is conservative to use the AH-64A LEP percentage. The AH-64A loads are converted to percentages for application to ART design. Separate load-life factors are used for different materials and applications.
This analysis is intended to provide a dual engine power number that can be used to calculate fatigue life in the drive system. Because aircraft are used differently, and torque is not recorded, individual aircraft fatigue lives will vary. This analysis is limited to available data: the primary mission spectrum and engineering test data. Also, the load-life exponent for gears traditionally used by AGMA is challenged by recent NASA research.

Load-Life Relationship

The common use S-N equation:

$$S = N^P * K$$

and the definition form of the load-life relationship:

$$N = (C/F)^p$$

are the same when $C = qK$, $p = -1/P$, $F = qS$ where q is a units conversion constant

The AGMA published S-N curve is a load-life relationship for gears that has been in use and widely accepted for years. The AGMA load-life exponent is 17.2 (Figure 20) [12]. NASA research determined the load-life relationship for AISI 9310 spur gears to be 4.3 [18]. A long accepted load-life exponent for bearings is 3 for ball type and 10/3 for roller type [19].

L1 Life equations describe a trade-off of load vs. life for a given reliability. There is no infinite life. This relationship allows varying torque levels to be combined into a Life Equivalent Power.

The LEP is a generality of the Root Mean Cube (RMC) power. The RMC power is equivalent to the LEP when the load-life exponent (p) is 3.

The numbers 3 and 17.2 therefore bound the load-life exponent for this analysis. Lower numbers indicate less sensitivity of life to maximum spectrum load.

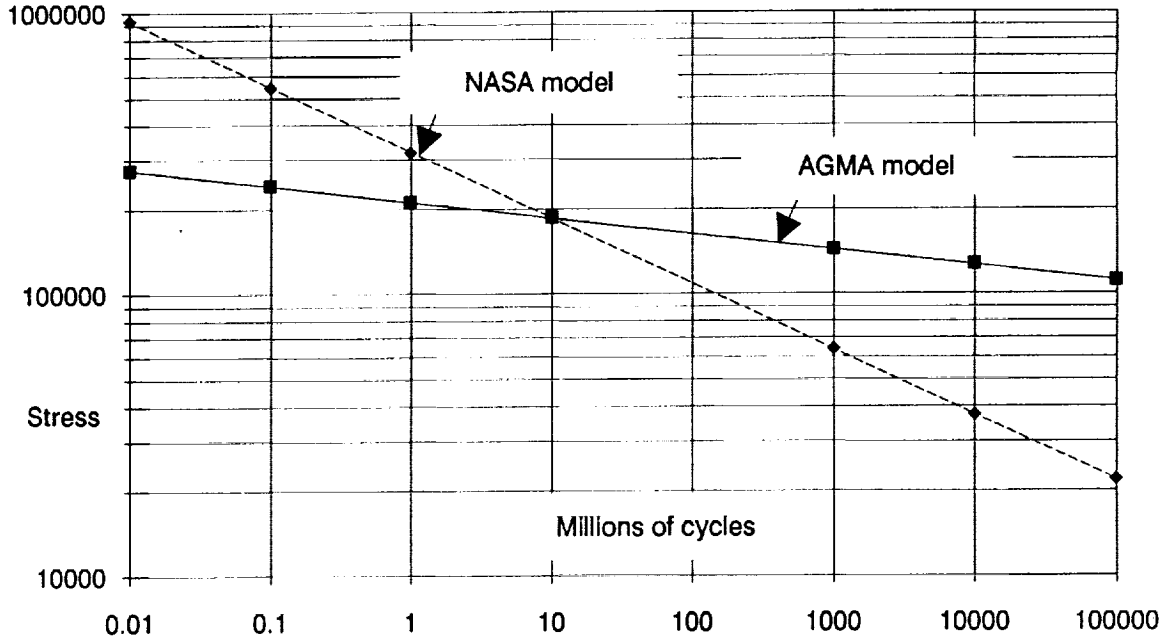

Figure 21. S-N Curve for AGMA and NASA

Mission Spectrum Averaging

To determine the fatigue life of a component or system which is not run at a single power level, the Palmgren-Minor linear damage rule is used. This rule states that the varying power levels can be combined by determining the fraction of life consumed at each power level. The fraction is the number of cycles at the load over the allowable cycles at that load. The fractional lives at differing power levels are then added up. For L_{10} lives:

$$L_e/l_{10,e} = l_1/l_{10,1} + l_2/l_{10,2} \cdots + l_n/l_{10,n}$$

The life equivalent power is obtained by setting N in the load-life equation to the L_{10} life, and then substituting. Solving for Fe:

$$F_e = [\ (\text{sum}\ (F_i^p * N_i) / \text{sum}\ (N_i)\ ]\ 1/p = LEP$$

AH-64A LEP

The AH-64A Apache has a Max Continuous Power (MCP) of 2828 HP. The AH-64A Apache primary mission [21] (Table 19) defines the power spectrum. The numbers for power were compared to the engineering test data, Reference [22]. It was found that for the flight conditions listed in the primary mission, the power usage was accurate to within a few percent.

Since the ship flies other profiles besides the primary mission, a few other curves were generated using the primary mission along with other flight profiles. This is an attempt to generate the most plausible power usage profile and come up with a more accurate LEP. The effect of mission spectrum and load-life factor is analyzed in Figure 22.

The base profile (0) is the primary mission spectrum. It is highly unlikely that any ship flies only the primary mission for its entire life.

Profile 1 includes the reserve as listed on the primary mission. The 30 minutes of best cruise represent deployments and other non-critical operations.

Profile 2 includes 3 hours best cruise for every mission. This is the low-usage spectrum. To provide an upper bound, the primary mission and 5 minutes of MCP was used (Figure 22, Profile 3). The highest and lowest profile was combined to produce a profile of mostly cruise with a few minutes of MCP (Figure 22, Profile 4).

The curves have different slopes in Figure 22, because the high operating points tend to dominate as the load-life factor increases.

	Load-Life Factor	LEP Factor
Gear Bending	31.0	88
Gear Compressive	17.2	80
Ball Bearing	3.0	65
Roller Bearing	3.33	66

ART LEP

The ART profile is obtained by scaling up the AH-64A Apache profile by 5000/2828. Applying Mission spectrum averaging to the profile using the component load-life exponents yields the component LEP factor. For gears, AGMA-based numbers were used since the NASA data does not extend out to the very high cycle counts required by 5000 hours operation.

TABLE 19. LIFETIME POWER PROFILES

	Profile	Primary	w/res	w/ferry	w/mcp	w/ferry & mcp
		0	1	2	3	4
Maneuver	HP					
warmup	2063	8	8	8	8	8
cruise A	1431	15	15	15	15	15
cruise B	1127	6	6	6	6	6
hover A	2201	12.5	12.5	12.5	12.5	12.5
cruise C	2508.2	5	5	5	5	5
cruise D	1188	15	15	15	15	15
cruise E	957	6	6	6	6	6
hover B	1843	12.5	12.5	12.5	12.5	12.5
reserve	1285		30	180	0	180
MCP	2828				5	5

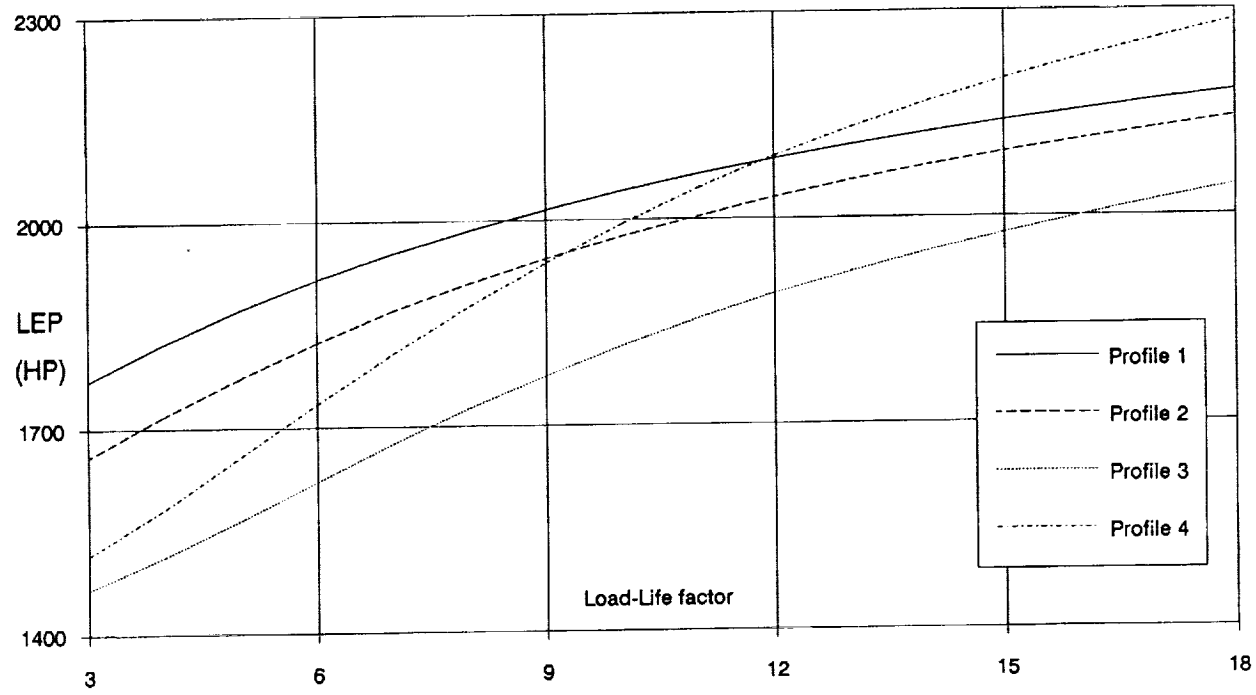

Figure 22. Effect of Load-Life Factor on Life Equivalent Power

Because drive systems consist of many different materials and components which react differently to varying mission profiles, LEP is a function of component and type of stress. For gears, assurance that bending failures will not occur is obtained by the requirement that an ultra-high (1.5) reliability factor be used. This results in less than 1/10,000 bending failures over the 15,000 hour life of the transmission, and during a 30 minute One Engine Inoperative (OEI) event per gearset.

Component Design Requirements

Translating from the above conditions to design requirements requires component-specific calculations.

Bearing lives are generated using Anti-Friction Bearing Manufacturers Association (AFBMA) standard section 9, with factors for improved materials and lubrication. As the design progresses, the predictions are refined by using the more sophisticated A.B. Jones program. This program takes shaft lengths, temperature, and lubrication film thickness into account.

Gear lives are calculated using AGMA standard methodology. The total number of cycles required is calculated:

$$\text{Cycles} = 15{,}000 \text{ hours} * 60 \text{ min/hour} * \text{rpm} * \text{Cycles/rpm}$$

The cycles required are used to obtain a pitting resistance life factor Cl:

$$C_l = 2.466 * \text{cycles}^{-.056}$$

The contact stress allowable (S_{ac}) is then modified by Cl.

$$S_1 = S_{ac} * C_l$$

This yields the L1 life stress allowable for use as input to the ART reliability model. In the late stages of design, the MDHC stress analyst refined these calculations and delivered L_{10} life directly to the reliabilty engineer.

Automation of the Reliability Process

A computer model of transmission reliability was developed using an equation-solving software. The model relates critical component lives to overall transmission MTBR. The software allows what-if analysis and constraint solving. The transmission was modeled to obtain reliability requirements expressed as L1 or L_{10} lives. Then as the design progressed, the predicted lives were fed back into the model to evaluate the design. This allowed fine tuning the design for minimum weight. The impact of going to twelve vs. six planetary bearings, an additional face gear bearing, and using different weibull parameters were among the trades studied. The additional bearings did not impact the design very much (<1% change in component L_{10} life required) and was adopted. The use of different Weibull parameters had a great impact on the required component L_{10} lives. It is important for continuing work that the shape parameter be as accurate as possible.

Another possibility studied was the two stage design recommended after the results of the face gear testing done at NASA-Lewis. This concept reduces the parts count by 8 gears and 15 bearings. The required L_{10} life is reduced by 27.1%. This increases the allowable stresses by 1.02%. Unfortunately, this is not enough to overcome the weight penalty due to the very large gear sizes. This design will be kept in mind as further face gear data becomes available.

Using the data in Table 20, the MTBR of the finalized transmission design was calculated.

This results in an L50 system life of 5927 hours and an MTBR of 6269 hours (Figure 23). Although the accuracy is not 100 percent, this analysis demonstrates that the design is definitely on track.

TABLE 20. RELIABILITY PARAMETERS FOR CALCULATION OF ART MTBR

Gear L_{10} hours	Number	Bearing L_{10} hours	Number	Miscellaneous Failure Rates
8200000	2	50000	4	.000017379
8600000	2	50000	4	.0000289
62800000	2	50000	2	.0000289
8660000	2	28315	2	.00000372
62800000	2	22484	2	
10600000	1	44256	2	
971000	1	21926	2	
2240000	1	50000	1	
12287000	6	50000	1	
1.3E9	6	50000	1	
6.5E8	1	16629	6	
87216	1	20000	1	
5602	1	14735	1	
17181	1	21379	1	
		39409	1	

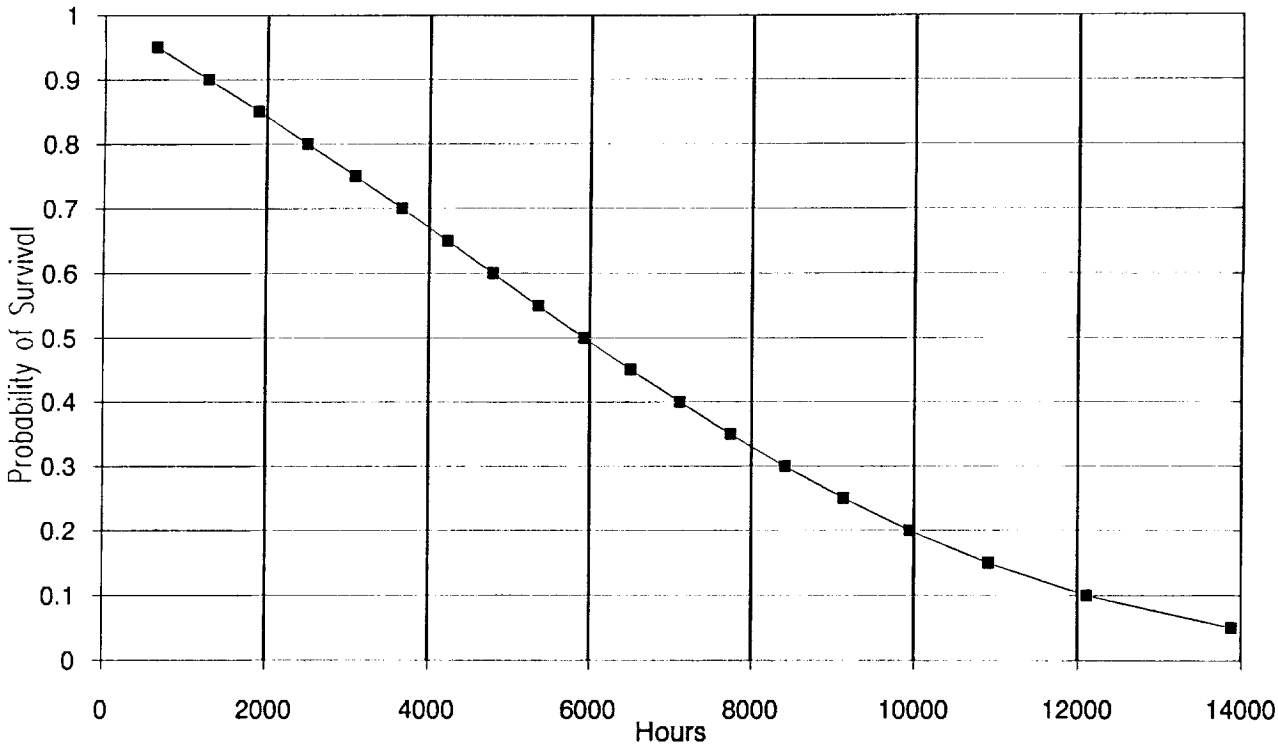

Figure 23. ART Reliability vs. Hours

IV.F.4 MAINTAINABILITY

This section contains maintainability information and analysis applicable to the design of the ART, and focuses on feedback from the field. Expert maintenance personnel have identified specific problem areas that are helicopter transmission maintenance drivers. They have made suggestions based on their day-to-day experiences maintaining transmissions. Figure 24 presents the most common discrepancies found during transmission overhaul [23,24]. When a transmission comes in, these are the most commonly found discrepancies. Notice that there are many more discrepancies found than the primary reason for the transmission removal. This additional maintenance is often due to problems induced by the removal: missing hardware, gouges, or wires cut. Therefore, removal avoidance is a big issue. We have used these expert customer comments with a statistical analysis of transmission failures to determine the major maintainability issues. This section includes:

1. Design criteria
2. Failure mode history of similar hardware from the AH-64A Apache helicopter ranked by frequency of occurrence. The design should minimize the effect and impact of these potential failures (see Figures 19, 25, 26, and 27).
3. Aggressive maintainability Line Replaceable Unit (LRU) recommendations.
4. Maintainability analysis and evaluation of the design.

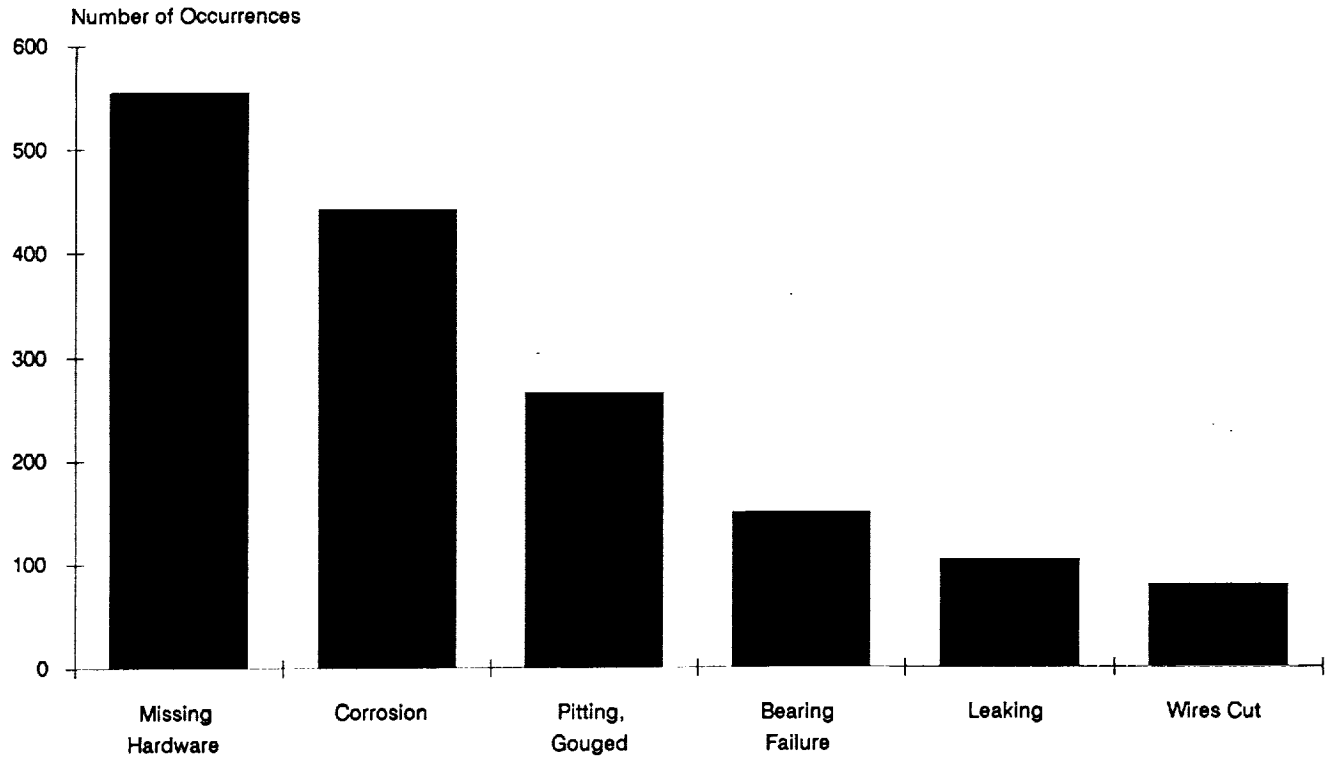

Figure 24. Most Commonly Found Discrepancies

IV.F.4 1 Design Criteria

1. The equipment shall represent the least complex design consistent with functional requirements and expected service conditions.
2. The ART shall be designed so its operation, maintenance and repair can be accomplished by personnel with a minimum of training.
3. All ART component's removal/installation shall be accomplished with the use of common tools from the maintainer's toolbox and existing handling equipment.
4. Components with the highest predicted failure rate (lowest MTBR) shall be most accessible.
5. The ART system design shall be such that the replacement of a failed LRU does not require the removal of a non-failed component for access.
6. Where seals are used within the system, they shall have an operational life equal to or greater than the operating life of the component that requires the seal. (See Seals)
7. All mounting hardware shall be standardized to match that used throughout the aircraft.
8. All components of the ART system shall withstand exposure to a salt-sea atmosphere, sand/dirt particles and humidity conditions up to 100%.
9. Component MTBR should not be degraded due to a 6 month storage, nor should there be maintenance or restoration required prior to installation on an aircraft.

Figure 20 presents reasons for transmission removals. Each of these removal categories show the way that we improved our design to reduce failures leading to removals; and the amount of that improvement will be described.

Contamination

Of 218 AH-64A transmissions returned to depot, 76 of them were removed for contamination as illustrated in Figures 25 and 26. Twenty-four of these had inadequate data to determine the original cause of the contamination. Of the 48 transmissions removed for oil contamination and where the source of the failure could be determined, 34 of these were caused by the Accessory Gearbox (AGB) and its accessories. These are primarily due to the Shaft Driven Compressor (SDC) and the Auxiliary Power Unit (APU). Contamination is due to dynamic component wear, internal corrosion, and insufficient sealing.

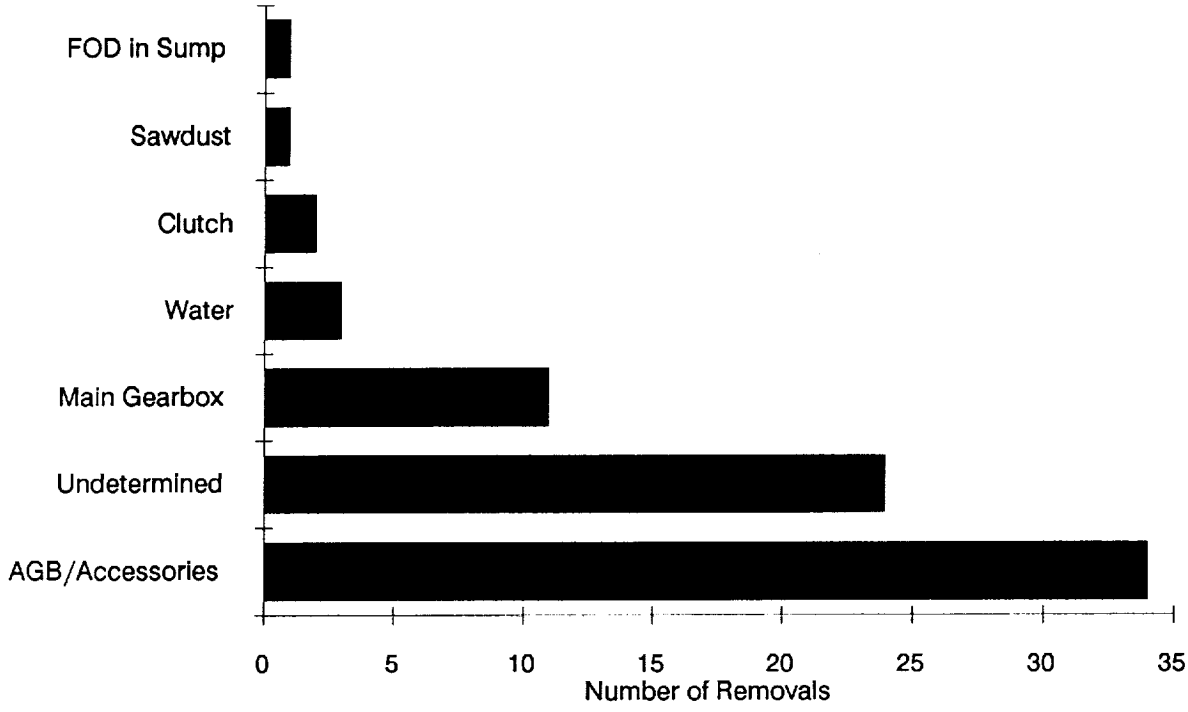

Figure 25. Causes of Contamination

SDC induced Damage

SDC failures cause secondary failures of the transmission. These failures are due to increased wear of the input drive quill and to contaminated oil which is shared between the SDC and the transmission.

1. Contaminated oil. Lubrication systems for the transmission should be separate from all other components. Internal failures of the SDC have caused secondary failures within the transmission due to the oil supply shared between the AGB, SDC, and transmission.
2. Bearing failures. Secondary failure of bearings within the transmission can occur when externally mounted units fail. Failures of the SDC have caused failure of the bearings that support the quill shaft drive for the SDC and the generator.

APU Induced Damage

Teardown of transmissions at depot have revealed failure of the APU gear in the AGB. These failures were caused by an overtorque condition external to the transmission. Depot experts believe that the APU power take-off clutch is grabbing or slipping, causing an overtorque condition.

Recommendations

1. Modularize the AGB.
2. Use separate lubrication systems for the AGB and the main gearbox.
3. Monitor vibration of all accessories. (See Integrated Diagnostics)
4. Drive splines should be isolated and sealed from the gearbox so accessories may be removed and replaced at field level.

Evaluation

The AGB has been separated from the main transmission. This reduces the high-speed seal count by 4.

The lube system improves on the AH64A's design in the following ways:

1. Three micron fine filtration keeps particles from damaging the dynamic components.
2. Screens at the oil ports keep contaminants out during maintenance.
3. The Desiccant/breather keeps water from getting inside the gearbox to significantly reduce internal corrosion.
4. The Quantitative Debris Monitor generates a current pulse proportional to the mass of the captured particles. The electronics package then converts the signal into diagnostic data suitable for expert system processing. This information is used for detecting failure onset, severity, and progression rate.

Contamination was eliminated from the Miscellaneous Failure Mode calculations and represented under Dynamic Component wearout.

Leaking

Leakage problems are the second highest cause for removal of the AH-64A transmission (see Figure 26). The top four failed seals are lip seals in the AGB. External seals of helicopter gearboxes have not been designed as field replaceable items, but seal replacement has usually been assigned to Aviation Unit-level Maintenance (AVUM) level for cost reasons. These seals are often installed incorrectly, damaged during installation, or allow gearbox contamination during seal replacement.

Lip seals

Lip seals are inexpensive relative to carbon face seals. The AH-64A experienced poor reliability of the lip seals until they were upgraded to the spring-loaded type. This improvement helped, but did not solve the problem.

Because lip seals wear a groove in turning shafts, seal replacements often sit in the original groove, and do not seal.

Carbon seals

Carbon seals are expensive and difficult to install. The carbon seal on the AH-64A engine input quill has a failure rate which is tied with two lip seals for the third highest failing seal. Even highly skilled aircraft mechanics misunderstand the carbon seal after years of experience with it. This seal works best when there is a reservoir of oil behind the seal which must be held back.

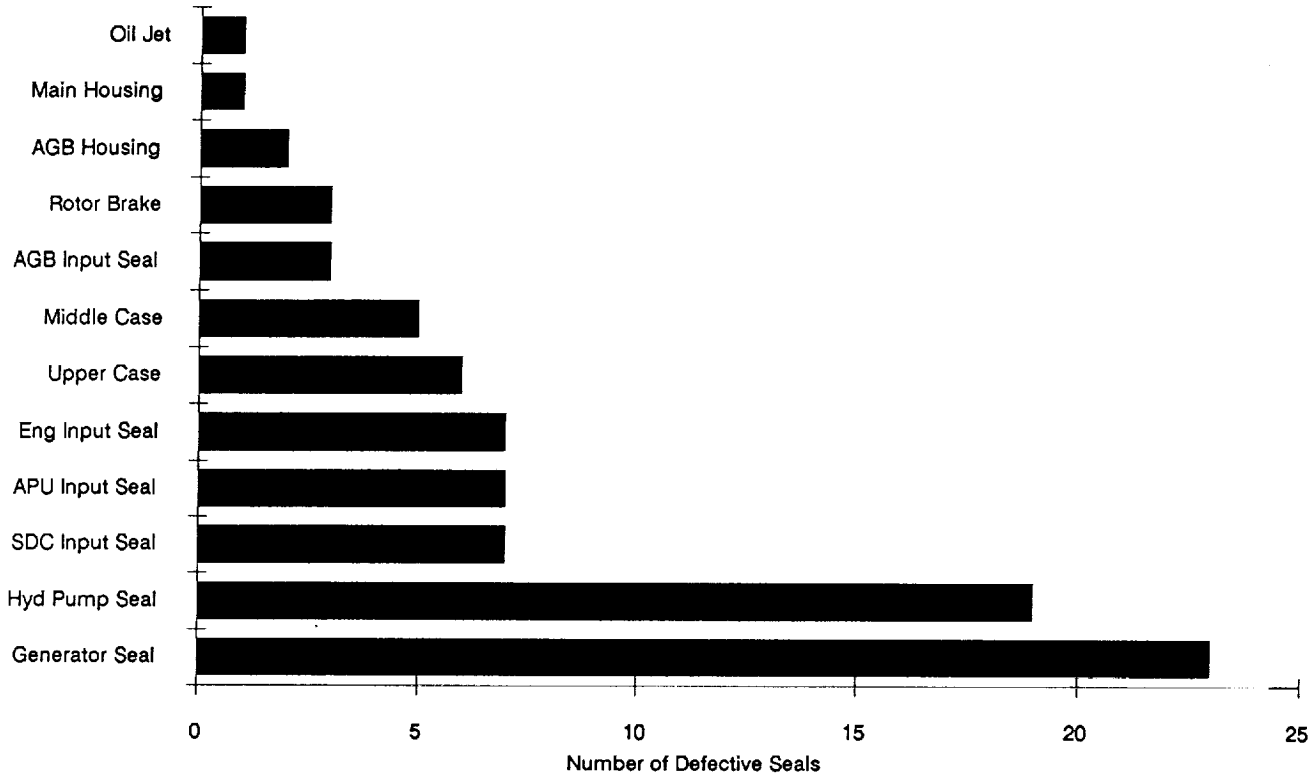

Figure 26. Causes of Leaking

Recommendations

1. Use spring-loaded lip seals wherever possible.

2. A SpeediSleeve should be installed on all gearshafts where a lip seal is used. The lip seal would wear a groove in the replaceable sleeve, and save the expensive gear. SpeediSleeve is replaceable at Aviation Intermediate Maintenance (AVIM) or Service Center level maintenance, preventing a trip to depot.

3. Make lip seals shimmable. This would place the replacement seal at an unworn place on the gearshaft, allowing two or more seal replacements per SpeediSleeve installation.

4. Design all seals in housing assemblies to prevent the effect of incorrect installations. Replacement would be accomplished by removing the bolts attaching the seal/housing assembly, sliding out this assembly, and replacing it with a new seal/housing assembly. This would assure proper alignment of the seal with the shaft centerline and minimize handling of a seal surface by the mechanic. There is a recognized trade-off in weight.

5. Use carbon seals only where shaft speed is more than 10,000 feet per minute or a reservoir of oil which must be held back.

6. Provide a source of oil to all seals for cooling and lubrication to extend seal life.

Evaluation

There are 2 magnetic seals on the input shafts of the ART. There will be oil behind these seals. The housings have been designed to allow field servicing. Field personnel will need to be specially trained to replace these seals but for the shaft speed, these are the best alternatives. An indexed fit is provided to prevent damage on installation.

The lip seal on the NOTAR output is designed to be field-replaceable. The housing around the lip seal can be removed to access the lip seal with the transmission in-place. In addition, there is a sleeve around the shaft to protect the shaft surface from wearing.

The seal on the main rotor output was designed to protect the transmission from spray washing and other maintenance. The output will normally be sealed up at the rotor hub. This seal also has a sleeve to prevent scratching of the mating surface and failure of the expensive planetary carrier.

The static shaft tube in the center of the ART has a dual O-ring seal to the housing. This part is included in the removal-inducing failure category (see Figure 24) with a failure rate of $1/8.8 * 10^{7}$. With 2 in parallel, the resulting failure rate is $1/1.72 * 10^{8}$.

The ART transmission was rated at a 90-percent reduction of leaking failures compared to the Apache.

Corrosion

Corrosion is the highest occurring failure mode of parts repaired or replaced at depot (see Figure 24 and Figure 27). Maintenance personnel at depot spend an average of 20 hours reworking each transmission for corrosion alone. The easiest way to begin the fight against corrosion is with a highly corrosion resistant housing material. The two choices for an aircraft transmission are magnesium and aluminum.

External corrosion on the AH-64A transmission develops at split casting lines, in the o-ring grooves at mating surfaces between the main housing and the accessory cover and between the main housing and the intermediate support, and in water traps of the casting, i.e. generator and hydraulic pump attachment points.

Magnesium

Magnesium

New high strength and high purity magnesium alloys (WE43A and AZ91E) are now available for use as transmission housing materials. These magnesium alloys are highly corrosion resistant, but the standard protection against galvanic corrosion is still required. Additional testing is being performed by MDHC's Materials, Processes, and Specifications (MP&S) Department, Reference [25].

1. Corrosion. The major disadvantage to using magnesium in the past has been its poor corrosion resistance. Recent advancements in magnesium corrosion control using high purity magnesium have resolved these arguments for all but marine applications.

2. Casting. Magnesium transmission housings can be cast with oil passages, bosses and mating surface flanges to within 0.005 inch due to the stable shrink rate of magnesium. This means that bosses and other normally machined areas can be used "as cast", saving time and money in machining costs.

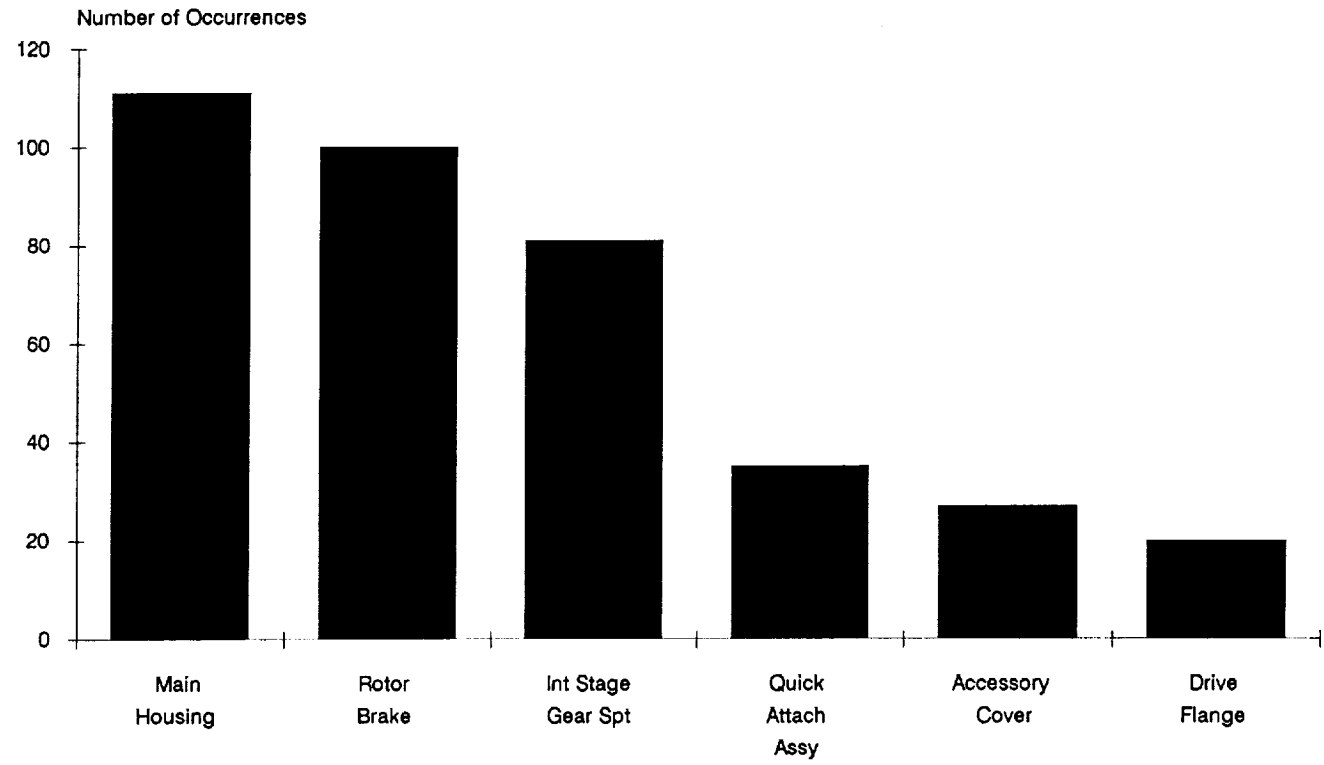

Figure 27. Parts With Corrosion

3. Tooling. Magnesium has a toolability factor of 5.00. Compared to aluminum's toolability factor of 2.85, this means that tools used to machine magnesium will last 3 to 4 times longer than those used on aluminum.

4. Weight. Magnesium is lighter than aluminum. Magnesium weighs about 0.065 lb/cu. inch, 35% less than aluminum's 0.1 lb/cu. inch.

5. Strength to weight ratio. Magnesium has a good strength to weight ratio. It offers the lightest weight per unit volume without sacrificing strength and rigidity.

Aluminum

There are a variety of properties which make aluminum an economical and attractive material, such as: appearance, light weight, fabricability, physical and mechanical properties, and corrosion resistance.

1. Corrosion. The excellent corrosion resistance of aluminum is a major factor for its consideration in helicopter transmissions. The aluminum inherently forms an oxide protective surface layer when exposed to air. The alloys used in aircraft transmissions have a high resistance to seawater corrosion.

2. Casting. Sand casting is the most economical method of casting aluminum due to the size and shape of most housings. Oil passages and bosses can also be cast into the housing using sand casting. However most housings will have to have some machining to obtain dimensional requirements, resulting in higher cost for manufacturing.

3. Tooling. Aluminum is more expensive to tool than magnesium due to its toolability factor of 2.85 compared to 5.00 for magnesium. This will reduce tool life by 3 to 4 times.

4. Weight. Aluminum would add weight to the transmission. It is 50% heavier than magnesium.

5. Strength to weight ratio. Aluminum is comparable to magnesium for equal strength to weight ratio. However, it is about half the stiffness to weight ratio of magnesium.

Recommendations

1. Make the transmission housings from high purity magnesium alloy (AZ91E, WE43A, or a combination of the two).
2. Take all available precautionary steps against galvanic corrosion. Use zinc plated bolts and aluminum 5000 series washers. Manufacture spacers and drive plates from 5000 series aluminum. MP&S will have additional guidelines for the chosen housing material. Their investigation is ongoing.
3. Take all available precautionary steps against environmental corrosion. Blind tap bolt holes to prevent the access of water to thread surfaces in critical areas.
4. Place drain holes where accumulation of water may occur.
5. Use a desiccant breather for air flow into the transmission with a check valve. For air out flow, use another line with check valve.
6. High quality shipping containers should be considered a mandatory part of the maintainability and reliability requirements for this transmission. Pre-shipping treatments should be included, and all transmissions should be shipped with desiccant and a desiccant indicator on the container. Investigate: For shipping, attach a recirculation line from the oil output to the oil input. Attach a flange with a hand-crank adapter to the input. Include instructions to crank the transmission at regular intervals to provide oil circulation while in storage. Possibly provide crank and access integrated with the shipping container. This part of the transmission's life is critical with respect to internal corrosion.

Evaluation

The above guidances have been implemented into the design. The material chosen for the housing (WE43A) represents the best alternative for non-sea operation. For sea-based operation, aluminum should be substituted. The weight penalty of aluminum housing components is estimated at 50% of the weight of the magnesium components, an additional 70 lb or 7 percent.

The reduction in corrosion caused removals is estimated at 50 percent.

Freewheeling Unit

The AH-64A currently has a 1,000 hour Time Between Overhaul (TBO) interval for the freewheeling unit due to slipping and excessive drag clip wear. All types of freewheel units experience wear during the overrunning mode. With the higher times accumulating on on-condition gearboxes, it is more likely that wear will progress to the point where the freewheel unit will not operate satisfactorily; it is likely that excessive freewheel unit wear will become more prominent as a primary failure mode. There is a pawl-based clutch design that does improve wear characteristics.

Recommendations

Freewheeling units should be field replaceable, or modularized. Investigate use of pawl-based clutch design.

Evaluation

The pawl-based clutch is field replaceable. Although new to helicopters, the design should minimize wear due to its synchronizing positive engagement feature. This will, in turn, reduce metal particles in the oil.

Summary

Under conservative assumptions, we have a transmission design that can run 5000 hours MTBR. Areas for improvement at this point are: bearing life, and reducing failures from other than contact stress. The latter include failures due to housing cracking or breaking, corrosion, lubrication system failures, and leaks. The failure history of the AH-4A transmission, in providing lessons learned to MDHC transmission designers, assures reliability improvement.

The risks areas in this design are identified and addressable. With advance testing the risks will be reduced allowing the benefits of this design to be used in an FAAV.

IV.F.5 Supportability Discussion

The miscellaneous failure rate is the reliability driver in this design. Although it will take weight to add features like field-replaceable seals and housing strength, the benefits of this more balanced approach will be a larger reduction in required weight of gears and bearings.

It is perhaps more difficult to design large, reliable bearing than gears. Bearings often need volume in areas where volume is at a premium. This was the case in the idler pinion design, the notar output gear, and the planetary.

The integrated diagnostics section indicates that a QDM is the basic diagnostic component. This is the best way to detect problems pending further work on other failure detection methods (acoustic, proximity, etc).

Continuing work in the supportability area will have a large impact on the operational characteristics of the transmission. The trade-offs depend on the target application more as the design gets into greater detail, i.e., if a military mission is envisioned, bearing cage hardening might be preferable. This research has opened some issues to trade off analysis, including:

1. Case material, thickness, and corrosion prevention
2. Transmission sealing and field-replaceable assurance
3. Instrumentation strategy

For final production design, these considerations can feed an "Evaluator Function" methodology implemented in a computer model. The numerical values to weigh features of design alternatives can be obtained through the Analytic Hierarchy Process, Reference [26], applied to end-users. This would provide more detailed application-specific feedback to the design.

As the ART program progresses, Supportability will continue to work closely with design, making recommendations as appropriate. We are maintaining a library of papers and reports relevant to helicopter transmission supportability. Among them is a valuable history of lessons learned, including the lesson that design for supportability is a differentiating factor among otherwise equal technical proposals.

Summary/Conclusions

The Supportability features of the ART design have been evaluated. Supportability criteria were developed. This data provided input to further refine the design.

Under conservative assumptions, we have a transmission design that can make 5000 hours MTBR. This can still be increased. Areas for improvement at this point are: bearing life, and reducing failures from other than contact stress. The latter include failures due to housing cracking or breaking, corrosion, lubrication system failures, and leaks. The failure history of the AH-64A transmission, in providing lessons learned to MDHC transmission designers, assures reliability improvement.

Achievement of the reliability goal depends on what happens between design and production. It is important to retain design intent throughout the ART program. The risks areas in this design are identified and addressable. With advance testing the risks will be reduced allowing the benefits of this design to be used in a FAAV. This is being addressed by MDHC design.

IV.G ACOUSTIC ASSESSMENT

IV.G.1 Summary

The acoustic goal for the Advanced Rotorcraft Transmission (ART) program of 10 dB noise reduction was essentially met with a predicted overall noise reduction value of 9.6 dB. Perhaps more importantly, the analytical procedures that were developed and validated in this program represent a "design to noise" capability that has not been previously available. Preliminary parametric studies indicate a strong potential for further acoustic improvement of the MDHC ART design while essentially maintaining the current extraordinary weight results. The ART acoustics evaluation presented here is based on validated analytical techniques. The methodology employs the use of finite element methods to determine the dynamic response of the gear box casing. It is the excitation of the casing, due to the gear meshing forces, which results in radiated noise. This information is then used for the acoustic calculations, which are accomplished by two distinctly different procedures. A deterministic approach, based on the boundary element method, was used for determining the radiated noise at the lowest gear mesh frequencies. Given the limitations of the computer resources available, it was necessary to supplement this method with a stochastic approach, based on statistical energy analysis (SEA), for evaluation of the higher frequencies. SEA could not be used exclusively because of its limited precision at the lower frequencies where the boundary element method performed best. The combined dynamic and acoustic analyses were validated by application to an existing rotorcraft transmission and comparing the results to a vibro-acoustic database obtained during a comprehensive sound intensity survey of the transmission operating on a regenerative test stand. The methodology was then applied to the MDHC ART design.

IV.G.2 Introduction

Rotorcraft interiors typically exhibit noise levels much higher than those of fixed-wing commercial aircraft. A major contributor to the overall cabin noise environment is the main transmission, or gearbox. Since state-of-the-art rotorcraft transmissions are still inherently noisy, efforts to solve interior noise problems on rotorcraft have been aimed at minimizing the transfer of gearbox vibration energy through the airframe structure and into the cabin.

Recently, increased emphasis has been placed on reducing noise at the source rather than modifying its transmission path. Consequently, noise control has become a high priority in the design process for newer, advanced rotorcraft transmissions. One of the key objectives in designing new transmissions is to reduce its noise to levels which minimize the need for airframe modifications and treatment of the interior to meet the accepted standards for passenger comfort. To incorporate noise control features in new transmission designs, it is necessary to possess the capability to predict its noise emissions analytically. Rotorcraft cabin noise is influenced largely by structurally-transmitted gear box vibration. However, the airborne noise component is also a direct result of gear box vibrations. If the case-radiated noise can be reduced, then the underlying assumption is that the vibration levels transmitted through its mounting structure and into the airframe will also be reduced.

The prediction of transmission noise to date has generally been based on empirical methods and projection of current trends using measured data on existing transmissions. Since there is no analytical basis in such an approach, the noise estimates thus obtained can be quite different from the actual values. It is also not possible to establish or quantify approximately the amount of error involved in the estimates when such an approach is used. In order to address these issues and to provide technology growth in the area of structural noise

prediction, a detailed effort utilizing combined dynamic and acoustic analyses was undertaken as part of the noise prediction methodology for the MDHC ART design. The goal of this effort was threefold - (1) to develop the necessary analytical procedures, (2) to apply these procedures to an existing transmission to both validate this approach and to get an idea of the level of error involved, and (3) to apply the validated approach to predict the noise levels for ART. Additionally, once the framework for analysis has been established, and the models to be used in the analysis have been developed, it will be possible to use this methodology to identify potential design changes that would further reduce the radiated noise levels. Performing these design iterations could lead to a design that is optimized for the lowest possible noise levels.

Analytical procedures do exist at present to compute transmission noise, Reference [27]. But these rely on dynamic test data from the transmission to generate analytical models, and do not provide a viable approach for predicting transmission noise at the design stage. The technique developed for ART, therefore, employs the use of finite element analysis for model generation. The data required for such modeling are usually readily available during or after the completion of a preliminary design. Dynamic analyses are performed using the transmission finite element model, the results from which are used in the subsequent acoustic analyses.

Computation of the structurally-radiated noise is accomplished by using both deterministic and stochastic methods. These methods have previously been used for predicting helicopter interior noise. Aerospatiale used the former approach, based on finite element and boundary element methods, to evaluate the airframe structure-borne noise in an SA365N Dauphin helicopter [28]. Analysis of noise measurements obtained inside the bare cabin of the SA365N during flight showed that the main gear box is the major contributor to overall cabin noise levels. Therefore, the analysis focused mainly on the transfer of vibration energy from the gear box to the airframe structure. Predicted cabin noise levels were within 3 dB of the measured values up to 1870 Hz. Due to the constraints imposed by the mesh density of the model, correlation between measured and predicted values naturally decreased at higher frequencies.

The stochastic approach, based on statistical energy analysis (or SEA), has been used extensively by Sikorsky on the S-76 helicopter [29,30], and by Bell on the Advanced Composite Airframe Program (ACAP) helicopter [31]. The advantage of SEA results from the statistical treatment of resonant modes, which allows a significant reduction in the number of degrees of freedom in the model. This greatly reduces the effort and cost otherwise required to implement deterministic methods for analysis at high frequencies. The dynamic responses of both helicopter models were obtained by measurement during actual flight. These measurements were used as input to the SEA models for the acoustic calculations. Reasonable agreement between measured and predicted cabin noise levels was demonstrated with the S-76 and ACAP models. The discrepancies that did occur are likely caused by the statistical description of the power flow between subsystems (e.g., plates, beams, etc.) of the model. Since a finite element model was used to describe the dynamic response of ART, structural coupling of subsystems in the SEA model was not required. SEA, therefore, was used to compute only the sound radiated by each subsystem individually.

To evaluate the radiated noise of new systems under design, its dynamic response must be determined by analysis. Therefore, a numerical method such as finite element analysis is necessary to define the energy input for both the boundary element method and SEA.

By combining the methods described above, MDHC has implemented a procedure for calculating the direct case-radiated noise of rotorcraft transmissions without the need for vibration data from existing hardware. It can be used during the early design stages of a gear box, and can assist the engineer in the application of effective

noise control design features. The methods have been successfully validated by numerically modeling the AH-64 Apache helicopter transmission and comparing the results with measured acoustical data. The correlation studies were used to ascertain the accuracy of the predictions as well as to identify the limitations of the analyses and the bounds within which the analyses are valid.

The following discussion begins with a general overview of the methodology employed, followed by the application to the AH-64 helicopter transmission. A description of the experimental test program which produced the acoustic and vibration data used in the validation is also included. Next, the noise prediction technique is applied to ART. Experience gained from the Apache transmission modeling and correlation studies is utilized in the ART analysis. To illustrate the utility of the noise prediction methodology in achieving a low noise design by parametric studies, a modification to the baseline ART design is considered. It is shown that the modified design yields a lower overall noise level than the original design. In a similar fashion, it is possible to consider various potential changes in the design of the casing and/or gears and evaluate their impact on the noise levels, thus leading to an improved design with lower noise.

IV.G.3 Methodology

The first task in the noise prediction methodology is the development of analytical procedures to represent as accurately as possible the various aspects of noise generation in the transmission. The uneven transfer of motion between meshing gear pairs is generally recognized as the main source of noise in transmissions. This is induced by the nonuniform deflections of the gear teeth in mesh, which in turn is caused by the varying combined stiffness of the geartooth pair as the pair moves through one complete mesh cycle. This phenomenon repeats itself for each successive pair of gearteeth, leading to a periodic variation of the gear deflections. Consequently, even under ideal conditions, the meshing gears are subjected to dynamic excitations at the gearmesh frequency and its higher harmonics. In practice, imperfections in gear teeth or operation would introduce excitations at additional frequencies (sidebands) equal to the gearmesh harmonics plus or minus integer multiples of the rotational speeds of the gears. Sidebands are also introduced in planetary systems due to the motion of the planets, occurring at gearmesh harmonics plus or minus multiples of the planet-pass frequency. As a result of the excitations induced at the gearmesh, the gears undergo vibrations which are transmitted through the bearings to the casing. The ensuing dynamic response of the casing leads to the radiation of noise at all the excitation frequencies. It follows that in order to predict this radiated noise, the excitations at the gear mesh must be determined first. Once these excitations are known, they are applied to an analytical model of the transmission to determine the vibration levels on the casing. The finite element method is used in the present methodology to generate the transmission analytical model. The surface velocities of the casing are obtained from the dynamic analysis of the transmission model subjected to the gearmesh excitations.

The surface velocities serve as the basis for the acoustic calculations. For the lowest gearmesh frequencies and harmonics, the velocities are input directly to the boundary element method. At the higher harmonics, statistical energy analysis is employed. Here, the velocities are spatially averaged over specific areas of the transmission casing. These areas are then represented by generalized subsystems such as rib-stiffened plates and cylindrical shells in the SEA model. The overall noise prediction scheme is illustrated in Figure 28.

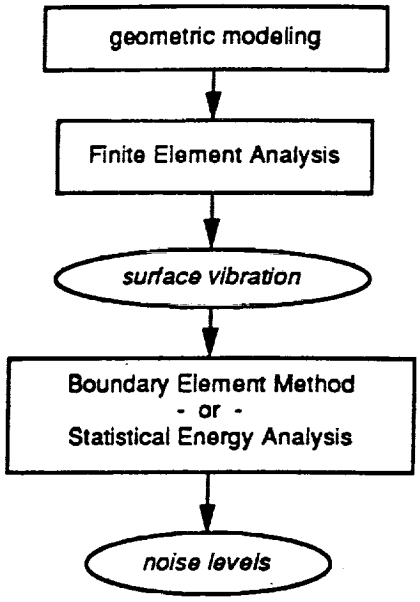

Figure 28. Transmission Noise Prediction Scheme

A significant advantage of the boundary element method is the fact that it is deterministic. This means that sound pressure levels can be determined at any point in the acoustic field, or on the surface of the model. By coupling its output with post-processing software, noise contours can be plotted on the surface of the boundary element model to help identify the "hot spots" on the transmission casing. This feature is very useful for determining where design changes are needed in the housing to reduce noise radiation. With SEA, on the other hand, only the spatially averaged total sound pressure can be computed. The various aspects of the dynamic and acoustic analyses are discussed in the following sections.

IV.G.3.i Transmission Finite Element Analysis

At present, the most commonly used method to develop analytical models for predicting structural vibrations is finite element analysis (FEA). The semi-empirical noise prediction techniques currently in use do not encompass all of the possible design parameters. There is a need for a more scientific approach to the problem, especially during the design phases where trade-off studies are required. Therefore, finite element analysis seems to be a superior alternative.

While FEA has been successfully employed in other fields over the last two decades, it has not found effective use in transmission design and analysis until recently. Despite the fact that FEA models of individual gears have been used to locate and solve problems involving troublesome resonant frequencies [32,33], proving the efficacy of the technique, detailed finite element analysis of transmission systems has not been attempted to date. In an earlier effort, described in Reference [27], individual components were modeled using alternative approaches rather than FEA, and combined using component mode synthesis to obtain the overall model.

Application of FEA to model the transmission as a whole, including all of the various components, has usually involved simplifying assumptions such as the representation of the gears as concentrated masses and springs [33,34]. No systematic study of the validity of these assumptions and their effects on the final results has been made, however. Efforts to develop detailed models in the past were hampered by limited and expensive computational resources. With the recent advances in computing capabilities, however, the creation and analysis of large models in a reasonable time and at a reasonable cost is now feasible. On the other hand, including too many details that do not influence the accuracy of the model may result in an excessively large model that is unwieldy. This would prevent the effective use of the model during design stages for trade-off studies due to the high computational cost and the increased difficulties in handling large, complex models.

It is therefore essential to determine the level of sophistication required in modeling the various components of the transmission, so that an adequately small and sufficiently detailed finite element model can be developed for the whole transmission and used to study and optimize the transmission configuration to meet the specified requirements. To this end, studies have been performed, particularly with respect to the modeling of the internal components in the transmission, to evaluate the level of detail necessary [35]. The findings from this study were made use of in building models for the Apache and ART transmissions. The approach adopted is such that the resulting transmission model will require only the input data that are readily available during the design stages. Detailed discussions on Apache and ART model development are provided in later sections.

IV.G.3.ii Gear Mesh Excitation Analysis

The transmission finite element model, once complete, is subjected to gear mesh induced excitations to determine the casing vibration levels necessary for acoustic analysis. Since the mechanism that causes these vibrations involves varying gear teeth deflections through the mesh cycle, the process of computing the excitations begins with the evaluation of the compliance of the gear teeth at various points along the tooth. Based on the combined compliance of the driving and driven geartooth pair, the steady load transferred between the gears, and the number of geartooth pairs in mesh, the load shared by each pair and the relative deflection of one gear with respect to the other are determined. This relative deflection between the gears along the line of action is known as the static transmission error [36].

Because of the repeating gear meshing action of successive pairs of gear teeth, the static transmission error is a periodic function with a period equal to the inverse of the gearmesh frequency. It can be considered as an enforced relative displacement between the gears, and in this sense used as an excitation in the dynamic analysis of the transmission. Since the response of the transmission is desired at harmonics of the gearmesh frequencies, the harmonics of the static transmission error are extracted through a Fourier analysis. These harmonics are used as excitations and the response of the transmission is determined by performing frequency response analyses at all the frequencies of interest.

In using the static transmission error as an excitation, it is implied that it represents the relative displacement between the gears when they are in operation. But the actual relative displacement would also depend on the dynamic response of the gears themselves in response to this imposed motion. The excitations induced at the gearmesh are thus coupled to the response of the system, and therefore cannot strictly be determined independent of the system response. However, if the gearmesh frequencies (or its harmonics) are not in the vicinity of the resonant frequencies of the meshing gears, then it can be assumed that the dynamic response of the system does not significantly affect the excitation amplitudes determined from the static transmission error. This is assumed to be the case in the present analysis. It is assumed that all the gears are operating away from the critical speeds corresponding to gearmesh frequencies, and that conditions such as tooth separation do not occur.

A survey was conducted to determine if any of the gear analysis codes currently available such as GRDYNMULT, DANST, and PGT could be used to compute the excitations as discussed above [37]. After a review of the various features incorporated into these codes, it was decided that GRDYNMULT would be used for obtaining the tooth compliance data. The gear tooth model used in evaluating the tooth compliance is discussed, for example, in Reference [38].

A separate program was developed to compute the static transmission error and its harmonics using the compliance data from GRDYNMULT. This approach was adopted since GRDYNMULT does not compute the transmission error harmonics needed in the present analysis directly. The transmission error is computed in DANST but it does not incorporate the capability to handle external-internal meshes such as the planet-ring mesh in the planetary system. Furthermore, GRDYNMULT can be used with helical gears which is not the case with the other programs. Application of this procedure to calculate the excitations for the Apache and ART transmissions is discussed in later sections.

IV.G.3.iii Boundary Element Method

When the boundary element method is used, the Helmholz integral equation is solved numerically to determine sound pressure on the surface of a vibrating structure. The integration is performed over the discretized surface (boundary element model). For exterior radiation problems, this equation has the form (Reference [39]):

$$c(P)\, p(P) = \int_S [\, p(Q)\, y'(P,Q) + I\, w\, r_o\, k\, v_n(Q)\, y\,(P,Q)] \; dS(Q)$$

where P is the point at which the total sound pressure p is to be calculated, Q is an arbitrary point on the surface S, and p(Q) is the sound pressure at Q. c(P) is the Helmholz coefficient whose value is determined by the location of the field point P, and the local geometry if P lies on the surface S. The Helmholz coefficient is described by Cheng and Seybert in Reference [39]. The normal surface velocity v_n is determined by finite element analysis, r_o is the density of air, and $I = \sqrt{-1}$. The wave number $k = w/c_o$ where c_o is the speed of sound, y is the free-space Green's function, and y' is the normal derivative of the free-space Green's function. The integration is performed over the surface S of the boundary element model (i.e., transmission casing).

A computer code developed at the University of Kentucky, called BEMAP (Boundary Element Method for Acoustic Predictions), employs a numerical method based on the Helmholz integral equation. Version 2.44 of this code was used in this investigation. Previous studies by Oswald and Seybert [40] have demonstrated that when the vibratory responses on the surface of a structure are reliably defined, BEMAP can accurately predict the resultant noise.

When solving for pressure on the radiating surface S, the Helmholz equation is discretized into N nodes, and a system of N simultaneous algebraic equations is produced in terms of sound pressures p and normal surface velocities v_n. The values for v_n are determined from finite element analysis. The equations are then easily solved for p. Once all the values of p and v_n are known, the total sound pressure at any point in the acoustic field can be calculated using Gaussian quadrature. But rather than quantify transmission noise in terms of sound pressure at numerous field points, the total acoustic energy emitted can be evaluated conveniently by a single value of sound power in Watts. First, the sound intensity I at each point Q on the surface is calculated from the exact formula:

$$I = \frac{1}{2}\, \mathrm{Re}\, [p * v_n]$$

where Re is the real part of the expression in brackets. Integration of the sound intensity vectors over the entire surface S produces the total sound power W:

$$W = \int I \, dS$$

Application of the boundary element method to exterior radiation problems is subject to the difficulties associated with nonunique solutions at certain characteristic frequencies, or wave numbers. BEMAP employs a variation of the Combined Helmholz Integral Equation Formulation (CHIEF) method to overcome the problem of nonuniqueness. This method is described by Cheng and Seybert [39] and is used to improve the solution to the Helmholz integral equation. A procedure for checking the convergence of the solution is also provided in BEMAP.

IV.G.3.iv Statistical Energy Analysis

Statistical energy analysis (SEA) permits the statistical treatment of the dynamic behavior of complex structures by analysis of a generalized model. This type of model is comprised of a series of substructures, or sub-systems, such as plates, cylindrical shells, and beams. SEA provides a means for calculating the energy flow between connected sub-structures, and to the sound field. The mathematical basis for SEA is described in detail by Lyon in Reference [41].

AutoSEA is a vibro-acoustic design software package based on SEA, and was developed by Vibro-Acoustic Sciences, Ltd. of Australia. It runs on the Apple Macintosh family of desktop computers. Version 1.0.3 was used to evaluate the noise produced at the higher gear mesh frequencies of the transmission.

To obtain a basic understanding of the mathematical basis for this technique, consider a subsystem with total energy E in the frequency bandwidth Dw, centered at w, and a damping loss factor h. The power dissipation W from that subsystem to the acoustic field can be obtained from the formula, References [42,43]:

$$W = whE$$

Since the energy of each subsystem in the transmission model is determined from the finite element model, we need not be concerned with the coupling between subsystems in the statistical energy model.

SEA is normally applied to dynamical systems excited by incoherent, or broadband noise sources. Lyon shows in Chapter 4 of Reference [41] how narrow band sources are equivalent to broadband sources when system averages are taken, and that the results can be generalized, with proper care, to pure tones. It is important to be aware of the potential for high coupling of generalized subsystems with the acoustic field at the gear mesh frequencies being analyzed. For example, if a component of the transmission is represented as simple plate flexure, high coupling will occur at some discrete frequency which depends on the geometry and material properties of the plate. If this frequency lies within the same bandwidth as the gear mesh frequency being analyzed, the solution to the power balance equation will be unstable. Since simple plate flexure would typically be an over-simplified representation of an actual gearbox casing, the problem of high coupling at a discrete frequency can be avoided by adding rib-stiffening to the plate.

The AutoSEA User's Guide [43] references several sources where standard equations for loss factors of various structures (e.g. plates, cylinders, beams, etc.) are available. There are also standard equations available in the literature which describe the relationships between the surface mean-square velocity $<v^2>$ of simple vibrating structures and the emitted acoustic energy. These can be simply expressed in the form:

$$<v^2> = A <p^2>$$

where A is a function of the structural geometry and material properties and $<p^2>$ is the mean-square pressure. Note that, unlike the boundary element method, SEA requires knowledge of the material properties, including density, thickness, and wave propagation speed.

IV.G.4 Description of the AH-64 Apache Transmission

Figure 29 is a cutaway view of the AH-64 Apache helicopter transmission. It is a 3-stage transmission rated at 2828 HP and weighs 678 pounds. There are two input drive shafts, one for each engine, turning at 9841 rpm. The 1st-stage consists of the two input pinions, each driving a spiral bevel gear with a mesh frequency of 4756 Hz. These drive the 2nd-stage which consists of two helical pinions driving a single "combining" gear with a mesh frequency of 2634 Hz. The combining gear then drives the 3rd-stage. Here, a sun gear drives six planetary gears with a mesh frequency of 665 Hz. This planetary system drives the output rotor shaft at 289 rpm. Figure 30 shows the transmission casing.

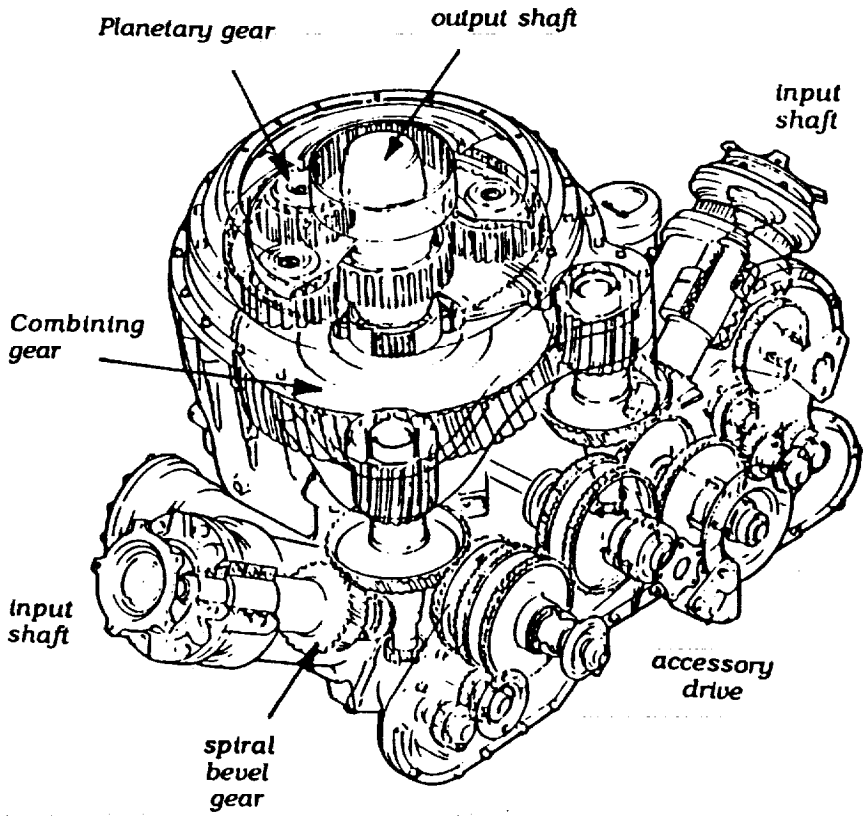

Figure 29. The AH-64 Apache Helicopter Transmission (cutaway view)

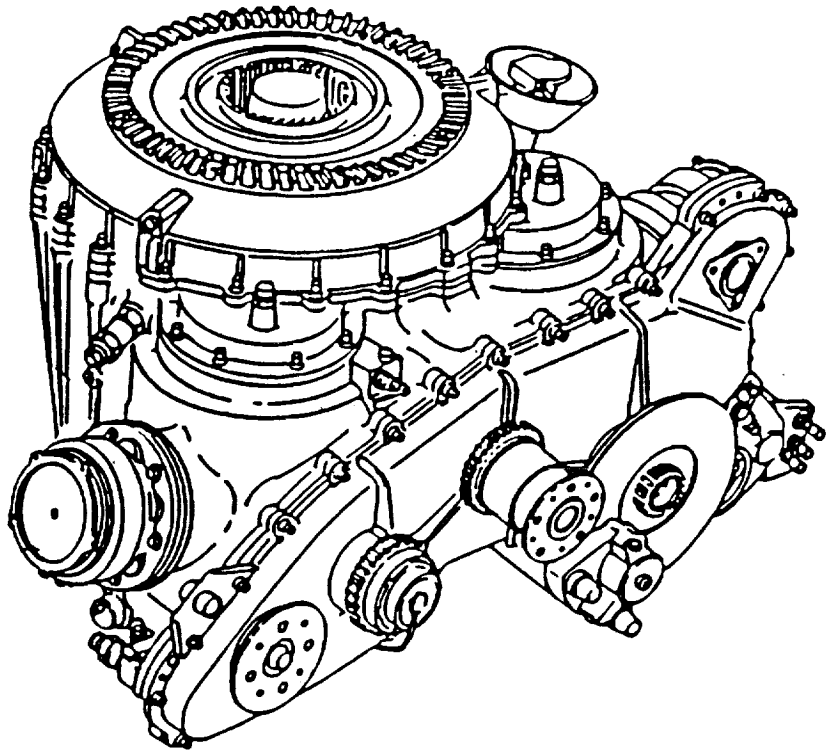

Figure 30. The AH-64 Apache Helicopter Transmission Outer Casing

IV.G.5 Application of Methodology to the AH-64 Transmission

First, a finite element model was developed for the AH-64 Apache helicopter transmission. A finite element (FE) analysis was then performed to determine the complex velocity distribution over the surface of the outer casing during operation at maximum power. These results were compared with accelerometer measurements obtained during the experimental test program. The FE analysis was then refined by adjusting the overall system damping ratio until there was reasonable correlation between the measured and computed velocities. A parametric study was performed to determine the influence of overall system damping on radiated sound. These results are presented in the section on comparison between analysis and experiment.

IV.G.5.i Finite Element Model

The NASTRAN finite element model of the AH-64 transmission that was used to compute the dynamic response of the casing for acoustic analysis is described in this section. Development of this model, referred to as the reduced model, was based on a more detailed model generated by Lucas Western Incorporated (LWI). This developmental effort was undertaken with the objective of obtaining a model that can be run in reasonable time so that it could be used for repeated parametric studies, while at the same time retaining the essential frequency response characteristics of the full LWI model. The model reduction procedure and the excitations used to determine the vibration levels on the casing are discussed.

Model Reduction. The detailed LWI model of the transmission used to obtain the reduced model is shown in Figure 31. This detailed model includes fine representations of many areas of the casing, and thus is somewhat large. The model contains in excess of 10,700 grid points and 64,000 degrees of freedom. It was found that it was impractical to use this model for parametric studies where, for example, the model has to be run for a range of values of a parameter to determine the optimum value for this parameter. For such occasions, it is worthwhile to develop a smaller model which possesses similar response characteristics as the full model, but for which the results can be obtained more rapidly.

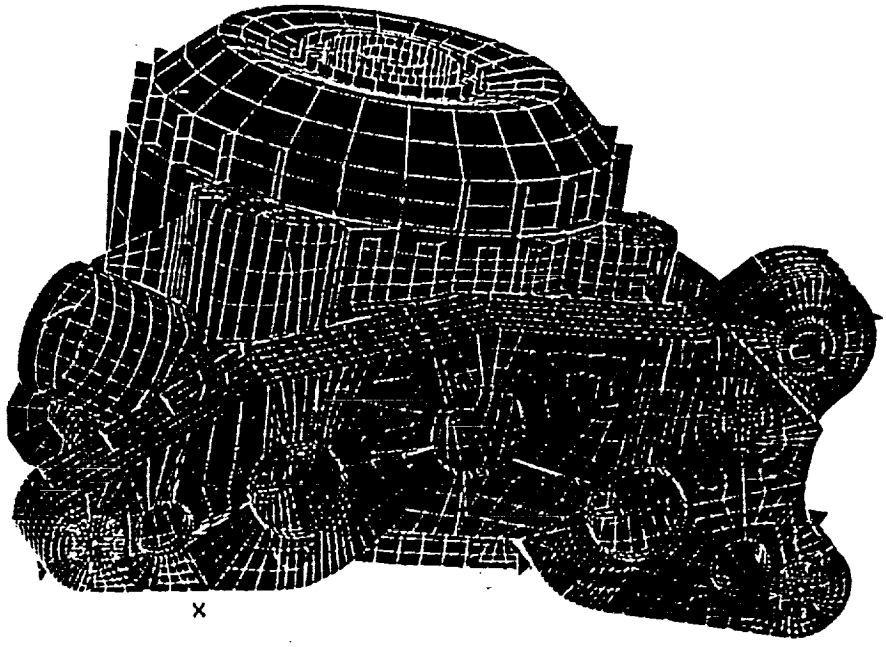

Figure 31. LWI FE Model of the AH-64 Apache Helicopter Transmission

The reduced model uses the full model as the starting point, and involves decreasing the element density in areas of the full model that do not have much impact on the accuracy of the response. In order to facilitate this reduction procedure, the full model is divided into smaller components if necessary. Reduction is applied to each of these components, leading to a smaller model for each component. Both the detailed and the reduced component models are analyzed and the results compared to ensure that any loss in accuracy incurred due to reduction is within acceptable limits. Finally, all the smaller component models are assembled together to obtain the overall reduced model.

Application of the reduction procedure to the LWI model involved reducing each of the major casing components, namely the top cover, the intermediate gear support, the lower casing, and the accessory drive cover. Two dimensional quadrilateral and triangular elements (QUAD4 and TRIA in NASTRAN) were used throughout to represent all the components. In addition, the central combining (cluster) gear and the planet carrier were also modeled with two-dimensional elements.

Most of the reduction in size was achieved by increasing the element size in particular areas that were deemed to have less impact on model accuracy. But the maximum element size was kept approximately the same in the reduced model as in the full model. This meant that the frequency range in which the reduced model is useful would be the same as for the full model. The reduction effort was accompanied by concurrent analysis of both the full and reduced models to make sure that there were no errors introduced during the reduction procedure, and also to check the accuracy of the reduced model and its acceptability.

Verification of the Reduced Model. Comparison between the reduced and full component models to establish acceptability and the range of validity of the reduced models was accomplished using several means. One of the methods involved correlating the frequencies and mode shapes of the corresponding component models. This included both the comparison of individual modes between the two models in the lower frequency range, and a comparison of the number of modes in a specified frequency range (modal density) in the two models at higher frequencies. Another means of comparison that was adopted to investigate the accuracy of the reduced models was to examine the frequency response functions before and after reduction.

Based on all the correlations obtained using different criteria, it has been determined that the reduced model of the casing, shown in Figure 32, possesses essentially the same characteristics as the full model up to about 3000 Hz, beyond which the two models start deviating from each other. The actual accuracy of either model can be determined only by comparing the model results with test data.

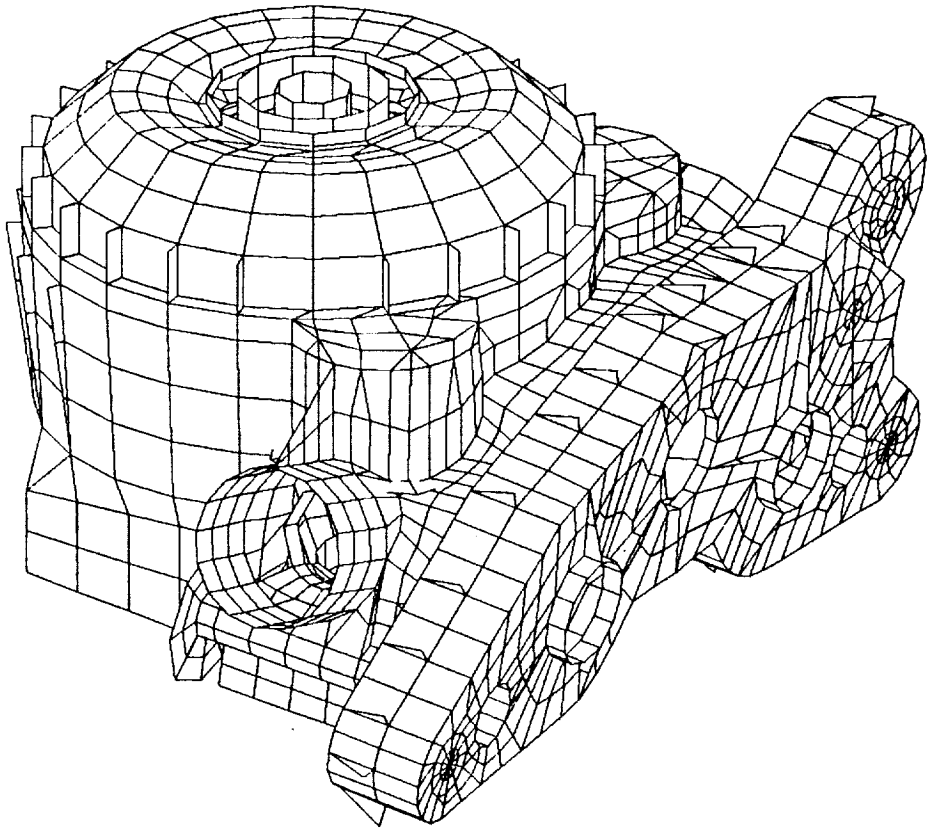

Figure 32. Reduced FE Model of the Apache Helicopter Transmission Casing

IV.G.5.ii Modeling of the Interior Elements

Gears. In the original LWI model, all the internal components with the exception of the cluster gear and the planet carrier were modeled as one-dimensional BAR elements. But subsequent studies have revealed that for some of the gears this type of modeling would be inadequate. The gear dynamic response plays a significant role in transmitting the excitations generated at the gear mesh to the housing through the bearings. This is particularly important when the excitation is not purely torsional, as would be the case for helical or spiral bevel gears where the thrust loading at the mesh could excite the bending modes of the gear web. In such instances, the gears were modeled using one-dimensional elements for the central gearshafts and two-dimensional elements for the webs. The nodes around the inside circumference of the 2-D web model were rigidly connected to the central shaft node, consistent with the assumption of plane cross-sections remaining plane for the bending of the gear shaft. But for those gears which were not directly in the load paths of any of the excitations of interest, the one-dimensional representations of the original LWI model were retained.

For the cluster gear which was originally modeled with two dimensional elements, model reduction was carried out as in the case of the casing components. The sun gear, which is splined to the cluster gear, was modeled together with the cluster gear as one component. The resulting model for all the gears is shown in Figure 33.

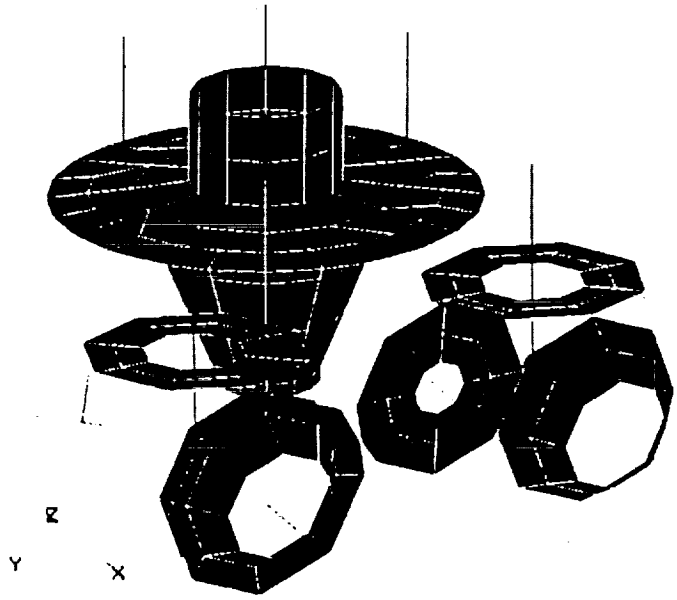

Figure 33. Finite Element Model of the Apache Transmission Gears

Bearings. The bearings were incorporated into the reduced model as linear elastic springs and viscous dampers (CELAS in NASTRAN). Stiffnesses for the springs used were determined from the procedure described in Reference [44]. These stiffnesses are functions of both the loads transmitted and the shaft speeds. Values specified in the model correspond to 100% torque and 100% RPM conditions, since the correlations with experimental data were performed under these conditions only. For all the gears that were not involved in the gearmesh frequency range of interest (such as the accessory drive gears whose meshing frequencies are above 5 kHz), a representative bearing stiffness value of 300,000 lb/in was specified as in the original LWI model.

The viscous damping values for bearing dampers were chosen based on a literature survey. Experimental data for bearing stiffness and damping are reported in References [45,46]. While a range of values is given in these references for different conditions, it was decided that a damping to stiffness ratio of 0.00005 would be used for all the bearings in the transmission model. Thus all the bearings in the model were assigned damping parameters equal to their stiffnesses multiplied by this ratio, where the bearing stiffnesses are determined as described above.

The manner in which the bearings were included in the model is as follows. For each bearing, the springs and dampers representing the bearing were connected between the central shaft grid point and another grid point coincidental with the shaft grid. The deflections of this coincidental grid point were constrained to be the average of the deflections of the surrounding grid points on the housing (RBE3 element in NASTRAN). In cases where the gearshafts were modeled in detail as 2-dimensional elements, two coincidental grid points were defined on the shaft axis at each bearing location. One of these was connected by an RBE3 element to the surrounding grids on the housing, while the other was connected to surrounding grids on the shaft, also through an RBE3 element. The coincidental grids in turn were connected through the spring and damper elements representing the bearing. Bearing springs are specified in both translational and rotational degrees of freedom, but dampers are used in translation only.

IV.G.5.iii Gearmesh Modeling

Meshing between the various gears was represented in the model as linear springs with stiffness values proportional to the face width of the gear teeth. The following equation, used in the LWI model, was also used in the reduced model [47].

$$K = (2{,}900{,}000 \times F) / C$$

where K is the gearmesh stiffness, F is the face width in inches, and C is a correction factor of 1.15. In reality, the gearmesh stiffness varies through the meshing process, and the variation is periodic with a period equal to the inverse of the gearmesh frequency. Values used in the model are therefore approximations based on typical gear tooth proportions and average mesh stiffnesses.

Since the load transfer at the gear mesh is along a direction normal to the teeth in contact called the line of action, the springs representing the gear mesh were oriented along the lines of action for the different meshes. In order to accomplish this, coordinate systems were defined such that the x-axis of each system was directed along the line of action of a given mesh. At the location of the mesh, if grid points did not exist already for each of the meshing pair of gears as a part of the gear models, additional grids were created and connected by rigid elements to the respective shaft grids. This resulted in two coincidental grid points, one for each gear in mesh, at the mesh location. Gearmesh springs were then specified between the coincidental grids along the x-axis of the coordinate system defined for that mesh. This procedure was implemented for all the meshes in which the excitations consisted of at least one frequency component in the frequency range of interest. The remaining meshes such as those in the accessory drive area were not modeled, since these have a minimal effect on the casing response at lower frequencies.

IV.G.5.iv Structural Damping Representation

There are several sources of damping within the transmission including the bearings, seals, gearmesh damping, and structural damping due to the gearshafts and the casing. Some of these involve damping in specific regions such as the bearings and seals, while structural damping is distributed throughout the transmission. Damping effects due to sources such as gearmesh damping are usually much higher than structural damping. All damping effects, except those due to bearings which are taken into account in the bearing models, are represented as a single equivalent structural damping coefficient in the model. The value of this coefficient will in general be higher than usual structural damping as it includes all the other effects. If necessary, however, damping due to seals and the gearmeshes could be represented as viscous dampers at the appropriate locations if the corresponding damping factors could be found. For example, if the viscous damping factor at the location of a gearmesh is known, it can be incorporated as a damping element between the same nodes that are used for the gearmesh stiffness connections. Likewise, dampers for seals could be specified at appropriate locations. But since reliable estimates for damping coefficients of seals and gearmeshes are not available at present, these effects have been lumped together with the structural damping coefficient in the model.

The actual value for the structural damping coefficient was chosen based on correlations with experimental data to be discussed later. Since the major contribution to structural damping comes from the casing, the value specified depends on the damping properties of the casing material, which in this case is cast magnesium alloy. In Reference [48] (Lazan), magnesium alloys are reported to have structural damping in the range 0.001 - 0.17 depending on the stress level in the material. A value of 0.1 (equivalent to 5% critical damping) was chosen based on test data, which is within the reported range.

IV.G.5.v Overall Model

Assembling the various reduced casing components and internal element models resulted in an overall model size of about 3,730 nodes and 22,000 degrees of freedom (Figure 34). This is roughly 1/3 the size of the original transmission model, which made it feasible to run different cases for parametric studies where the damping was varied to improve correlation with test data. The complete model was first subjected to static analyses to verify the integrity of the model. A typical stress contour plot from a gravity loading analysis, where deflections and stresses in the transmission due to its own weight are computed, is shown in Figure 35. After such verification, the model could be used to evaluate the casing response needed for noise estimation.

IV.G.5.vi Computation of Mesh Excitations

Calculation of mesh excitations to be applied to the Apache transmission model followed the procedure described in a previous section. For each mesh, relevant data needed to compute gear tooth compliance were extracted from the gear drawings and specified as input to the program GRDYNMULT. The tooth compliance information, along with profile modification data obtained from the drawings, was used to determine the transmission error for the mesh. A Fourier transform of the transmission error yielded the amplitudes of the gearmesh harmonics which are used as excitations in the analysis.

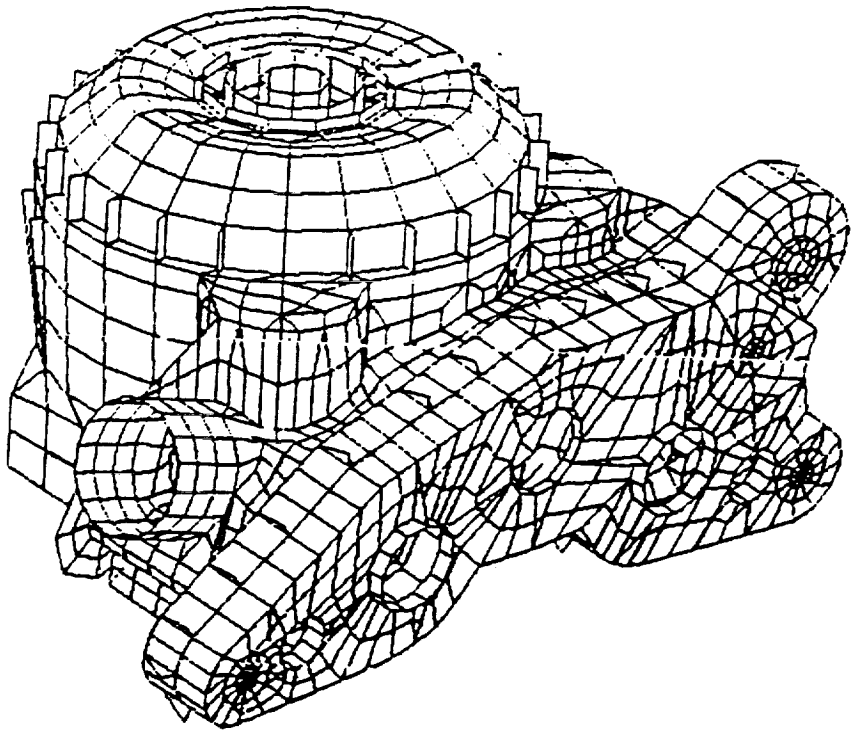

Figure 34. Finite Element Model of the Apache Helicopter Transmission

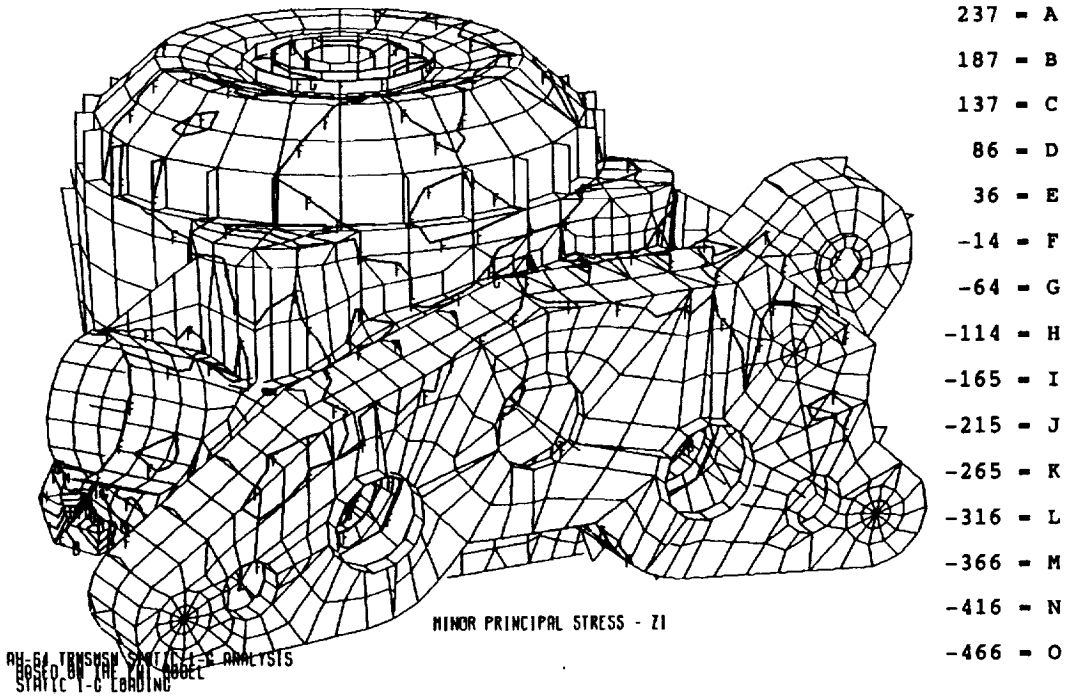

Figure 35. Typical Stress Contour Plot from a Gravity Loading Analysis (stresses in psi)

At each frequency of interest, the harmonic amplitude which constitutes the excitation at this frequency is specified as the relative displacement between the driving and driven gears at the mesh point in the model; i.e., it is imposed as the relative displacement along the line of action between the two coincident grid points corresponding to the meshing gears at the meshing location. Since the excitation consists of imposed dynamic displacements rather than forces, it cannot be applied directly. One of the methods of applying this excitation, employed in the present case, is to specify large masses where the displacements are to be imposed, and then apply a force equal to this large mass times the acceleration corresponding to the imposed displacement. The excitations for the planetary system (3rd stage) are applied simultaneously at all the sun-planet and ring-planet mesh locations. The phasing between the planets is determined from the number of sun and ring gear teeth and the number of planets, as described in Reference [49]. For the second stage where two drive pinions mesh with the combining gear, the phasing between the two meshes is again determined from the number of teeth on the combining gear and the angular separation between the drive pinions. The first stage mesh was not considered in the analysis as the model was deemed too coarse for application at this frequency. This is discussed in more detail below. Likewise, sideband excitations were not considered since the phenomena that cause such excitations could not be modeled easily and could vary from one transmission specimen to another.

IV.G.5.vii Dynamic Analysis

The maximum element size used in a finite element model imposes restrictions on the frequency range in which it can be relied upon to yield reasonable results. For the Apache transmission model, the maximum element size is about 3.7 inches. Based on this dimension, it was considered inappropriate to employ this model in response analysis for frequencies greater than about 3000 Hz. This precludes the first stage mesh occurring at a frequency of 4756 Hz. In any event, analysis at this frequency would still be difficult, even if a more detailed model with smaller elements was available. This is due to the fact that the first stage mesh involves spiral bevel gears, and there are no gear tooth analysis procedures available at present that accommodate such gear types. Hence reliable estimates for the excitations could not be computed. As a consequence, gear mesh excitation analyses were performed for the 2nd and 3rd stages only, viz. the combining gear and the planetary stages. For the planetary system, the analysis frequency range was restricted to include up to the fourth harmonic of the meshing frequency, which is up to about 2659 Hz. In the case of the combining gear, analysis was restricted to the fundamental meshing frequency (2634 Hz).

IV.G.5.viii Acoustic Analysis

It was estimated that this model should be capable of analysis at discrete frequencies up to 3000 Hz with reasonable confidence. This would exclude the spiral bevel gear mesh (4756 Hz), which typically produces the highest amplitudes of vibration on transmission housings. However, a NASA/Army investigation [50] into gearbox-related cabin noise aboard an OH-58 helicopter indicated that, although spiral bevel gears produce high vibration levels on the gear box casing, very little of this energy actually gets transmitted to the cabin and manifests itself as noise. The acoustic data indicated that this gear excitation is not the dominant source of noise in the helicopter cabin. In fact, it is typically the planetary system which contributes most to cabin interior noise. This was also evident from flight test noise data obtained on the Apache helicopter. This will be discussed later under the section which describes the experimental noise test. The noise generated in the cabin from transmission vibration is dependent on the energy transfer function between the gear box and the cabin interior and the acoustic efficiency of the process. Therefore, the design of quiet transmissions depends primarily on the ability to predict the noise generated by the planetary system, and perhaps the 2nd-stage gear set, in this case, a helical combining gear at 2634 Hz.

The complex velocities were determined by FE analysis at each of 1670 nodes that make up the elements on the surface of the model. These values were then compared with measured values from the vibro-acoustic test described by Hardesty and Hudson [51]. The test data provided a quality control measure for the FE analysis. The model could be modified and the overall system damping ratio adjusted until reasonable correlation existed between the measured and computed velocity values.

IV.G.5.ix Boundary Element Model

Figure 36 shows the boundary element model of the AH-64 Apache helicopter transmission. It was derived from the finite element model by removing its internal components. The elements used for modeling the interior components are not required for the acoustic calculations since it is the outer casing which actually radiates noise. Cantilevered elements were also removed from the finite element model and shaft openings were "capped off" and to produce a closed boundary element model. Of the 1920 linear elements in this model, 1416 were quadrilateral and 504 were triangular.

The boundary element model and computed velocities were then used to compute the radiated noise in terms of sound power in Watts. These values were then compared with the measured acoustic data. This procedure was executed for each of the gear mesh frequencies and associated harmonics up to 3 kHz.

The FE model of the Apache transmission was developed using linear elements. The surface pressures and velocities are assumed constant over each element. Seybert and Khurana [52] reported that this piecewise constant approximation has been used with good results, although a higher density model becomes necessary when the surface is irregular. Seybert and Khurana [52] suggest that the mesh density of the model be at least 4 linear elements per acoustic wavelength. The frequency range of analysis provided by the boundary element

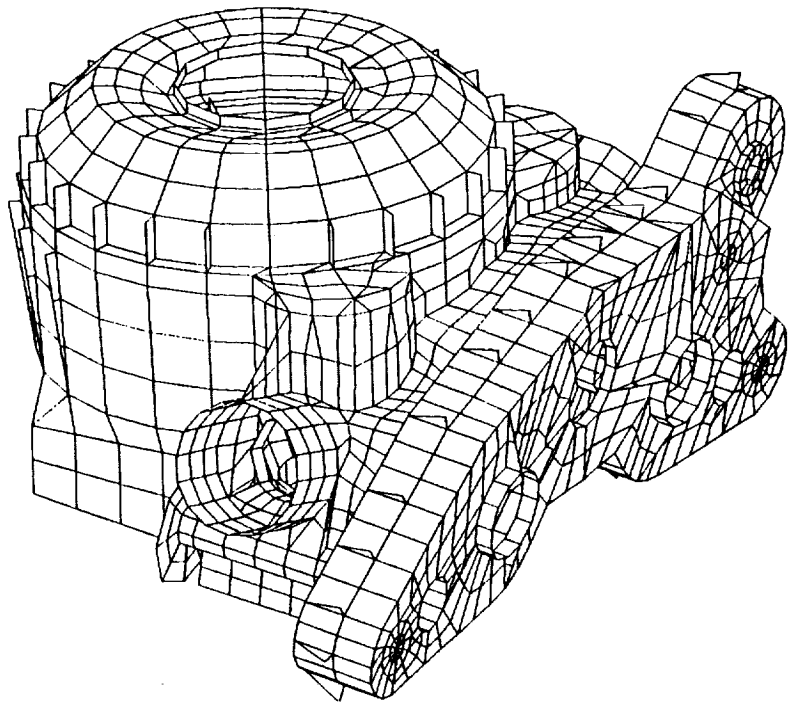

Figure 36. Boundary Element Model of the AH-64 Apache Helicopter Transmission

model is determined by the relative size of the elements in the mesh and the acoustic wavelength at the highest frequency of interest. The finite element analysis, on the other hand, is limited by the structural wavelength at the highest frequency of interest. This varies with the material properties and geometry of the structure. But the acoustic wavelength is dependent only on the ambient conditions and is assumed to be relatively constant. Therefore, although the finite element model provided dynamic response analysis up to 3 kHz, the acoustic analysis using the boundary element model was limited to frequencies below approximately 1500 Hz.

For BEMAP to predict acoustic emissions at gear mesh frequencies above 1500 Hz would have required an increase in the mesh density of the model. This would have meant approximately a 4-fold increase in the number of elements for the analysis to include the 2nd-stage (combining) gear mesh frequency at 2634 Hz. The deterministic approach described above would have been computationally impractical, even with the super-computer resources available. For the higher frequencies, rather than explicitly describe the velocity and pressure at each node, it might be sufficient to obtain a statistical mean-squared average. This statistical, or stochastic approach, reduces the complexity of the analysis by space-averaging the velocity distribution. Consequently, the method of statistical energy analysis was explored as an option for predicting transmission noise at the higher frequencies .

IV.G.5.x SEA Model

The Apache transmission was represented by a combination of rib-stiffened plates and cylinders as shown in Figure 37. The dynamic input to SEA was in the form of an average velocity over each sub-system and was obtained from the finite element model. The upper frequency range of the SEA model was limited only by the input data provided by the finite element model (<3000 Hz). The total sound power dissipation from each component in the SEA model was then computed. The combined total was then compared to the measured sound power levels.

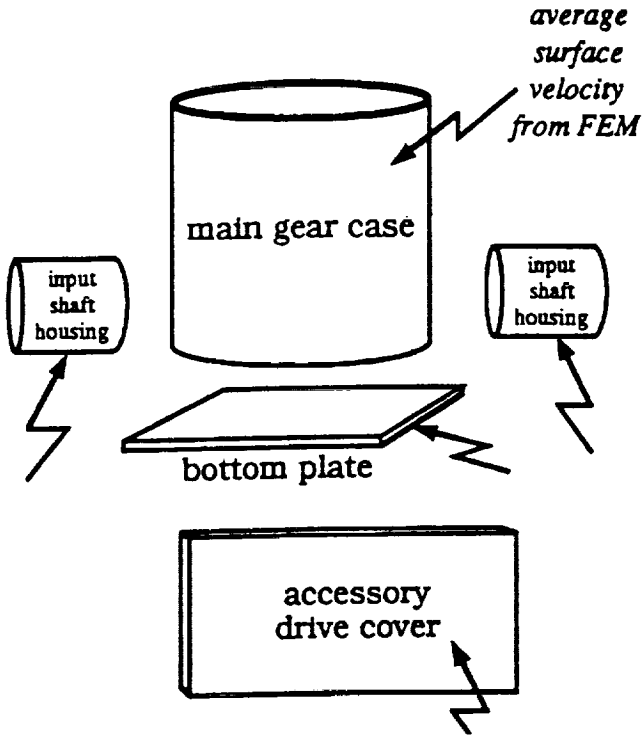

Figure 37. SEA Model of the AH-64 Apache Helicopter Transmission

IV.G.6 Experimental Program

To develop a methodology for predicting the noise generated by a rotorcraft transmission, it is necessary to validate such a method with a comprehensive vibro-acoustic database from an isolated transmission. The intent is to predict the noise radiating directly from the transmission housing. Therefore, the test transmission was installed on a regenerative test stand in an instrumented test cell. Because of the semi-anechoic nature of the test environment, it was necessary to measure sound intensity, using spacial averaging techniques, over a control volume around the gearbox. Noise reflective surfaces in the test cell were covered with 4 inch foam panels to minimize potential error in the sound intensity measurements. Vibration measurements were obtained simultaneously at several location on the casing. The intensity measurements were integrated over the surface area of the control volume to produce the overall sound power level (PWL). Two transmissions were tested so that data repeatability could be established. The difference in overall PWL between each transmission was within 0.5 dB. The test procedures and data were reported by Hardesty and Hudson [51].

Figure 38 is a 1/3-octave band plot of the measured sound power levels obtained from the transmission noise test described in Reference [51]. The acoustic data shown here is for the Apache transmission operating at 100% RPM and 100% torque (2828 HP). The 1/3-octave bands containing the gear mesh frequencies and related harmonics are indicated. A narrow band spectral analysis indicates the presence of an anomalous tone at 1640 Hz. It is not associated with any of the gear mesh harmonics. Although it was not positively identified, it is speculated that the tone is the 10th harmonic of the input drive shaft speed of 164 Hz. The highest noise level is exhibited by the spiral bevel (input) gear in the 5 kHz 1/3-octave band. The accelerometer data also indicate that this gear produces the highest vibration levels on the casing. This is consistent with the NASA/Army vibration measurements on the OH-58 helicopter transmission [50].

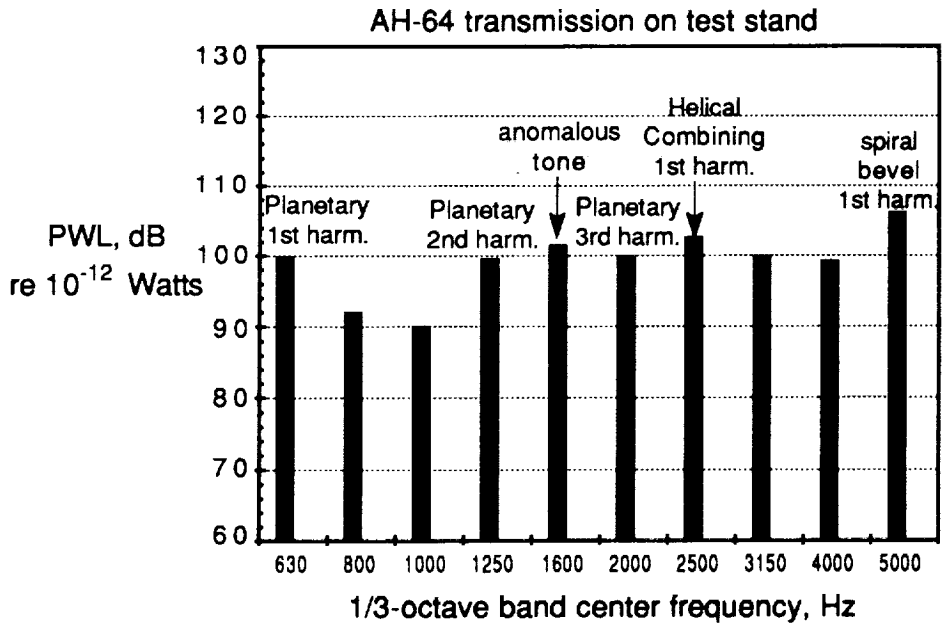

Figure 38. Measured Sound Power Spectrum of the Apache Helicopter Transmission

Figure 39 is a narrow band spectral plot of the noise measured inside the Apache helicopter in the pilot cockpit. This data clearly shows that very little of the vibration energy produced by the spiral bevel gear actually gets transmitted through the airframe and manifests itself as noise in the cockpit. This finding is also consistent with the acoustic data obtained in a NASA/Army investigation. Therefore, the discrete tones produced by the planetary system and the combining gear are of primary concern in the design of quiet transmissions. The data in Figure 39 also shows no indication of the anomalous tone at 1640 Hz.

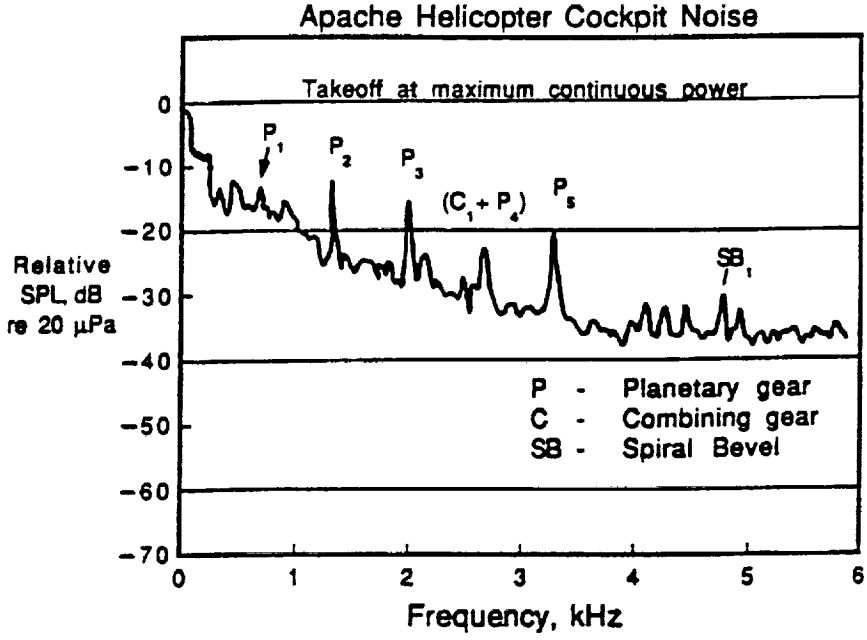

Figure 39. Measured Noise Levels in the Cockpit of the Apache Helicopter

IV.G.7 Comparison Between Analysis and Experiment

IV.G.7.i Correlation of Vibration Levels

At all the gearmesh frequencies of interest, the transmission finite element model is used to determine the vibration levels on the transmission casing. Accelerations at three specific locations on the casing obtained from analysis are compared to data measured during vibro-acoustic tests on an Apache transmission in Table 21. Boundary conditions used in analysis to obtain these results simulated the test configuration as closely as possible. Since the transmission was fixed to a solid aluminum plate around the curvic coupling area during tests, this region of the top cover in the model was grounded. In addition, the input and the output shaft ends in the model were grounded through soft and stiff torsional springs to simulate the effect of the peripheral components.

The results presented in Table 21 show that the model yields vibration levels that are comparable to measured data at lower frequencies. But at higher frequencies, the deviation between the model and the measurements becomes significant. The correlation deteriorates more rapidly in the case of the two measurements made at location 3.

Some general observations can be made based on the comparisons provided in Table 21. The model results are closer to the measured data at some locations than others. Thus it is difficult to extrapolate from these results and estimate the error that might be involved in noise computations, since vibration data from all the surface grid points are used in such computations. Also, since only the response normal to the surface is used in acoustic analysis, large deviations from measured data in the other directions may not necessarily lead to large deviations in noise estimates. Finally, at higher frequencies, the model tends to overpredict the response and thus would lead to conservative noise estimates. In light of these considerations, useful results could still be obtained from the model in the high frequency range, in spite of the decreased accuracy. The correlations suggest, however, that the model would produce unacceptable results at very high frequencies (>3000 Hz).

TABLE 21. COMPARISON BETWEEN MEASURED AND PREDICTED VIBRATION LEVELS (in g's)

Location No.	Accelerometer No.		Planetary Harmonics 1st	2nd	3rd	4th	Combining Gear (1st only)
			Meshing Frequency (in Hz)				
			664.7	1329.4	1994.1	2658.8	2634.4
1	1	Test	2.0	1.8	2.3	1.7	2.0
		Analysis	5.2	5.6	0.1	4.2	21.8
	2	Test	2.7	3.3	3.4	2.3	3.8
		Analysis	4.0	2.8	14.0	4.1	12.0
2	3	Test	0.3	1.8	0.8	1.5	1.8
		Analysis	0.3	0.5	4.5	3.1	9.5
3	4	Test	3.1	1.1	2.0	1.8	1.8
		Analysis	2.1	2.7	16.0	21.0	26.7
	5	Test	4.9	1.8	11.3	4.3	2.6
		Analysis	3.0	8.4	36.0	28.0	25.2

The decreasing accuracy of the model with frequency is directly attributable to the maximum element size used. But decreasing the element size would lead to an overly large model that would be difficult to handle. For example, halving the element size in the model would mean more than tripling the number of grid points and the associated degrees of freedom.

There are also other approximations in the analysis that could be additional sources of error. First among these is the fact that the planetary system behavior is not reproduced in the model. When the transmission is operating, the planets are revolving around the sun gear and the meshing locations are changing continuously around the sun and the ring gears. Thus every point in the ring gear experiences a load at the planet-pass frequency. Furthermore, the motion of the planets results in periodic changes in the stiffness and mass distributions of the planetary system. These effects are not simulated in the model where the planets are assumed to be stationary. Other sources of error include the approximations made(for modeling ease) in representing the transmission housing geometry, the assumptions involved in gear mesh excitation computations, and the boundary conditions used in the analysis.

IV.G.7.ii Correlation of Acoustic Data

Figure 40 is a plot comparing the measured sound power spectrum with the BEMAP-predicted noise levels of the planetary and the combining gears. The values for the planetary gear 1st and 2nd harmonic are over-predicted by 4.8 dB and 2.6 dB, respectively. Values for the planetary 3rd harmonic and the combining gear are grossly over-predicted. Recalling the mesh density requirement of 4 linear elements per acoustic wavelength, it is expected that the accuracy of the boundary element method would diminish at frequencies above the 2nd planetary gear harmonic which lies in the 1250 Hz 1/3-octave band. This is apparent from the results in Figure 40.

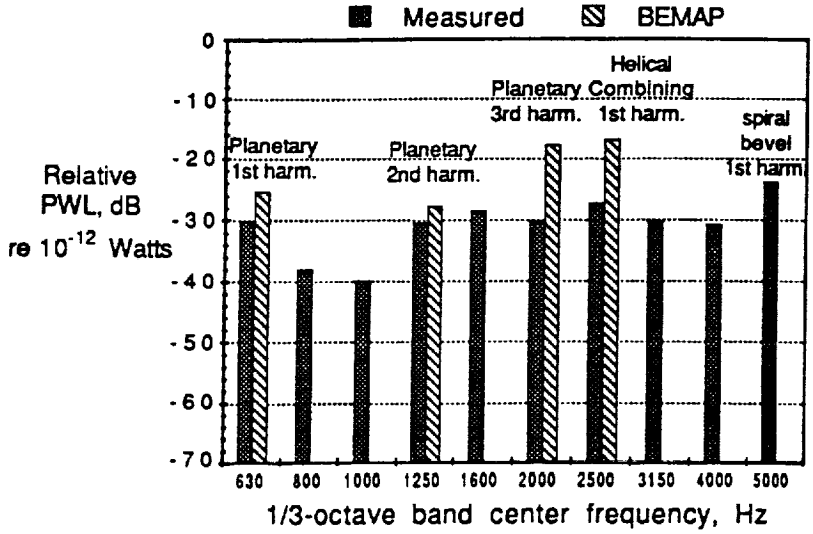

Figure 40. Measured vs. BEMAP-Predicted Sound Power Levels

In Figure 41, the predicted values from SEA for the combining gear frequency (2634 Hz) are plotted against the measured data. At the lowest gear mesh frequencies (e. g. planetary 1st and 2nd harmonics), SEA under-predicts the values by 6 to 7 dB. The accuracy improves at the planetary 3rd harmonic and combining gear mesh. As described earlier in the methodology section, certain assumptions are necessary for application of SEA. These assumptions appear to be valid at these higher frequencies as the results

here are good. Results for the spiral bevel gear frequency (4756 Hz) are also shown. However, the vibration data for this frequency was obtained from the measured accelerometer data since the FE model was limited to analysis at frequencies below 3 kHz. The combined result from both the boundary element method and statistical energy analysis is shown in Figure 42. The results are listed numerically in Table 22.

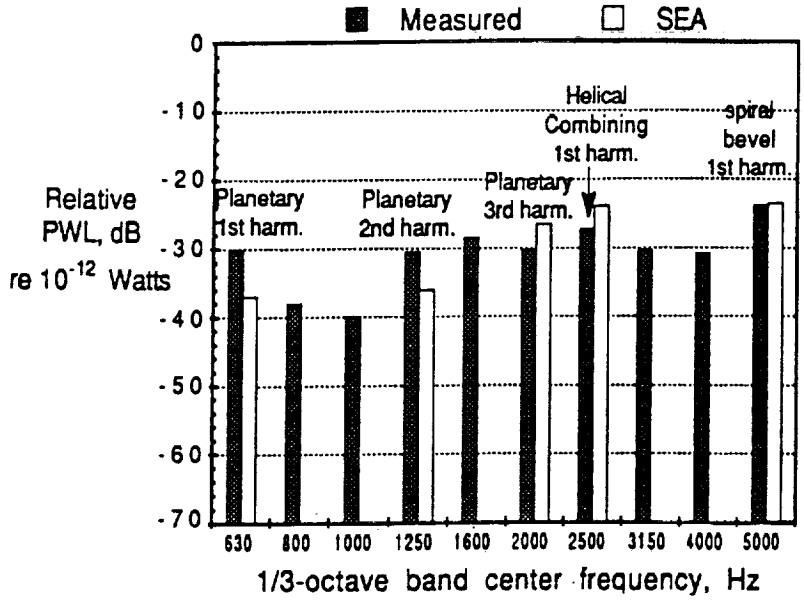

Figure 41. Measured vs. SEA-Predicted Sound Power Levels

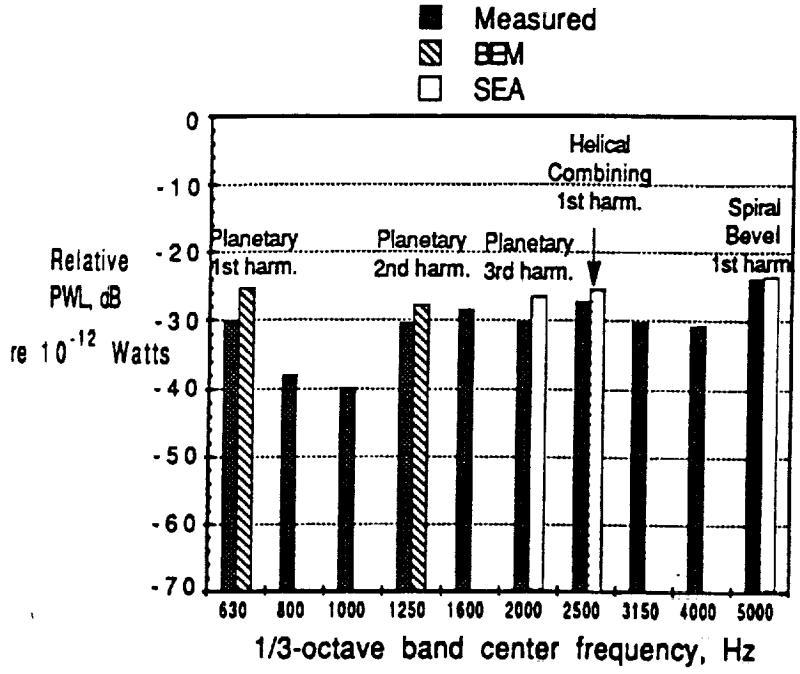

Figure 42. Measured vs. Combined (BEM and SEA) Predicted Sound Power Levels

TABLE 22. TRANSMISSION NOISE PREDICTION VALIDATION
(AH-64 Apache helicopter transmission)

Gear Mesh Harmonic		Frequency Hz	1/3-octave Center Freq, Hz	Measured PWL, dB re 10^{-12} Watts	Predicted PWL, dB re 10^{-12} Watts	DPWL dB
Planetary:	1st harm	664.7	630	99.9	104.7	+4.8
	2nd harm	1329.0	1250	99.6	102.2	+2.6
	(Unknown)[1]	1640.0	1600	101.5	-	-
	3rd harm	1994.0	2000	99.8	103.5	+3.7
	4th harm	2659.0	2500	102.7[2]	106.0	+3.3
Combining:	1 harm	2634.0				
Spiral Bevel:	1st harm	4756.0	5000	106.2	-	-

[1]An anomalous harmonic excitation was observed at 1640 Hz during the AH-64 transmission noise test. This frequency does not correspond with any of the known gear mesh frequencies of the transmission or the input drive system of the regenerative test stand.
[2]Combination of planetary 4th harmonic and combining gear 1st harmonic

The sound pressure or sound intensity distribution on the surface of the transmission, computed by BEMAP, can be conveniently plotted on the boundary element model. An example is shown in Figure 43. The post-processor used in this case is PDA/PATRAN™. Plotted here are the surface sound pressure levels at the planetary gear mesh frequency of 665 Hz. The highest levels are observed in the vicinity of the input shaft and pinion gear housings on both sides, near the accessory gear box (dark shading). There are also some "hot spots" where high sound pressure levels are radiating from the front face of the gear box. Apparently, the planetary gear mesh loads are transmitted through the shaft bearings at the planetary and combining gears, and ultimately, through the 1st-stage gear housings. A similar sound pressure distribution was observed at the planetary 2nd harmonic.

The FE/BE model was fine-tuned by adjusting the damping ratio in the finite element model. This was a total system damping ratio distributed over the entire structure (e. g. shafts, housing, etc.). Acoustic power radiated at the planetary gear mesh frequency was evaluated over a range of damping ratios. Figure 44 shows the sensitivity of the predicted sound power level to the system damping. A damping ratio of 5% critical was chosen as a nominal value for the final predictions. The transmission gears, shafts, and bearings are made of steel, and are therefore fairly stiff. But the housing is made of a cast magnesium alloy. Reference [48] (Lazan) shows that test specimens made from such alloys have structural damping ratios as high as 17 percent. The combination of a stiff drive train, a housing with relatively high damping, and lubrication in the gears, suggests that an overall damping ratio of 5% critical (10% structural) is a reasonable estimate.

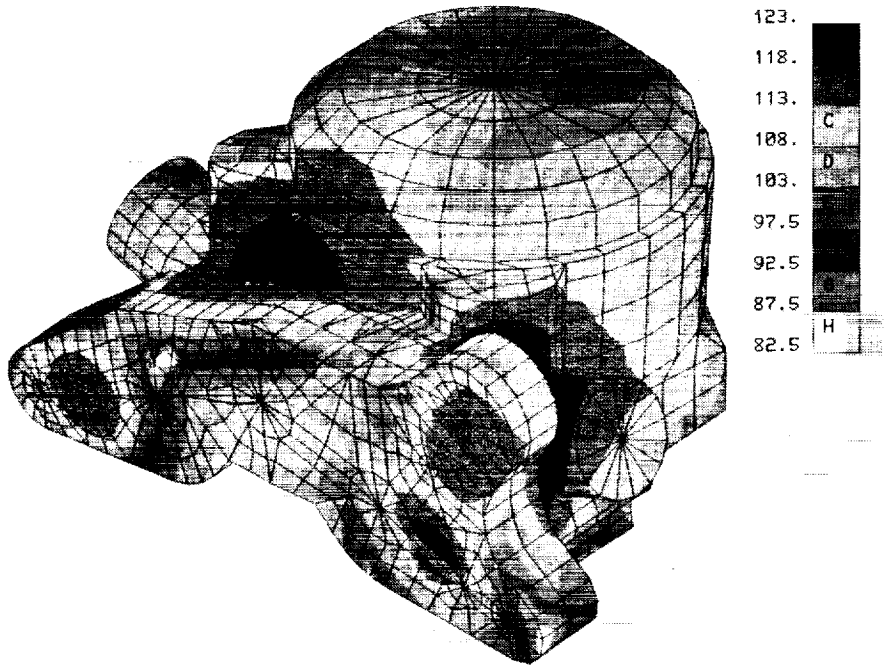

Figure 43. Surface Noise Contour on Transmission Housing at Planetary Gear Mesh (665 Hz)

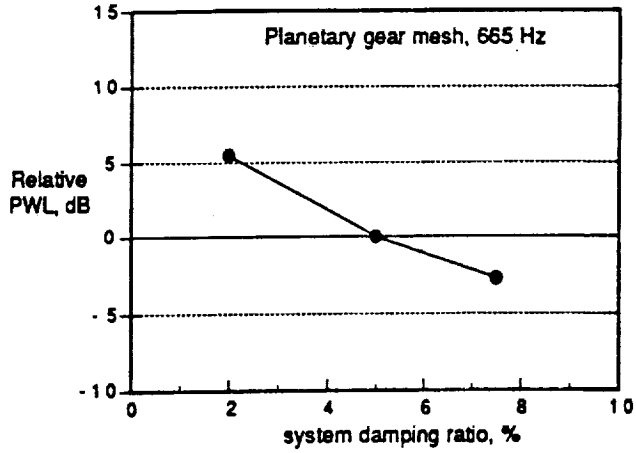

Figure 44. Effects of Structural Damping on Predicted Gearbox Noise Levels

IV.G.8 Description of the MDHC Advanced Rotorcraft Transmission

The interior components of ART are illustrated in Figure 45. It is a 3-stage transmission rated at 5000 HP and weighs 815 pounds. The 1st-stage consists of two input pinions turning at 20952 rpm, each driving a pair of face gears with a mesh frequency of 9778 Hz. The 4 face gears drive the 2nd-stage which consists of four spurs driving a single combining gear with a mesh frequency of 3107 Hz. The combining gear then drives the 3rd-stage. Here, a sun gear drives six high contact ratio (HCR) planetary gears with a mesh frequency of 797 Hz. This planetary system drives the output shaft at 290 rpm. The key features of the gear design which are expected to help reduce radiated noise are the split-torque configuration and the HCR planetary gears.

Figure 46 shows the transmission casing which has about 50% more radiating surface than the Apache transmission. Currently, there is no added rib-stiffening in the gear casing for noise reduction. The BEMAP analysis indicated a casing noise radiation efficiency comparable to that of the Apache transmission casing. The option of casing modification can be investigated to optimize its design for low noise radiation efficiency.

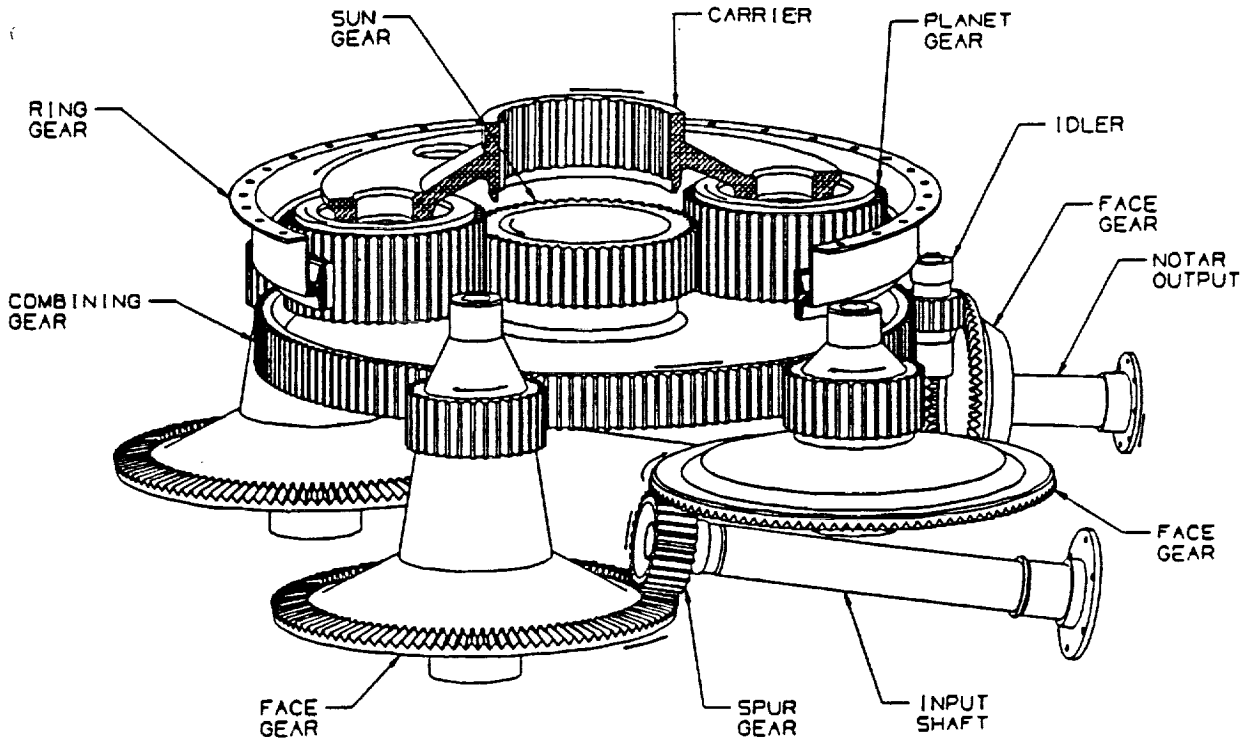

Figure 45. ART Gear Arrangement

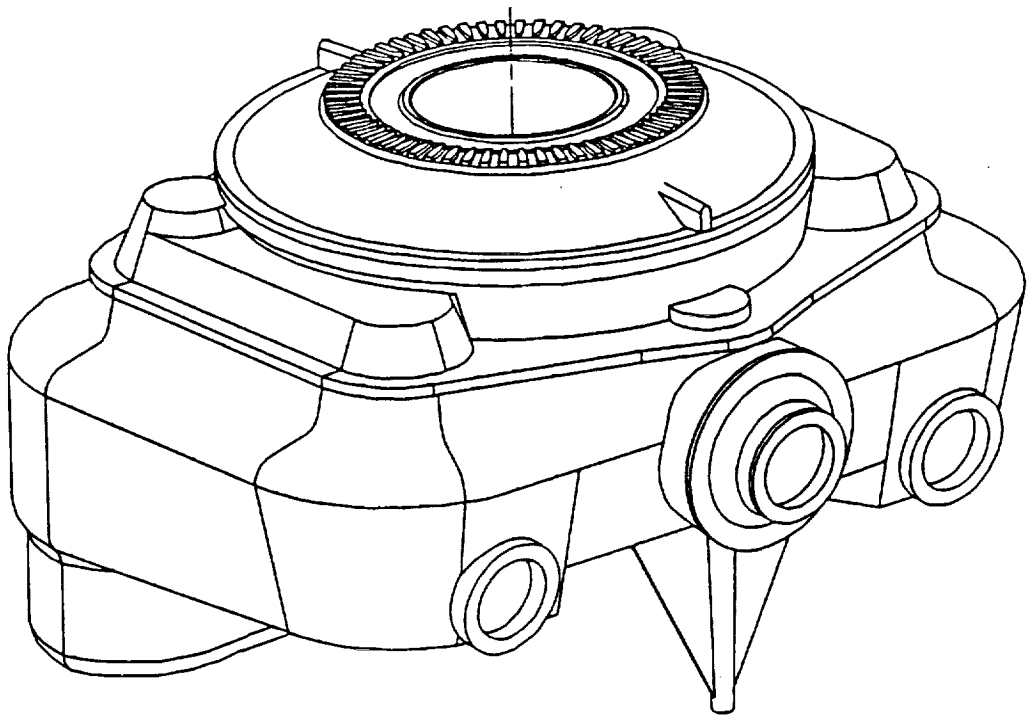

Figure 46. ART Outer Casing

IV.G.8.i Baseline Transmission Noise Level

The estimated noise level for a state-of-the-art 5000 HP transmission was based on measured acoustic trend data obtained from the 2828 HP Apache helicopter transmission operating over a range of torque settings. This data is plotted in Figure 47. The measured overall sound power level (OAPWL) for the Apache helicopter transmission is 110.8 dB re 10^{-12} Watts at 2828 HP. The trended noise data indicate an increase of 1.2 dB going from a 2828 HP transmission to 5000 HP. The 5000 HP SOA transmission is expected to produce a 112 dB overall sound power level. The ART goal would be 10 dB less, or 102 dB. However, if we disregard the anomalous tone in the 1600 Hz 1/3-octave band, the measured Apache overall noise level drops by 1.3 dB to 109.5 dB. This approach, in effect, sets an even stricter noise goal for ART. Additionally, as indicated earlier, the 1st-stage gear mesh frequencies in both the Apache transmission and ART are beyond the range of the analytical models. Since it has been well established that the 1st-stage gear mesh is not a major contributor to the vehicle interior noise levels, the measured noise produced by the spiral-bevel gear in the Apache model is also disregarded. This again is in the interest of conservativism in establishing a noise goal for ART. Therefore, the measured noise levels produced by the Apache transmission planetary system and combining gear totals 106.7 dB. Consequently, the estimated state-of-the-art baseline noise level (+1.2 dB) becomes 107.9 dB, and the corresponding noise goal for ART is 97.9 dB (10 dB less). The mesh frequency of the 1st-stage (face gear) in ART is 9778 Hz, approximately twice that of the spiral-bevel gear in the Apache transmission. This places it well beyond the speech interference range of the frequency spectrum. The SOA baseline transmission noise level is shown in Table 23.

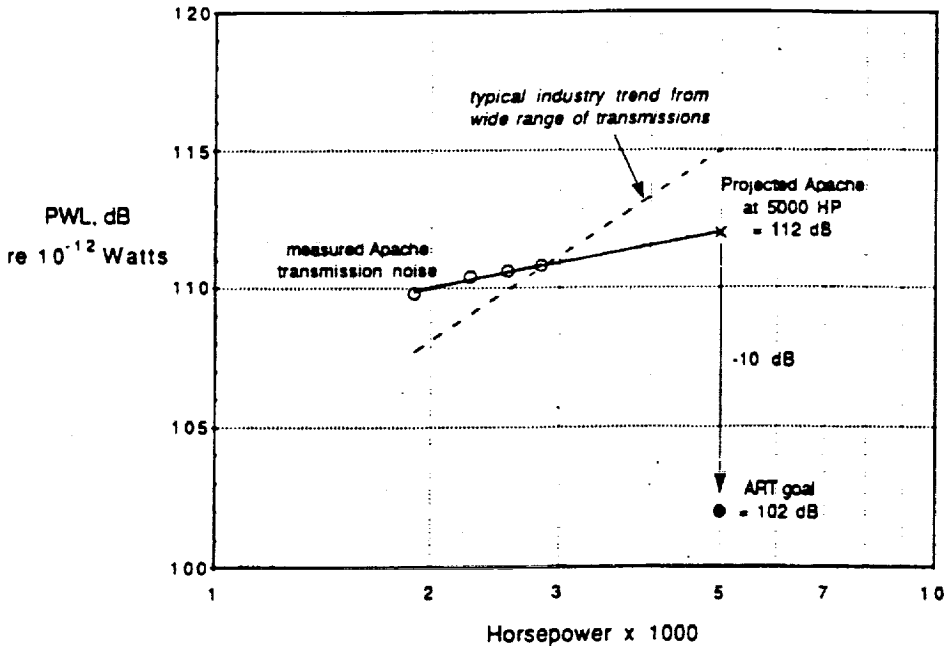

Figure 47. ART Transmission Noise Goal from Apache Transmission Noise Trend Data

TABLE 23. ESTIMATED NOISE LEVEL FOR BASELINE TRANSMISSION

	OAPWL (dB re 10^{-12} Watts)
Measured Apache transmission noise *(planetary and combining gear mesh frequencies only)*	106.7
Baseline 5000 HP (+1.2 dB)	**107.9**

IV.G.9 Application of Methodology to ART

IV.G.9.i Finite Element Model

The procedure followed in developing the ART finite element model parallels that used for the Apache transmission model. As in the case of the Apache model, ART was divided into several components, each of which was modeled separately. The overall model was obtained by assembling the individual component models.

Figure 48 depicts the representation used for the internal components. The planet carrier, the ring gear, the combining gear, and the gearwebs were modeled with quadrilateral and triangular plate elements. The gearshafts were modeled with one-dimensional bar elements and rigidly tied to the webs. The top, intermediate, and lower ART casing models are shown in Figures 49, 50, and 51. Plate elements were used in most regions, combined with solid elements to represent the flanges in some areas. The maximum element size in the model is about 2.7 inches, which is smaller than the maximum size in the Apache model. It follows that the ART model can be expected to produce results of comparable accuracy at higher frequencies than the Apache model. This is essential since the range in which results are required for ART is higher (up to 3200 Hz compared to about 2700 Hz for the Apache).

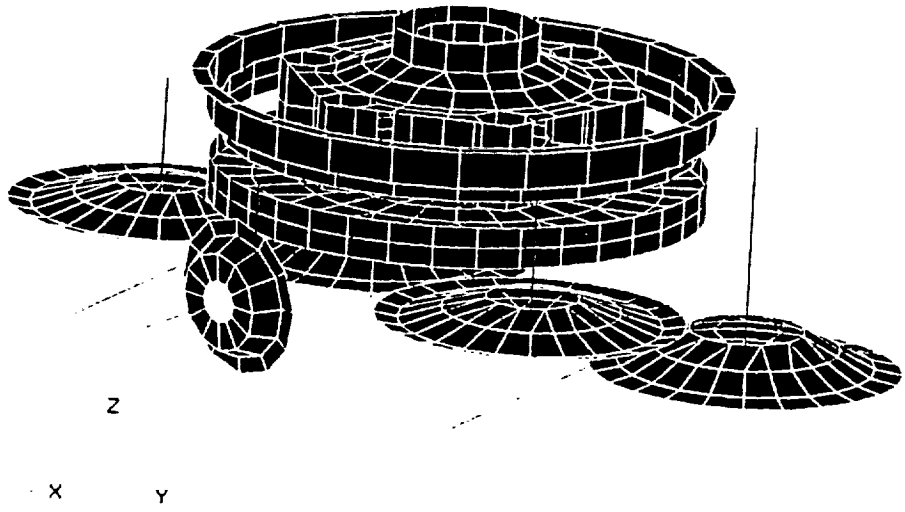

Figure 48. FEM of ART Internal Components

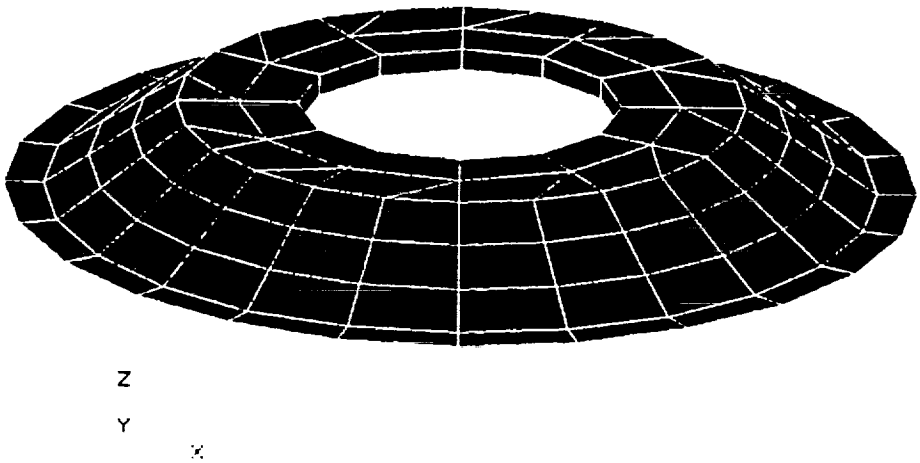

Figure 49. ART Top Cover

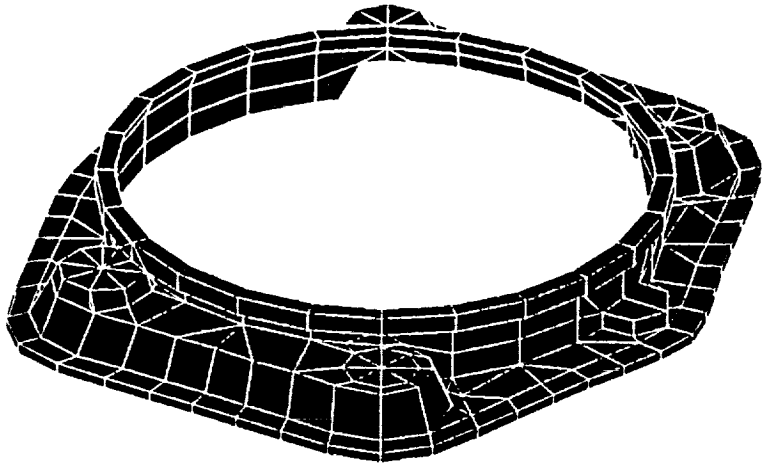

Figure 50. ART Intermediate Casing

Techniques used to model the bearings and gearmeshes of the Apache transmission were also used for ART. The complete model obtained by combining the various components is illustrated in Figure 52. This model possesses approximately 3600 nodes and 3450 elements. Typical stresses obtained from a static gravity loading analysis are shown in Figure 53.

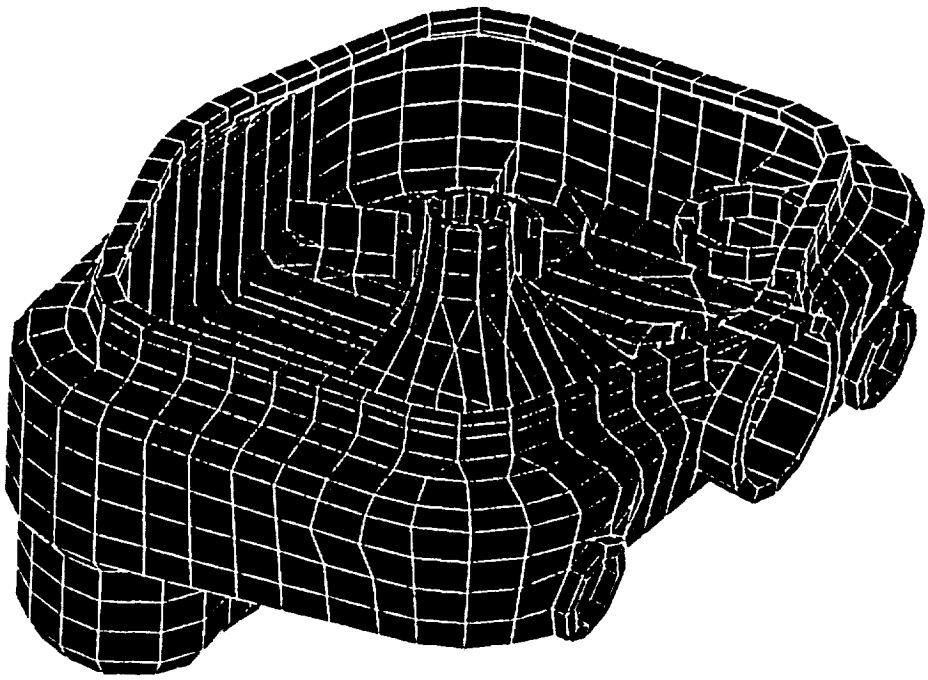

Figure 51. FEM of ART Lower Casing

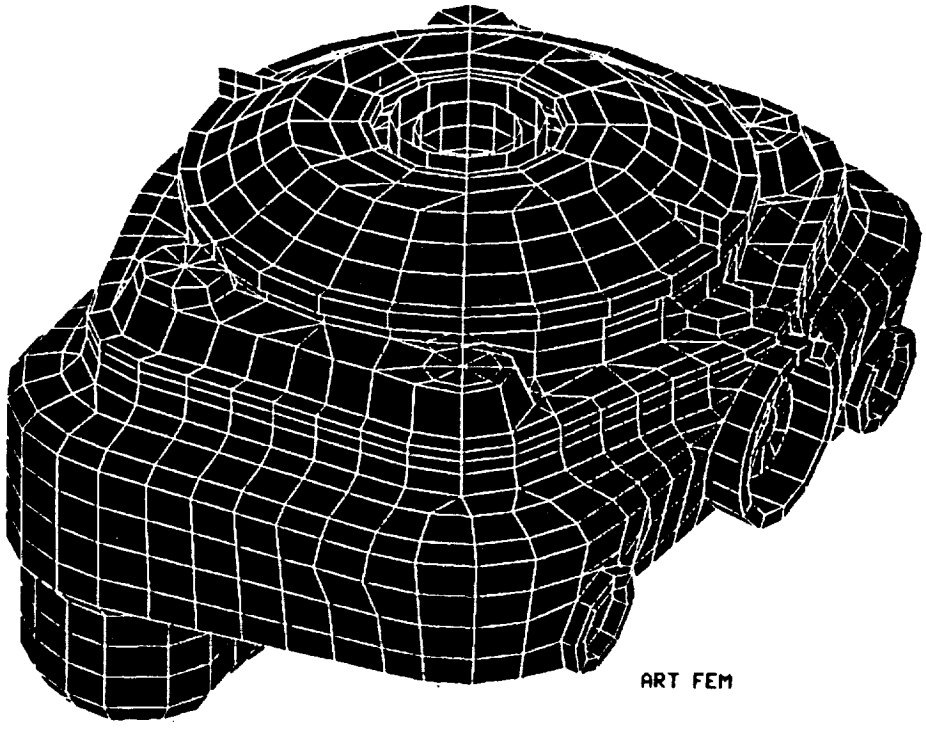

Figure 52. Complete FEM of ART

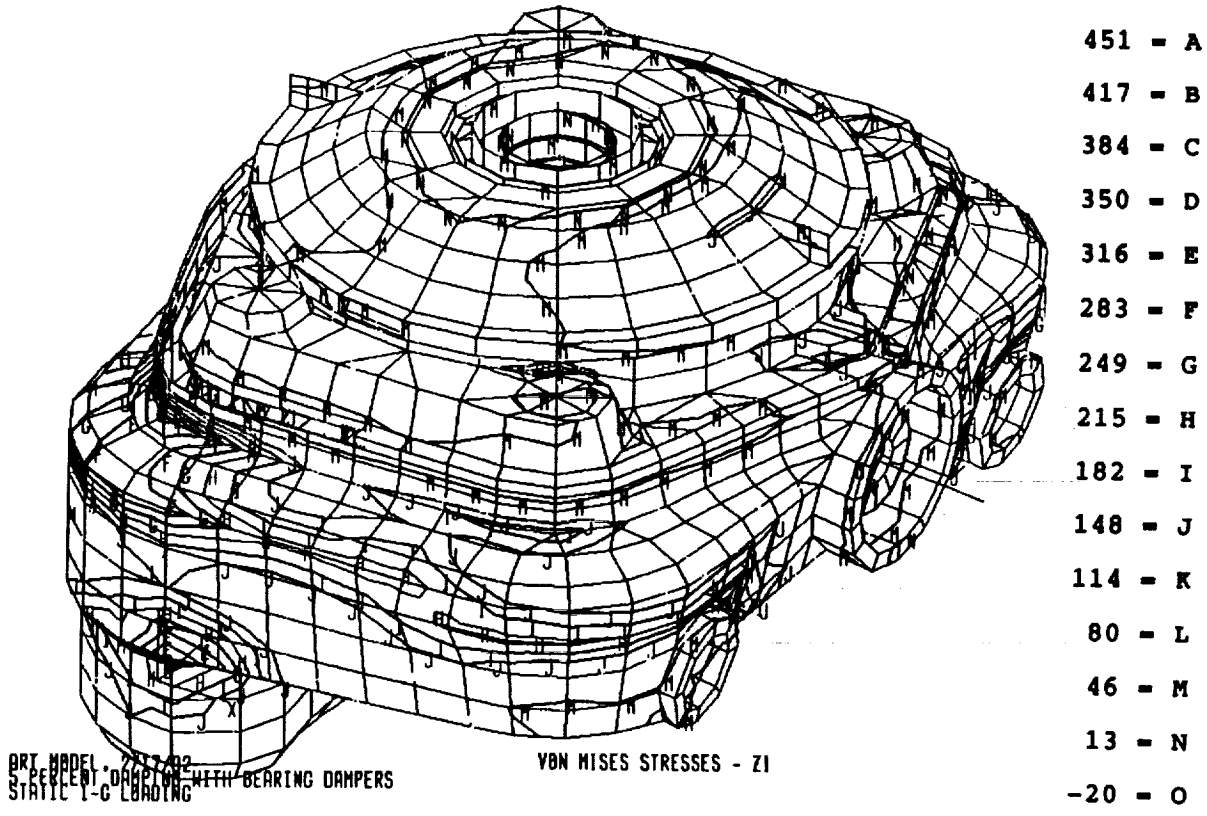

Figure 53. Stress Contour Plot from Static Gravity Loading (stresses in psi)

IV.G.9.ii Gear Mesh Excitation

Gear mesh excitations for ART were computed using procedures discussed earlier. Only the second and third stage meshes, consisting of the combining and the planetary gears, were considered in the analysis. Response to gear mesh excitations were computed at the first four harmonics of the planetary system and the first harmonic of the second stage mesh. Fundamental frequency of the planetary mesh is 797 Hz, while the meshing frequency for the combining gear is 3107 Hz. The first stage face gear meshes were not included in the analysis since these occur at a very high frequency (>9000 Hz).

The gear tooth dimensions needed to calculate tooth compliance were obtained from design data. In computing the transmission error from the compliance data for each mesh, various tooth profile modification amounts were specified and the excitation harmonics determined. The modification amounts that resulted in the lowest amplitudes for the harmonics of the transmission error were used in the analysis. These optimum tooth profile modification data are listed in Table 24 for each mesh. The casing response was obtained with the resulting excitations at all the frequencies of interest.

TABLE 24. LINEAR PROFILE MODIFICATION DATA FOR GEAR TEETH

Gear	Roll Angle at Start of Tooth Modification (deg)	Amount of Modification at Tip (in.)
Sun	24.0	0.0008
Planet	26.0	0.001
Ring	16.9	0.001
2nd Stage Pinion	27.3	0.00085
2nd Stage Gear	27.0	0.00085

IV.G.9.iii Boundary Element Model

Figure 54 shows the boundary element model of the MDHC ART design. It was derived from the finite element model in a manner similar to that of the Apache transmission and consists of 1754 elements. The geometry of the ART casing is somewhat simpler than that of the Apache model. Since the ART finite element and boundary element models were carefully developed with the specific application in mind, they are a better representation of the actual geometry than those developed for the Apache transmission models.

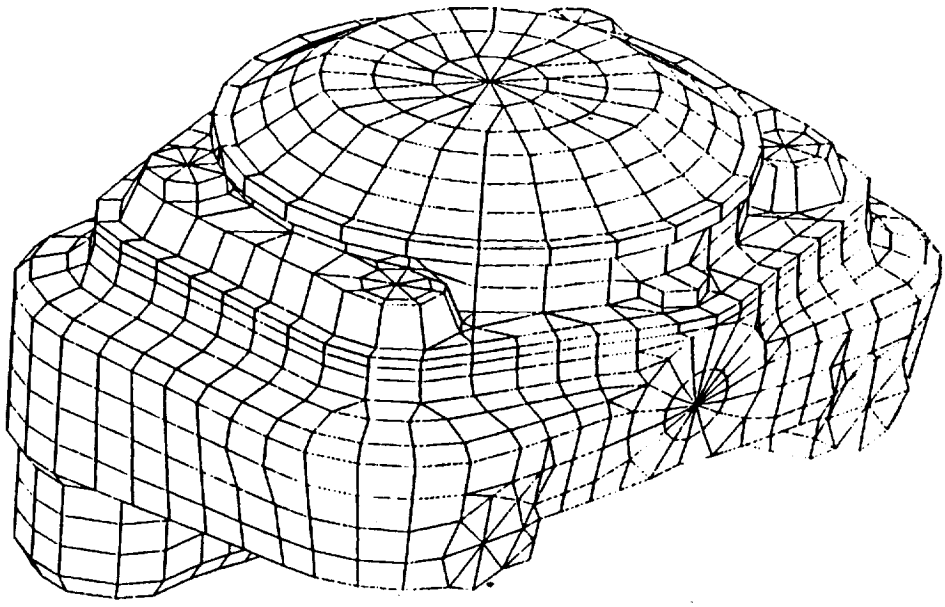

Figure 54. ART Boundary Element Model

IV.G.9.iv SEA Model

For application of statistical energy analysis at the combining gear mesh and the planetary 3rd and 4th harmonics, ART was represented by a combination of cylindrical shells and flat plates. The average surface velocity over each subsystem was obtained from the finite element model in a manner similar to that used for the Apache transmission. The sound power dissipation from all subsystems were combined to give the total radiated sound power.

IV.G.10 Discussion of Results

To quantify the predicted noise emissions for ART, it was necessary to establish a correction factor which represents the error margin associated with the noise prediction methodology. The correction factor would then be applied directly to the ART noise prediction. This necessitated a direct comparison between the noise levels predicted for the Apache transmission and the corresponding measured values. These comparisons are summarized in Table 25. Rather than apply corrections to each individual harmonic in the ART evaluation, the error margin was determined for the combined total noise level. This, as it turns out, is a more conservative approach. A total correction factor of -3.6 dB (measured-predicted) was derived for the overall sound power level. This correction factor was applied to the predicted overall sound power level for ART.

TABLE 25. TRANSMISSION NOISE PREDICTION ERROR CORRECTION
(AH-64 Apache helicopter transmission)

Gear Mesh Harmonic		Frequency Hz	Octave Center Freq, Hz	Measured PWL, dB re 10^{-12} Watts	Predicted PWL, dB re 10^{-12} Watts
Planetary:	1st harm	664.7	500	99.9	104.7
	2nd harm	1329.0	1,000	99.6	102.2
	3rd harm	1994.0	2,000	99.8	103.5
	4th harm	2659.0	4,000	102.7[1]	106.0[1]
Combining:	1st harm	2634.0			
OAPWL				106.7	110.3

[1]Combination of planetary 4th harmonic and combining gear 1st harmonic.

Table 26 summarizes the noise predictions for MDHC's current ART design. The predicted noise levels were obtained by implementing the same procedures used in the Apache transmission noise evaluation. When the 3.6 dB correction factor from Table 25 is applied to the predicted value for OAPWL, a total noise reduction of 9.6 dB is achieved in the current MDHC ART design, relative to the baseline transmission noise level of 107.9. The reduction in overall transmission noise level is due primarily to a combination of several design features. The analysis demonstrated that a high contact ratio (CR) between the sun-planet (CR=2.24) and ring-planet (CR=2.48) gear meshes provides a significant reduction in the dynamic response of the meshing forces, and subsequent reduction in noise produced at the planetary gear mesh harmonics. The contact ratios used in the Apache transmission are 1.5 and 1.67, respectively. Reduced noise levels were also indicated by increasing the contact ratio from 1.64 (in the Apache transmission) to 1.7 at the combining gear stage. Another major contribution to overall system noise reduction was accomplished by optimizing the tooth profile modification at the planetary and combining gear stages. The finite element analysis provided a means to evaluate the effects of such modifications on the system dynamic response and noise. Finally, mass stiffening of various components including the ring gear web, sun gear shaft, and the gear box casing, indicated further potential for optimizing the ART design for low acoustic emissions. Planetary gear phasing was also employed as a noise reduction feature in the ART design. However, this is considered a state-of-the-art noise control feature which already exists in the baseline transmission design.

TABLE 26. ART NOISE PREDICTIONS

Gear Mesh Harmonic		Frequency Hz	Predicted PWL, dB re 10^{-12} Watts		Plus Correction (-3.6 dB)
Planetary:	1st harm	797.0	98.0	(BEM)	
	2nd harm	1594.0	95.9	(BEM)	
	3rd harm	2391.0	90.0	(SEA)	
	4th harm	3188.0	84.0	(SEA)	
Combining:	1 harm	3107.0	96.0	(SEA)	
OAPWL			101.9		**98.3**

IV.G.11 Summary of Results

The acoustics assessment of the MDHC Advanced Rotorcraft Transmission (ART) is based on validated analytical techniques. The methodology employs the use of finite element methods to determine the dynamic response of the gear box casing. This excitation of the casing, due to the gear meshing forces was used for calculating the case-radiated noise. The acoustic calculations were accomplished by a combination of a deterministic approach, based on the boundary element method, and a stochastic approach, based on statistical energy analysis (SEA). It was necessary to employ both of these methods to evaluate the gear mesh harmonics in the frequency range of interest. The combined dynamic and acoustic analyses were validated by

application to an existing AH-64A transmission and comparing the results to a vibro-acoustic data base obtained during a comprehensive sound intensity survey of the transmission operating on a regenerative test stand. The validation provided a high degree of confidence in both the dynamic and acoustic models used in the ART noise assessment. The validated methodology was then applied to the MDHC ART design. Major noise reduction features were incorporated in the design which were evaluated by using advanced dynamic and acoustic prediction methodologies. These features can not be evaluated using conventional analytical techniques. Results indicate an overall noise reduction of 9.6 dB relative to a current state-of-the-art transmission rated at the same horsepower. Although this falls short of the program goal of 10 dB noise reduction, the analytical procedures allow for "design-to-noise" capability. Preliminary parametric studies indicate a strong potential for optimizing the ART design to achieve maximum noise reduction without exceeding the weight goal.

V. MISSION EFFECTIVENESS

The mission effectiveness analysis of a Future Attack Air Vehicle (FAAV) which uses the Advanced Rotorcraft Transmission (ART) is presented herein.

The FAAV is visualized by MDHC as a twenty-first century air vehicle that is versatile, highly maneuverable, serviceable and stealthy. It will be capable of air-to-air (ATA), air-to-ground, anti-armor, and special electronic mission aircraft (SEMA) missions conducted worldwide, day or night, in all weather conditions.

Several key performance parameters of the FAAV are evaluated herein to determine the benefits that would be derived from the performance characteristics of the selected ART configuration. This analysis focuses on the system, not just the transmission, and it considers the synergism of the transmission performance on the FAAV as a total system.

This section is segmented into three subsections:

- Mission Analysis
- Reliability
- Life-Cycle Costs

Mission Analysis is an assessment of lethality and survivability of the aircraft. As part of the ART program, an evaluation of how the improved transmission impacted mission effectiveness was studied. Although the changes being considered affected all areas of mission performance, past experience indicated that the most demanding area would be a close-in, air-to-air engagement. Accordingly, the air-to-air engagement was the focus of this analysis.

FAAV Reliability will be much improved over current generation aircraft. The amount of improvement is estimated by trending previous and current design reliabilities. Assuming the FAAV is a next-generation design, the trend is to double reliability requirements every generation. This results in an FAAV system reliability of 18 hours with mission reliability increasing from 22 to 75 hours.

Life Cycle Costs (LCC) estimates were made for three configurations: baseline FAAV, ART improved FAAV, and optimized FAAV with ART. This report contains the estimates and a discussion of the techniques and assumptions used to make those estimates. The LCC estimate is reflective of the technological advances (composites and integrated mission equipment) and operating conditions inherent in designing and fielding an aircraft in the next century.

V.A MISSION ANALYSIS

As part of the Advanced Rotorcraft Transmission (ART) project, there was a requirement to evaluate the effect on mission effectiveness of using an advanced rotorcraft transmission of lighter weight, variable RPM, and greater reliability in a conceptual Future Attack Air Vehicle (FAAV). The proposed design changes affect the aircraft's ability to perform its mission, and can be translated into a comparison of the lethality and survivability of FAAV equipped with the candidate transmission designs. Although the changes being considered affect all

areas of mission performance, past experience indicated that the most demanding area would be a close-in air-to-air engagement. Accordingly, the air-to-air engagement was the focus of the analysis.

V.B APPROACH

The primary changes incorporated, or considered, in the candidate ART designs were the following:

- Weight reduction of 622 lb compared to an upgraded Apache-type transmission
- 5000 horsepower capability
- Increase in mean-time-between-removals (MTBR) to 6200+ hours
- Ability to temporarily increase rotor RPM to 120 percent.

The aircraft selected to evaluate the ART was a conceptual FAAV, modeled as a follow-on Apache design, with upgraded capabilities. Specifically, the FAAV included:

- Engines of 3000 HP each (6000 HP total)
- 5-bladed rotor system with 25-inch blade chord
- NOTAR anti-torque system

The baseline aircraft used for comparison was the FAAV mentioned above, equipped with an upgraded Apache-type transmission. This configuration is referred to as the baseline FAAV in this section. The second configuration referenced in this section is the ART improved FAAV. This is the same FAAV aircraft, modeled as a follow-on Apache design, equipped with the 5000 HP ART transmission. The third configuration is referred to as the optimized FAAV with ART. This configuration assumes that the aircraft was designed from the ground up with the ART transmission. Operation of the main rotor at 120% RPM is assumed for this configuration to evaluate potential mission analysis and cost benefits.

The scenario used was an air-to-air engagement between the three FAAV aircraft configurations and selected threat helicopters. The basic engagement was between two Blue aircraft and four Red aircraft, to ensure the Blue aircraft were properly stressed.

V.C THREATS

The threat was represented by the MI-28 "HAVOC," and the KA-35 "HOKUM."

V.D ENGAGEMENT MODEL

The Air Land Engagement Simulation (ALES) was used to evaluate the air-to-air encounters. The few-on-few ALES model simulates the performance of the aircraft and their weapons systems, and evaluates the outcome.

A total of ten combinations of initial headings for the aircraft were evaluated for each test case. The aircraft configurations and weapons loads that were modeled are given in Table 27.

TABLE 27. AIRCRAFT CONFIGURATIONS AND WEAPONS LOADS

	CONFIGURATION #		
	1	2	3
Description	**Baseline FAAV**	**FAAV with ART**	**FAAV with ART @ 120% RPM**
Gross Weight (lb)	17,336	16,714	16,714
Transmission	Upgraded Apache-type with 5000 HP capability	ART	ART
Main Rotor RPM	100%	100%	100%
Anti-torque System	NOTAR	NOTAR	NOTAR
Weapons for all configurations:			
Stingers	8		
Rockets	38		
Rounds 30mm	1200		

The capability to temporarily increase rotor RPM could not be modeled directly. The model runs for this situation were made with rotor RPM at 120 percent for the whole run.

The input variables that were changed were gross weight and rotor RPM. Specifically, the numbers of interest were gross weights of 17,336 and 16,714 lb, and RPM of 100 and 120 percent. The effect of increased reliability was assessed separately, with the Sustained Combat Evaluation Tool (SCET) described later. The engagements were modeled at sea level/standard day conditions. This was done to ensure that there would always be at least 5000 HP available to use the full capability of the ART.

Although cases with missiles and guns, and "guns only" were modeled, the "guns only" cases were more informative.

Although there is some maneuvering required to attain a missile-firing position, the results, to some degree, become a function of the attributes of the type of missile used. This tends to obscure the performance contribution of the ART. For this reason, the "guns only" cases were analyzed more closely for their sensitivity to ART attributes, and only the "guns only" cases are displayed on the results charts.

As indicated in Table 27, the only differences between the configurations were gross weight and rotor RPM. All three aircraft configurations were run against both types of threat helicopter. The measures of effectiveness were:

Lethality - Threat helicopters destroyed

Survivability - Blue helicopters surviving

Exchange Ratio - Red losses divided by Blue losses

Firing Opportunities - Blue firing opportunities for a given run (equal to the number of bullets expended by Blue)

Engagement Time - The total time required to complete the engagement.

As indicated, the "firing opportunities" represents the number of rounds fired by the guns of the Blue aircraft. Since a round is not fired unless the targeting constraints are met, the firing of each round was considered a firing opportunity.

The total engagement time is an average of all engagement times for a given set of circumstances, and is a measure of the efficiency of the weapon system.

The FAAV aircraft were also evaluated with the SCET model. This is a program that calculates the impact of combat losses, combat availability, resupply times, and initial force levels on combat sustainment. This tool evaluates the mission impact of the increased availability of the ART, in addition to any increased combat effectiveness.

V.E RESULTS AND CONCLUSIONS

V.E.1 Results

The ALES program uses an imbedded helicopter performance model called the Maneuver Criteria Evaluation Program (MCEP). Prior to running the ALES program, the necessary MCEP parameters must be generated for the specific aircraft conditions of interest. These parameters are then used by MCEP during the ALES runs to provide performance information for the ALES model. Three MCEP runs were completed. The first two were at 100 percent rotor RPM with different gross weights. The third was at 120 percent rotor RPM, at the lighter of the gross weights. The speed-power polar plots generated during these runs provided interesting insight into the effects of increasing rotor RPM.

Figure 55 shows a comparison of the three cases, the two 100% RPM cases and the lighter gross weight at 120% RPM. From Figure 55 it can be seen that at 160 kts, there are still approximately 1,300 excess horsepower available for the 100% case, Configuration 2. However, the aircraft is transmission limited (5000 HP) at approximately 150 kts for the 120% case, Configuration 3. An investigation of the associated MCEP parameters indicated the cause. The combination of increased rotor RPM and increasing forward speed caused the main rotor tip speed to enter the trans-sonic range. At Mach numbers above 0.9, the compressibility effects begin to dominate power requirements. For example, at 100% RPM and 160 kts, the power required to overcome compressibility effects is 555 HP. For the same airspeed at 120% rotor RPM, 2540 HP is required to overcome compressibility effects.

This situation obviously affected the amount of excess power available (which is directly related to vertical rate of climb (VROC), for the 120% RPM case. In the extensive maneuvering of air-to-air engagements, VROC is very important. The results of the ALES runs generally verified the importance of excess power in air-to-air engagements. The Configuration 2 (16,714 lb, 100% RPM) cases were consistently more effective than the other two cases. The reduced weight provided additional excess power that translated to additional VROC. As shown in Figure 56, Configuration 2 produced more Blue survivors, resulting in consistently higher exchange ratios (17 to 22% higher than Configuration 1, and 52 to 73% higher than Configuration 3).

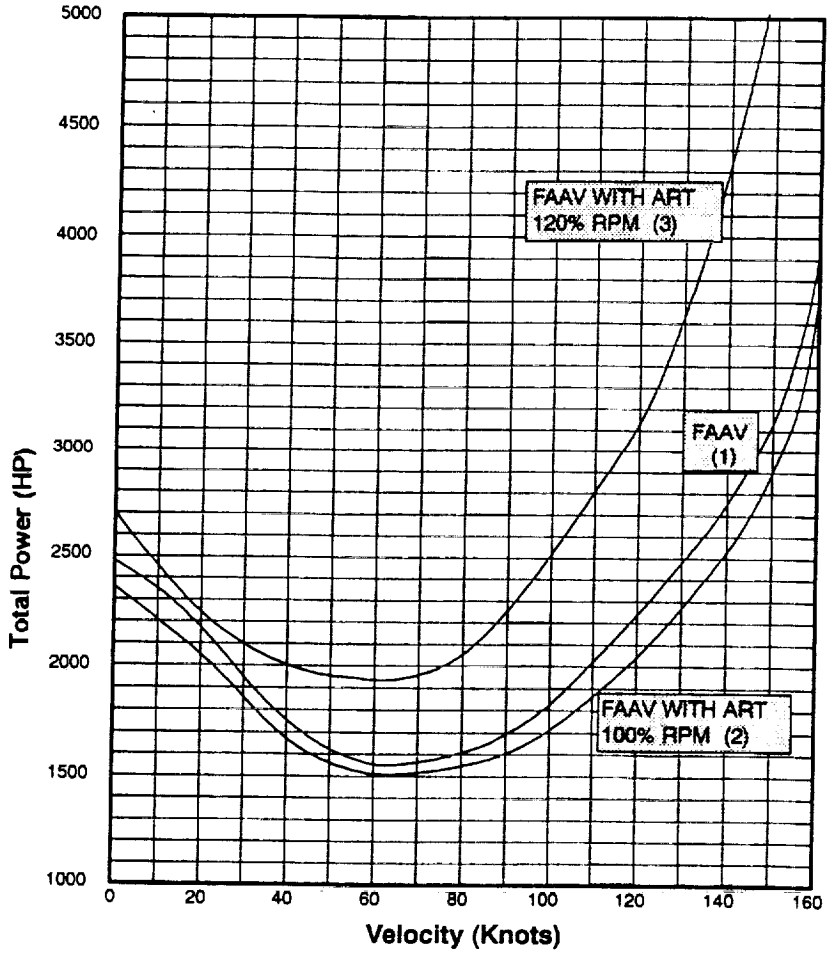

Figure 55. Speed Power Polar Comparison Apache FAAV (Configurations 1, 2, and 3)

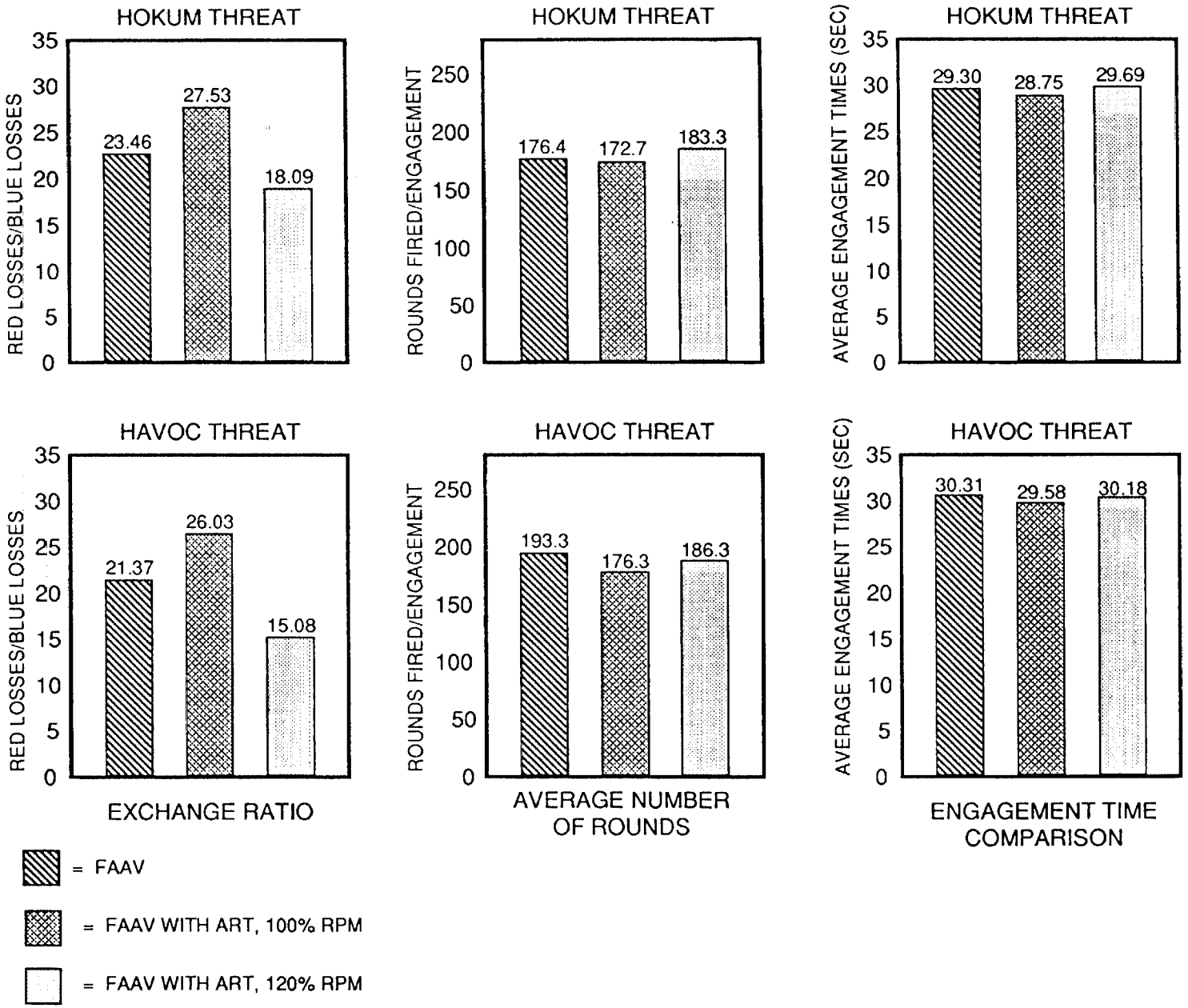

Figure 56. FAAV Configurations

Configuration 3, though lighter than Configuration 1, suffered a serious lack of excess power, due to the compressibility power requirements discussed earlier. This 120% RPM case was consistently less effective than either of the other two (23 to 42% lower exchange ratio). The above statements hold for engagements against both threat helicopters. An analysis of firing opportunities and total engagement time indicated the Configuration 2 aircraft required fewer rounds, and less time to complete the engagement, demonstrating slightly greater efficiency and significantly better effectiveness.

The evaluations with the SCET tool indicated that the combination of increased reliability and better exchange ratio of the ART equipped FAR (100% RPM), resulted in 12.80% improvement in the capability to sustain a given level of combat operations.

These results are significant in that they show the relative effectiveness of the different versions of the FAAV against a given threat helicopter. The reported numbers of Blue and Red kills are not predictions of the results of actual combat, they are analytical results dependent on many assumptions and modelling variables. The performance of the threat aircraft is based on unvalidated individual performance models. In the case of the Hokum, this model is based on "best estimates of performance." Although comparisons of the different FAAV aircraft configurations against the same threat are valid, it is not valid to compare results of a given FAAV variant against different threats.

V.E.2 Conclusions

- The use of the ART transmission (100% case) produces a 17 to 22% increase in the loss exchange ratio of Red losses to Blue losses, compared to the baseline FAAV.

- The ability to sustain rotor RPM at 120% provided no advantages, and, due to the substantial additional power required, resulted in a 24 to 42% decrease in loss exchange ratio when compared to the 100% RPM case, at the same gross weight. Use of varying RPM during engagement was not modeled.

- In all cases, the FAAV with ART, 100% RPM case was more effective than the other two configurations.

V.F RELIABILITY

V.F.1 FAAV Mission Reliability

Because the FAAV is a next-generation design, the trend is to double reliability requirements every generation (see Figure 57). This analysis is based on substituting an ART for a AH-64A transmission. The reliability equation for this substitution is:

$$1/(\text{ART MTBF}) = \text{SUM} \quad 1/\text{Standard MTBF's} \; -1/\text{AH-64A Transmission Mission MTBF} \; +1/\text{ART Mission MTBF}$$

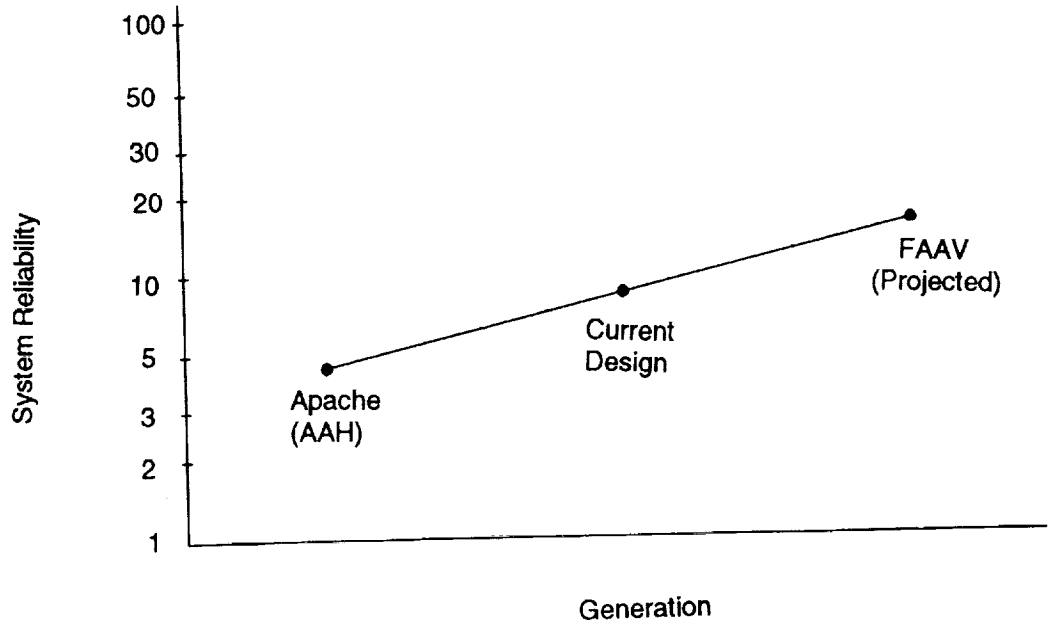

Figure 57 . Trend in Military Helicopter System Reliability

The design features which enhance transmission reliability, improving MTBR from 1500 hours (2) to 5000 hours, will have a proportional improvement on mission (and system) reliability.*

ART Mission MTBF = ART MTBF/AH-64A Transmission MTBR
*AH-64A Transmission Mission MTBF

Using the current actual mission reliability of the AH-64A, transmission of 354 hours MTBF ([53]:

ART Mission MTBF = 500/1500*354 = 1180 hours

Using the current actual mission MTBF of the AH-64A of 22 hours [53]:

ART-AH-64A Mission MTBF = 1/(1/22 - 1/354 + 1/1180) = 23 hours

For an Apache equipped with an ART, mission reliability will increase 4.5% from 22 to 23 hours MTBF.

For the FAAV with the projected mission reliability of 88 hours:

ART-FAAV Mission MTBF = 1/(1/88 - 1/354 + 1/1180) = 107 hours

For an FAAV equipped with an ART, mission reliability will benefit 22% from 88 to 107 hours MTBF.

*Mission reliability accounts for any failure in the system which causes a mission abort. This includes chip detector lights coming on (whether justified by a transmission problem or not) and even perceived failures such as excessive vibration. System reliability accounts for any system failures.

V.F.2 FAAV System Reliability

The current system reliability of the Apache drive system is 61.6 hours [53]. ART-related improvements will increase this number proportional to the MTBR improvement:

$$\text{ART System MTBF} = 5000/1500*61.6 = 205$$

Substituting the ART for conventional transmission shows the impact to the FAAV:

$$\text{ART-FAAV MTBF} = 1/(1/18 - 1/61.6 + 1/205) = 22.6$$

An FAAV equipped with an ART will benefit by an increase in system reliability of 25.5% from 18 to 22.6 hours. Consequently, aircraft availability will also improve.

V.G LIFE CYCLE COSTS

An LCC estimate was completed for the baseline FAAV, ART improved FAAV, and optimized FAAV with ART.

V.G.1 Methodology

The LCC estimate is broken down into three phases: Investment, Research and Development, and Operating and Support.

Parametric and analogous cost estimating techniques were the primary methods employed in determining the LCC impacts associated with the Advanced Rotorcraft Transmission (ART) and the Future Attack Air Vehicle (FAAV).

Parametric estimating is accomplished by correlating design parameters to historical costs through a regression analysis that describes the relationship of cost to those parameters.

The GE PRICE (Parametric Review of Information for Costing and Evaluation) hardware model was employed in estimating airframe and mission equipment mechanical and electrical (development and production) costs. Technological advances in mission equipment resulted in the following adjustments to the PRICE model:

- Reduced risk due to commonality of modules between weapon systems such as the Advanced Tactical Fighter and FAAV
- Reduced integration costs, resulting from a fully integrated system which allows for the elimination of special test equipment currently required to perform system checkout.

Analogous estimating is based on the known cost of a similar item in a prior system. Adjustments are made to the known costs to account for differences in relative complexities of the performance, design, and operational characteristics of the compared items. The analogous systems used for comparison were the AH-64A, AH-1T, and the Advanced Composite Airframe Program (ACAP). The lines of code for airborne and ground system software were based on similarities to the F-15 and Advanced Tactical Fighter Programs using the Ada software

language. The estimate and a discussion of the techniques and assumptions used to make those estimates are included in the following paragraphs.

V.G.2 System Description

The estimate for each configuration was broken down to the subsystem level. This was necessary to show the impact of incorporating the ART into the FAAV aircraft.

Subsystem Breakdown:

- Structure
- Armor
- Landing Gear
- Propulsion
- Rotor
- Drive
- Flight Control
- Hydraulic/Pneumatic
- Electrical
- Fuel
- Environmental Control System
- Furnishings and Equipment
- Crewstation
- Mission Equipment

V.G.3 Acquisition Cost Estimates (Ground Rules and Assumptions)

The following set of ground rules and assumptions were used to develop the acquisition cost for the baseline FAAV, ART improved FAAV, and optimized FAAV with ART air vehicle configurations.

Economic Base Year. All cost data and estimates are reported in base year 1988 dollars.

Development Quantity. Nine prototype air vehicles are assumed.

Production Quantity. This estimate assumes that 600 aircraft will be procured for each configuration.

Schedule. The acquisition schedule as provided:

	Start	First Article	Completion
DEM/VAL	Jan/2000	-	Dec/2003
Full-Scale Development	Jan/2003	Dec/2004	Dec/2006
Production	Jan/2005	Dec/2006	Dec/2013

Production Buildup. The production rate buildup schedule based on an evaluation of current programs:

FY06	FY07	FY08	FY09	FY10	FY11	FY12	FY13
12	24	48	72	120	120	120	84

Software. Three million lines of code will be developed with the programmer averaging 2.5 manhours per line of code based on an evaluation by the software development organization.

Cost Exclusions. The following acquisition elements were not considered in this estimate:

- Retrofit
- Industrial Facilities
- Operational Site Activation

Development Methodology. Research and Development (R&D) cost is defined, in general, to be the sum of all costs resulting from applied research engineering design, analysis, development, test, evaluation and managing development efforts related to a specific material system. The Department of the Army Pamphlet 11-2, "Research and Development Cost Guide for Army Material Systems," addresses the following cost elements:

1.0 Research and Development Cost

1.01 Development Engineering
1.02 Producibility Engineering and Planning
1.03 Tooling
1.04 Prototype Manufacturing
1.05 Data
1.06 System Test and Evaluation
1.07 System/Project Management
1.08 Training
1.09 Facilities
1.10 Other

Parametric and analogous cost estimating techniques were used to drive the total aircraft R&D cost estimates shown in Table 28. The range from low to high reflects uncertainty in the estimate which is typical during the conceptual phase of the program. The GE PRICE H-Model was the primary estimating tool. Analogies to AH-64A, AH-1T, and ACAP were used to develop the subsystem manufacturing complexities which are an integral part of the PRICE estimating process.

Cost Estimating Relationships (CER's) developed from in-house sources were used in conjunction with the PRICE H output to develop the complete estimate.

TABLE 28. TOTAL R&D

	Baseline FAAV	ART Improved FAAV	Optimized FAAV with ART
Total R&D	$2000M - $2247M	$1984M - $2227M	$1967M - $2206M
NOTE: Costs in millions of dollars (M)			

The transmission/drive system R&D estimates were derived using the same approach as the total aircraft. The development cost for each configuration is referenced in Table 29.

TABLE 29. TRANSMISSION R&D ESTIMATE

	Baseline FAAV	ART Improved FAAV	Optimized FAAV with ART
Total R&D	$52.2M - $62.5M	$43.2M - $51.8M	$43.2M - $51.8M
NOTE: Costs in millions of dollars (M)			

Production Methodology. Production (investment) cost is defined, in general, to be the sum of all costs resulting from the production and introduction of the material system into the Army's operational inventory. The Department of the Army Pamphlet 11-3, "Investment Cost Guide for Army Material Systems," addresses the following cost elements:

2.0 Investment Cost

- 2.01 Non-Recurring Investment
- 2.02 Production
- 2.03 Engineering Changes
- 2.04 System Test and Evaluation
- 2.05 Data
- 2.06 System/Project Management
- 2.07 Operational Side Activation
- 2.08 Training
- 2.09 Initial Spares and Repair Parts
- 2.10 Transportation
- 2.11 Other

The PRICE H files used in the development estimate were retained for use in creating the air vehicle production estimate. Table 30 depicts the total investment cost for each configuration.

The Advanced Rotorcraft Transmission (ART) recurring production costs were derived based on AH-64A data. The data was provided via the Material Pricing Section, i.e., purchase order data. The systems and their respective costs are listed in Table 30. The systems, where sufficient data was available, were fitted to a curve and the appropriate sloes and first unit cost determined.

The objective is to project a baseline transmission cost based on the present Apache transmission. The baseline transmission has a power requirement of 5000 HP.

TABLE 30. INVESTMENT

	Baseline FAAV	**ART Improved FAAV**	**Optimized FAAV with ART**
Investment	$9582M - $11,641M	$9487M - $11,525M	$9400M - $11,418M
NOTE: Costs in millions of dollars (M)			

Two approaches were taken in determining the cost of the baseline transmission. Approach one, makes use of a study described in Reference [54]. The Drive System's cost estimating relationships (CER's) provided recurring production cost as a function of weight and quantity. Adjustment factors were derived based on AH-64A historical data and applied to the algorithms to compensate for up-to-date technology.

The second approach used the GE PRICE H parametric hardware model. Based on the average unit cost of the first four lots of the AH-64A system, the model was adjusted and complexity factors derived, characteristic to each individual system. These factors, along with the system weights, were input into the model and new costs derived.

The results of the two approaches, along with the weights and costs of the McDonnell Douglas Helicopter Company (MDHC) AH-64A and the MDHC Light Helicopter 500E model, were fitted to a curve by employing techniques of linear regression. The results yielded an algorithm that estimates transmission cost as a function of weight. The results of this analysis are shown in Table 31.

TABLE 31. ART RECURRING PRODUCTION COST

	1,792-lb ART	**1,350-lb ART**
Recurring Production	$530K	$420K
NOTE: Costs shown in thousands of dollars (K) and includes drive system (shafts, couplings)		

V.G.4 Operating and Support Cost Estimate

The following set of ground rules and assumptions were used to develop the O&S cost for the baseline FAAV, ART Improved FAAV and FAAV with ART air vehicle configuration.

Economic Base Year. All data and estimates are reported in economic base year 1988 dollars.

Operational Scenario. An operating scenario of 420 flight hours per year for 25 years was used based on direction from NASA.

Maintenance Concept. Two level maintenance (Aviation Unit and Depot) concept was assumed.

Exclusions. The following elements of cost were excluded from the estimate:

- Other direct support operations
- Unit training
- Transportation
- Translents, patients, and prisoners
- Medical support
- Training devices
- Software maintenance

Operating and Support Methodology

Operating and Support (O&S) cost is defined in general to be the sum of all costs resulting from the operation, maintenance and support of the weapon system after it is accepted into the Army inventory. The Department of the Army Pamphlet 11-4, "Operating and Support Guide for Army Material Systems," addresses the following cost elements:

3.0 Operating and Support Cost
- 3.01 Military Personnel
- 3.02 Consumption
- 3.03 Depot Maintenance
- 3.04 Modifications, Material
- 3.05 Other Direct Support
- 3.06 Indirect Support

The O&S costs shown in Table 32 were generated using the Quick Look II model. The in-house model is based on CER's developed through the AVSCOM Maintenance Operating and Support (AMOS) cost model and AH-64A historical data. The Quick Look II model is used to calculate subsystem O&S cost as a function of unit cost and Reliability/Maintainability (R&M) characteristics of the helicopter.

TABLE 32. O&S COST

Total O&S		
Baseline FAAV	**ART Improved FAAV**	**Optimized FAAV**
$21,058M - $22,824M	$20,970M - $22,715M	$20,892M - $22,621M
NOTE: Costs in millions of dollars.		

The FAAV aircraft will have lower operating costs than the current generation of helicopters based on the following: significant increases in reliability common module architecture, reduction in false failures, reduction in line replaceable units, isolation of failure through self-diagnostics, and standardization of airframe manufacturing components. Further improvements are probable as technological advances are incorporated into the system.

Direct Operating Cost Methodology

Direct Operating Cost (DOC) is a subelement of O&S cost and consists of the following cost elements:

3.012 Direct Maintenance
3.021 Replenishment Spares
3.022 Petroleum, Oil and Lubricants
3.031 Depot Labor
3.032 Depot Material

The Quick Look II files used in the O&S estimate were retained for use in creating the DOC estimate. The difference in direct operating cost shown in Table 33 is attributed to incorporation of the ART into the air vehicle configurations. The mean time between removal for the ART is 5000 hours versus 1,500 hours for the AH-64A transmission. This results in a DOC saving for the transmission of approximately 33 percent.

TABLE 33. DOC

	Baseline FAAV	**ART Improved FAAV**	**Optimized FAAV with ART**
Direct Operating Cost	$1,476 - 1,807	$1,460 - 1,787	$1,448 - 1,772
Transmission (only)	$66 - 79	$44 - 53	$44 - 53
NOTE: Costs shown in dollars per flight hour.			

V.H CONCLUSIONS

Inherently, a reduction in empty weight of an aircraft enables improvements in most areas of performance. Relative to the Baseline FAAV, the FAAV with ART offers a choice of added range, ordnance payload, and improved agility, which is critical in the air-to-air combat environment. Mission Analysis shows that the FAAV with ART produces a 17 to 22 percent improvement in the loss exchange ratio (Red losses to Blue losses) when compared to the baseline FAAV.

Reliability is improved as well. The FAAV with ART offers much improved mission reliability with a 22 percent increase in MTBF (88 hours for FAAV baseline vs. 107 hours for FAAV with ART). System reliability increased 25.5% in MTBF (18 hours vs. 22.6 hours). Significant decreases in the estimated life cycle costs are as shown in Table 34.

TABLE 34. WEIGHT/LIFE CYCLE COST COMPARISON

	Baseline FAAV	ART Improved FAAV	Optimized FAAV with ART
• Transmission weight, lb	1792	1170	1170
• Aircraft empty weight, lb	10,391	9769	9769
• Aircraft gross weight, lb	17,336	16,827	16,600
• Aircraft development cost, $ per unit	3.33M - 3.74M	3.31M - 3.71M	3.28M - 3.68M
• Transmission acquisition cost, $ per unit	0.64M - 0.77M	0.49M - 0.59M	0.49M - 0.59M
• Aircraft acquisition cost, $ per unit	19.30M - 23.15M	19.12M - 22.92M	18.94M - 22.71M
• Transmission direct operating cost, $ per flight hour per unit	66 - 79	44 - 53	44 - 53
• Aircraft direct operating cost, $ per flight hour per unit	1,476 - 1,807	1,460 - 1,787	1,448 - 1,772
• Transmission fleet life cycle cost, total $	800M - 960M	571M - 688M	571M - 688M
• Aircraft fleet life cycle cost, total $	32.64B - 36.71B	32.44B - 36.47B	32.26B - 36.25B

NOTE: Included list of assumptions. Also, run at least one case where:

number of aircraft = 600

life cycle period = 25 years

annual utilization = 420 flight hours

VI. MATERIAL CHARACTERIZATION TESTS

VI.A INTRODUCTION

Five near-net forged gear materials and three transmission housing materials were tested as part of the ART program. The gear materials tested were X53 Pyroware, CBS 600, M50NIL, AISI 9310 and M300. The tests performed for these were gear tooth scoring tests, single tooth bending tests, Charpy impact energy tests and compact tension fracture toughness tests. The housing materials tested were C355T7 aluminum, WE43 Magnesium, and ZE41A magnesium alloys. Tensile tests and compact tension fracture toughness tests were performed for these. The tests, gear materials, AMS specifications and test quantities are summarized in the following tables.

Tooth Scoring Tests, Single Tooth Bending Fatigue Tests, and Charpy Impact Energy Tests - Gear Materials

These tests were performed on specimens fabricated from five different steels as tabulated.

		Number of Tests		
Material	Spec.	Tooth Scoring	Tooth Bending	Charpy
M50NIL	6278	70	20	12
X53 Pyro.	6308	72	20	12
CBS 600	6255	6	12	12
AISI 9310	6265	96	24	12
300M	6514	6	12	12

Fracture Toughness Tests - Gear and Housing Materials

These tests were performed on specimens fabricated from two magnesium alloys, one aluminum alloy, and two steel alloys, as tabulated.

Material	Spec.	Heat Treatment	No. of Tests
WE43	N/A	Solution Heat Treat	7
ZE41A	4439A	Solution Heat Treat	7
C355T7	4215	Solution Heat Treat	6
M50 NIL	6278	Pseudocarburized/Hardened	6
X53 Pyro.	6308	Pseudocarburized/Hardened	7

Tensile Tests - Housing Materials

These tests were performed on specimens fabricated from two magnesium alloys and one aluminum alloy as tabulated.

Material	Spec.	Heat Treatment	No. of Tests
WE43	N/A	Solution Heat Treat	24
ZE41A	4439A	Solution Heat Treat	24
C355T7	4215	Solution Heat Treat	24

The selected gear material tests were chosen to allow determination of the relative resistance to tooth scoring, relative bending strength, impact toughness and fracture toughness of the five materials. Near-net forged test gears were employed in the single tooth bending and scoring tests to determine if any additional benefits could be derived from gears produced using the near-net-shape forging process. The AISI 9310 and M300 steels were intended as baseline gear materials for use in comparison with the high-hot-hardness X53, CBS 600 and M50NIL steels and with existing test data.

The tests of the three housing materials were chosen to determine impact toughness and tensile strength of the materials. The ZE41A magnesium served as a baseline for comparison with the more advanced WE43 magnesium and C355T7 aluminum alloys.

VI.B TEST PROGRAMS

VI.B.1 Gear Tooth Scoring Tests

VI.B.1.i Introduction

The objective of the tooth scoring tests was to compare the relative scoring resistance of near net forged gears made from various advanced gear materials. Tests were run at McDonnell Douglas Helicopter Company on 252 specimens consisting of X53 Pyroware, CBS 600, M50NIL, AISI 9310 and M300 gear materials. The test rig capabilities and test operating conditions were selected to assure that tooth scoring precipitated in all test specimens. Test conditions were monitored and recorded for each test run, and operating parameters were measured with calibrated instrumentation. Following the tests, comparisons made from failure data determined the ranking of the materials in terms of resistance to scoring. The flash temperature index and probability of scoring were also determined from the test data for the materials. Recommended design operating temperatures were then determined for the materials based on mean value, one sigma and two sigma standard of deviation of the test data.

VI.B.1.ii Test Article Description

Five gear materials consisting of two baseline gear steels and three high-hot-hardness gear steels were selected for the tooth scoring tests. AISI 9310 and M300 served as the baseline steels for the tests, while X53 Pyroware, CBS 600 and M50NIL gear steels were tested as high-hot-hardness candidates for selection in the advanced

rotorcraft transmission. The gear materials and test quantities used in the tooth scoring tests are identified as follows:

Part Number	Material	AMS Spec	Heat Treatment	Make From	No. of Tests
42499-21-1	M50NIL	6278	Carburized and Hardened	42499-21-6 Forging	70
42499-22-1	M50NIL	6278	Carburized and Hardened	42499-21-6 Forging	
42499-21-2	X53 Pyro	6308	Carburized and Hardened	42499-21-7 Forging	72
42499-22-2	X53 Pyro	6308	Carburized and Hardened	42499-22-7 Forging	
42499-21-3	CBS 600	6255	Carburized and Hardened	42499-21-8 Forging	6
42499-22-3	CBS 600	6255	Carburized and Hardened	42499-22-8 Forging	
42499-21-4	AISI 9310	6265	Carburized and Hardened	42499-21-9 Forging	96
42499-22-4	AISI 9310	6265	Carburized and Hardened	42499-22-9 Forging	
42499-21-5	300M	6514	Through Hardened	42499-21-10 Forging	6
42499-22-5	300M	6514	Through Hardened	42499-22-10 Forging	

The test gears were rough-formed using the near-net forging process. This process was selected because it has the potential for increasing gear fatigue life and improving the endurance limit. The process also makes more efficient use of raw materials and greatly reduces or even eliminates the need for secondary machining, depending on the quality class of gear required. The five near-net forged materials were produced by The Eaton Corporation in Willoughby Hills, Ohio.

The material certificates and chemical compositions are outlined in Tables 35 and 36. All heat treatment operations were conducted at Lucas Western, Inc. Table 37 outlines the specific heat treatments applied to each material, and the actual case depth and hardness measured from test gears. Each group of test specimens manufactured from the same material were from one heat treat and melt of the material and were heat treated in the same lot to minimize variation of the test population.

TABLE 35 . MATERIAL CERTIFICATES

Material	AMS Spec.	Producer	Heat No.	Product Form	Grain Size
M50NIL	6278	Teledyne Vasco	8904A	1.5" f bar	5-3/4
Pyroware X53	6308	Carpenter	80238	1.5" f bar	8-9
CBS 600	6255	Latrobe	E3891	1.5" f bar	5-1/2
9310	6265	Teledyne Vasco	8755A	1.5"f bar	6-1/4
Maraging 300	6514	Teledyne Vasco	1280B	1.5" f bar	7

TABLE 36. CHEMICAL COMPOSITIONS

	Element (%)								
Material	**C**	**Mn**	**P**	**S**	**Si**	**Co**	**Cr**	**Ni**	**Cu**
M50NIL	0.14	0.28	0.013	0.001	0.21	0.02	4.15	3.33	0.02
Pyroware X53	0.11	0.34	0.006	0.002	0.82	-	1.04	2.02	2.09
CBS 600	0.17	0.55	0.008	0.001	1.09	-	1.43	0.06	0.06
9310	0.12	0.58	0.004	0.001	0.27	-	1.20	3.20	0.09
Maraging 300	0.006	0.01	0.004	0.0004	0.07	9.35	0.28	18.83	0.05

	Element (%)							
Material	**Mo**	**V**	**W**	**Ti**	**Al**	**B**	**Zr**	**Ca**
M50NIL	4.23	1.23	0.01	-	-	-	-	-
Pyroware X53	3.23	0.09	-	-	-	-	-	-
CBS 600	0.98	-	-	-	0.04	-	-	-
9310	0.12	-	-	-	-	-	-	-
Maraging 300	4.86	-	-	0.70	0.08	0.0027	0.01	0.05

TABLE 37. SPECIFIC HEAT TREATMENTS

Material	Carburize	Hardening	Refrigera-tion	Temper	Core Hardness	Case Hardness	Case Depth (in.)
9310	1700°F, 3 hr	Temper 1150°F, 2 hr Austenitize 1500°F, 1 hr, Salt Quench	-125°F, 3 hr	300°F, 3 hr	RC 35-40	RC 63	0.032 - 0.036
M50NIL	1750°F, 2 hr	Temper 1300°F, 2 hr Preheat 1625°F, 0.5 hr Austenitize 1990°F, 0.5 hr, Gas Quench	-120°F, 3 hr	1000°F, 2+2+2 hr	RC 42-43	RC 60	0.030 - 0.035
Pyroware X53	1700°F, 1 hr, 1750°F, 2 hr	Temper 1350°F, 2 hr Austenitize 1675°F, 1.5 hr, Oil Quench	-120°F, 3 hr	350°F, 2 hr	RC 37-40	RC 63	0.035 - 0.042
CBS 600	1700°F, 3 hr	Temper 1150°F, 2 hr Austenitize 1625°F, 1 hr, Oil Quench	-120°F, 3 hr	600°F, 3+3 hr	RC39-41	RC58-59	0.030
Maraging 300		Aging 900°F, 6 hr			RC 53-54		

The test specimens were fabricated to fit the MDHC Tooth Scoring Test Fixture. The machined specimen configurations are summarized briefly as follows:

Pinion Part Number	42499-21-1 thru -5
Type of Pinion	Involute Spur
No. of Teeth	20
Pitch Diameter	2.500
Pressure Angle	25 degrees
Circular Tooth Thickness	0.1948
Face Width	0.250
Root Diameter	2.176
Outside Diameter	2.750
Minimum Fillet Radius	0.044
Pilot ID Reference Diameter	1.00025
Maximum Surface Finish	32 RMS or 29 AA

Gear Part Number	42499-22-1 thru -5
Type of Gear	Involute Spur
No. of Teeth	30
Pitch Diameter	3.750
Pressure Angle	25 degrees
Circular Tooth Thickness	0.1933
Face Width	0.500
Root Diameter	3.426
Outside Diameter	4.000
Minimum Fillet Radius	0.037
Pilot ID Reference Diameter	1.00025
Maximum Surface Finish	32 RMS or 29 AA

VI.B.1.iii Test Rig Description

The tests were performed on a hydraulically-powered, closed-loop, self-contained tooth pitting-scoring test fixture designed to test a single set of spur gears operating at a center distance of 3.125 inches at a maximum pinion speed of 15,000 RPM. An isometric view of the NASA-Lewis Gear Fatigue Test Fixture, which also illustrates principal components of the MDHC scoring fixture's test gearboxes, is shown in Figure 58. A photograph of the MDHC scoring test fixture is shown in Figure 59. The maximum torque capacity of the scoring test fixture is 3100 in.-lb, applied to the test pinion. The fixture contains separate lubrication systems for the test gearbox and the slave gearbox, with each system containing a separate oil cooler. The lubrication system for the test gears also incorporates an oil heater to provide a constant oil supply at the required oil temperature. The fixture uses a three micron oil filter for the test gear lubrication system and incorporates chip detectors. The test fixture provides lubrication and cooling oil to the test gears through one oil jet. Providing oil into mesh, this jet has one 0.045-inch diameter hole directing the oil flow. The stand has two inspection ports with removable transparent covers for viewing the condition of the test gear teeth.

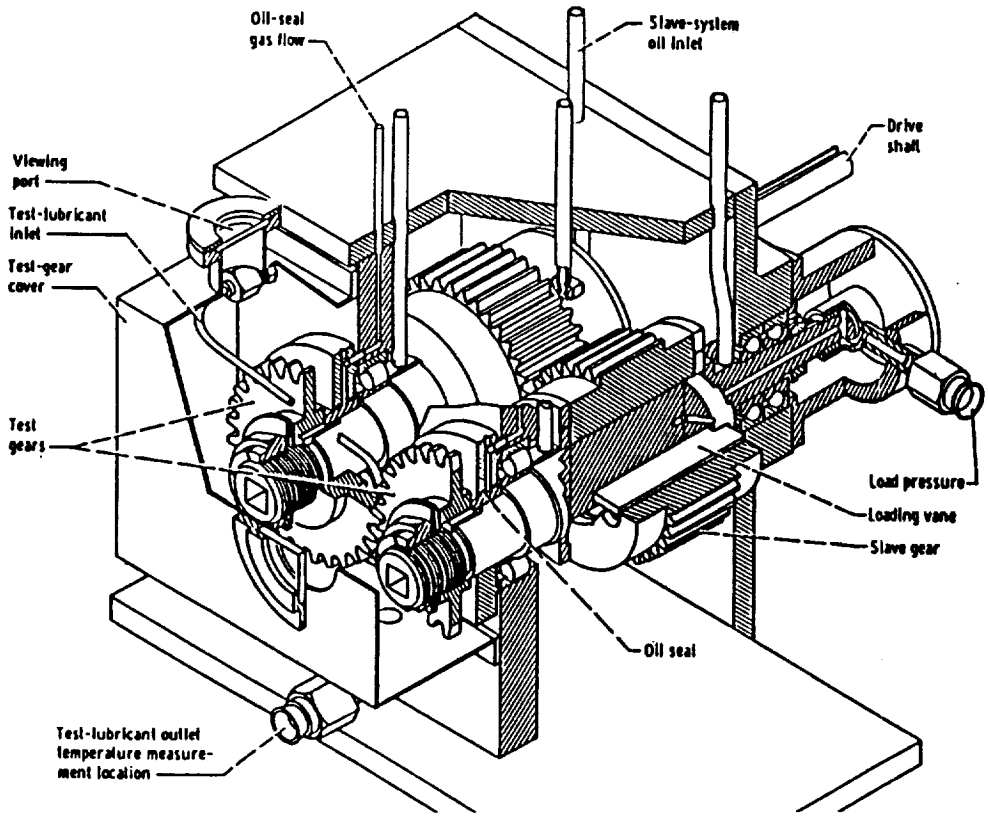

Figure 58. NASA-Lewis Gear Fatigue Test Fixture

Figure 59. MDHC Tooth Scoring Test Fixture

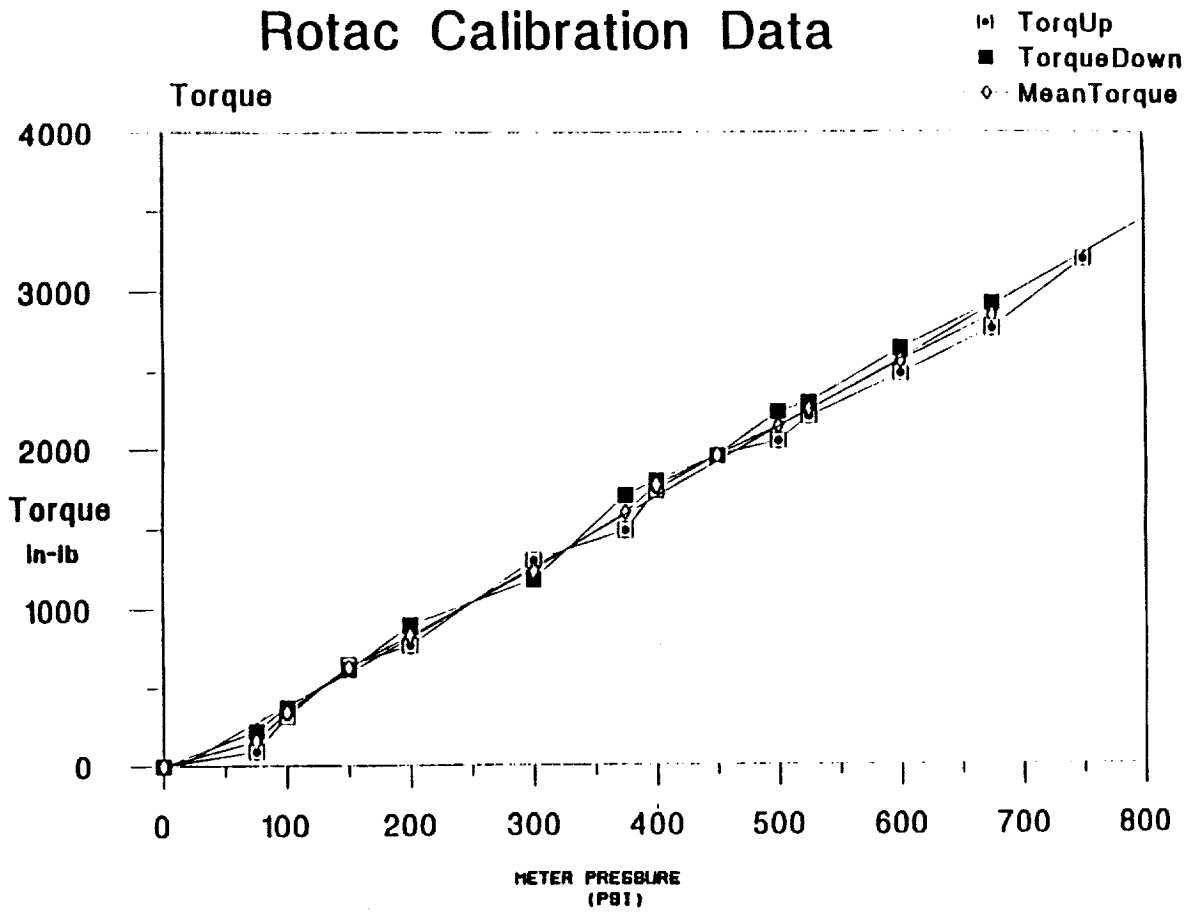

Figure 60. Scoring Test Fixture Calibration Curve

The test fixture is instrumented with a display panel containing digital readouts and fault isolation lights with provisions for recording equipment. It has a chip detector circuit which illuminates an indicator light and automatically shuts off the fixture if the test specimens generate magnetic debris. The fixture has control features including automatic shutdowns for overspeed, high oil and bearing temperatures, and low oil pressure or excessive pressure differential across the oil filter. The stand also is capable of reading test time in tenths of an hour.

The test fixture contains a Rotac hydraulic vane torque applier that was calibrated for fixture torque as hydraulic pressure was applied in 75 psi (gage) increments from 0 to 750 psi and then decreased back to 0. A straight line fit of the torque vs. pressure data was found to be the accurate approximation of the values recorded as shown in Figure 60.

VI.B.1.iv Test Procedure

During testing, each test gear set was mounted in the gear scoring fixture so that the pinion was fully engaged with the exception of about 0.02 inch of its face width. This was done to avoid tooth overlap on the face of the gear member during subsequent tests with another pinion run on that same face. During tests, the test gear load and direction were such that the 20-tooth pinion was always the driving member, the bulk oil temperature was stabilized at 165°F, and the test gear oil pressure was set to 24.0 psi.

The gear sets were subjected to a break-in procedure prior to testing. The test gears were run 12 minutes at reduced RPM and torque with the test gearbox oil temperature and pressure set to the operating conditions.

After break-in, the pinion gear tooth load was started at 600 in.-lb torque at 10,000 RPM for the first load step. Each gear specimen was operated in a series of load steps starting at 600 in.-lb for 5-minute intervals. The pinion torque was increased by 100 in.-lb for each interval until scoring was observed after shut down. The tests were shut down after each 5-minute interval so the test gears could be visually inspected for scoring. The inspections were made through the inspection port following easy removal of the inspection cover located on the right side of the test gearbox housing.

Data recorded for each test included the test specimen material, part number, serial number, test date, start and end time for each run, RPM for break-in and tests, torque for break-in and tests with pressure conversion, oil temperature into the gearbox, test gearbox oil pressure, slave gearbox oil pressure, inspection record and test comments and operator's name and initials.

VI.B.1.v Results

A summary of the test data is provided in Table 38. The test torque data, along with test speed, oil reservoir temperatures and gear geometric parameters, were used to calculate flash temperatures [4]. Standard summary statistics were then run against the flash temperatures. This data is charted in Figures 61 and 62. The most important determinant is the temperature at which a high percentage of the samples resist scoring. This is indicated by the "mean - Standard Deviation (S.D.)" and "mean - 2 S.D." values in the figure. Mean minus S.D. is the temperature in these tests at which there was a 15.87 percent chance of scoring (medium scoring risk). Mean minus 2 S.D. is the test temperature at which there was a 2.28 percent chance of scoring (low scoring risk). In the AGMA tests, the medium scoring risk area was bounded on the upper side by a 30 percent chance of scoring and on the lower side by a 5.5 percent chance of scoring. Using the minus 1 and minus 2 S.D. as a bound for this area, in the MDHC tests, is a more conservative approach. Based on this criteria, the M50Nil material and the CBS 600 have the highest scoring resistance, followed by X53, M300 and lastly AISI 9310. Table 39 provides a summary of scoring flash temperatures of medium (-1 S.D.) and low (-2 S.D.) risk.

TABLE 38. SUMMARY OF SCORING TEST DATA

Torque Level, in.-lb (25% Surface Scoring Observed)											
Test	**600**	**700**	**800**	**900**	**1000**	**1100**	**1200**	**1300**	**1400**	**1500**	**No. of Tests**
M50NIL	-	-	-	-	6	27	21	12	3	1	70
X53	-	-	-	14	18	13	18	5	4	-	72
CBS 600	-	-	-	-	1	1	2	1	1	-	6
9310	1	4	26	41	23	1	-	-	-	-	96
300M	-	-	1	4	1	-	-	-	-	-	6
											* 250

* 252 tests were actually completed. Two test points run during early tests at 200°F oil reservoir temperature (oil temp In) were invalidated due to tooth contact occurring on both the drive and coast sides of gear teeth.

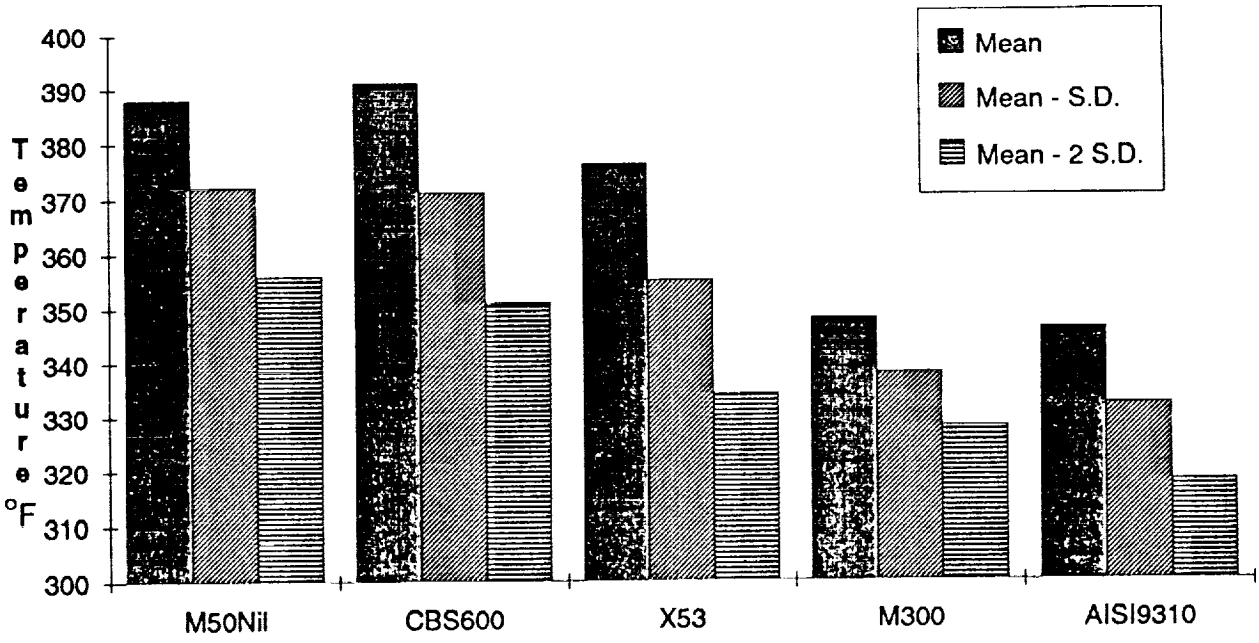

Figure 61. Scoring Test Flash Temperatures

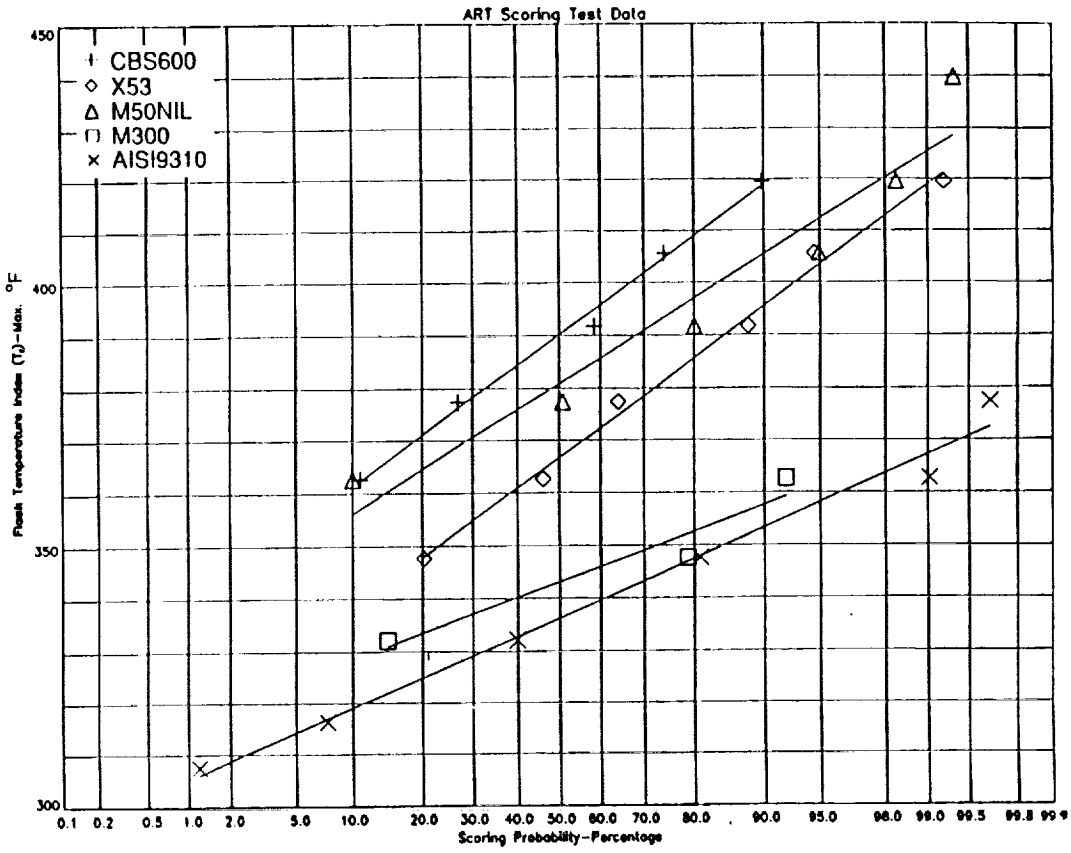

Figure 62. Flash Temperature vs. Probability of Scoring

TABLE 39. FLASH TEMPERATURES (°F), SCORING RISK

Materials	Medium Risk Mean - 1 S.D.	Low Risk Mean - 2 S.D.
M50NIL	372	356
CBS 600	371	351
X53	355	334
M300	338	328
AISI 9310	332	318

VI.B.1.vi Discussion of Results

The significance of the results is that based on a scoring mode of failure, using the best gear steel (M50NIL) in this test would provide an increase of 389 in.-lb of operating torque with the same probability of scoring as the AISI 9310 steel (at -2 S.D.). AISI 9310 steel was rated at 700 in.-lb with a -2 S.D. probability of scoring, so this represents a 56% improvement in load carrying capability. Also at -2 S.D. probability, CBS 600 provides an increase of 221 in.-lb torque (32% improvement), X53 an increase of 112 in.-lb torque (16% improvement) and 300M an increase of 33 in-lb torque (5% improvement). As can be seen in Table 40, only six samples of the CBS 600 and M300 test materials were used. This gives their results a lower confidence level than the other materials.

TABLE 40. TEST SPECIMEN MATERIALS AND QUANTITIES

Material	Spec.	Heat Treatment	No. of Tests
M50 NIL	6278	Carburized and Hardened	20
X53 Pyro.	6308	Carburized and Hardened	14*
CBS 600	6255	Carburized and Hardened	12
AISI 9310	6265	Carburized and Hardened	17**
300M	6514	Through Hardened	12

*Will be 20 tests of X53 when completed (reference page 122)
**Will be 24 tests of AISI 9310 when completed (reference page 122)

Modern gear steels exhibit increased resistance to scoring that can be used to advantage. These benefits should expand the envelope of gear design. Based on a scoring mode of tooth failure, results from the MDHC scoring tests indicate a 56% improvement in load-carrying capacity with use of M50NIL steel, 32% improvement with use of CBS600 steel, 16% improvement with use of X53 Pyroware and 5% improvement with use of 300M steel. Results of other types of gear tests can be used in conjunction with this and previous scoring test results to provide a recommended gear material for future aircraft application.

VI.B.2 Single Tooth Bending Fatigue Tests

VI.B.2.i Introduction

Gear tooth bending strength is one of the most important gear design parameters in drive system engineering. This report describes the test procedure and test results of single tooth bending fatigue tests performed on advanced gear materials manufactured from near-net forgings. The objective of the tests was to compare the relative bending strength of five advanced near-net forged gear steels. In addition, comparisons were made with single tooth bending test results existing for standard forged gears of these materials. Tests were run at LWI, on 88 specimens consisting of X53 Pyroware, CBS 600, M50NIL, AISI 9310 and M300 gear materials. The test rig was designed to allow accurate placement of load at the highest point of single tooth contact on the test gear teeth. Test conditions were accurately determined using a calibrated load cell, load frequency and cycle count measurement, strain gaged test gear teeth, and carefully recorded test data. AGMA bending stress was calculated from raw test data, and best fit S-N curves for mean data and mean minus three sigma standard of deviation were plotted for each material.

VI.B.2.ii Test Article Description

Five near-net forged gear materials consisting of X53 Pyroware, CBS 600, M50NIL, AISI 9310 and M300 were selected for tests of single tooth bending fatigue strength. The AISI 9310 and M300 steels were intended as baseline gear materials for use in comparison with the high-hot-hardness X53, CBS 600 and M50NIL steels. The near-net forging process was selected because it has the potential to increase gear fatigue life and improve the endurance limit. The process also makes more efficient use of raw materials and can greatly reduce or even eliminate the need for secondary machining, depending on the quality class of gear required. The gear materials and test quantities used in the single tooth bending tests are identified as follows.

Part Number	Material	AMS Spec.	Heat Treatment	Make From	No. of Tests
42499-21-11	M50 NIL	6278	Carburized and Hardened	42499-21-6 Forging	20
42499-21-12	X53 Pyro.	6308	Carburized and Hardened	42499-21-7 Forging	20
42499-21-13	CBS 600	6255	Carburized and Hardened	42499-21-8 Forging	12
42499-21-14	AISI 9310	6265	Carburized and Hardened	42499-21-9 Forging	24
42499-21-15	300M	6514	Through Hardened	42499-21-10 Forging	12

The five near-net forged materials were produced by the Eaton Corporation in Willoughby Hills, Ohio. The material certificates and chemical compositions are outlined in Tables 41 and 42.

Each group of test specimens manufactured from the same material were from one heat and one melt of the material and were heat treated in the same lot to minimize variation of the test population. One gear of each material was evaluated after carburizing for microstructure and case depth at the profile and root. All the heat treatment operations were conducted at LWI Table 43 outlines the specific heat treatments applied to each material, and the actual case depth and hardness measured from the test gears. In addition, one gear of each material was evaluated for case depths at the same two locations after finish grinding.

TABLE 41. MATERIAL CERTIFICATES

Material	AMS Spec.	Producer	Heat No.	Product Form	Grain Size
M50NIL	6278	Teledyne Vasco	8904A	1.5" f bar	5-3/4
Pyroware X53	6308	Carpenter	80238	1.5" f bar	8-9
CBS 600	6255	Latrobe	E3891	1.5" f bar	5-1/2
9310	6265	Teledyne Vasco	8755A	1.5"f bar	6-1/4
Maraging 300	6514	Teledyne Vasco	1280B	1.5" f bar	7

TABLE 42. CHEMICAL COMPOSITION

	Element (%)								
Material	**C**	**Mn**	**P**	**S**	**Si**	**Co**	**Cr**	**Ni**	**Cu**
M50NIL	0.14	0.28	0.013	0.001	0.21	0.02	4.15	3.33	0.02
Pyroware X53	0.11	0.34	0.006	0.002	0.82	-	1.04	2.02	2.09
CBS 600	0.17	0.55	0.008	0.001	1.09	-	1.43	0.06	0.06
9310	0.12	0.58	0.004	0.001	0.27	-	1.20	3.20	0.09
Maraging 300	0.006	0.01	0.004	0.0004	0.07	9.35	0.28	18.83	0.05

	Element (%)							
Material	**Mo**	**V**	**W**	**Ti**	**Al**	**B**	**Zr**	**Ca**
M50NIL	4.23	1.23	0.01	-	-	-	-	-
Pyroware X53	3.23	0.09	-	-	-	-	-	-
CBS 600	0.98	-	-	-	0.04	-	-	-
9310	0.12	-	-	-	-	-	-	-
Maraging 300	4.86	-	-	0.70	0.08	0.0027	0.01	0.05

The machined single tooth bending test specimen configurations are summarized briefly as follows:

Type of Gear	Involute Spur
Diametral Pitch	8
Number of Teeth	20
Face Width	0.250
Pressure Angle	25 degrees
Pitch Diameter	2.500

Base Diameter	2.266
Outside Diameter	2.750
Root Diameter	2.176
Minimum Fillet Radius	0.054
Circular Tooth Thickness	0.1933

Eight of the 20 gear teeth were removed to eliminate possible interference with the test fixture. As shown in the Figure 63 view taken from Lucas Western drawing 42499-21, there were four test teeth on each test gear. Before starting the tests, the circular tooth thickness, fillet radius, root diameter, outside diameter, and root surface finish of each gear were measured and recorded. These values were used to accurately calculate the AGMA bending stress [55] for each gear.

TABLE 43. HEAT TREATMENTS, CORE/CASE HARDNESS AND CASE DEPTH AT PITCH LINE

Material	Carburize	Hardening	Refrigera-tion	Temper	Core Hardness	Case Hardness	Case Depth (in.)
9310	1700°F, 3 hr	Temper 1150°F, 2 hr Austenitize 1500°F, 1 hr, Salt Quench	-125°F, 3 hr	300°F, 3 hr	RC 35-40	RC 63	0.032 - 0.036
M50NIL	1750°F, 2 hr	Temper 1300°F, 2 hr Preheat 1625°F, 0.5 hr Austenitize 1990°F, 0.5 hr, Gas Quench	-120°F, 3 hr	1000°F, 2+2+2 hr	RC 42-43	RC 60	0.030 - 0.035
Pyroware X53	1700°F, 1 hr, 1750°F, 2 hr	Temper 1350°F, 2 hr Austenitize 1675°F, 1.5 hr, Oil Quench	-120°F, 3 hr	350°F, 2 hr	RC 37-40	RC 63	0.035 - 0.042
CBS 600	1700°F, 3 hr	Temper 1150°F, 2 hr Austenitize 1625°F, 1 hr, Oil Quench	-120°F, 3 hr	600°F, 3+3 hr	RC39-41	RC58-59	0.030
Maraging 300		Aging 900°F, 6 hr			RC 53-54		

VI.B.2.iii Test Rig Description

The test rig for single tooth bending tests included a single tooth bending test fixture (shown in Figures 64 and 65), designed by LWI, and an MTS Model 800 materials test system. The test fixture was mounted on the base plate of the MTS load frame. The MTS Model 810 machine is a servohydraulic, closed-loop control system designed for test of fracture mechanics, fatigue and basic material properties. The single tooth bending test fixture was designed so that the test tooth was loaded at the highest point of single tooth contact, based on a 1:1 gear ratio, while the reaction tooth was loaded at the lowest point of single tooth contact. The fixture design allows tests of 1.5 to 6.0-inch pitch diameter spur gears with face widths up to 0.5 inch. Both the load and reaction anvils can be repositioned to accommodate various tooth heights along the line of action for involute spur gears. The fixture also has strip chart recorder and signal generator compatibility. A drip lubrication system is incorporated to prevent spalling of the test specimens. Other features include a crack detector circuit enabling automatic shutdown of the fixture, an oil filter and a digital readout. The fixture also has a custom furnace which can be used for elevated temperature tests at up to 800°F.

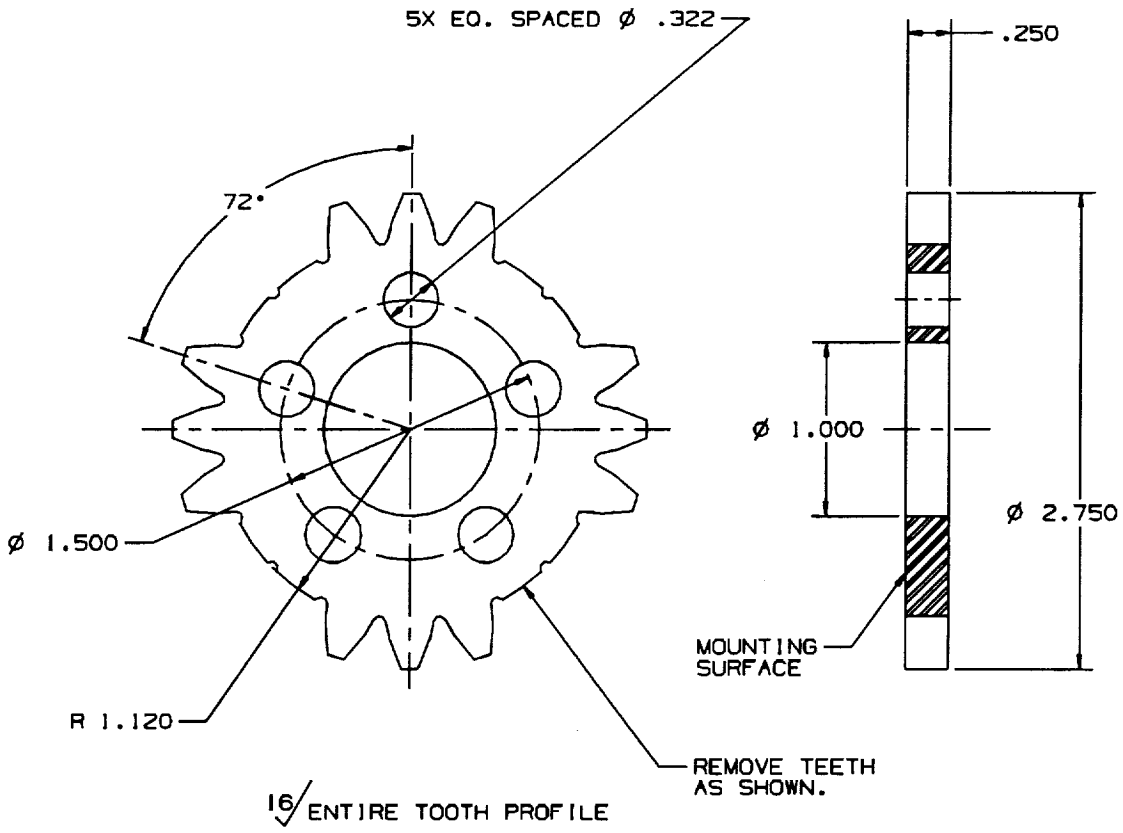

Figure 63. Detail Views of Test Gears

Load applied to the test gear was measured with a calibrated commercial load cell which was mounted under the loading stud, as shown in Figures 64 and 65. The load cell was calibrated per ASTM standards. The load anvil was adjusted to the desired contact position by stroke control of the loading stud. The test gear was then mounted on the fixture and the reaction anvil was slightly adjusted so that both load and reaction teeth were in contact. A load of 100 lb was then applied to the test tooth, and the positioning of anvils rechecked. The minimum load was maintained at 100 lb during all tests to ensure that constant contact was maintained and impact loads were avoided. Thus the mean load was always 100 lb higher than the alternating load during test runs.

The crack detector circuit was employed through instrumentation of all test teeth with crack wires to ensure that each test could be stopped at a fixed crack length of approximately 0.070 inch at the root fillet area. The wire was bonded to both sides of the test tooth at approximately 1/32-inch from the root radius, and then integrated into the control circuit of the test machine. Failure was defined as a crack which progressed through the wire until the crack wire broke. In addition to automatic test rig shutdown due to crack wire breakage, the system would also be shut down due to detection of error in the load range value, detection of error in limit values for both load and stroke, and manual emergency stop.

Figure 64. Test Tooth and Load Anvil

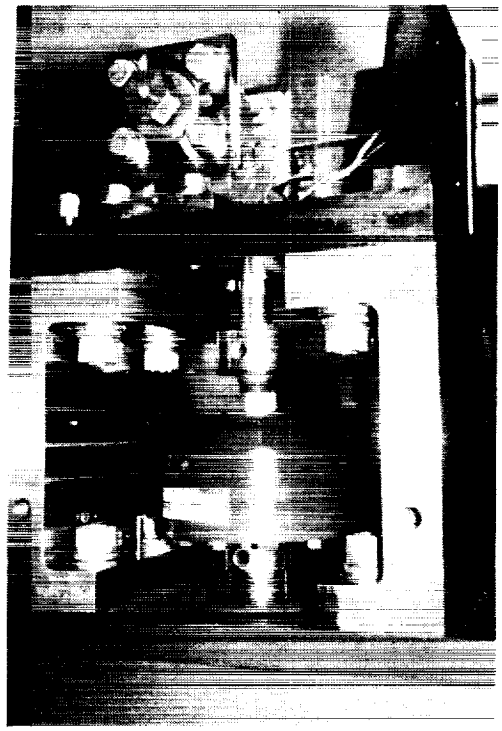

Figure 65. Single Tooth Bending Fatigue Test Fixture

VI.B.2.iv Test Procedure

All single tooth bending fatigue tests were executed at the LWI, Applied Technology Division facility using the previously described test fixture mounted on an MTS servo-controlled, closed-loop, hydraulic test machine. Prior to testing, the test gear teeth were instrumented with strain gages as shown in Figure 66 so that actual gear tooth root stress could be measured and plotted against the applied normal load. The strain gages were located at the point on the tooth root of AGMA maximum bending stress [55]. Strain gages of 0.015-inch length were selected based on the test gear root configuration. A cast was made of the tooth space and used as a template for laying and pressing the two strain gages at the desired locations.

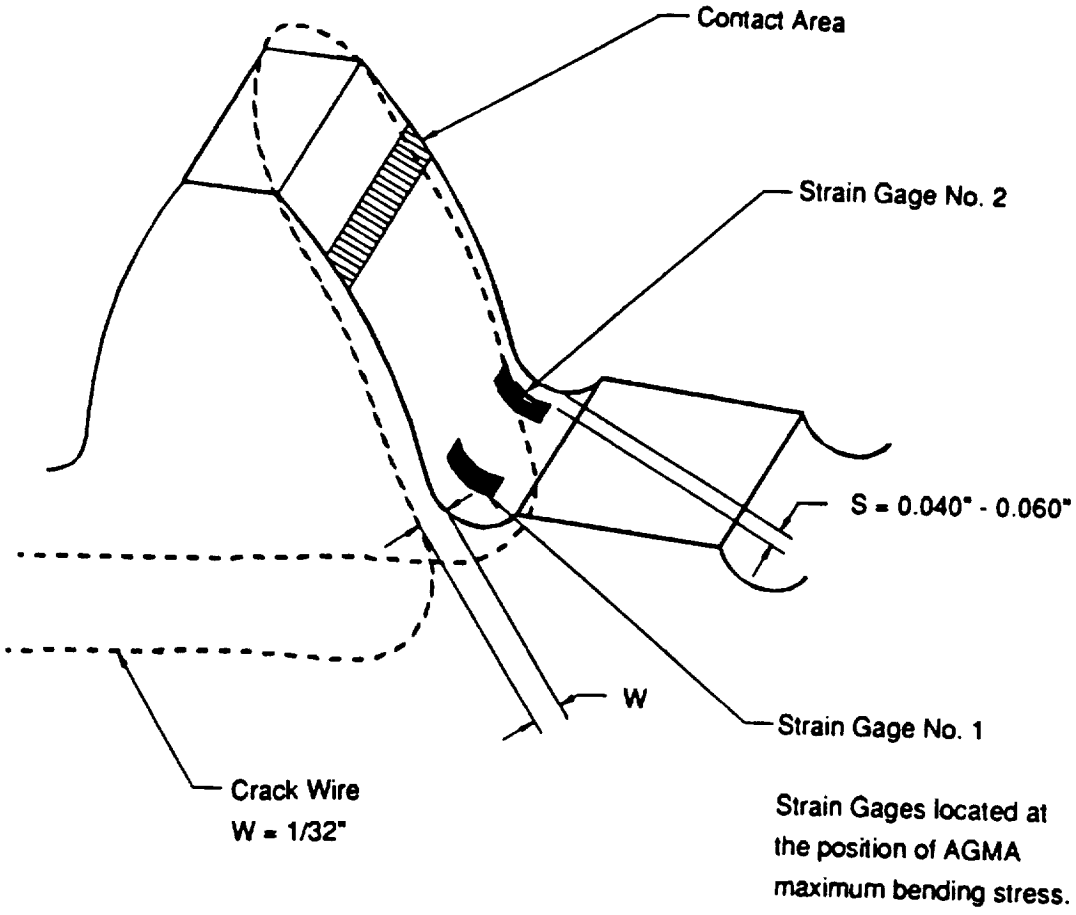

Figure 66. Strain Gage and Crack Wire Placement

The loading frequency for all tests was 30 Hz. Any gear tooth which ran at a specific load level for $3x10^6$ cycles was considered a run-out for this single tooth bending fatigue test program. The first tests of the M50NIL, X-53 and CBS 600 material gears were run at approximately 2031 ± 1931 lb (280 ksi maximum). The first 9310 steel gear test was run at approximately 2172 ± 2072 lb (300 ksi maximum), while that of maraging 300 steel maximum was run at 1748 ± 1648 lb (240 ksi maximum). If the first test was a runout, load was increased to yield a 40 ksi maximum bending stress increase for the second test. If the first test yielded a tooth failure, load

was decreased to yield a 20 ksi drop in maximum bending stress. Subsequent tests were increased or decreased in a similar manner, with the goal of attaining a few run-outs and having most of the remaining failure points clustering about the bend or "knee" of the S-N curve attained for each material. In addition, the load levels at which failures occurred were usually run for more than one test to give some idea of the test result variance seen at the same loads.

Data recorded for each test run included test gear serial number, test gear material conditions, test gear configuration data, test tooth number, applied normal loads (maximum and minimum), calibrations of strain gaged tooth, cycles to failure, failure mode, frequency of applied load, and test temperature.

The equivalent bending stresses for the test load values were calculated, based on the AGMA tooth bending stress formula [55], as follows:

$$St = \frac{Wt\ Ko\ Pd\ Ks\ Km}{Kv\ F\ J}$$

Where

St = Calculated tensile bending stress at the root of the tooth, psi
Wt = Transmitted tangential load at operating pitch diameter, lb
Ko = Overload factor
Kv = Dynamic factor
Pd = Diametral pitch
F = Face width, inch
Ks = Size factor
Km = Load distribution factor
J = Geometry factor

For this testing program,

$$Ko = Kv = Ks = Km = 1.0 \text{ and } Wt = Wn \cos(\phi)$$

Where,

Wn = Applied normal load
ϕ = Pressure angle at the pitch diameter

Therefore,

$$St = \frac{Wn \bullet \text{Cos}(\phi) \bullet Pd}{F \bullet J}$$

In this single tooth bending test program, the load was applied at the worst load position, i.e., at the highest point of single tooth contact. The "J" factor was calculated by the Lucas Western SHAG program which was developed according to AGMA Standard (55). So, for a 3000 lb applied normal load, the maximum bending stress was calculated as:

$$St = \frac{3000 \bullet \text{Cos}(25°) \bullet 8}{0.25 \bullet 0.4104035}$$

$$= 212 \text{ ksi}$$

VI.B.2.v Results

The basic raw data is shown in Tables 44, 45, 46, 47, and 48. All the fatigue lives were rounded to the nearest 100 cycles. The real significance of this data can only be gaged when it is subjected to a statistical evaluation. Five bending strength formulae were investigated and applied to the fatigue test spur gear configurations - Lewis, Dolan-Broghamer, Heywood, Kelly-Pederson, and AGMA. The AGMA method gave the smallest deviation from the measured stress for spur gears (56). Therefore, S-N curves were fitted to the tooth fatigue data with respect to AGMA calculated stress in this gear tooth bending fatigue test program. The general approach involved analyzing the data statistically in order to define the sample mean, the standard deviation, and the mean endurance limit. This data then can be used to compare various materials and to make reasonable projections of the allowable bending stress for a given material under realistic design conditions. Runouts from the fatigue test data were not included when determining a best fit curve. Runouts were shown in the S-N curve for information only and were clearly distinguished from the finite life data points by the use of arrows. The number of arrows indicates the number of tests that were run at that specific stress level. Because the S-N relationship was reasonably approximated by a curve for a specific interval of stress, it was not recommended that the S-N curve be extrapolated outside the interval of testing (57).

TABLE 44. M50NIL SINGLE TOOTH BENDING FATIGUE TEST DATA

Material: Carburized M50NIL Steel per AMS 6278		
Test Temperature: RT	**Case Depth (Inch): 0.030-0.035 (at pitch line)**	**Case Hardness: RC 60** **Core Hardness: RC 42-43**
Test No.	**AGMA Max. Bending Stress, ksi**	**Cycles to Failure**
1	280	369,300
2	260	Run Out
3	320	41,100
4	280	Run Out
5	320	10,000
6	340	19,500
7	300	32,000
8	340	4,900
9	300	18,100
10	300	24,800
11	280	Run Out
12	290	22,600
13	290	157,000
14	290	22,900
15	290	52,200
16	290	38,200
17	280	Run Out
18	320	31,100
19	340	5,000
20	280	91,500

TABLE 45. X53 SINGLE TOOTH BENDING FATIGUE TEST DATA

Material: Carburized X53 Steel per AMS 6278

Test Temperature: RT **Case Depth (Inch): 0.035-0.042 (at pitch line)** **Case Hardness: RC 63 Core Hardness: RC 37-40**

Test No.	AGMA Max. Bending Stress, ksi	Cycles to Failure
1	280	Run Out
2	320	52,600
3	340	8,200
4	300	1,791,600
5	320	16,700
6	340	10,500
7	300	55,000
8	300	26,400
9	290	Run Out
10	300	781,600
11	300	Run Out
12	320	88,400
13	340	9,300
14	300	553,400
15	320	33,200
16	340	23,600
17	295	75,100
18	360	15,900
19	360	7,100
20	360	7,600

TABLE 46. CBS 600 SINGLE TOOTH BENDING FATIGUE TEST DATA

Material: Carburized CBS 600 Steel per AMS 6255		
Test Temperature: RT	**Case Depth (Inch): 0.030 (at pitch line)**	**Case Hardness: RC 58-59 Core Hardness: RC 39-41**
Test No.	**AGMA Max. Bending Stress, ksi**	**Cycles to Failure**
1	280	Run Out
2	320	19,700
3	300	15,200
4	290	Run Out
5	320	23,800
6	300	74,400
7	290	33,900
8	290	34,200
9	280	Run Out
10	290	Run Out
11	340	12,200
12	340	17,500

Figures 67, 68, 69, 70, and 71 show the mean S-N curve (50 percent failure) and the curve of the mean minus 3 sigma for each material. The mean endurance limits, standard deviations, and the mean endurance limit minus 3 sigma are shown in Table 49 and Figures 67 through 71. For comparing the bending fatigue strength, all the mean S-N curves of the five materials are plotted in Figure 72.

The failure modes have been evaluated and all were the typical failures of the tooth root fillet bending fatigue. Cracks were found in the root areas of either one side or both sides of test teeth with a length of approximately 0.070 inch.

VI.B.2.vi Discussion of Results

Based on the specific heat treatments of each material (as previously shown in Table 43), Pyroware X53 has the greatest tooth bending fatigue strength. AISI 9310 is the material of the least bending fatigue endurance. The five materials are rated in terms of tooth bending fatigue strength as follows:

1. X53
2. CBS 600
3. M50NIL
4. Maraging 300
5. 9310

TABLE 47. 9310 SINGLE TOOTH BENDING FATIGUE TEST DATA

Material: Carburized 9310 Steel per AMS 6265

Test Temperature: RT | **Case Depth (Inch): 0.032-0.036 (at pitch line)** | **Case Hardness: RC 63 Core Hardness: RC 35-40**

Test No.	AGMA Max. Bending Stress, KSI	Cycles to Failure
1	300	1,800
2	280	6,600
3	260	3,800
4	240	16,200
5	240	5,100
6	200	219,300
7	180	Run Out
8	200	760,000
9	220	27,000
10	220	9,200
11	210	19,000
12	190	Run Out
13	210	Run Out
14	220	17,100
15	220	12,000
16	200	16,500
17	200	Run Out
18	210	2,155,900
19	240	7,400
20	190	Run Out
21	210	29,000
22	210	56,200
23	200	50,000
24	200	30,000

TABLE 48. M300 SINGLE TOOTH BENDING FATIGUE TEST DATA

Material: Through-hardened Maraging 300 Steel per AMS 6514		
Test Temperature: RT	**Case Depth (Inch): (at pitch line)**	**Case Hardness: RC** **Core Hardness: RC 53-54**
Test No.	**AGMA Max. Bending Stress, KSI**	**Cycles to Failure**
1	240	121,400
2	220	687,700
3	260	35,900
4	220	120,800
5	200	Run Out
6	240	42,500
7	260	89,100
8	210	141,300
9	200	Run Out
10	280	30,000
11	280	39,900
12	210	93,100

Comparing the single tooth test results of these five near-net forged materials with that of Lucas Western's conventional test gears made from bar stock, it is concluded that:

- The tooth bending fatigue strengths of near-net forged X53, CBS 600, M50NIL, and Maraging 300 are only slightly better than that of conventional gears.
- The tooth bending fatigue strength of conventional 9310 gears is greater than the near-net forged 9310 gears.

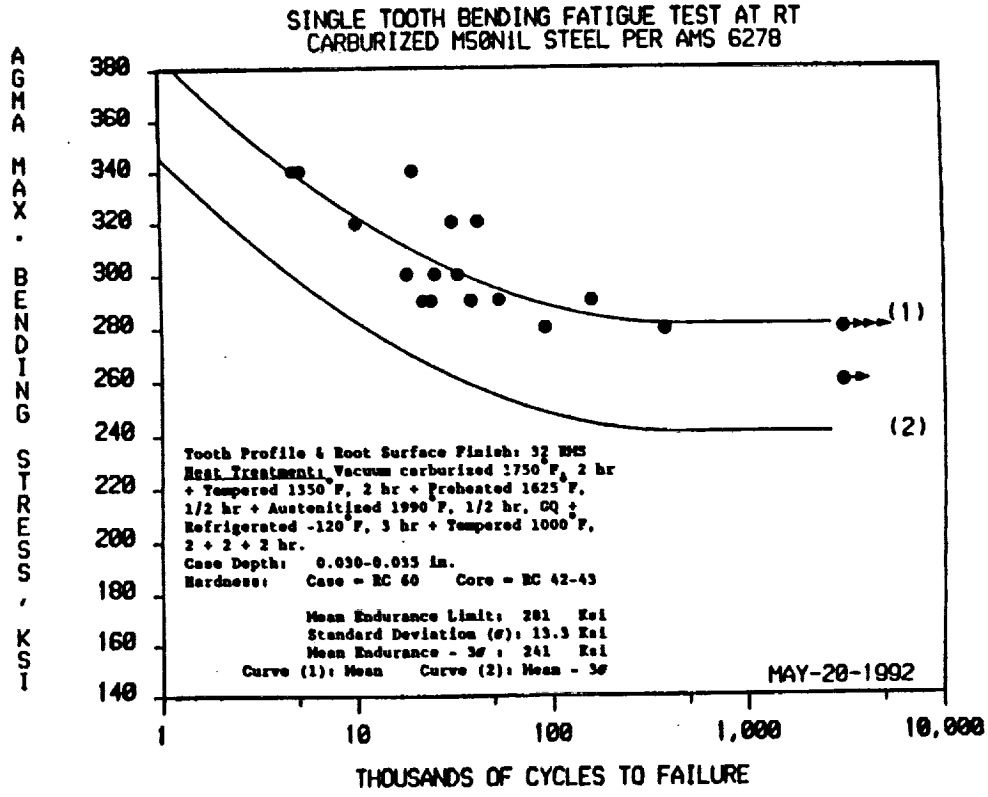

Figure 67. Best Fit S-N Curve of Single Tooth Bending Fatigue Tests
Material: M50NIL

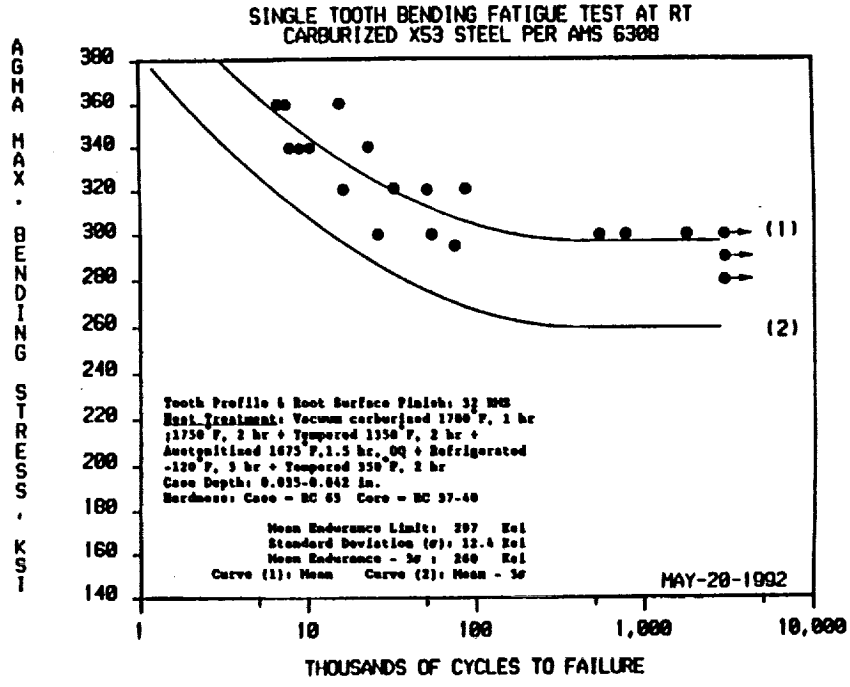

Figure 68. Best Fit S-N Curve of Single Tooth Bending Fatigue Tests
Material: X53

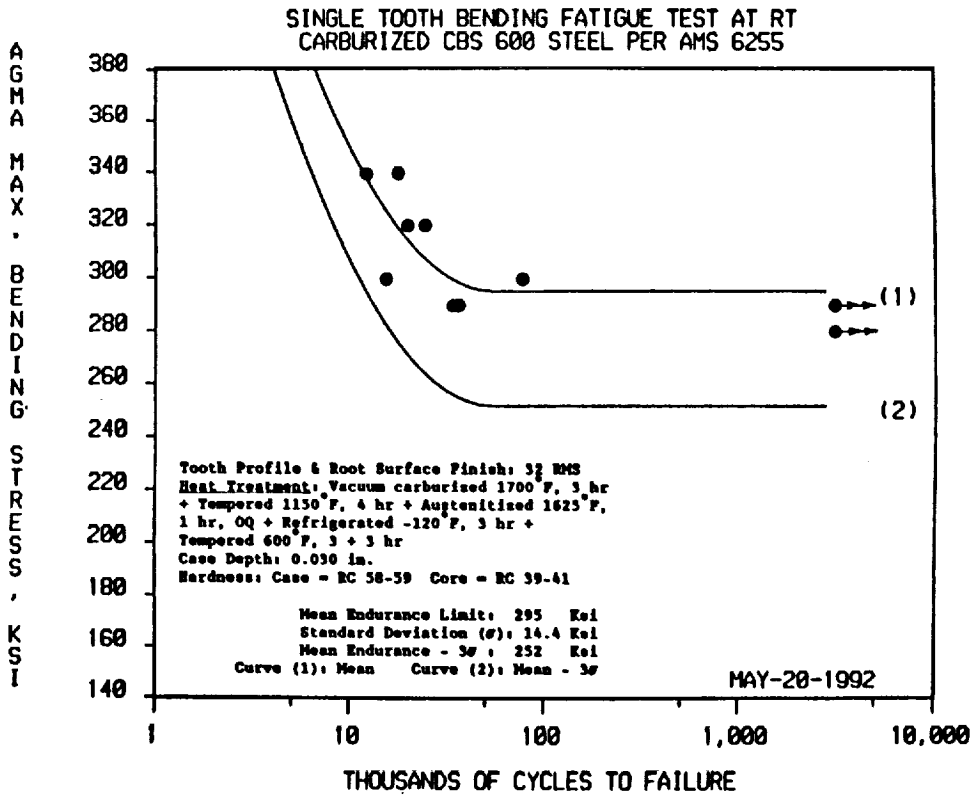

Figure 69. Best Fit S-N Curve of Single Tooth Bending Fatigue Tests
Material: CBS 600

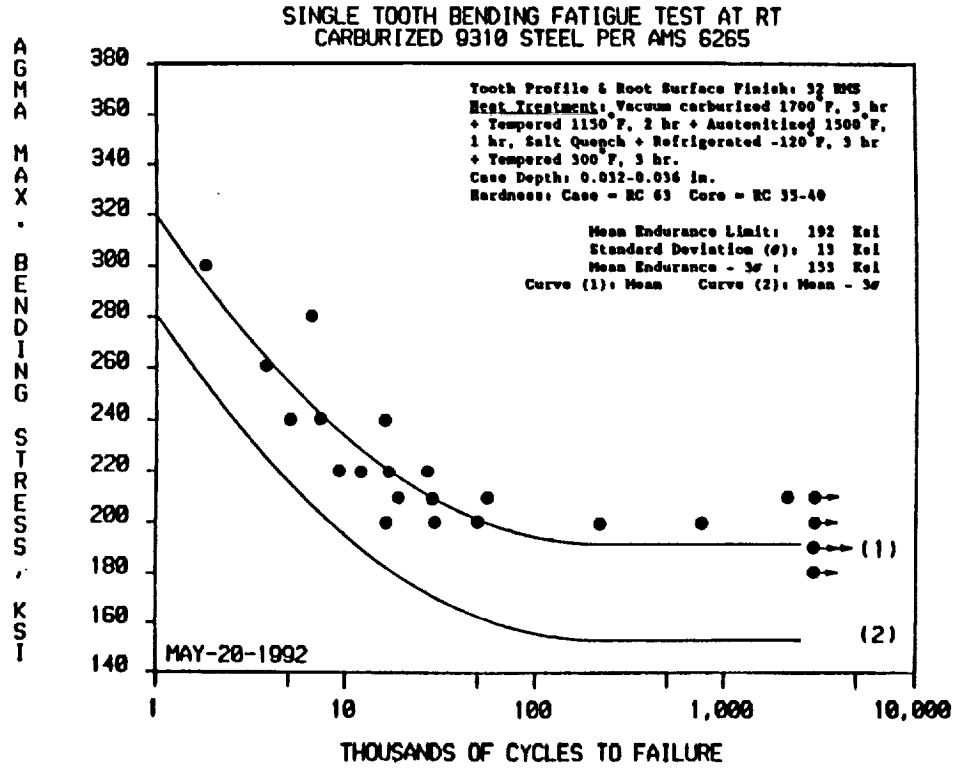

Figure 70. Best Fit S-N Curve of Single Tooth Bending Fatigue Tests
Material: 9310

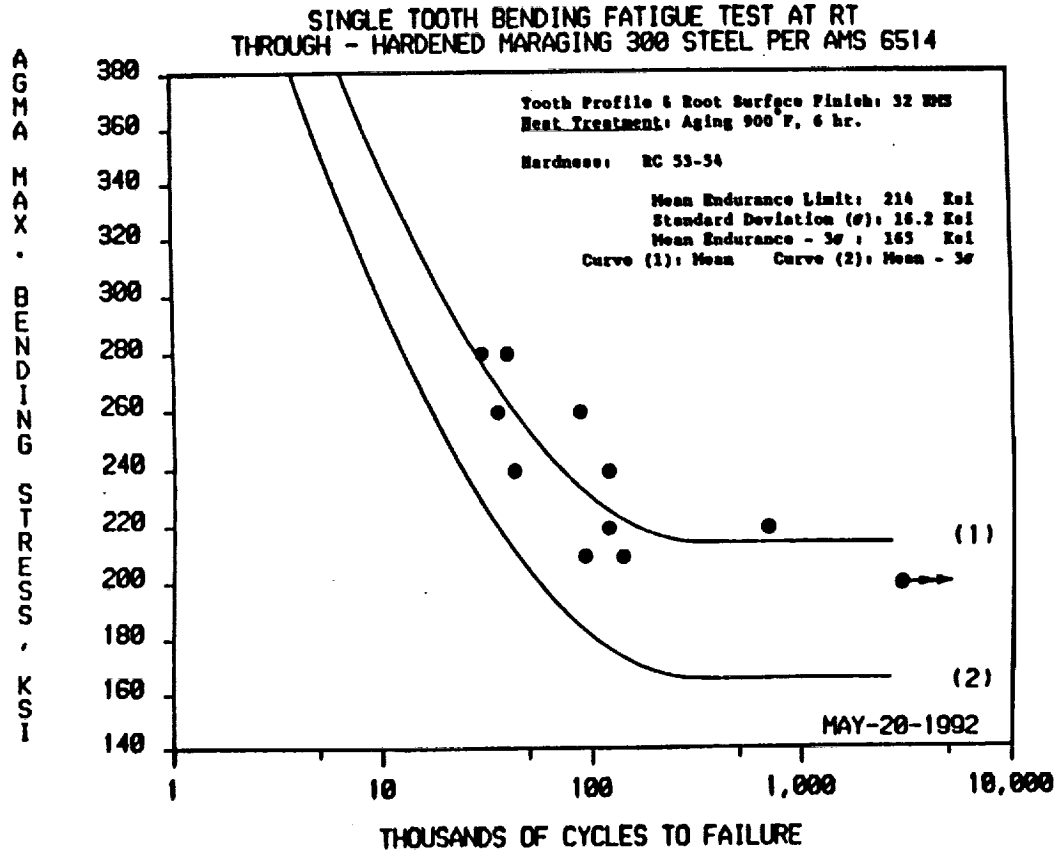

Figure 71. Best Fit S-N Curve of Single Tooth Bending Fatigue Tests
Material: Maraging 300

TABLE 49. STATISTICAL EVALUATION OF TEST DATA

The mean endurance limits, standard deviations, and the mean endurance limits minus three sigma of single tooth bending fatigue strength.

m = mean endurance limit

σ = standard deviation

m-3σ = mean endurance limit minus three sigma

Material	m, ksi	σ, ksi	m-3σ, ksi
X53	297	12.4	260
CBS 600	295	14.4	252
M50NIL	281	13.3	241
Maraging 300	214	16.2	165
9310	192	13.0	153

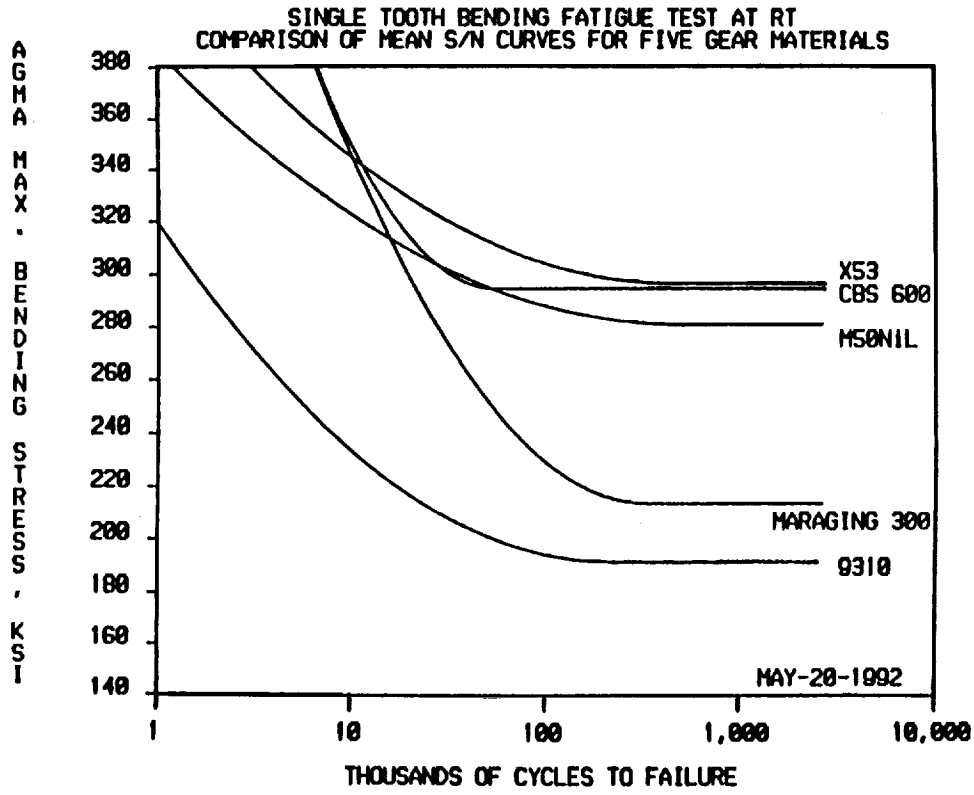

Figure 72. Comparison of Best Fit S-N Curves for Five Gear Materials

The possible reasons for the fatigue strength differences between near-net forged gears and conventional gears are outlined below:

1. Size Effect. The conventional test gears have a greater size (8 DP, 3.75-inch pitch diameter).

2. Case Depth. Some case depth of carburized conventional gears are only 0.020 inch, which is shallower than the near-net forged gears.

3. Due to the Difference in Gear Manufacturing Processes. Further research work may be necessary to investigate the bending fatigue strength difference between the near-net forged gears and conventional gears.

In order to obtain more data in the high cycle fatigue range and reduce the standard deviations, more single tooth tests of material CBS 600 and Maraging 300 are required to achieve a better statistical evaluation of test data. Also, to compare the tooth bending fatigue strength between near-net forged gears and conventional gears, it is recommended that two groups of test gears with the identical gear size/configuration and the same case depth should be used to conduct the single tooth bending fatigue tests.

Finally, the AGMA formula of tooth bending stress was selected to correlate the test data, since AGMA calculated stress best matched experimentally measured stress. Since the LWI Shag Program is based on AGMA equations [55], it also allows the data derived herein to be used for design and analysis directly. Since the test gears used are actual full sized gears and not specimens, the data obtained from the testing does not need to be adjusted to size.

The data, however, does have to be adjusted to reflect the actual conditions which may be encountered in an actual gear system. These conditions include dynamics and alignment effects as well as blank construction and tooth geometry effects. The S-N data may be used directly only with an appropriate safety factor applied. In most cases, the gears are analyzed by the conventional AGMA methods, thus the allowables must be adjusted to reflect the unknowns in the AGMA analysis.

VI.B.3 Charpy Impact Energy Tests - Gear Materials

VI.B.3.i Introduction

A number of advanced, high-temperature steels have recently been introduced and proposed for use in elevated-temperature gear and bearing applications. The integrity and performance of such steels must be precisely determined and understood in order to ensure that the correct design and application are achieved. To assess the suitability of five such steels at room temperature, the conventional impact testing (Charpy V) was included in the material test schedule of the Advanced Rotorcraft Transmission program. The five steels tested were Pyroware X53 (AMS 6308), M50NIL (AMS 6278), CBS 600 (AMS 6255), AISI 9310 (AMS 6265) and Maraging 300 (AMS 6514).

VI.B.3.ii Test Article Description

For the test specimens, the material certificates, chemical compositions, specimen size, specimen configuration, and specimen orientations are detailed in Tables 50, 51, and 52. Figure 72 shows the Charpy impact test specimen configuration. Each Charpy impact specimen, except CBS 600, was machined with the crack-plane orientation transverse to the rolling direction of the bar (designated R-C in ASTM E399). The CBS 600 specimens were machined in L-C orientation because of material availability.

The heat treatment process is critical in affecting the impact energy and the strength of the finished components. Table 53 outlines the specific core heat treatments applied to each material, as well as the core hardness and tensile yield strengths generated by each heat treatment. All heat treatment operations were conducted at LWI, Applied Technology Division.

TABLE 50. MATERIAL CERTIFICATES

Material	AMS Spec.	Producer	Heat No.	Lucas Western Lab Serial No.	Product Form	Process	Grain Size
9310	6265	Carpenter	89580	840183	4.5" ϕ bar	VIM VAR	7/8
M50NIL	6278	Latrobe	E3729	900255	4.5" ϕ bar	VIM VAR	5.5
Pyroware X53	6308	Carpenter	95320	900164	4.5" ϕ bar	VIM VAR	7/8
CBS 600	6255	Latrobe	E3891	900270	2.0" ϕ bar(1)	VIM VAR	5
Maraging 300	6514	Cytemp	6L1202	900078	4.5" ϕ bar	VIM VAR	7

(1) 4.5" ϕ bars were not available at the time of preparing the test specimens.

TABLE 51. CHEMICAL COMPOSITION

Material	Element (%)													
	C	Mn	P	S	Si	Co	Cr	Ni	Cu	Mo	V	W	Ti	Al
9310	0.10	0.65	0.006	0.004	0.27	-	1.31	3.21	0.03	0.15	-	-	-	-
M50NIL	0.12	0.21	0.015	0.004	0.17	0.02	4.15	3.48	0.04	4.28	1.24	0.03	-	-
Pyroware X53	0.12	0.28	0.009	0.00016	0.66	-	0.96	1.97	1.90	3.21	0.10	-	-	-
CBS 600	0.17	0.54	0.005	0.001	1.12	-	1.46	0.02	0.06	0.93	-	-	-	0.05
Maraging 300	0.01	0.01	0.001	0.004	0.05	9.17	0.28	18.52	0.05	4.91	-	-	0.68	0.12

VI.B.3.iii Test Rig Description

The Charpy Impact Tester, made by Tinius Olsen, is a pendulum-type testing machine of rigid construction and capacity more than sufficient to break the specimen in one blow. The machine used was verified on April 4, 1990, which was within one year prior to the January 1991 testing month. The test results using this machine were within the allowed variation range of the National Institute of Standards and Technology (NIST).

TABLE 52. SPECIMEN SIZE, SPECIMEN CONFIGURATION, AND SPECIMEN ORIENTATION

Material	AMS Specification	Specimen Size	Specimen Configuration(1)	Specimen Orientation(2)
9310	6265	0.394" x 0.394", Full	Charpy (Simple Beam) V-Notch, Type A	RC
M50NIL	6278	0.394" x 0.394", Full	Charpy (Simple Beam) V-Notch, Type A	RC
Pyroware X53	6308	0.394" x 0.394", Full	Charpy (Simple Beam) V-Notch, Type A	RC
CBS 600	6255	0.394" x 0.394", Full	Charpy (Simple Beam) V-Notch, Type A	LC
Maraging 300	6514	0.394" x 0.394", Full	Charpy (Simple Beam) V-Notch, Type A	RC

(1) See Figure 72.
(2) Use the crack plane orientation code in ASTM E399.
L = direction of maximum grain flow (the direction normal to the crack plane).
R = radial direction (the direction normal to the crack plane).
C = circumferential or tangential direction (the expected direction of crack propagation).

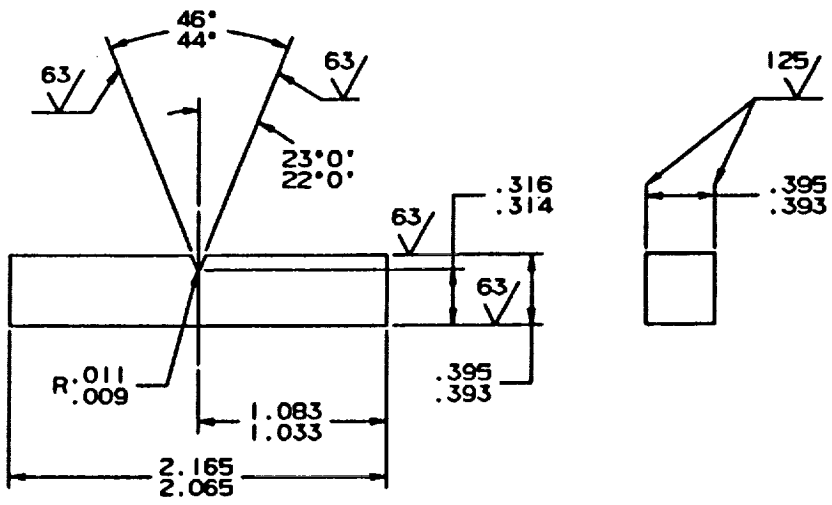

Figure 73. Charpy V Impact Specimen

TABLE 53. CORE HEAT TREATMENTS AND REQUIRED MECHANICAL PROPERTIES AT ROOM TEMPERATURE

Material	Pseudo-carburize	Hardening	Refrigeration	Temper	Hardness	Yield Strength 0.2% Offset, ksi
9310	1700°F, 3 hr	Temper 1150°F, 2 hr Austenitize 1500°F, 1 hr, Oil Quench	-125°F, 3 hr	300°F, 3 hr	RC 37-38	142
M50NIL	1750°F, 2 hr	Temper 1300°F, 2 hr Preheat 1625°F, 0.5 hr Austenitize 2000°F, 0.5 hr, Gas Quench	-100°F, 3 hr	1000°F, 2+2+2 hr	RC 42-43	162
Pyroware X53	1700°F, 1 hr, 1750°F, 2 hr	Temper 1350°F, 2 hr Austenitize 1675°F, 1.5 hr, Oil Quench	-110°F, 2 hr	350°F, 2 hr	RC 37-38	143
CBS 600	1700°F, 3 hr	Temper 1150°F, 2 hr Austenitize 1625°F, 1 hr, Oil Quench	-120°F, 3 hr	600°F, 3+3 hr	RC41-42	138
Maraging 300		Aging 900°F, 6 hr			RC 54-55	296

VI.B.3.iv Test Procedure

The Charpy-V impact tests were performed in accordance with the ASTM E23 standard method for "notched bar impact testing of metallic materials." All tests were performed at room temperature. The broken specimens were inspected and then stored for further reference. The impact energy absorbed lateral expansion, and fracture appearance were determined based on ASTM E23, Procedure 11.2.4 and are included in this report.

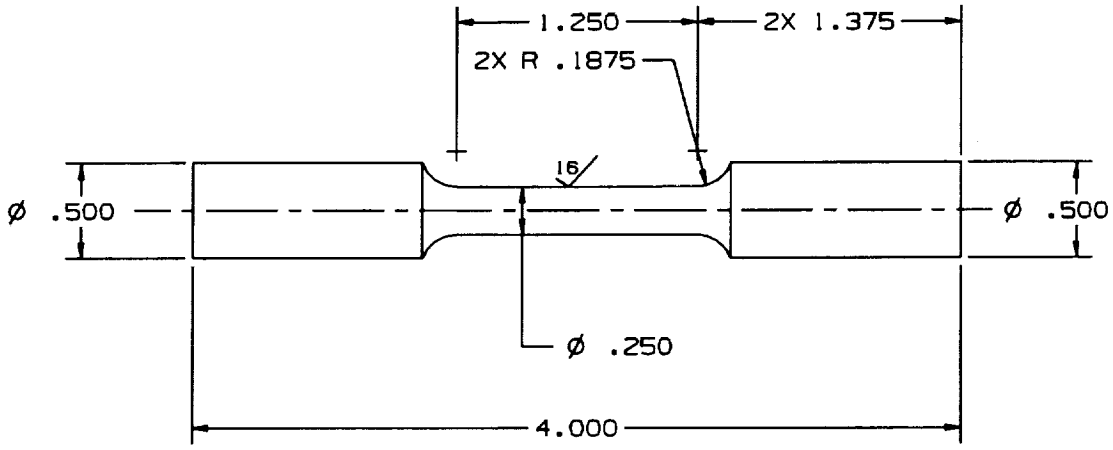

Figure 74. Tension Test Specimen

In addition to the Charpy impact tests, five tensile tests of each material were performed at room temperature to check the validity of the heat treatment cycles. The tensile bars were heat treated in the same batch with the Charpy rectangular bars, prior to machine finishing. Figure 73 shows the tensile test specimen configuration. All tensile testing was carried out in accordance with ASTM E8.

VI.B.3.v Results

Following tests, the percent shear fracture was determined and recorded. Lateral expansion was measured from the two halves of each broken specimen. The impact energy data was statistically analyzed and Table 54 presents a summary of the impact energy mean values, standard deviations and predicted ranges of mean value at 99 percent confidence level. Also included in the table are the average tensile test properties for tensile test specimens of the five materials.

Based on the core heat treatments conducted for each material and summarized in Table 4, AISI 9310 is the toughest material and M50NIL is the least tough. Pyroware X53 was found to be the second toughest, with CBS 600 third, and maraging 300 fourth. These results used in conjunction with results of other tests contained in this report, as well as results of previously performed tests, provide the design engineer with good indication of the material to choose for the requirements of his application.

TABLE 54. SUMMARY - CHARPY V IMPACT ENERGY TEST RESULTS

Impact Energy Tests Data Specimen Failure Points (ft–lb)	Impact Energy Tests ft–lb				Tensile Test Results		
	M*	D*	S*	% Shear	Yield Strength ksi	Tensile Strength ksi	Elongation %
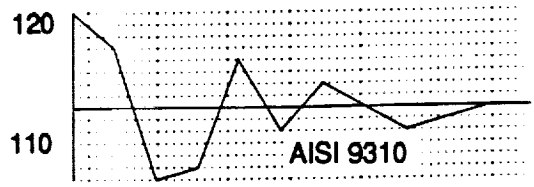	113	109–117	4.0	90	142	181	18
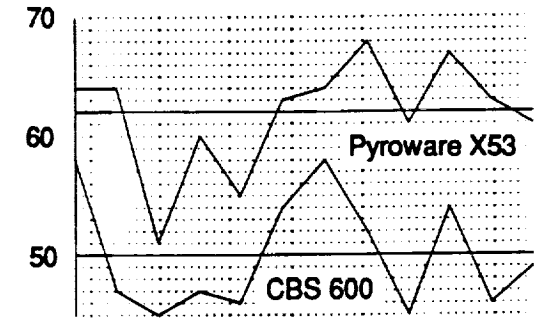	62	58–66	4.8	59+	142	179	16
	50	46–54	4.9	36–	138	185	18
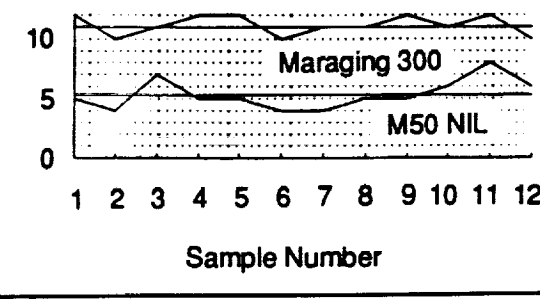	11	10–12	.83	<10	296	305	11
	5.3	4.2–6.4	1.2	<5	162	197	20

* M = Mean value impact energy
D = Predicted range of mean value with a 99% confidence level
S = Standard deviation of impact energy data

VI.B.4 Fracture Toughness Tests

VI.B.4.i Introduction

Two advanced, high-temperature steels and three housing materials were tested at room temperature to provide fracture toughness (K_{1c}) measurements. The gear materials tested were X53 Pyroware (AMS 6308) and M50NIL (AMS 6278). These two steels have been introduced and proposed for use in elevated temperature gear and bearing applications. The housing materials tested were WE43 and ZE41A magnesium alloys and C355T7 aluminum alloy. These are candidate housing materials for the design of future gearboxes operating at elevated temperatures.

The property K_{1c} determined in this program characterizes the resistance of a material to fracture in a neutral environment in the presence of a sharp crack under severe tensile constraint, such that the state of stress near the crack front approaches tri-tensile plane strain, and the crack-tip plastic region is small compared with the crack size and specimen dimensions in the constraint direction.

A K_{1c} value is believed to represent a lower limiting value of fracture toughness. This value may be used to estimate the relation between failure stress and defect size for a material in service wherein the conditions of high constraint described above would be expected. Background information concerning the basis of this test method herein in terms of linear elastic fracture mechanics (LEFM) may be found in References [58] and [59].

VI.B.4.ii Test Article Description

For the test specimens, the material certificates, chemical compositions, specimen sizes, specimen configurations, and specimen orientations are detailed in Tables 55, 56, and 57. The fracture toughness specimens of the two steel materials (M50NIL, Pyroware X53) were machined with the crack-plane orientation transverse to the rolling direction of the bar (designed R-C in ASTM E399). This crack-plane orientation is similar to the crack direction of the single tooth bending fatigue test gears of an earlier Lucas Western test program performed. This single tooth bending fatigue test program used the same 4.5-inch diameter bar stock as the fracture toughness test specimens, providing a good basis for comparison of material performance in single tooth bending and fracture toughness.

Prior to testing, the specimen geometry was carefully measured to verify that it was within machining tolerances, and then it was checked against the size validity expectation.

The condition of plane strain is affected by the thickness of the specimen and the size of the plastically deformed zone around the crack tip. For ductile materials, the plastic zone area can be large, so large specimens are required to provide restraint adequate to prevent excessive plastic deformation. For brittle materials, almost all the deformation at the crack tip is elastic so small specimens are required, based on the linear elastic fracture mechanics theory.

In order to obtain valid fracture toughness (K1c) values, various specimen sizes (from 0.75 to 1.5-inch thickness) were used, based on the available stock of material in this program. One of the configurations, that of the 1-inch thick specimens, is shown in Figure 75. This is similar to the 0.75 inch, 0.95 inch and 1.50 inch specimen configurations also used in the tests.

TABLE 55. MATERIAL CERTIFICATES

Material	AMS Spec.	Producer	Heat No.	Product Form	Process	Grain Size
WE43	N/A	Magnesium Elektron	--	1" Thick Plate	Sand Cast	-
ZE41A	4439A	Magnesium Elektron	--	1" Thick Plate	Sand Cast	-
C355T7	4215	Teledyne Cast Products	08310C	1.25" Thick Plate	Sand Cast	-
M50NIL	6278	Latrobe	E3729	4.5" ϕ Bar	VIM VAR	5.5
Pyroware X53	6308	Carpenter	95320	4.5" ϕ Bar	VIM VAR	7/8

The heat treatment process critically affects the fracture toughness. The two steel alloys are carburizing materials. They were not case hardened; they were heat treated to test the core fracture toughness. Both materials received the thermal processing cycle most applicable to current service requirements, which are the same as the heat treatment of the Charpy impact test specimens. These two steel materials were heat treated at Lucas Western Inc., Applied Technology Division.

The magnesium alloys, WE43 and ZE41A, were treated at Magnesium Elektron, Inc. Aluminum alloy, C355T7, was produced and heat treated by Teledyne Cast Products. All the housing material received the same heat treat cycles as the tensile test specimens. Table 58 outlines the specific heat treatments applied to all the test materials.

VI.B.4.iii Test Rig Description

The testing machine used was a MTS 810 series material test system, located at LWI, Applied Technology Division. It has three control modes:

Load Control:	up to $\pm$ 20,000 lbs
Stroke Control:	$\pm$3 inches displacement
Strain Control:	up to $\pm$15% strain (axial extensometer)
C.O.D. Gage:	up to 0.150 inches displacement

To minimize bending, specimen fixtures were such that the major axis of the specimen closely coincided with the load axis. The maximum bending strain determined was 1% of the average axial strain. 5% is the maximum allowable bending strain per ASTM standard E466 and E606. During testing the stress distribution was uniform through the specimen thickness and symmetrical about the plane of the prospective crack. The measured fatigue precrack front and the fracture appearance of the broken specimens are uniform and symmetrical.

TABLE 56. CHEMICAL COMPOSITION

Element (%)								
Material	**Y**	**Zr**	**Nd**	**Yb**	**Zn**	**Dy**	**Mn**	**Cu**
WE43	5.42%	0.44%	2.55%	0.14%	0.094%	0.48%	0.0064%	0.0059%
ZE41A	-	0.58%	-	-	4.52%	-	0.0069%	0.0061%
C355T7	-	-	-	-	<0.10%	-	<0.10%	1.1%

Element (%)							
Material	**Fe**	**Si**	**Ni**	**Mg**	**Ce**	**Al**	**Ti**
WE43	0.0053%	0.0070%	0.010%	REM	-	-	-
ZE41A	-	-	0.0017%	REM%	1.31%	-	-
C355T7	0.06%	5.3%	-	0.50%	-	REM	0.16%

Element (%)						
Material	**C**	**Mn**	**P**	**S**	**Si**	**Co**
M50NIL	0.12	0.21	0.015	0.004	0.17	0.02
Pyroware X53	0.12	0.28	0.009	0.00016	0.066	-

Element (%)						
Material	**Cr**	**Ni**	**Cu**	**Mo**	**V**	**W**
M50NIL	4.15	3.48	0.04	4.28	1.24	0.03
Pyroware X53	0.96	1.97	1.90	3.21	0.10	-

TABLE 57. SPECIMEN SIZE, SPECIMEN CONFIGURATION, AND SPECIMEN ORIENTATION

Material	AMS Specification	Specimen Size Thickness, inch	Specimen Configuration	Specimen Orientation
WE43	N/A	0.75 1.00	C(T)-Straight Through	N/A
ZE41A	4439A	0.75 0.95* 1.00	C(T)-Straight Through	N/A
C355-T7	4215	0.75	C(T)-Straight Through	N/A
M50NIL	6278	1.00	C(T)-Straight Through	RC
Pyroware X53	6308	1.00 1.50	C(T)-Straight Through	RC

*The material was only available for machining 0.95-inch thick specimens.

VI.B.4.iv Test Procedure

All the fracture toughness (K_{1C}) tests were performed in accordance with ASTM Standard E399 (Plane-Strain Fracture Toughness of Metallic Materials) and the following reference standards:

B645: Plane-strain Fracture Toughness Testing of Aluminum Alloys
E8: Methods of Tension Testing of Metallic Materials
B557: Method of Tension Testing Wrought and Cast Aluminum - and Magnesium-Alloy Products

All tests described below were conducted at room temperature.

To provide tensile properties for performing fracture toughness (K_{1C}) tests, tensile tests were first carried out in accordance with ASTM E8 and B557. Five tensile tests of each steel alloy (M50NIL, Pyroware X53) were conducted and the tensile properties are shown in Table 59. Table 59 also contains the tensile properties determined from the 24 tensile tests of each housing material (WE43, ZE41A, C355T7).

Tests for fracture toughness determination involve a two-part test procedure each with its own set of constraints. The first phase is the fatigue precrack section; the second phase is the tensile test of the precracked specimen.

Within the fatigue precrack phase, the maximum stress intensity factor in the initial portion of the fatigue cycle was kept below 80 percent of the estimated K_{1C} value of the material, and the terminal value of K_{max} was maintained at less than 60 percent of the K_Q value.

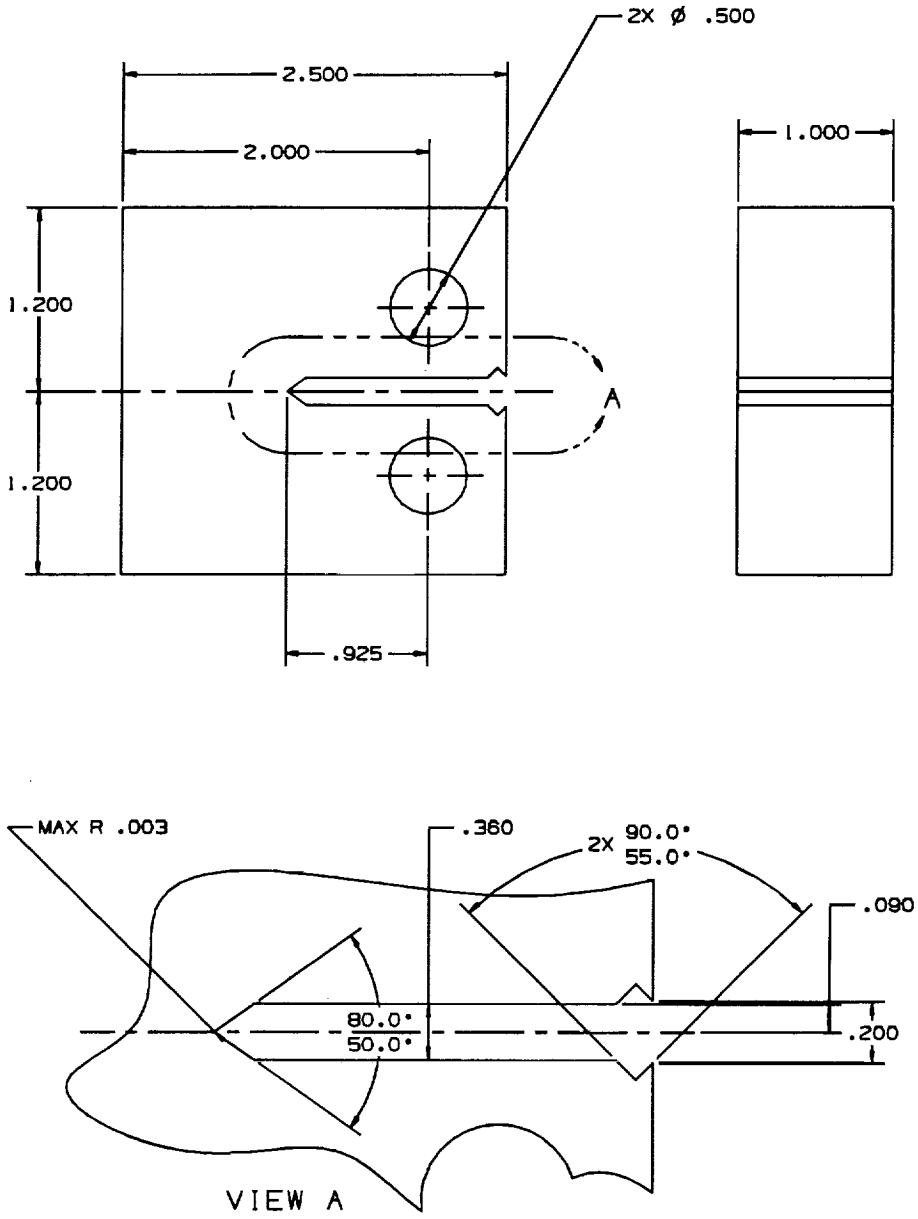

Figure 75. Fracture Toughness (K_{1C}) Specimen, B = 1.00"

TABLE 58. HEAT TREATMENTS AND HARDNESS

Material	Solution Heat Treatment	Aging Treatment	Hardness
Magnesium Alloy ZE41A (Condition T5)	2 hrs at 626°F, cool in air	16 hrs at 356°F	BHN 60
Magnesium Alloy WE43 (Condition T6)	8 hrs at 977°F, hot water quench at 140°F - 176°F	16 hrs at 482°F	BHN 71
Aluminum Alloy C355T7 (Condition T7)	12 hrs at 980°F, water quench at 70°F	8 hrs at 440°F	BHN 81

Material		Material			
Material	**Pseudo-carburize**	**Hardening**	**Refrigeration**	**Temper**	**Hardness**
M50NIL	1750°F, 2 hr	Temper 1300°F, 2 hr Preheat 1625°F, 0.5 hr Austenitize 2000°F, 0.5 hr, Gas Quench	-100°F, 3 hr	1000°F, 2+2+2 hr	RC 42-43
Pyroware X53	1700°F, 1 hr, 1750°F, 2 hr	Temper 1350°F, 2 hr Austenitize 1675°F, 1.5 hr, Oil Quench	-110°F, 2 hr	350°F, 2 hr	RC 37-38

A nominal loading rate range of 30-150 (ksi • $in.^{1/2}$)/minute was used in the fracture tests, based on ASTM E399, Procedure 8.3. The actual load and displacement data values that made up the load-displacement curves were stored through a PC-based data acquisition system. These data files were used for data reduction and stored for further studies of the material properties.

It is recommended by ASTM E399 that at least three replicate tests be made for each material condition. For this test program, at least six tests of each material were conducted and used to define the fracture toughness. In an effort to obtain valid K_{1c} values, seven tests of WE43, ZE41A and X53 were performed.

VI.B.4.v Results

The values of fracture toughness (K_{1c} or K_Q) and the average values are listed in Table 60. A typical detail data summary (WE43 alloy, 1-inch thick, specimen I.D.1) is given in Table 61. A typical load-displacement curve (WE43, specimen I.D.1) is shown in Figure 76.

TABLE 59. TENSILE PROPERTIES

Material	Nominal Gage Section Diameter, in.	Nominal Area in^2	Yield Strength 0.2% Offset Ksi	Tensile Strength Ksi	Elongation %	Reduction of Area %	Modulus of Elasticity* $X10^6$psi
WE43	0.250	0.0491	26.7	39.9	8.2	-	6.478
ZE41A	0.250	0.0491	21.0	32.0	4.6	-	6.462
C355T7	0.250	0.0491	35.1	41.3	2.5	-	10.640
M50NIL	0.250	0.0491	162.0	197.0	20.0	74.0	29.4
Pyroware X53	0.250	0.0491	143.0	179.0	16.0	65.4	28.4
*The modulus of elasticity was calculated from the proportional section of the stress-strain curve.							

VI.B.4.vi Discussion of Results

The fracture toughness tests of WE43 were unable to obtain a valid K_{1c} because:

- P_{max}/P_Q exceeded 1.10.
- Surface crack length less than 0.050 inch (B = 1.00" only).

The invalid ratio of P_{max} to P_Q indicates that a larger specimen should be used to determine K_{1c}.

Magnesium Elektron, Inc., used the same thickness specimen (0.75-inch) as this test program to determine fracture toughness. The WE43 fracture toughness values provided by Magnesium Elektron, 14.5 ksi, $in.^{1/2}$ is quite close to the K_Q values (14.6 ksi, $in.^{1/2}$) of this test result.

Pyroware X53 is too ductile for the tested specimen size. Calculated specimen sizes per ASTM E399, procedure 7.1.3, have shown that specimens thicker than 3 inches would be required to meet the validity requirements of E399. It is considered impractical to test K_{1c} of 3-inch thick specimens to obtain valid results, so alternative methods to obtain valid fracture toughness of X53 should be employed. The J integral technique (ASTM E813) can be used as an alternate, conservative method for estimating K_{1c} on materials that lack sufficient brittleness or specimens that lack sufficient thickness to be tested for K_{1c} per ASTM E399.

K_Q is a conditional value of the fracture toughness test and may be used for preliminary design purposes as long as the hardware thickness is not greater than the specimen thickness used to generate the K_Q result.

TABLE 60. FRACTURE TOUGHNESS TEST RESULTS

Material	Fracture Toughness Ksi - $in.^{1/2}$	Average of K_{1c} Ksi - $in.^{1/2}$
WE43	14.45 (K_Q)	
	14.57 (K_Q)	
	13.81 (K_Q)	
	13.76 (K_Q)	
	15.84 (K_Q)	
	14.65 (K_Q)	
	15.35 (K_Q)	14.6 (K_Q)
	Reference Data [60]:	14.5
ZE41A	11.52 (K_Q)	
	11.69 (K_Q)	
	11.89 (K_Q)	
	11.53 (K_Q)	
	12.12	
	12.21	
	12.67	12.3
	Reference Data [60]:	12.0
C355-T7	17.56	
	17.37	
	17.57	
	16.98 (K_Q)	
	17.85	
	15.66 (K_Q)	17.6
	Reference Data: None Found	

TABLE 60. FRACTURE TOUGHNESS TEST RESULTS (Continued)

Material	Fracture Toughness Ksi - $in.^{1/2}$	Average of K_{1c} Ksi - $in.^{1/2}$
M50NIL	57.3	
	58.2	
	52.2 (K_Q)	
	61.5	
	62.9	
	56.8	59.3
	Reference Data [61]:	58.8
Pyroware X53*	124.5 (K_Q)	
	143.2 (K_Q)	
	129.9 (K_Q)	
	118.0 (K_Q)	
	126.5 (K_Q)	
	133.4 (K_Q)	
	133.2 (K_Q)	130.0 (K_Q)
	Reference Data [62]:	115.0

*Fracture toughness of Pyroware X53 were tested at Dickson Testing Company, Inc., due to the load limit of Lucas Western's testing machine.

TABLE 61. K_{1C} DATA SUMMARY

MATERIAL: WE43 **SPECIMEN I.D.1**

Form: Separately sand cast block, 1-inch thickness

Heat Treat: T6 **Specimen Type:** C(T) - Straight I.D.1

Specimen Parameters	Data	ASTM E399 Reference Paragraph
Crack Plane Orientation	N/A	5.1.3
Specimen Thickness (B), inch	0.747	8.2.1
Specimen Width (W), inch	1.506	A4.4.1
Crack Starter Notch Length, inch	0.650	A4.4.1
0.2% offset Yield Strength, ksi	26.7	7.1.1
Ultimate Strength, ksi	39.9	7.1.1
Modulus of Elasticity, ksi	6478	7.1.1
Fatigue Precracking	**Data**	**Reference Paragraph**
Temperature	RT (66-68 F)	A2.4.4
Number of Cycles (initial stage)	11,500	A2.4.1
Number of Cycles (final stage)	8,500	A2.4.2
K_{max} (initial stage), ksi, $in.^{1/2}$	6.2	A2.4.1
K_{max} (final stage), ksi, $in.^{1/2}$	4.9	A2.4.2
ΔK (final stage), ksi, $in.^{1/2}$	4.4	A2.1.2
Fracture Test	**Data**	**Reference Paragraph**
Test Temperature	RT (66-68 F)	A2.4.4
Relative Humidity	54-56	10.2.7
P_{max}, kip	1.63	9.1.1
P_Q, kip	1.36	9.1.1
P_{max}/P_Q	1.20	9.1.2
Loading Rate, ksi, $in.^{1/2}$	49.4	8.3
Load - Displacement Record	Type I	9.1.1
Fracture Appearance, % Oblique	7%	9.2

TABLE 61. K_{1C} DATA SUMMARY (Continued)

MATERIAL: WE43		**SPECIMEN I.D.1**
Form: Separately sand cast block, 1-inch thickness		
Heat Treat: T6		**Specimen Type:** C(T) - Straight I.D.1
Fracture Test	**Data**	**ASTM E399 Reference Paragraph**
Crack Length:	0.712	8.2.2
At Left Surface, inch	0.745	8.2.2
At Left of Center, inch	0.760	8.2.2
At Left of Crack Front, inch	0.762	8.2.2
At Right of Center, inch	0.750	8.2.2
At Right Surface, inch	0.756	8.2.2
Average Crack Length, inch		
Criteria of Validity	**Data**	**Reference Paragraph**
$K_{max} \leq 0.8\ K_{1c}$ (initial stage)	Valid	A2.4.1
$K_{max}/E \leq 0.002$ in.$^{1/2}$ (final stage)	Valid	A2.4.2
$K_{max}/E \leq 0.6\ K_Q$ (final stage)	Valid	A2.4.2
Fatigue Crack Plane Symmetry	Valid	8.2.4
Average Crack Length	Valid	7.2.1
Inner Crack Length Difference	Valid	8.2.2.[58]
Smaller Crack Front	Valid	8.2.2.[60]
Surface Crack Length	Valid	8.2.2.[60]
Surface Crack Length Difference	Valid	8.2.2.[60]
Loading Rate (Fracture Test)	Valid	8.3
$P_{max}/P_Q \leq 1.1$	Invalid	9.1.2
$B \geq 2.5\ (K_Q/\sigma_{ys})^2$	Valid	9.1.3
$a \geq 2.5\ (K_Q/\sigma_{ys})^2$	Valid	9.1.3
Calculation of K_Q and R_{sc}	**Data**	**Reference Paragraph**
K_Q, ksi, in.$^{1/2}$	14.45	A4.5.3
K_{1C}, ksi, in.$^{1/2}$	N/A	9.1.3
Strength Ratio, R_{SC}	1.09	A4.5.4

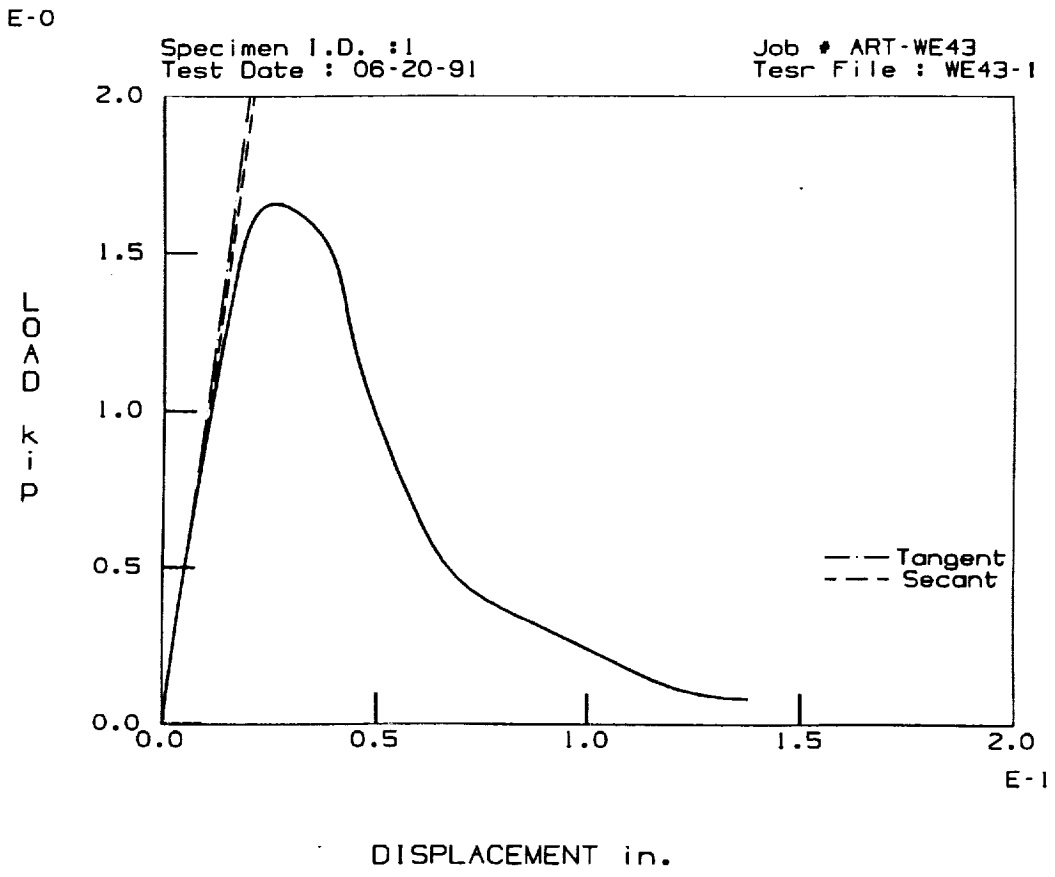

Figure 76. K_{1C} - Load Versus Displacement

VI.B.5 Tensile Tests - Housing Materials

VI.B.5.i Introduction

Two advanced magnesium-based alloys (WE43, ZE41A) and one promising aluminum alloy (C355T7) were tested at room temperature to provide comparative information on the strength and ductility of materials under uniaxial tensile stress. This information will be used in material selection for design of future helicopter transmissions. This tensile properties data was also used in performance of the fracture toughness (K_{1c}) tests.

VI.B.5.ii Test Article Description

The material certificates and chemical compositions are detailed in Tables 62 and 63. The specimen sizes and specimen configurations are shown in Figures 77 and 78. Only nine tests of C355T7 (specimens 16-24) used the button head specimens (Figure 78) due to material availability. All the specimens were finish machined after the final heat treatment. The diameters of the specimen gage section were measured to the nearest 0.001 inch. The dimensional measurement data are shown in Tables 64, 65, and 66.

TABLE 62. MATERIAL CERTIFICATES

Material	AMS Spec.	Producer	Product Form	Process
WE43	N/A	Magnesium Elektron	1" Thick Plate	Sand Cast
ZE41A	4439A	Magnesium Elektron	1" Thick Plate	Sand Cast
C355T7	4215	Teledyne Cast Products	0.75" f Bar	Sand Cast

TABLE 63. CHEMICAL COMPOSITION

	Element (%)							
Material	**Y**	**Zr**	**Nd**	**Yb**	**Zn**	**Dy**	**Mn**	**Cu**
WE43	5.42%	0.44%	2.55%	0.14%	0.094%	0.48%	0.0064%	0.0059%
ZE41A	-	0.58%	-	-	4.52%	-	0.0069%	0.0061%
C355T7	-	-	-	-	<0.10%	-	<0.10%	1.1%

	Element (%)						
Material	**Fe**	**Si**	**Ni**	**Mg**	**Ce**	**Al**	**Ti**
WE43	0.0053%	0.0070%	0.010%	REM	-	-	-
ZE41A	-	-	0.0017%	REM%	1.31%	-	-
C355T7	0.06%	5.3%	-	0.50%	-	REM	0.16%

The heat treatment process can often be the greatest single influence affecting the material strength and ductility. Each material must receive accurate control of the thermal processing cycles. Magnesium alloys, WE43 and ZE41A, were heat treated at Magnesium Elektron, Inc. Aluminum alloy C355T7 was produced and heat treated by Teledyne Cast Products. Table 67 outlines the specific heat treatments applied to each material and the associated hardness.

VI.B.5.iii Test Rig Description

The testing machine is a MTS 810 series material test system with three control modes:

Load Control: Up to ±20,000 lb
Stroke Control: ±3 inches displacement
Strain Control: Up to 15% strain

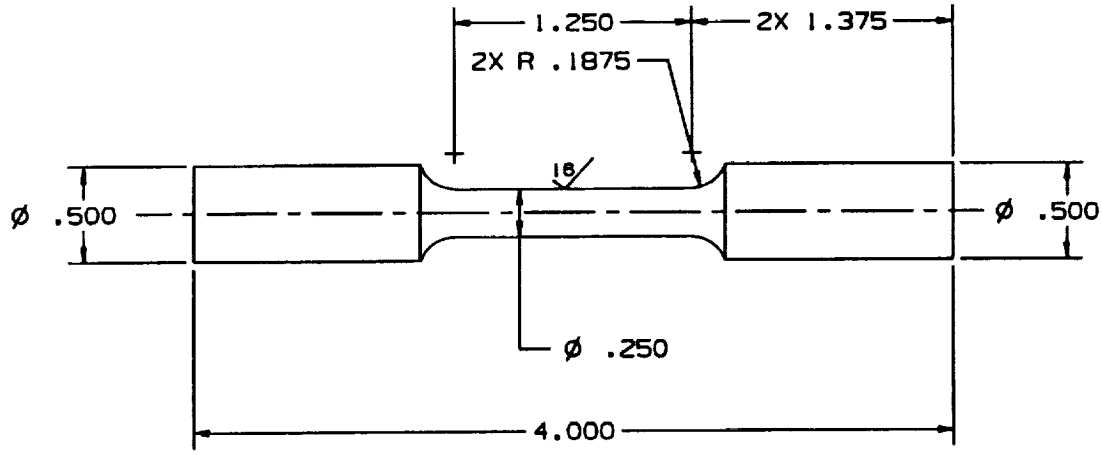

Figure 77. Tensile Specimen (Plain Cylindrical Ends)

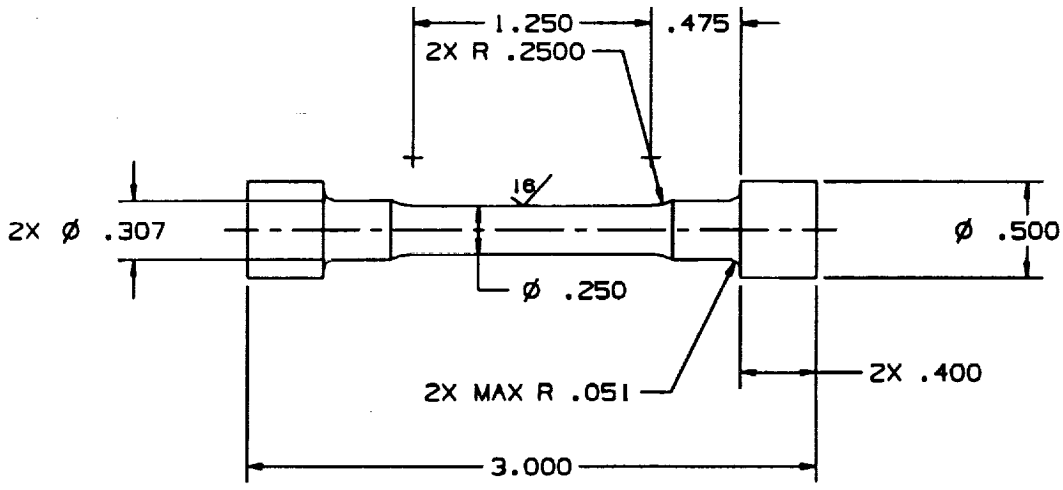

Figure 78. Tensile Specimen (Button Head Ends)

The test stand is located at LWI, Applied Technology Division, City of Industry, California. This machine was calibrated by a certified MTS service engineer on May 28, 1991. All the calibrations were within the range of ASTM standards.

To minimize bending strains, specimen fixtures were aligned such that the major axis of the specimen closely coincided with the load axis. The maximum bending strain determined was 1 percent of the average axial strain. Five percent is the maximum allowable bending strain per ASTM Standard E466 and E606.

VI.B.5.iv Test Procedure

All the tensile tests were performed in accordance with ASTM Standard B557 and reference standards of ASTM A370 and E8. The broken specimens were inspected and stored for further references. Load control testing at a nominal stress rate of 86 ksi/minute was used, based on the recommendation of ASTM B557, Procedure 7.2.7.2. A typical stress-time curve obtained during testing (WE43 magnesium alloy, Specimen #8) is shown in Figure 79. The actual load and strain data values that made up the stress-strain curves (see Results section) were stored through a PC-based data acquisition system. These data files were used for data reduction and archived for further studies of the material properties. Twenty-four tests of each material were used to calculate and determine the tensile properties.

VI.B.5.v Results

A typical stress-strain curve (WE43 magnesium alloy, Specimen #8) from the tensile tests is shown in Figure 80. The data summaries for all tests are shown in Tables 64, 65, and 66. There are slight deviations in calculated moduli of C355T7 due to the different specimen configuration (shown in Figures 77 and 78). To have comparative information, only 15 test data (Specimen Nos. 1-15) of C355T7 cylindrical end specimens (Figure 77) were used for statistical analysis. The mean values of yield strength, tensile strength, elongation, and modulus were determined and listed in Tables 68, 69, and 70. The yield strength was determined by the "offset method" at an offset of 0.2 percent from the stress-strain diagrams. The modulus of elasticity was calculated from the proportional section of the stress-strain curves.

The yield strength, tensile strength, elongation, and the usable high temperatures of these three gear case materials are compared in Table 71, along with published reference data.

VI.B.5.vi Discussion of Results

WE43, ZE41A, and C355T7 are candidate housing materials for the design of future gearboxes operating at elevated temperatures. As derived from these tests, WE43 is the most ductile material. Also, the tensile strength of WE43 is similar to C355T7, but the yield strength of WE43 is only about 76 percent that of C355T7.

As shown in Table 71, WE43 has the highest service temperature (up to 572°F). Magnesium alloy also is approximately two-thirds the weight of aluminum alloy. These are critical factors in the design of advanced helicopter transmissions.

The tensile tests from this program were conducted at room temperature. For future testing, it is recommended that elevated temperature tensile tests be performed to determine mechanical properties at anticipated operating temperatures of around 325 to 400°F. The creep properties of these three materials at elevated temperatures should also be determined by future tests.

TABLE 64. TEST DATA OF WE43

Specimen No.	Diameter (in.)	Area ($in.^2$)	Yield Strength 0.2% Offset (ksi)	Tensile Strength (ksi)	Elongation* %	Modulus of Elasticity (ksi)
1	0.251	0.0495	25.7	38.8	9.6	6483
2	0.250	0.0491	25.5	39.1	8.3	6438
3	0.251	0.0495	28.5	42.2	9.6	6491
4	0.250	0.0491	28.1	41.6	7.9	6515
5	0.251	0.0495	25.9	38.7	7.1	6516
6	0.250	0.0491	25.2	36.9	5.3	6511
7	0.250	0.0491	26.0	39.3	7.9	6439
8	0.249	0.0487	26.4	39.9	8.3	6470
9	0.250	0.0491	29.6	43.0	9.8	6554
10	0.249	0.0487	26.0	39.2	8.2	6507
11	0.250	0.0491	25.4	39.7	10.1	6545
12	0.249	0.0487	27.9	41.3	6.8	6549
13	0.250	0.0491	27.9	40.9	7.1	6446
14	0.250	0.0491	25.9	39.2	7.9	6441
15	0.250	0.0491	28.0	38.6	3.6	6563
16	0.250	0.0491	25.9	39.7	8.9	6474
17	0.250	0.0491	28.4	40.8	6.4	6510
18	0.249	0.0487	25.4	39.6	9.5	6494
19	0.249	0.0487	26.0	39.2	8.3	6459
20	0.250	0.0491	25.9	38.8	8.7	6421
21	0.249	0.0487	25.5	40.1	13.3	6314
22	0.250	0.0491	29.3	43.1	8.8	6537
23	0.249	0.0487	25.8	38.7	7.9	6458
24	0.250	0.0491	25.8	38.2	7.6	6326

*Original gage length = 1 inch

TABLE 65. TEST DATA OF ZE41A

Specimen No.	Diameter (in.)	Area ($in.^2$)	Yield Strength 0.2% Offset (ksi)	Tensile Strength (ksi)	Elongation* %	Modulus of Elasticity (ksi)
1	0.250	0.0491	21.4	32.1	4.6	6462
2	0.252	0.0499	21.3	31.4	3.7	6576
3	0.250	0.0491	21.1	32.5	5.1	6497
4	0.253	0.0503	21.4	32.1	4.6	6438
5	0.251	0.0495	20.9	32.5	5.0	6538
6	0.250	0.0491	21.2	32.2	4.6	6469
7	0.250	0.0491	21.3	32.4	4.9	6430
8	0.252	0.0499	20.9	31.5	4.1	6473
9	0.249	0.0487	20.3	31.5	4.4	6453
10	0.250	0.0491	21.4	31.9	4.2	6701
11	0.251	0.0495	20.5	32.1	5.0	6436
12	0.250	0.0491	20.5	31.6	4.6	6374
13	0.250	0.0491	20.7	32.2	5.0	6359
14	0.250	0.0491	21.3	32.2	4.6	6317
15	0.250	0.0491	21.2	31.9	4.2	6471
16	0.251	0.0495	21.0	31.6	4.2	6415
17	0.249	0.0487	20.5	32.2	4.7	6567
18	0.251	0.0495	20.8	31.8	4.5	6567
19	0.250	0.0491	20.9	32.4	4.9	6461
20	0.250	0.0491	21.4	32.3	4.8	6392
21	0.250	0.0491	20.8	32.0	4.8	6502
22	0.250	0.0491	20.9	31.7	4.5	6378
23	0.250	0.0491	21.6	32.5	5.0	6399
24	0.250	0.0491	21.3	31.9	4.4	6404

*Original gage length = 1 inch

TABLE 66. TEST DATA OF C355T7

Specimen No.	Diameter (in.)	Area ($in.^2$)	Yield Strength 0.2% Offset (ksi)	Tensile Strength (ksi)	Elongation* %	Modulus of Elasticity (ksi)
1	0.250	0.0491	33.8	39.6	2.1	10589
2	0.252	0.0499	35.7	42.5	3.1	10776
3	0.250	0.0491	35.4	40.7	2.0	10619
4	0.251	0.0495	35.4	42.4	3.5	10427
5	0.251	0.0495	36.2	43.4	3.3	10604
6	0.250	0.0491	35.6	42.0	2.5	10888
7	0.250	0.0491	35.3	41.7	2.5	10498
8	0.251	0.0495	35.3	41.7	2.7	10765
9	0.251	0.0495	35.2	42.4	3.2	10479
10	0.251	0.0495	34.0	41.3	3.0	10854
11	0.250	0.0491	35.3	42.0	2.9	10577
12	0.250	0.0491	35.6	39.8	2.0	10495
13	0.249	0.0487	33.0	39.4	2.3	10581
14	0.251	0.0495	35.3	40.3	2.0	10660
15	0.250	0.0491	35.3	40.3	2.0	10762
16	0.252	0.0499	36.3	44.0	4.5	11246
17	0.252	0.0499	36.7	43.6	3.6	11651
18	0.252	0.0499	34.2	41.0	2.9	11610
19	0.252	0.0499	36.0	40.2	2.0	12048
20	0.252	0.0499	37.1	45.2	5.0	12667
21	0.253	0.0503	34.4	40.5	2.3	12295
22	0.253	0.0503	34.7	41.1	2.5	12203
23	0.253	0.0503	36.2	42.9	3.0	11986
24	0.253	0.0503	34.6	43.0	5.9	11781

*Original gage length = 1 inch

TABLE 67. HEAT TREATMENTS AND HARDNESS

Material	Solution Heat Treatment	Aging Treatment	Hardness
Magnesium Alloy ZE41A (Condition T5)	2 hrs at 626°F, cool in air	16 hrs at 356°F	BHN 60
Magnesium Alloy WE43 (Condition T6)	8 hrs at 977°F, hot water quench at 140°F - 176°F	16 hrs at 482°F	BHN 71
Aluminum Alloy C355T7 (Condition T7)	12 hrs at 980°F, water quench at 70°F	8 hrs at 440°F	BHN 81

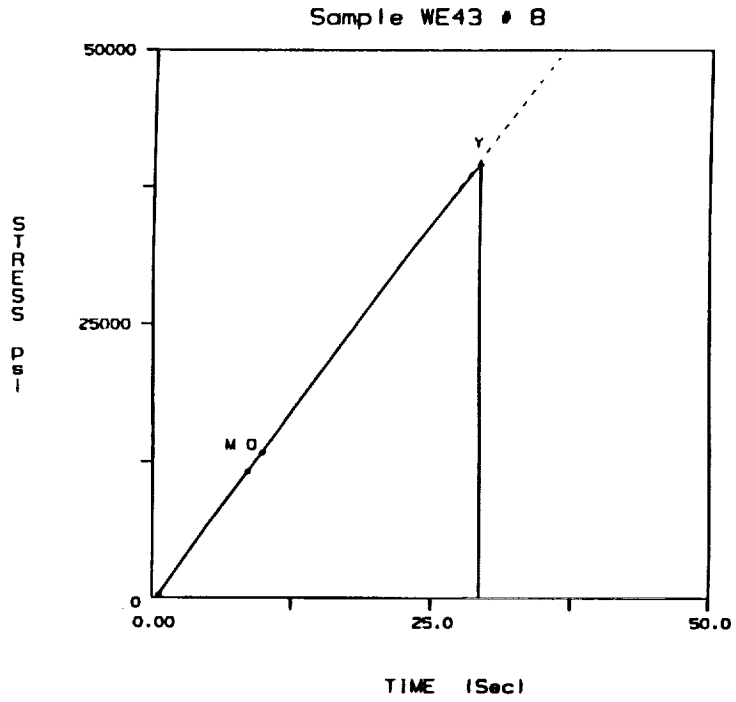

Figure 79. WE43 Stress-Time Curve

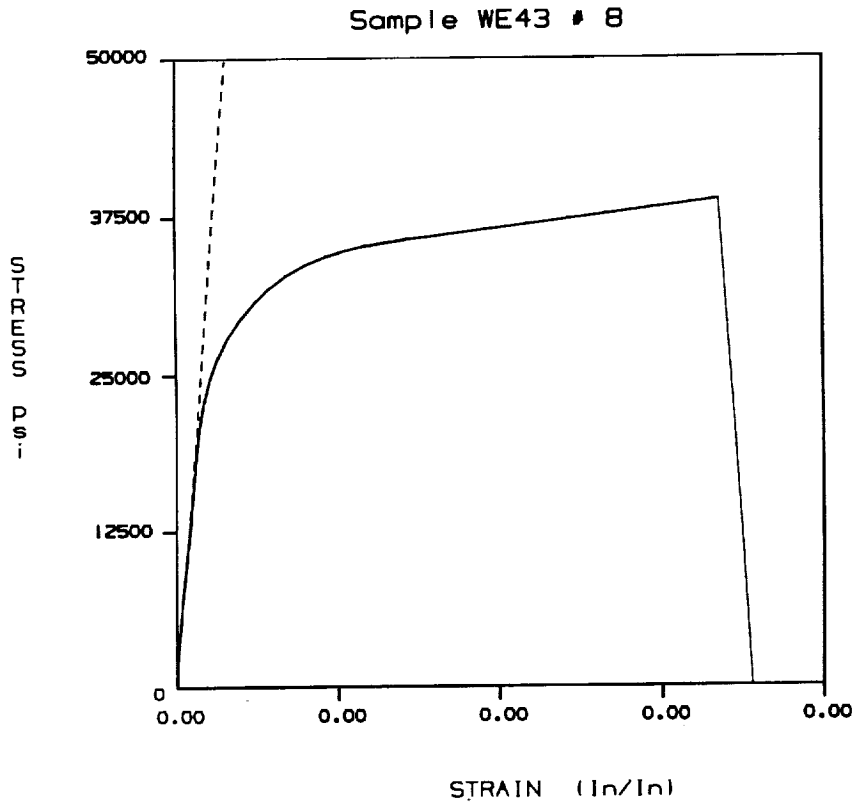

Figure 80. WE43 Stress-Strain Curve

TABLE 68. TENSILE PROPERTIES (MATERIAL: WE43)

	Mean	Standard Deviation
Diameter, in.	0.250	0.001
Area sq, in.	0.0490	0.0003
Peak Load, lb	1954	76
Yield Strength, 0.2% offset, ksi	26.7	1.4
Tensile Strength, ksi	39.9	1.5
Elongation, %*	8.2	1.8
Modulus of Elasticity, ksi	6478	63
*Original gage length = 1 inch		

TABLE 69. TENSILE PROPERTIES (MATERIAL: ZE41A)

	Mean	Standard Deviation
Diameter, in.	0.250	0.001
Area sq, in.	0.0492	0.0004
Peak Load, lb	1576	18
Yield Strength, 0.2% offset, ksi	21.0	0.4
Tensile Strength, ksi	32	0.3
Elongation, %*	4.6	0.3
Modulus of Elasticity, ksi	6462	84
*Original gage length = 1 inch		

TABLE 70. TENSILE PROPERTIES (MATERIAL: C355T7)

	Mean	Standard Deviation
Diameter, in.	0.250	0.001
Area sq, in.	0.0493	0.0003
Peak Load, lb	2034	68
Yield Strength, 0.2% offset, ksi	35.1	0.8
Tensile Strength, ksi	41.3	1.2
Elongation, %*	2.5	0.6
Modulus of Elasticity, ksi	10640	142
*Original gage length = 1 inch		

TABLE 71. TENSILE TEST RESULTS SUMMARY

Material	Yield Strength 0.2% Offset, ksi	Tensile Strength ksi	Elongation %	Usable High Temperature*
WE 43	26.7 (26.8 average)	39.9 (38.4 average)	8.2 (7.0 average)	572°F
ZE41A	21.0 (22.6 average)	32.0 (29.0 average)	4.6 (3.0 average)	320°F
C355T7	35.1 (35.0 min.)	41.3 (38.0 min.)	2.5 (2.0 min.)	400°F

( ) Published reference data are shown in parenthesis.

*Usable high temperatures and reference data of WE43 and ZE41A were suggested by Magneslum Elektron, Inc., and 400°F service temperature and reference data of C355T7 was from Lucas Western Specification MPS 49500B415.

VI.B.6 Face Gear Capacity Tests

VI.B.6.i Introduction

Experimental tests on face gears were performed in the NASA Lewis spiral bevel gear rig (Handschuh, et al., 1992) [63]. The face gears tested, shown in Figure 81, were basically a half-size version of the MDHC/Lucas ART design. The gears were 16 pitch with 28 teeth on the pinion and 107 teeth on the face gear. The shaft angle was 90 degrees to accommodate the rig.

VI.B.6.ii Test Article Description

A limited amount of test gears were available for test (four pinions and four face gears). The gears were made of Maraging 300 steel per AMS 6514. The pinions were nitrided and ground with a case hardness of Rc 58. The face gears were shaper cut and hardened to Rc 52. A method for grinding face gears has not been developed yet, although this is the subject of an additional MDHC/LWI IR&D program currently underway.

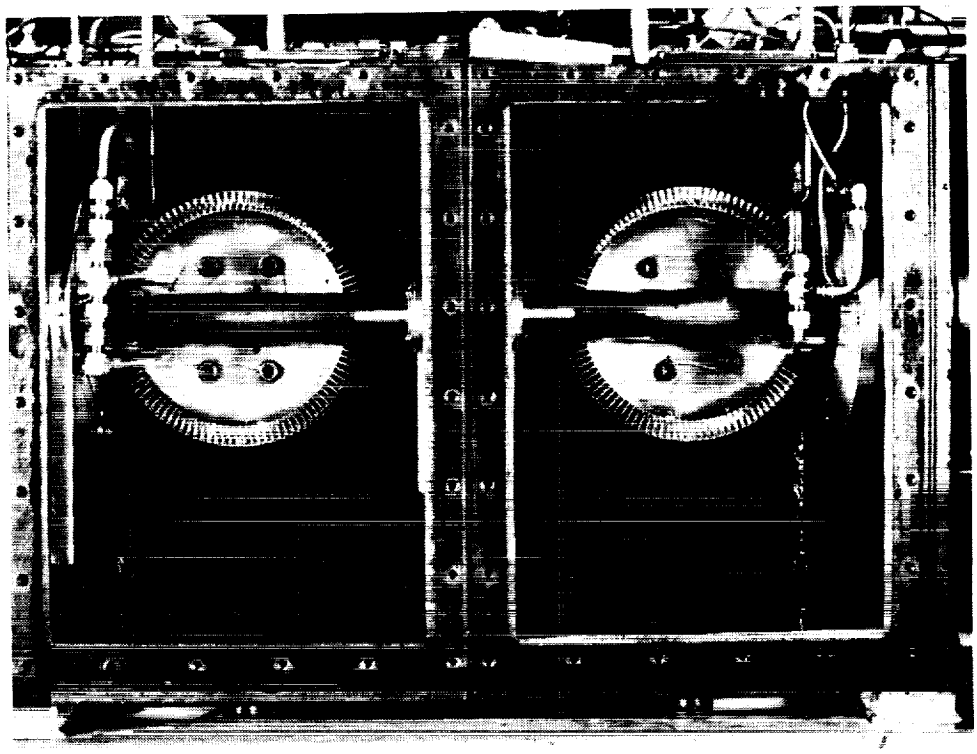

Figure 81. Gears Installed in Test Stand

VI.B.6.iii Test Rig Description

The NASA-Lewis spiral bevel gear rig, shown in Figure 82, operates on a closed loop or torque-regenerative principle. Two sets of pinion/face gears are used in the loop with the two pinions connected by a cross shaft. The outputs of the two face gears are connected through a helical gear mesh. A hydraulic loading system is connected to the helical mesh which puts a thrust load on the mesh, and thus, the torque in the loop. A variable speed motor is connected by a belt to the loop and powers the test stand.

VI.B.6.iv Test Procedure

The objective of the tests was to demonstrate the feasibility of face gears and determine the failure modes for high power applications. For the tests, 100-percent design speed and torque were defined as 19,000 rpm pinion speed and 68 N-m (600 in.-lb) pinion torque for a power of 135 kW (180 HP). The gears were run at 74°C (165°F) oil inlet temperature using an ample supply of DOD-L-85734 lubricant at about 0.8 gpm per mesh.

VI.B.6.v Results

Four sets of gears successfully completed 26-hour ($30x10^6$ pinion cycles) endurance runs at 100 percent speed and torque. The contact pattern on the teeth was good and developed on the full tooth of the face gear. The pinion teeth showed normal wear. The face gear teeth, however, had some surface distress. The teeth from the test side (pinion driving the face gear) had moderate wear and were in good condition. The teeth from the slave side (face gear driving the pinion) had small pit lines in some instances in the middle region of the teeth.

The gears were subsequently run 26 hours at 200-percent torque and 100-percent speed. One test (two sets of gears) lasted the 26 hours with the pinions showing moderate wear and the face gears showing increasing surface distress. The second test (the additional two sets of gears) was suspended after about 10.5 hours due

to a tooth breakage on one of the face gears (slave side). The breakage originated from the surface pit line from the previous test.

VI.B.6.vi Discussion of Results

The results, although limited, demonstrated the feasibility of face gears in high-speed, high-load applications. The tests did show surface distress with the face gears, however. The use of a hardened, ground gear steel (in use for conventional aircraft gears today but not presently available for face gears since manufacturing techniques do not exist to grind face gears) would significantly increase the surface durability and make face gears available for high-power application.

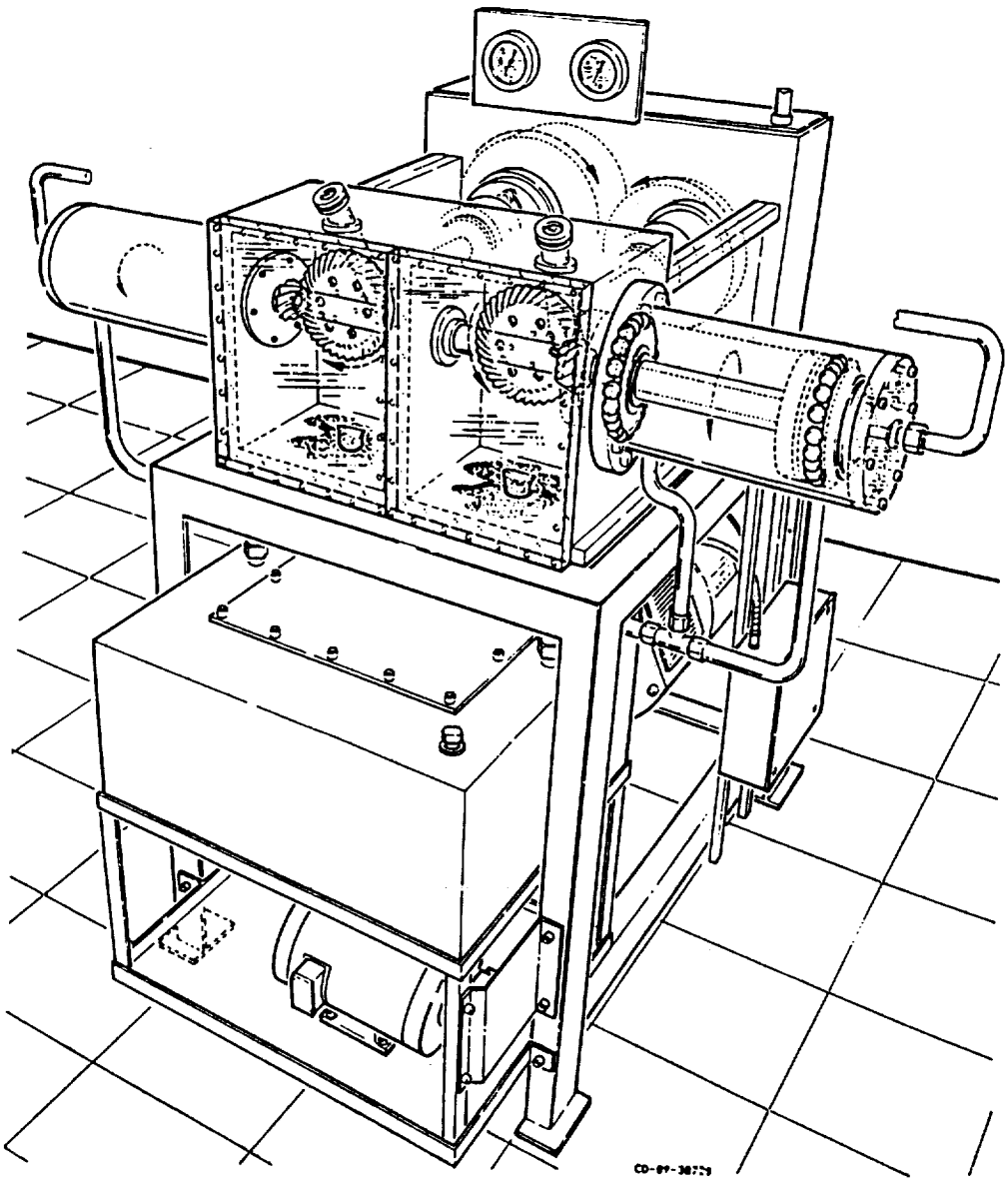

Figure 82. NASA Spiral Bevel Gear Rig

VII. SUMMARY OF RESULTS - CONCLUDING REMARKS

The McDonnell Douglas Helicopter Company (MDHC) and teammate Lucas Western, Inc. (LWI) have completed the design of a 5000-horsepower Advanced Rotorcraft Transmission (ART) within Phase I of the Army/Nasa ART Program. The innovative split torque configuration using face gears has met or exceeded the Army/NASA weight, noise and reliability goals set for the program. In working to achieve the goals, transmission design and analysis processes were performed interactively to attain the desired design characteristics.

The weight goal for the ART Program was to attain a 25 percent weight reduction for the 5000 HP transmission relative to a state-of-the-art (SOA) baseline design. A 5000 HP upscaled Apache main transmission served as the SOA baseline transmission for goal progress comparisons. The MDHC/LWI ART design, weighing 815 lb, reached a 40 percent weight reduction relative to the 1347 lb SOA baseline transmission weight. This was 195 lb below the 1010 lb goal, and was achieved through use of the novel split torque configuration, an optimized combination of gear ratios, and weight-conscious design of individual components. The use of face gears in the ART first stage was found to be a significant weight and space savings development. Face gear geometry allows torque splitting from a single input pinion, with second stage torque recombination then occurring directly, as all second stage pinions rotate in the same direction and in a single plane above. Implementation of the high contact ratio planetary provided additional weight reduction, as did the detail design of the ART transmission subsystems. The positive engagement overrunning clutch yielded a weight-competitive design having enhanced reliability characteristics and reduced cooling requirements. The advanced lubrication system decreased the transmission installation weight. A lightweight secondary lubrication system employing low flow rate oil misters provides oil for more than one hour of emergency operation.

The ART program reliability goal was 5000 hours Mean-Time-Between-Removal (MTBR). The split torque ART transmission was analyzed during the design process to achieve this goal. Reliability requirements were apportioned to the transmission component level. This was done both for dynamic components and for those which could contribute to miscellaneous failures. Loading and cycling of individual dynamic components were evaluated to attain at least the 14,100-hour component lives required to yield the 5000-hour system life. In addition, other components which affect removal intervals such as seals and housing sections were designed to operate for the duration of their required lives. The MTBR obtained for the ART transmission as a result of the design and analysis processes is 6269 hours, exceeding the 5000-hour goal.

The ART program noise goal was to reduce source noise by 10 dB relative to a 5000 HP SOA baseline transmission. The noise level identified as meeting this goal by the MDHC/LWI team was 97.9 dB. This is 10 dB below the 107.9 dB noise level obtained from the upscaled 5000 HP Apache baseline transmission. The 107.9 dB noise level was based on extrapolated Apache transmission test data. The predicted source noise level for the ART is 98.3 dB, which is 9.6 dB below the 107.9 dB SOA noise level, essentially meeting the goal. In working to achieve the 10 dB reduction, gear web, rim and shaft deflections were analyzed during the design process to minimize noise. The transmission housing structural shape, ribs and stiffeners were designed to minimize vibratory deflections. Also, the high contact ratio (HCR) dropped-tooth planetary was implemented mainly to facilitate noise reduction. The planetary design, in addition to having HCR tooth modifications, incorporates tooth phasing methods and a cantilevered ring gear in minimizing noise. Use of nonstandard tooth proportions in the second stage gear designs also contributed to noise reduction.

Significant aircraft mission performance improvements and cost savings are realized from use of the ART transmission. The improvement in loss-exchange ratio during combat is 17 to 22 percent. A 12 percent improvement is seen in the ability to sustain a given level of combat operations. The Mean-Time-Between-

Failure (MTBF) increase represents a 22 percent improvement. Use of the ART would also result in a transmission acquisition cost savings of 23 percent or $165K, per unit. An average transmission direct operating cost savings of 33 percent, or $24 per flight hour, would also be realized.

The ART three-stage split torque design with face gears offers several areas for future investigation which should yield substantial technology gains. Of primary interest is the first and second stage split torque section of the transmission. Proof-of-concept split torque tests were initiated by the MDHC/LWI team in late 1992. Using results of these tests as a guide, follow-on design, fabrication and testing will be proposed to refine the concept and maximize its potential. Also, the need to perform additional face gear capacity tests in conjunction with the above is apparent, and such tests with ground face gears are planned. Face gear grinding technology development is currently underway. Another effort will evaluate transmission configurations for uses in future higher horsepower versions of the Apache. A two-stage ART transmission design, having only the two split torque stages, will be compared with designs of the three stage ART and a configuration similar to the existing 2828 HP Apache transmission. The evaluations will compare the designs on the basis of the U.S. Army weight, noise and reliability goals, as well as mission effectiveness, flight performance and cost parameters.

Follow-up work should be performed on other portions of the ART Phase I design as well. The proposed rotorcraft application of a pawl and ratchet-based positive engagement clutch merits a detail design, fabrication and test program to compare this to existing rotorcraft clutch designs. The high contact ratio planetary, implemented as the third stage of the Phase I ART design, is worthy of fabrication, evaluation testing and comparison with standard planetary designs. Such planetary tests should be performed in conjunction with an acoustic modeling effort to investigate correlation of actual versus predicted noise levels.

The MDHC/LWI ART offers considerable improvements to SOA rotorcraft transmission design. Substantial progress was made in meeting or exceeding the U.S. Army/NASA weight, noise and reliability goals. The three stage split torque single planetary transmission can provide significantly increased capabilities for a fielded aircraft.

APPENDIX A

POSITIVE ENGAGEMENT CLUTCH ANALYSIS

The analysis section below covers curvic coupling stress analysis, helical spline stress analysis, resonant frequency analysis, pawl balance calculation, hydroplaning analysis, spring stress analysis, and engagement system analysis. Individual clutch components are illustrated in Figure 4 of the Transmission Configuration section.

CURVIC COUPLING STRESS ANALYSIS

Curvic coupling stress analysis is based on the Gleason system:

$$D = 3\sqrt{T/1,310}$$

where,

D is the coupling outside diameter
T is ultimate torque in in.-lb

Face length is 0.125 x outside diameter and material ultimate strength is 150,000 psi. The design uses a 2.0 inch outside diameter, 0.25 inch face length and 9310 steel with an ultimate strength of 250,000 psi. The ultimate allowable torque is:

$$2^3 \times 1,310 \times 250,000/150,000 = 17,467 \text{ psi}$$

Maximum continuous applied torque is:

$$63,025 \times 3,000 \text{ HP}/20,950 \text{ rpm} = 9,025 \text{ in.-lb}$$

Ultimate torque is:

$$1.5 \times 9,025 = 13,538 \text{ in.-lb}$$

Margin of Safety (M. S.) is:

$$17,467/13,538 - 1 = +0.3$$

HELICAL SPLINE STRESS ANALYSIS

The helical spline is 8/16 pitch, 17 teeth and 45-degree helix angle, one half of the teeth carry load.

Shear stress is:

$$8T/\pi D^2 F (\sin \psi) = 8 \times 9,025/\pi \times 2.125^2 \times 1 \times 0.707 = 7,200 \text{ psi}$$

M. S. = Large

Compressive stress is:

$2T/D\ N\ F\ (\sin \psi) = 2 \times 9{,}025/2.125 \times 17 \times 1 \times 0.707 = 706.7$ psi
M. S. = Large

RESONANT FREQUENCY ANALYSIS

This section contains the natural frequency analysis of the pawl about its center of rotation. The polar mass moment of inertia of the pawl was calculated by the integration of 16 element sections, see Figure 83 and Table 72. A helical tension spring was sized for 31 lb/in. The spring rate is easily modified by changing any or all of three variables: wire diameter, coil diameter, and number of coils. Thus, the optimum spring rate can be found readily by experiment.

Spring rate is:

$$K = G\ d^4/8D^3\ N$$

where,

G is Modulus of Rigidity = 11,500,000 psi

d is Wire diameter = 0.035 inch

D is Coil mean diameter = 0.325 inch

N is Number of coils = 2 coils/pawl

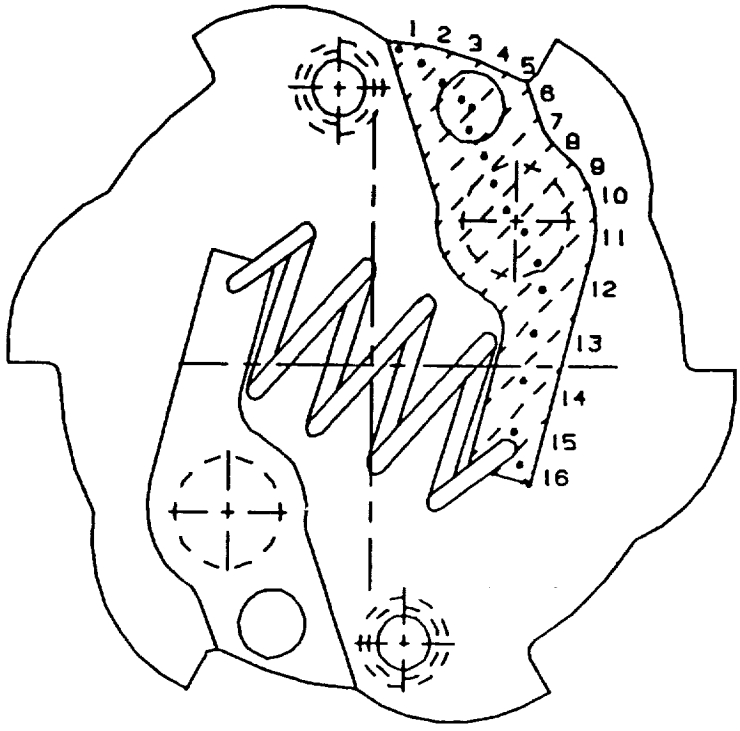

Figure 83. Section Integrated System Used to Calculate Polar Mass Moment of Inertia and Centrifugal Force Moment of Pawl

TABLE 72. PAWL POLAR MASS MOMENT OF INERTIA, J

Element No.	t Thickness (inch)	A Area ($inch^2$)	r Radius (inch)	tAr^2 ($inch^5$)
1	0.20	0.055 x 0.050	0.375	77.34×10^6
2	0.20	0.05 x 0.110	0.333	121.98
3	0.20	0.05 x 0.157	0.285	127.52
4	0.20	0.05 x 0.210	0.240	120.96
5	0.20	0.05 x 0.255	0.315	253.02
6	0.20	0.05 x 0.260	0.133	45.99
7	0.20	0.05 x 0.275	0.078	16.73
8	0.20	0.05 x 0.295	0.025	1.84
9	0.20	0.05 x 0.300	0.025	1.88
10	0.20	0.05 x 0.260	0.078	15.82
11	0.20	0.05 x 0.215	0.133	38.03
12	0.20	0.05 x 0.200	0.208	86.53
13	0.20	0.05 x 0.205	0.295	178.40
14	0.20	0.05 x 0.195	0.385	289.04
15	0.20	0.05 x 0.095	0.450	192.38
16	0.20	0.02 x 0.030	0.480	27.65
Hole	0.20	$\pi/4\ (0.11)^2$	0.213	-86.23
				1,508.9

$J = (0.0015089\ inch^5)\ (0.283\ lb/in^3)/386.05\ in/sec^2 = 1.105 \times 10^{-6}\ lb\text{-}in\text{-}sec^2$

Thus,

$$K = 11{,}500{,}000 \times (0.035)^4/8 \times (0.325)^3 \times 2 = 31\ lb/in$$

Resonant frequency is:

$$W = \sqrt{Ka^2/J}$$

where a is the distance from spring line of action to pawl pivot = 0.368 inch

$$W = [\ 31 \times (0.368)^2/1.105 \times 10^{-6}\ ]^{1/2}$$

$$W = 1{,}948\ radians/second$$

$$f = 1{,}948/2\pi = 310\ Hertz$$

PAWL BALANCE CALCULATIONS

The pawl moment due to centrifugal forces has been calculated by integrating section elements of pawl mass. The sectioning is as shown on Figure 83. The clockwise and counter clockwise section moments are given in Table 73 where l is the distance from the clutch rotational axis to the center of gravity of each sectional element and r is the distance from the pawl rotational axis to the center of gravity of each sectional element.

TABLE 73. PAWL CLOCKWISE AND COUNTERCLOCKWISE SECTION MOMENTS

Element No.	t Thickness (inch)	l Length (inch)	A Area ($inch^2$)	r Radius (inch)	tlAr ($inch^5$)
Clockwise					
1	0.20	0.583	0.055 x 0.050	0.375	120.24×10^{-6}
2	0.20	0.555	0.05 x 0.110	0.333	203.30
3	0.20	0.530	0.05 x 0.157	0.285	237.15
4	0.20	0.503	0.05 x 0.210	0.240	253.51
5	0.20	0.473	0.05 x 0.255	0.315	379.94
6	0.20	0.428	0.05 x 0.260	0.133	148.00
7	0.20	0.398	0.05 x 0.275	0.078	85.37
8	0.20	0.385	0.05 x 0.295	0.025	28.39
					1,455.90
Hole	0.20	0.500	$\pi/4\ (0.11)^2$	0.215	-204.32
Counterclockwise					
9	0.20	0.385	0.05 x 0.300	0.025	28.87
10	0.20	0.380	0.05 x 0.267	0.078	79.14
11	0.20	0.373	0.05 x 0.215	0.133	106.66
12	0.20	0.333	0.05 x 0.200	0.208	138.53
13	0.20	0.295	0.05 x 0.205	0.295	178.40
14	0.20	0.294	0.05 x 0.195	0.385	220.72
15	0.20	0.330	0.05 x 0.095	0.450	141.08
16	0.20	0.358	0.05 x 0.030	0.480	20.62
					914.02

$Q = \Sigma\ (t\ l\ A\ r)\ e/g\ (2\pi/60)^2\ (RPM)^2$

$= (1455.90 - 204.32 - 914.02)\ (.283/386.04)\ (2\pi/60)^2\ (20950)^2\ (10)^{-6}$

= 1.191 in-lb clockwise (nose down)

The nose down force of the pawl on the ratchet cylindrical surface is then the clockwise moment about the pawl center of rotation divided by the radius of action. The radius of action is found by constructing a line from the center of the pawl bearing face to the clutch rotational axis. The distance from this line to the pawl center of rotation is the radius of action. The nose down force is 0.907 in-lb/0.2 inch = 4.5 lb. Note that pawls are simple structures easily made to different design if test results indicate change would be advantageous.

HYDROPLANING ANALYSIS

The force of the pawl bearing face on the ratchet cylindrical surface is the sum of the spring generated force and the CF generated force.

Spring force is:

31 lb/inch x 0.21 inch extension x 0.368 inch/0.2 inch = 12.0 lb

CF force is:

1.191 in.-lb/0.2 inch = 5.95 lb

The area supporting the force is:

$0.2 \times 0.25 = 0.05$ inch^2

Hydroplaning load at 20,950 rpm is:

17.95/0.05 = 359 psi

Conventional hydrodynamic design is:

2,000 psi (approximate)

SPRING STRESS ANALYSIS

Analyses are shown for the conditions of ratcheting, hydroplaning, and going through resonance. Spring stress is:

$$S = 8 K P D/\pi d^3$$

where,

K is Stress concentration factor = 1 + 0.5/C

P is Force due to extension

D is Mean coil diameter = 0.325 inch

d is Wire diameter = 0.035 inch

C is D/d or 0.325/0.035 = 9.29

K = 1 + 0.5/C = 1 + 0.5/9.29 = 1.05

During:

Ratcheting: $P = 0.08 \text{ inch} \times 31 \text{ lb/inch} = 2.48 \text{ lb}$

Hydroplaning: $P = 0.21 \text{ inch} \times 31 \text{ lb/inch} = 6.51 \text{ lb}$

Resonance: $P = 0.24 \text{ inch} \times 31 \text{ lb/inch} = 7.44 \text{ lb}$

Ratcheting: $S = 8 \times 1.05 \times 2.48 \times 0.325/\pi \times 0.035^3 = 50{,}264 \text{ psi}$

Hydroplaning: $S = 8 \times 1.05 \times 6.51 \times 0.325/\pi \times 0.035^3 = 131{,}944 \text{ psi}$

Resonance: $S = 8 \times 1.05 \times 7.44 \times 0.325/\pi \times 0.035^3 = 150{,}793 \text{ psi}$

$S_{ult} = 250{,}000 \text{ psi}$

M. S. $= 250{,}000/150{,}793 \times 1.5 - 1 = 0.10$

ENGAGEMENT SYSTEM ANALYSIS

Pawl System

The pawl system of the positive engagement clutch provides the means for sensing the proper instant to initiate engagement and for operating the synchronizer to complete the engagement. It is essential that the engagement operation commence as soon as input speed has overtaken output speed and the face spline teeth are in alignment.

In the subject clutch, positive pawl system operation is assured by avoidance of pawl resonance during the time interval immediately preceding engagement.

The second design element required to assure reliable pawl system operation involves minimizing wear and fatigue of the pawl-ratchet system in long-term overrunning. By promoting pawl hydroplaning at all continuous overrunning conditions, metal-to-metal wear between pawls and ratchet teeth can be avoided and return spring cyclic motion minimized.

Figure 84 is a plot of pawl action versus differential input to output speed. By assuming uniform acceleration of the input from zero to full speed in 5 seconds, a scale of time to go to synchronous speed can be added to the abscissa; and by knowing the number of teeth in the ratchet, ratchet tooth exciting frequency can be added to the ordinate.

As the plot indicates, pawl system behavior passes through three distinct phases as differential speed changes:

1. Pawl hydroplaning, wherein differential speed between the pawls and the oil annulus carried in the ratchet is sufficient to support the pawl hydrodynamically.

2. Resonant behavior, where the speed differential will no longer support hydroplaning, so that the pawls become propelled by the ratchet teeth. When the ratchet pulses occur at the frequency which the pawls are unable to follow, then the pawls will tend to bounce at their natural frequency. A pin stop is provided to limit resonant excursions.

3. Coherent pawl and ratchet interaction occurs when the ratchet passage frequency becomes less than the pawl natural frequency and each pawl falls into each ratchet pocket as it comes by.

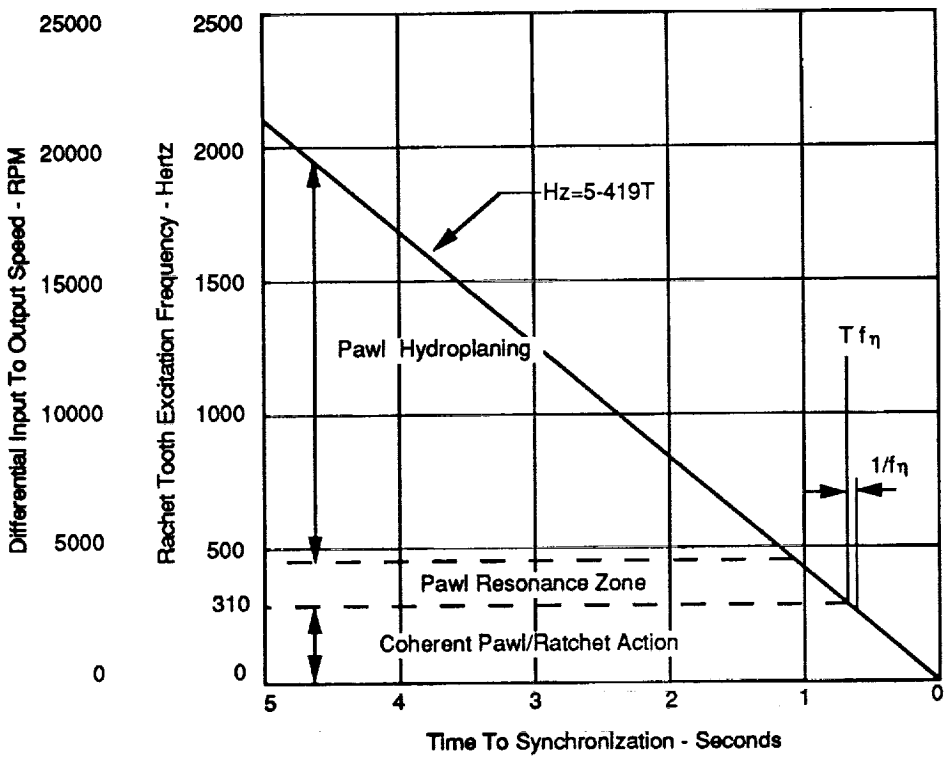

Figure 84. Pawl Behavior vs. Differential Input to Output Speed

The main thrust of pawl system design is to exercise control over the extent of these zones to promote reliable operation and long life.

The highest predicted natural frequency is 310 hertz while the shaft operating speed is 350 hertz. This proximity is not a cause for concern based on the following considerations:

Clutch Engaged

The pawl in the ratchet notch is submerged in the oil annulus formed by dams at either end of the ratchet. The oil annulus will resist displacement. There is friction at the pawl pivot which resists motion. The distance from the pawl tip to the ratchet face is the distance generated by the slope of the curvic coupling teeth in backing the pawl out of contact with the ratchet face. Any oscillation of the pawl would require alternately squeezing an oil film out from the radial face or the tangential face of the ratchet while the pawl moves a very small distance.

Clutch Overrunning

The design intent is that the pawls hydroplane on the cylindrical faces of the ratchet while overrunning. The margin shown is believed satisfactory. If resonant behavior is observed, it is a very simple matter to change the spring or the mass of the pawls.

Determination Of Ability Of Pawl To Engage Ratchet In The Available Time

In the ART drive system, it is possible for the speed differential between input and output to change rapidly as an engine accelerates up to engagement speed. It is assumed that this acceleration rate can be as high as 0 to 20,950 rpm in 5 seconds.

The plot given in Figure 81 shows that the input to output speed differential diminishes as the instant of synchronization (T_o) approaches. The rate of change of differential speed is:

20,950 rpm/5 seconds = 4,190 rpm/sec

Converting to rev/sec^2 results in:

4,190/60 = 69.8 rev/sec^2

Since there are 6 teeth in the ratchet, the rate of change of ratchet tooth exciting frequency is:

6 x 69.8 Hz thus,

f_t = 419 impacts/sec^2 (1)

where,

f_t = Ratchet tooth exciting frequency

Working back from the instant of synchronization (T_o), we can say that the last resonant pawl cycle must be completed at T_o or sooner. It can also be seen that the last opportunity for the start of that resonant cycle occurs when the ratchet tooth exciting frequency, f_t, just equals the pawl natural frequency, f_n.

The period of time for one resonant cycle is:

$1/f_n$

From (1), the time preceding T_o for f_t to equal f_n is:

$f_n/419$

As a minimum, let:

$1/f_n = f_n/419$

Therefore,

$f_n = \sqrt{419} = 20.47$ Hz

For a rotationally vibrating system,

$$f_n = 1/2\pi \sqrt{K_s/J}$$

where,

K_s = Spring rate of pawl return spring, lb-in./rad

J = Pawl polar mass moment of inertia = 1.105×10^{-6} lb-in. sec^2

Thus,

$$20.47 = 1/2\pi \sqrt{K_s/1.105 \times 10^{-6}}$$

and,

K_s = 0.0183 lb-in./radian

Note that this a minimum; any spring rate exceeding this value is satisfactory.

Spring force is:

31 lb/in x 0.21 extension = 6.51 lb

Spring Torque is :

6.51 lb x 0.368 inch from spring centerline to pawl pivot = 2.40 in-lb

Applied Angle is:

20° rotation to engage ratchet = 0.349 radians

Actual K_s is:

2.40 x 0.349 = 0.84 lb-in./radian
M. S. = Large

APPENDIX B1

LIFE AND RELIABILITY FOR SYSTEMS USING WEIBULL DISTRIBUTIONS

An equation relating system reliability to component reliabilities where the life of the system is dependent on all components surviving and the lives of the components are modeled as Weibull distributions.

Express life and reliability in terms of the 90 percent reliability life and the Weibull shape factor.

The two parameter Weibull function is widely used to model fatigue life:

$$R = e^{-\left(\frac{L}{N}\right)^{b}}$$

Lives of components are usually not expressed at the characteristic life (where 63.2 percent have failed), but at a 1 or 10 percent failed life. To relate the Weibull distribution to the L_{10} life: Take the log of the reciprocal of (1):

$$\ln\left(\frac{1}{R}\right) = \left(\frac{L}{N}\right)^{b}$$

and solve for N:

$$N = \frac{L}{\left(\ln\left(\frac{1}{R}\right)\right)^{\left(\frac{1}{b}\right)}}$$

From this we can equate characteristic lives for 90 percent reliability and general reliability.

$$N = \frac{L_{10}}{\left(\ln\left(\frac{1}{0.9}\right)\right)^{\left(\frac{1}{b}\right)}} = \frac{L}{\left(\ln\left(\frac{1}{R}\right)\right)^{\left(\frac{1}{b}\right)}}$$

Now solve for

$$\ln\left(\frac{1}{R}\right)$$

$$\ln\left(\frac{1}{R}\right) = \ln\left(\frac{1}{0.9}\right) \bullet \ln\left(\frac{L}{L_{10}}\right)^{b}$$

This equation relates life and reliability given the 90 percent reliability life and the Weibull shape factor.

Relate the system life to the component L_{10} lives.

For system life where the all components must be functioning:

$$R_S = \prod_{i=1}^{n} (R_i)$$

Take the log of the reciprocal:

$$\ln\left(\frac{1}{R_S}\right) = \sum_{t=1}^{n} \ln\left(\frac{1}{R_i}\right)$$

Substitute equation (1) into each component:

$$\ln\left(\frac{1}{R_S}\right) = \ln\left(\frac{1}{0.9}\right) \bullet \sum_{i=1}^{n} \left(\frac{L}{L_{10\,i}}\right)^{b_i}$$

This equation relates system life, system reliability, and component L_{10} life. When solving for system life (L) or a uniform component L_{10} life (L_{10}) it must be solved iteratively.

APPENDIX B2

FAILURE MODES EFFECTS AND CRITICALITY ANALYSIS (FMECA)

This section is provided as the basis of a full-scale FMECA for the production phase of the ART.

A FMECA consists of 2 parts:

1. Failure mode and effects analysis (FMEA)
2. Criticality Analysis

This section will present FMECA data in Table 74.

FMECA includes the preceding reliability analysis as a prelude to filling out the tables. The FMECA spec (MIL-STD-1629A) calls out activities (a-h) which support the design process including:

1. System definition. Completed by design with input from specialists.
2. Block diagrams. These diagrams, shown in Figure 85 are presented in a hierarchy, reflecting how reliability was apportioned and analyzed.
3. Interface failure modes. The integration of the system is an important part of the ART task. MDHC has considered all potential interfaces to the extent possible i.e. there is no FAAV design available for reference. When the pre-production version of the ship drawings become available, this effort can be completed.
4. Severity classification. Used to provide a qualitative measure of the worst potential consequences resulting from design error or item failure.
    a. Category I - Catastrophic. A failure which may cause death or loss of ship.
    b. Category II - Critical. A failure which may cause severe injury, major property damage, or major system damage resulting in mission abort.
    c. Category III - Marginal. A failure which may cause minor injury, minor property damage, or minor system damage which results in delay of loss of availability or mission degradation.
    d. Category IV - Minor. A failure not serious enough to cause injury, property damage, or system damage, but will result in unscheduled maintenance action.
    e. Failure detection methods are identified in the table.
    f. Corrective actions

TABLE 74. FAILURE MODES, EFFECTS AND CRITICALITY ANALYSIS

Part ID and Function	Failure Modes	Method of Detection	Failure Effect Subsystem	Failure Effect Air Vehicle	Maximum Severity, Compensating provisions	Probability/ Data Source (1)
ART assembly - Transmit torque to main rotor	Torque is not transmitted	Visual, flight characteristics, instrumentation	Inoperative	Safety of Flight	I, Autorotation forced landing	< 4/10,000 during 30 minute OEI condition / AGMA standards
	Torque is partially transmitted	Flight characteristics, instrumentation	Degraded function	Safety of Flight - condition of vehicle becomes OEI	II, Reduced power immediate landing (30 minute OEI designed in)	< 1/10,000 over 15,000 hour life of transmission / AGMA standards
	Excessive noise/ vibration	Audible, vibration, chip detectors	Failure of vibration-sensitive sensors and electronics.	Other system damage possible.	I, Non-vibration hardened equipment could be induced to fail: effect unknown.	Extremely unlikely. Helicopter components generally designed to 200 Gs.
	Excessive heat	Oil Temperature indication.	Reduced life, oil composition damaged	none	III, The ART is designed to run 30 minutes w/o oil.	Unlikely / Apache field Ops / Maint experience
	Seizure	Main rotor stops	System catastrophic failure	Safety of Flight	I, The ART is designed to run 30 minutes w/o oil.	0 / No Apache transmission seizures to date.
ART assembly - Transmit torque to accy. and NOTAR system	Torque is not transmitted	Visual, flight characteristics, instrumentation	Inoperative	Safety of Flight - Loss of anti-torque Possible forced landing	I, In forward flight, anti-torque is supplemented with tail-boom drag.	< 1/10,000 during OEI condition / AGMA gear bending failure calculations
	Excessive noise/ vibration	Audible, vibration, chip detectors	Failure of vibration-sensitive sensors and electronics.	Other system damage possible.	I, Non-vibration hardened equipment could be induced to fail: effect unknown.	Extremely unlikely. Helicopter components generally designed to 200 Gs.
	Excessive heat	Oil Temperature indication.	Reduced life, oil composition damaged	none	III, The ART is designed to run 30 minutes w/o oil.	Unlikely / Apache field Ops/Maint experience
	Seizure	Tail rotor stops	Loss of Anti-Torque	Safety of Flight - Loss of anti-torque Possible forced landing	I, In forward flight, anti-torque is supplemented with tail-boom drag.	0 / No Apache transmission seizures to date.
ART Assembly - Allow the rotor system to overrun the engine	Rotor system locked to engine	Main rotor and engine speed indications locked together.	Overrunning clutch failure	Reduced autorotation capability	IV, In autorotation, the rotor will be driving addt'l mass	no data
ART gears, bearings, shafts, flanges, and splines - transmit and change torque	Structural failure	Vibration, loss of power	Loss of power to main rotor and/or accy/NOTAR	Safety of Flight	I. Highest loads with Margin of Safety used in stress calculations	0/ No Apache structural failures to date.

TABLE 74. FAILURE MODES, EFFECTS AND CRITICALITY ANALYSIS (Continued)

Part ID and Function	Failure Modes	Method of Detection	Failure Effect Subsystem	Failure Effect Air Vehicle	Maximum Severity, Compensating provisions	Probability/ Data Source (1)
	Excessive gear and bearing wear-pitting and spalling	Quantitative Debris Monitor indication	Excessive noise and vibration	Excessive noise and vibration	IV. QDM will signal well in advance of critical problems	This mode calculated in previous section.
Over-running Clutch - Allows rotor to over-run engine, transmits torque	Unable to engage	Engine speed indication greater than rotor speed indication	Cannot transmit torque.	Possible loss of mission. System goes to OEI condition	III. 2 engine redundancy.	
	Unable to disengage	Engine and Rotor speed the same when collective dropped	Unable to disengage	Reduced autorotation capability	III. Autorotation not a normal procedure	no data
Housing - Provides structural support and torque reaction	Structural failure	Excessive Vibration	Cracking, breaking	Excessive vibration, loss of function	I. No Safety of flight related failures to date	3.72 E-5 / Apache UMSDC(2) failure data
	Corrosion	Visual, QDM	Reduced life	vibration, noise, Increases maintenance requirements, reduces life	IV. Fine filtration removes particles	2.9 E-5 / ART maintainability analysis
Housing - Retains oil	Gasket leak	Visible, hi temp, low oil pressure if excessive,	Loss of oil	Oil out operation	IV. ART designed for 30 min oil out operation.	0/ No Apache failures
Seals - prevent contamination of gearbox	Allow external contaminants to enter gearbox	QDM, Oil sample poor, oil leakage	Corrosion of internal parts, excessive wear	vibration, noise, Increases maintenance requirements, reduces life	IV. Fine filtration removes particles, Desiccant breather removes moisture	0 / ART maintainability analysis
Seals - prevent oil from leaking	Allow oil to leak	reduced oil level, visual, smell	none	Oil buildup on external surfaces	IV. Dual seal design	1.74 E-5 / ART maintainability analysis
Primary lube system - provide oil to gears and bearings for lubrication	Does not provide oil to gears and bearings	Pressure and Temperature indicators	Increased friction resulting in higher heat output	Reduced life	IV. Auxiliary lube system provides back-up	2.9 E-5 / ART maintainability analysis

NOTES:

(1) This is a summary. Please see preceding sections for analysis and basis.

(2) UMSDC is Unscheduled Maintenance Data Collection

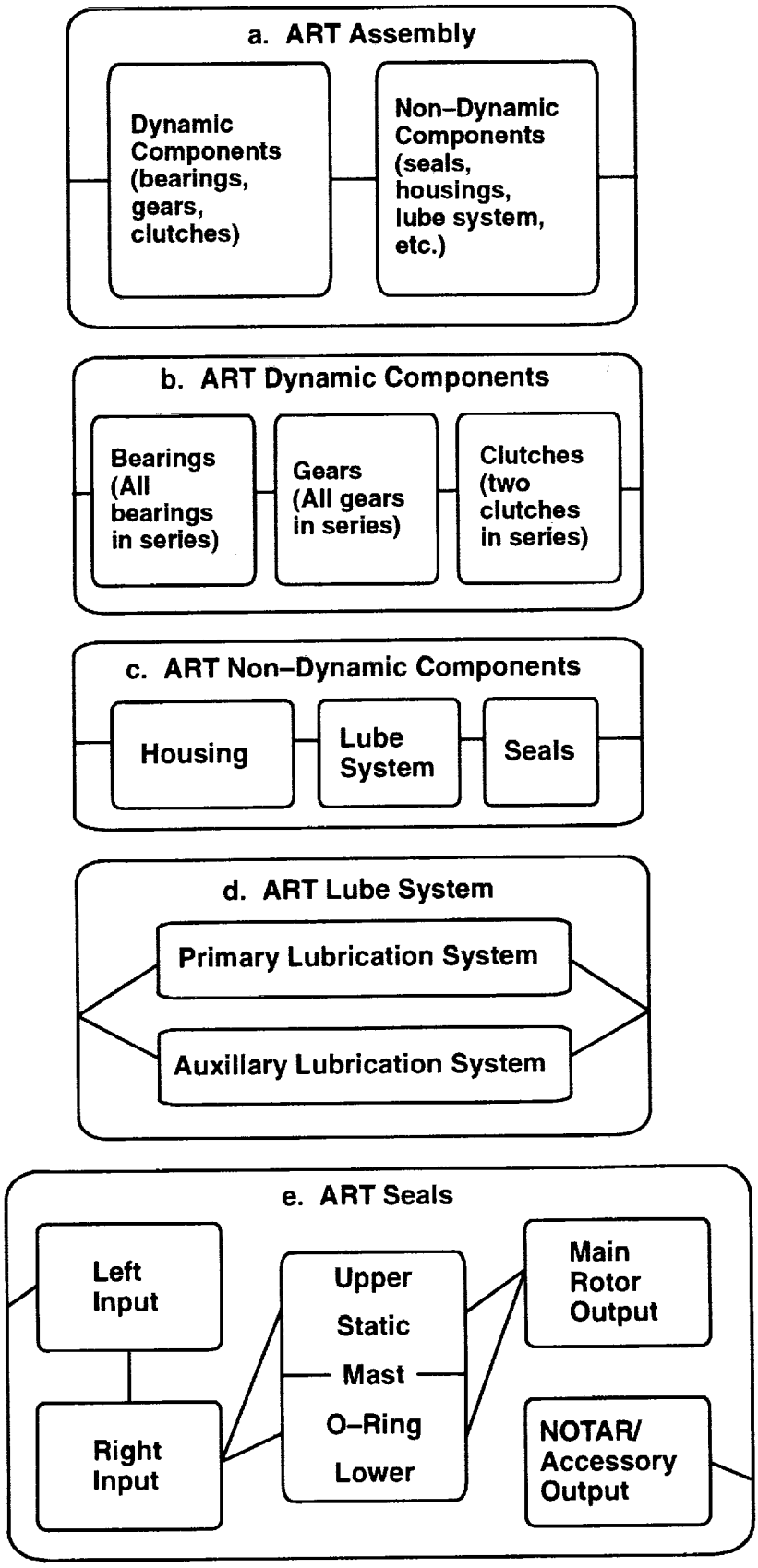

Figure 85. ART Reliability Block Diagrams

g. Effects of corrective actions: As the reliability specialist took part in the many design reviews, corrective actions were continuous and preempted erroneous design commitments. Specific examples include:

(1) Dynamic component L_{10} life design goals.

(2) Transmission failure type and frequency probability history.

(3) Reliability suggestions to design including those described in the maintainability section.

h. Residual problems are documented along with special controls which are necessary to reduce failure risk.

The risk items remaining are:

1. The ratchet-and-pawl clutch, in that it has not been used in a helicopter design. Reliability recommends that the clutch be tested in as realistic manner as possible.

2. The use of face gears in helicopter power transmissions. One precedent exists, and the design has used conservative models to predict life, although more testing is prudent.

3. The split-torque mechanism. This technology has been previously applied to helicopter design in various forms. This specific instance of the split-torque concept will benefit from the usual testing.

Low oil volume/High temperature lube system. This design will put increased demands on the reliability requirement of the lube system. Previous reliability data has indicated that the lube system tends to be highly reliable and is ready for performance growth.

REFERENCES

1. AGMA STD.216.01, Surface Durability (Pitting) Formulas for Spiral Bevel Gear Teeth, January 1964.

2. AGMA STD.223.01, Strength of Spiral Bevel Gear Teeth, January 1964.

3. AGMA STD.218.01, Rating the Pitting Resistance and Bending Strength of Spur and Helical Involute Gear Teeth, December 1982.

4. AGMA STD.217.01, Gear Scoring Design Guide for Aerospace Spur and Helical Power Gears, October 1965.

5. AFBMA STD.11-1978, Load Ratings and Fatigue Life for Roller Bearings, November 1978.

6. AFBMA STD.9-1978, Load Ratings and Fatigue Life for Ball Bearings, November 1978.

7. Schmidt, A.H., *A Method for Estimating the Weight of Aircraft Transmissions*, Society of Allied Weight Engineers, Technical Paper No. 1120, 1976.

8. Brikmanis, C.K. and Savage, M., *System Life and Reliability Modeling for Helicopter Transmissions*, Nasa Contractor Report 3967, April 1986.

9. *Failure Modes and Effects Analysis, Drive Train*, Report No. 205-939-008, Bell Helicopter Textron, October 1986.

10. *Helicopter Drive System On-Condition Maintenance Capability*, USAAMRDL-TR_75-57, Sikorsky Aircraft Division, July 1976.

11. *Analysis of Criteria for On-Condition Maintenance for Helicopter Transmissions*, USAAMRDL-TR-73, March 1973, by J.J. Dougherty III and S.J. Blewitt, Boeing Vertol Company.

12. *AGMA STD.211.02 for Surface Durability (pitting) of Helical and Herringbone Gear Teeth*, February 1969. Also see other AGMA STDs for gear surface durability.

13. Braddock, C.E., and Battles, R.A., *Design of an Advanced 500 HP Helicopter Transmission*, NASA Conference Publication 2210, June 1983, p. 125.

14. Mard, K.C., and Schlegel, R.G., *Transmission Noise Control - Approaches in Helicopter Design*, ASME Conference Publication 67-DE-58, May 1967, p. 8.

15. Litvin, F.L., *Design and Geometry of Face-Gear Drives*, ASME Journal of Mechanical Design, 1992.

16. Report No. 77-S-1401-2, *AH-64 Advanced Attack Helicopter Drive System Stress Analysis Report*, August 1982.

17. Haug, E.J., *Concurrent Engineering of Mechanical Systems*, Volume 1, Proceedings of the First Annual Symposium on Mechanical System Design in a Concurrent Engineering Environment, pp. 497-512, Ed., October 1989.

18. Townsend, D.P., Coy, J.J., Zaretsky, E.V., Experimental and Analytical Load-Life Relation for AISI 9310 Steel Spur Gears, Journal of Mechanical Design, January 1978, Vol. 100. Also see Transactions of the ASME, January 1978, Vol. 100.

19. Lundberg, G. and Palmgren, A., *Dynamic Capacity of Rolling Bearings*, Acta Polytech Mechanical Engineering Ser. 1, R.S.A.E.E., Nos. 3 and 7 (1947).

20. *Helicopter Drive System R&M Design Guide*, USARTL-TR-78-50, Cormier, K.R., Sikorsky Aircraft.

21. *DRC-S-H10000B System Specification for AH-64A Advanced Attack Helicopter*, April 1985, McDonnell Douglas Helicopter Company, Mesa, AZ.

22. Engineering Flight Test No. 470 Data, MDHC, May 4, 1989.

23. Expert testimony from the AH-64A Transmission Depot Maintenance Repair Facility was collected during a trip to that facility in Culver City. These experts were also consulted during the statistical analyses.

24. The AH-64A data consists of approximately 100,000 flight hours of AH-64A Sample Data Collection (SDC) field data, disassembly and inspection summaries, and McDonnell Douglas Helicopter Company Field Service Representative's Field Data Reports (FDR's).

25. Hawke, D.L., Hillis, J.E., Unsworth, W., *Preventative Practice for Controlling Galvanic Corrosion of Magnesium Alloys*, Technical Committee, International Magnesium Association, 1988.

26. Satty, T.L., *The Analytical Hierarchy Process*.

27. Bowes, M.A., Giansante, N., Bossler, R.B., and Berman, A., *Helicopter Transmission Vibration and Noise Reduction Program*, USAAMRDL-TR-77-14, June 1977.

28. Dussac, M., et. al., Aerospatiale, and Chabas, F., et. al., Office National d'Etudes et de Recherches Aerospatiales, *A Finite Element Method to Predict Internal Noise Levels at Discrete Frequencies for a Partially Composite Helicopter Fuselage*, American Helicopter Society 45th Annual Forum, May 1989.

29. Yoerkie, C.A., United Technologies Corporation, Sikorsky Aircraft Division, Moore, J.A. and Manning, J.E., Cambridge Collaborative, *Development of Rotorcraft Interior Noise Control Concepts - Phase 1: Definition Study*, NASA CR 166101, May 1983.

30. Yoerkie, C.A. and Gintoli, P.J., United Technologies Corporation, Sikorsky Aircraft Division, Moore, J.A., Cambridge Collaborative, *Development of Rotorcraft Interior Noise Control Concepts - Phase 2: Full Scale Testing*, NASA CR 172594, February 1986.

31. Mather, G., Bell Helicopter Textron, and Manning, J. and Quartararo, L., Cambridge *Collaborative, Analytical Prediction and Flight Test Evaluation of Bell ACAP Helicopter Cabin Noise*, American Helicopter Society 44th Annual Forum, June 1988.

32. El-Bayoumi, L.E., *Identification and Correction of Damaging Resonances in Gear Drives*, Paper No. 159.05, AGMA Fall Technical Meeting, Montreal, Canada, October 1983.

33. Albrecht, C., *Transmission Design Using Finite Element Method Analysis Techniques*, AHS Journal, April 1988.

34. Astridge, D. and Salzer, M., *Gearbox Dynamics - Modeling of a Spiral Bevel Gearbox*, Paper No. 50, Third European Rotorcraft and Powered Lift Aircraft Forum, France, 1977.

35. Meyyappa, M., Toossi, M., and Hashemi-Kia, M., *Modeling of Helicopter Transmissions for Vibration and Noise Prediction*, presented at the 46th Annual Forum of the AHS, Washington, D.C., May 1990.

36. Lee, C., Lin, H.H., Oswald, F.B., and Townsend, D.P., *Influence of Linear Profile Modification and Loading Conditions on the Dynamic Tooth Load and Stress of High Contact Ratio Gears*, NASA Technical Memorandum 103136, 1990.

37. Zakrajsek, J.J., *Comparison Study of Gear Dynamic Computer Programs at NASA Lewis Research Center*, NASA Technical Paper 2901, 1989.

38. Cornell, R.W., *Compliance and Stress Sensitivity of Spur Gear Teeth*, Journal of Mechanical Design, April 1981.

39. Cheng, C.Y.R. and Seybert, Andrew, University of Kentucky, *Recent Applications of the Boundary Element Method to Problems in Acoustics*, SAE Noise and Vibration Conference, Traverse City, MI, April 1987.

40. Oswald, Fred, NASA LeRC, Cleveland, OH, and Seybert, Andrew, et. al., University of Kentucky, *Comparison of Analysis and Experiment for Gearbox Noise*, NASA TM-105330, AVSCOM TR-91-C-030, 1992.

41. Lyon, Richard H., *Statistical Energy Analysis of Dynamical Systems: Theory and Applications*, The MIT Press, 1975.

42. Beranek, Leo, Noise and Vibration Control, McGraw-Hill, pp. 296-301, 1971.

43. Clifton, Scott, *AutoSEA Version 1.0 User's Guide*, Vibro-Acoustic Sciences, Ltd. (Australia), December 18, 1991.

44. Jones, A.B., *A General Theory for Elastically Constrained Ball and Radial Roller Bearings Under Arbitrary Load and Speed Conditions*, Journal of Basic Engineering, June 1960.

45. Kraus, J., Blech, J.J., and Braun, S.G., *In Situ Determination of Roller Bearing Stiffness and Damping by Modal Analysis*, Journal of Vibration, Acoustics, Stress and Reliability in Design, June 1987.

46. Walford, T.L.H. and Stone, B.J., *The Sources of Damping in Rolling Element Bearings Under Oscillating Conditions*, Proceedings of the Institution of Mechanical Engineers, Volume 197C, December 1983.

47. Dudley, D.W., *Handbook of Practical Gear Design*, McGraw Hill Book Company, 1984.

48. Lazan, Benjamin J., Prof., University of Minnesota, *Damping of Materials and Members in Structural Mechanics*, Pergamon Press, 1968.

49. Boyd, L.S. and Pike, J., *Multi-Mesh Gear Dynamics Program Evaluation and Enhancements*, NASA Contractor Report 174747, June 1985.

50. Coy, John, et. al., U.S. Army Propulsion Directorate, and Huff, R., et. al., NASA Lewis Research Center, *Identification and Proposed Control of Helicopter Transmission Noise at the Source*, NASA/Army Rotorcraft Technology Conference held at Ames Research Center, March 1987.

51. Hardesty, Mark and Hudson, Benjamin, McDonnell Douglas Helicopter Company, *Quantifying the Sound Power Generated by a Helicopter Main Transmission on a Regenerative Test Stand*, Internoise 89, Newport Beach, CA, December 1989.

52. Seybert, Andrew and Khurana, R., University of Kentucky, *Calculation of Sound Intensity and Sound Radiation Efficiency of Structures from Vibration Data*, prepared for presentation at the International Modal Analysis Conference in Orlando, FL, February 1-4, 1988.

53. Buresh, R.L., *Army Scored Unscheduled Maintenance Data for the AH-64*, 1989.

54. Beltramo and Morris, *Parametric Study of Helicopter Aircraft Systems Cost and Weights*, January 1989.

55. AGMA *Standard for Rating the Strength of Spur Gear Tooth*, AGMA 220.02, January 1964.

56. McIntire, W.L., Malott, R.C. and Lyon, T.A., *Bending Strength of Spur and Helical Gear Teeth*, AGMA 229.11, October 1967.

57. ASTM Standard E739, *Statistical Analysis of Linear or Linearized Stress-Life (S-N) and Strain-Life Fatigue Data*.

58. Brown, W.F., Jr., and Srawley, J.E., *Plane Strain Crack Toughness Testing of High Strength Metallic Materials*, ASTM STP 410, 1966.

59. Srawley, J.E., *Plane Strain Fracture Toughness, Fracture*, Vol. 4, Ch. 2, p. 45-68.

60. K_{1C} Values Provided by Magnesium Elektron, Inc.

61. M50NIL K_{1C} Values Provided by Latrobe Steel Company.

62. DiRusso, Robert, *Advances and Applications of Pyroware X53 in Helicopter Transmission System*, presented at the Rotary Wing Propulsion System Specialists' Meeting sponsored by the Southeast Region of the American Helicopter Society, Williamsburg, Virginia, November 12-14, 1986.

63. Handschuh, R.F., Lewicki, D.G., and Bossler, R., *Experimental Testing of Prototype Face Gears for Helicopter Transmissions*, NASA TM-105434, USAAVSCOM 7R-92-C-008, 1992.

REPORT DOCUMENTATION PAGE

Form Approved
OMB No. 0704-0188

1. AGENCY USE ONLY (*Leave blank*)	2. REPORT DATE	3. REPORT TYPE AND DATES COVERED
	January 1993	Final Contractor Report / Aug 88 - Jan 93

4. TITLE AND SUBTITLE

ADVANCED ROTORCRAFT TRANSMISSION (ART) PROGRAM - FINAL REPORT

5. FUNDING NUMBERS

WU-505-62-0K
C-NAS3-35454
PE-1L162211A47A

6. AUTHOR(S)

G. F. HEATH and R. B. BOSSLER, JR.

7. PERFORMING ORGANIZATION NAME(S) AND ADDRESS(ES)

McDonnell Douglas Helicopter Company
5000 E. McDowell Road
Mesa, Arizona 85205-9797

8. PERFORMING ORGANIZATION REPORT NUMBER

None

9. SPONSORING/MONITORING AGENCY NAMES(S) AND ADDRESS(ES)

Vehicle Propulsion Directorate
U.S. Army Research Laboratory
Cleveland, Ohio 44135-3191
and
National Aeronautics and Space Administration
Lewis Research Center
Cleveland, Ohio 44135-9797

10. SPONSORING/MONITORING AGENCY REPORT NUMBER

NASA CR-191057
ARMY RESEARCH LABORATORY
ARL-CR-14

11. SUPPLEMENTARY NOTES

D. F. LEWICKI
Project Manager
Vehicle Propulsion Directorate
Lewis Research Center
(216) 433-3970

12a. DISTRIBUTION/AVAILABILITY STATEMENT

Unclassified - Unlimited
Subject Category 37

12b. DISTRIBUTION CODE

13. ABSTRACT *(Maximum 200 words)*

Work performed by the McDonnell Douglas Helicopter Company and Lucas Western, Inc. within the U.S. Army/NASA Advanced Rotorcraft Transmission (ART) Program is summarized. The design of a 5000 horsepower transmission for a next generation advanced attack helicopter is described. Government goals for the program were to define technology and detail design the ART to meet, as a minimum, a weight reduction of 25 percent, an internal noise reduction of 10 dB plus a mean-time-between-removal (MTBR) of 5000 hours compared to a state-of-the-art baseline transmission. The split-torque transmission developed using face gears achieved a 40 percent weight reduction, a 9.6 dB noise reduction and a 6270 hour MTBR in meeting or exceeding the above goals. Aircraft mission performance and cost improvements resulting from installation of the ART would include a 17 to 22 percent improvement in loss-exchange ratio during combat, a 22 percent improvement in mean-time-between-failure, a transmission acquisition cost savings of 23 percent of $165K, per unit, and an average transmission direct operating cost savings of 33 percent, or $24K per flight hour. Face gear tests performed successfully at NASA Lewis are summarized. Also, program results of advanced material tooth scoring tests, single tooth bending tests, Charpy impact energy tests, compact tension fracture toughness tests and tensile strength tests are summarized.

14. SUBJECT TERMS

Helicopters; Rotorcraft aircraft; Transmission (machine elements); Gears

15. NUMBER OF PAGES

224

16. PRICE CODE

17. SECURITY CLASSIFICATION OF REPORT	18. SECURITY CLASSIFICATION OF THIS PAGE	19. SECURITY CLASSIFICATION OF ABSTRACT	20. LIMITATION OF ABSTRACT
Unclassified	Unclassified	Unclassified	